

**UNIVERSITY OF OKLAHOMA**

**GRADUATE COLLEGE**

**4DVAR RETRIEVAL OF PROGNOSTIC LAND SURFACE  
MODEL VARIABLES**

A Dissertation

SUBMITTED TO THE GRADUATE FACULTY

In partial fulfillment of the requirements for the

Degree of

Doctor of Philosophy

By

**DIANDONG REN**

Norman, Oklahoma

July 23rd, 2004

UMI Number: 3270680

### INFORMATION TO USERS

The quality of this reproduction is dependent upon the quality of the copy submitted. Broken or indistinct print, colored or poor quality illustrations and photographs, print bleed-through, substandard margins, and improper alignment can adversely affect reproduction.

In the unlikely event that the author did not send a complete manuscript and there are missing pages, these will be noted. Also, if unauthorized copyright material had to be removed, a note will indicate the deletion.

**UMI**<sup>®</sup>

---

UMI Microform 3270680

Copyright 2007 by ProQuest Information and Learning Company.

All rights reserved. This microform edition is protected against unauthorized copying under Title 17, United States Code.

ProQuest Information and Learning Company  
300 North Zeeb Road  
P.O. Box 1346  
Ann Arbor, MI 48106-1346

©Copyright by DIANDONG REN 2004

**All Rights Reserved.**

4DVAR RETRIEVAL OF PROGNOSTIC LAND SURFACE MODEL  
VARIABLES

A Dissertation APPROVED FOR THE SCHOOL OF METEOROLOGY

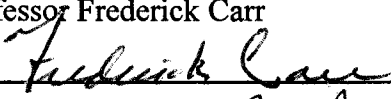
By



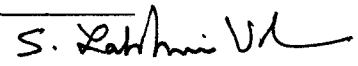
\_\_\_\_\_  
Professor Ming Xue

  
\_\_\_\_\_  
Professor Kelvin Droegemeier

\_\_\_\_\_  
Professor Frederick Carr

  
\_\_\_\_\_  
Professor Qin Xu

  
\_\_\_\_\_  
Professor S. Lakshmivarahan

  
\_\_\_\_\_  
Dr. Jidong Gao



## Acknowledgements

The people who have shaped this dissertation both personally and professionally are numerous. First, I must thank my advisor, Professor Ming Xue. He has taught me that no dream is too great. His diligence and perseverance is amazing, and I will never forget his honesty and kindness. I could not forget all the random drop-bys I made and he is always giving his supervision sincerely and with dedication. He revived my enthusiasm in meteorology after a series of setbacks (lack of funding during my M. S. study).

Thanks Professors Kelvin Droegemeier, Frederick Carr, Qin Xu, and Lakshmiarahan for serving on my committee. Thanks for your insightful questions during the general exam that guided and reshaped this study. Thanks Dr. Jidong Gao for the general technique for adjoint coding.

In addition to my dedicated committee, I feel obligated to thank several distinguished figures in the field of land surface modeling. Much of my knowledge about land surface modeling is from the communications with Professor Ann Henderson-Sellers, who is always a spiritual support for me. Professor Roger Pielke Sr. extended his kindness by introducing me to his active group members. Thanks for their precious time and nurture. Personal communications with them greatly lifted my knowledge level in this field of land surface modeling.

Thanks also are due all of CAPS. Jidong Gao, Dan Weber, Keith Brewster, Jerry Brotzge, Paul Nutter and Bill Martin, you taught me a lot. I could not have done this without your help. Friendship with Dr. Pengfei Zhang's family is long lasting and their introduction is valuable for me to get familiar with OU/SOM.

Finally and above all, I thank my wife and my parents. I have been blessed by all measure to have such an honorable and respected family. I thank my parents (Ren, Tongyu and Shi, Xiange). They opened my eyes to the world around me, filled me with wonder, and taught me what should be pursued and what is wrong. I thank my brothers (Dianhao, Dianxing, Dianshun and Dianwei) for their understanding and support. I will make up the caring of our parents as soon as possible. I thank the support from my dear wife (Xiaoning Li). She has patiently endured the long days and long nights associated with acquiring this degree. And in the times of trial, when I just wanted to quit, she always encouraged me to never give up. In retrospect, I never would have completed this task without Xiaoning her loving support. Thanks also go to my parents in law (Xingchai Li and Huixin Cao). Without their help in taking care of our daughter during this critical period, it is impossible for us to accomplish so much.

Supports for this study comes primarily through a DOT-FAA grant, and two NSF grants: ATM9909007 and ATM0129892.

# Table of Contents

<b>Acknowledgements .....</b>	<b>iv</b>
<b>List of Tables .....</b>	<b>viii</b>
<b>Abstract .....</b>	<b>ix</b>

## Chapter One

<b>General Introduction .....</b>	<b>1</b>
1.1. The Need for Land Surface Data Assimilation.....	4
1.2. Existing Methods for Soil Moisture Initialization .....	5
1.2.1. <i>Assimilation of Ground Surface Variables for Estimation of Surface Energy Balance Components</i> .....	7
1.2.2. <i>Estimation of Profile Soil Moisture/Temperature through Assimilation of Surface Measurements</i> .....	8
1.2.3. <i>Estimation of Land Surface Properties by Assimilating Screen-Level Atmospheric Observations</i> .....	9

## Chapter Two

<b>Data, Forward Model and General Framework for 4DVAR Retrieval .....</b>	<b>14</b>
2.1. OASIS Data.....	16
2.2. Forward Model.....	18
2.2.1. <i>Land Surface Components</i> .....	20
2.2.2. <i>PBL Scheme Used in this Study</i> .....	32
2.2.3. <i>Radiative Heating/Cooling</i> .....	42
2.3. Verification of Forward Nonlinear Model.....	45
2.4. Adjoint sensitivity and Variational Data Assimilation .....	65
2.4.1. <i>A General Statement of Sensitivity Study and Data Assimilation Using Adjoint</i> .....	65
2.4.2. <i>4DVAR Procedure and Definitions of Two Cost Functions Used in this Study</i> .....	70
2.4.3. <i>Analysis of the topology of the Cost Function</i> .....	75

## Chapter Three

<b>Development of Tangent Linear (TLM), Adjoint Models (ADM), and 4DVAR retrieval system.....</b>	<b>85</b>
3.1. Construction and Verification of the Tangent Linear and Adjoint Models .....	85
3.1.1. <i>Techniques for Coding Tangent Linear and Adjoint Models</i> .....	85
3.1.2. <i>Verifications of TLM and ADM</i> .....	90
3.2. Verification of The 4DVAR Data Assimilation System .....	91

## Chapter Four

<b>Initial Condition and Model Parameter Sensitivity Experiments .....</b>	<b>93</b>
4.1. Nonlinear Sensitivity Experiments .....	94
4.2. Tangent Linear Sensitivity .....	113
4.2.1 <i>Tangent Linear Verification for Forced Land Surface Model Runs</i> .....	114
4.2.2 <i>Tangent Linear Verification for Coupled Model Runs</i> .....	116
4.3. The Evolution of the Adjoint Variables and Period of Most Sensitivity .....	116
4.3.1. <i>Decomposition of Adjoint Sensitivities</i> .....	117
4.3.2. <i>Relative Parameter Sensitivities</i> .....	118

<b>Chapter Five</b>	
<b><i>Retrieval of Soil States Using Soil Skin Temperature Observations</i></b> .....	<b>119</b>
5.1. Data .....	120
5.2. Numerical Experiment Design .....	121
5.3. Observing Simulation System Experiment (OSSE) Retrieval.....	123
5.4. Retrieval Experiments with Real Data .....	143
5.4.1. <i>Initial value retrieval</i> .....	143
5.4.2. <i>Sampling strategy</i> .....	145
5.4.3. <i>The Effects of Assimilation Window Length</i> .....	148

<b>Chapter Six</b>	
<b><i>Retrieval of Soil States Using Atmospheric Observations Only</i></b> .....	<b>152</b>
6.1. Observing Simulation System Experiment (OSSE) Retrieval.....	154
6.1.1. <i>Convergence of the minimization</i> .....	155
6.1.2. <i>Robustness to Gaussian noise</i> .....	164
6.1.3. <i>Effects of observational accuracy</i> .....	166
6.2. Retrieval Experiments with Real Data .....	167
6.2.1. <i>Influence of the assimilation window length</i> .....	170
6.2.2. <i>Effects of preconditioning</i> .....	173
6.3. Extended Definition of the Cost Function .....	176
6.3.1. <i>Influence of the soil and vegetation</i> .....	178
6.3.2. <i>Identifying the Most Significant Model Errors</i> .....	180
6.3.3. <i>Effects of Atmospheric Forcing Conditions and Advection</i> .....	180

<b>Chapter Seven</b>	
<b><i>Summary and Conclusions</i></b> .....	<b>182</b>
<b>References</b> .....	<b>189</b>
<b>Appendix 1. General Philosophy of LSM-PBL Model</b> .....	<b>203</b>
A1.1. Land Surface Components.....	203
A1.1.1. <i>Soil Temperature</i> .....	204
A1.1.2. <i>Soil Moisture</i> .....	206
A1.2. Vertical Mixing in and above Convective Boundary Layer .....	210
A1.2.1. <i>Empirical Approximations of the Universal Functions</i> .....	212
A1.2.2. <i>Expressions for Turbulent Exchange Coefficients in terms of Universal Functions</i> .....	213
A1.2.3. <i>Integral Forms of Flux-Profile Relationships</i> .....	214
A1.2.4. <i>Expressions of the Monin-Obukhov Length L</i> .....	216
<b>Appendix 2. A Review of 4DVAR Data Assimilation Technology</b> .....	<b>218</b>
<b>Appendix 3. An example of hand coding adjoint and its verification</b> .....	<b>224</b>



## List of Tables

- Table 2. 1 Static soil and vegetation parameter setting at Norman site (Lat. 35 15' 20"; Lon. 97 29' 0"; characterized by flat terrain, and dynamic roughness of 0.004 m)
- Table 2. 2 Atmospheric model parameter setting
- Table 4. 1 Sensitivity to  $T_{sfc}$
- Table 4. 2 Sensitivity to  $T_{dp}$
- Table 5. 1 Parameters used in the selected period (August 4-27, 2000)
- Table 5. 2 Numerical experiment design for retrieval with stand-alone land surface model and its adjoint
- Table 5. 3 Initial states retrieval using synthetic data
- Table 6. 1 Retrieval experiment design for coupled model system
- Table 6. 2 Some statistics between initial guess and observation within the forecasting period
- Table 6. 3 Some statistics between retrieved and observation within the forecasting period
- Table 6. 4 Some statistics between initial guess and observation within the forecasting period
- Table 6. 5 Some statistics between retrieved and observation within the forecasting period
- Table 6. 6 Initial states retrieval using synthetic data
- Table 6. 7 Retrieved  $w_{sfc}$  with different measurement accuracies
- Table 6. 8 Some statistics between initial guess and observation within the forecasting period
- Table 6. 9 Some statistics between retrieved and observation within the forecasting period
- Table 6. 10 Preconditioning numerical experiments
- Table 6. 11 Simulating model error in vegetation coverage

## Abstract

For numerical weather prediction models, it is critically important to properly initialize its land surface model component. This study demonstrates successful variational retrievals of land surface states by assimilating either skin temperature or screen-level atmospheric measurements. For this purpose, the land surface model is first validated against the Oklahoma Atmospheric Surface Layer Instrumentation System (OASIS) measurements. Refinements to the model were found necessary.

Two distinct retrieval problems are tackled in this study. One uses skin temperature as the observation and one uses observations of near surface atmospheric variables. The former is done using a land surface model and its adjoint in a stand-alone mode, forced by observed meteorological parameters. A 4D variational (4DVAR) retrieval system is developed in which the cost-function is defined as a quadratic measurement of the model forecasting error in ground surface or skin temperature. The latter involves a 1D land surface-atmosphere model, the corresponding adjoint codes, and a definition of cost function that measures misfit between observed and modeled screen-level atmospheric temperature and specific humidity.

The major findings of the first type of retrieval are: Initial soil moisture contents as well as deep soil temperature can all be successfully retrieved, for realistic initial guess errors; the relative difficulty in retrieving superficial and deep soil moisture contents depends on the vegetation coverage and growth conditions; the revision to the soil temperature equations as documented in a separate paper is found critical in retrieval with real OASIS data; daytime observations are found much more effective because of their

higher signal to noise ratio; assimilation window length up to ten days is found to produce the better retrievals. This signifies the value of information contents.

For the second retrieval problem, the Medium Range Forecast (MRF) PBL model is implemented within the Advanced Regional Prediction System (ARPS), forming a coupled LSM-PBL model. We show that under ideal synoptic conditions, land surface prognostic variables can also be successfully retrieved from the screen-level atmospheric observations. The retrieval scheme is robust when subject to observational errors with magnitudes comparable to instrument accuracy, and for initial guess errors larger than typical model forecast errors. Compared to the early case, the validity period for tangent linearization is shorter due to feedbacks from atmospheric components. There exists an optimal assimilation window length resulting from the contest between degrading forecast accuracy and increasing necessary information content. For a moist period tested, taking the scheme efficiency into consideration, a length of about six hours seems to be a suitable assimilation window length.

# Chapter One

## *General Introduction*

Many studies have demonstrated the sensitivity of the surface energy budget and atmospheric fields to land-surface processes, on virtually all spatial and temporal scales (see, e.g., Zhang and Anthes 1982; Jacquemin and Noilhan 1990 for numerical weather prediction; Ookouchi *et al.* 1984; Santanello and Carlson 2001 for mesoscale modeling; Benjamin and Carlson 1986 for synoptic scale influences; Ye 1989; Mintz 1984; Milly and Dunne 1994; Henderson-Sellers *et al.* 1996 for climatology research). In a coupled land surface-atmospheric modeling system, the function of the land-surface model is to provide lower boundary conditions for latent heat flux, sensible heat flux and momentum fluxes, which will be used to predict the evolution of the planetary boundary layer (PBL). To do so, the land surface model requires the lowest atmospheric wind speed, temperature and relative humidity and other micrometeorological variables as its forcing.

Much research has established that the inclusion of a realistic formulation of land surface scheme improves the forecast of near surface and boundary-layer components (e.g., Abramopoulos *et al.* 1988; Betts and Hall 1996). Because, especially for weather prediction models, initialization of the land surface parameters is important, much research has also been devoted to better initialize the diagnostic and prognostic variables (e.g., Mahfouf and Viterbo 2001; Bouyssel *et al.* 1998) of land surface models. The initialization of the diagnostic/static variables includes the production of soil and

vegetation maps, whereas this work focuses on the analysis of the prognostic variables such as soil moisture and temperature in land surface models.

The land surface schemes employed in meteorology are designed to describe the thermodynamics and hydrology near the surface. Whereas the soil temperature at the surface is controlled by net radiation and the turbulent mixing with the overlying atmosphere in the form of sensible heat flux, temperatures in the soil medium distribute according to diffusion law. The hydrology components of a land surface scheme describe the basic evaporation processes at the surface together with the water partitioning between the vegetation transpiration, the drainage, the surface runoff, and that contained by soil. The bond connecting soil hydrology and thermodynamics is latent heat flux, the energy accompanying phase changes of water from vegetation transpiration and bare ground evaporation. One of the main difficulties in the use of land surface schemes is the initialization of the soil temperature and soil wetness.

Although soil moisture and temperature are of great importance, they are difficult to monitor routinely, especially at regional or continental scales (Jones *et al.* 2004). The situation calls for creative ideas for inferring soil moisture and temperature information from those related variables which are routinely measured. To date, there have been efforts to assimilate ground surface variables for estimation of surface energy balance components (Boni *et al.* 2001; Wetzel *et al.* 1984; van den Hurk *et al.* 1997; Xu and Qiu 1997; Xu and Zhou 2003), to assimilate surface measurements for estimation of profile soil moisture/temperature (Milly and Kabala 1986; Jackson *et al.* 1987; Entekhabi *et al.* 1995; Grunmann *et al.* 1999), and to assimilate screen-level atmospheric forcing for the

estimation of time-variant land surface properties (Mahfouf 1991; Callies *et al.* 1998). Most of these retrieval schemes are still in the research stage.

The goal of this study is to explore methods for land surface data assimilation, and to identify the issues that must be solved for successful data assimilation schemes for numerical weather prediction (NWP) purposes. This will be achieved by verifying and refining the forward land surface prediction scheme and by applying the four dimensional variational assimilation technique. Several outstanding issues such as sampling strategy, model error and model parameter uncertainties can be generalized using the variational formalism.

To these ends, two schemes are developed and retrieval experiments were conducted. For the first set, inspired by the previous work of Boni *et al.* (2001) and Grunmann *et al.* (1999), a retrieval scheme that assimilate ground temperature measurements from the Oklahoma Atmospheric Surface layer Instrumentation System (OASIS) is tested for estimating initial land surface variables such as soil moisture and temperature. The second set of experiments is more indirect and more demanding because they assimilate screen-level atmospheric measurements to estimate the initial soil model conditions (Mahfouf 1991; Callies *et al.* 1998; Bouyssel *et al.* 1998). Our successful retrieval experiments, especially with the real data, are based on a revision to the force-restore scheme (i.e., a compromise between the bucket (Manabe 1969) and multi-layered Richards (Richards 1931) equation-based methods) to correct a long time misuse in the mesoscale modeling community. The forward model system applies a planetary boundary layer scheme that gives an accurate description of the lower atmospheric daily evolution, yet is simple enough for coding its adjoint. The adjoint code,

a necessary component for the 4DVAR retrieval system (e.g., Le Demet and Talagrand 1986, Courtier and Talagrand 1987a&b), is hand-coded, with a commercial automatic differentiation tool used for a double check of the linearization.

In Subsection 1.1, the need for land surface data assimilation is outlined, followed by a detailed literature review on the current work in land surface modeling and its data assimilation (Subsections 1.2&1.3).

### *1.1. The Need for Land Surface Data Assimilation*

Because the evolution of the planetary boundary layer (PBL) is very sensitive to the specification of the soil moisture content in the hydraulically active layer (a top soil layer of a couple meters deep whose moisture can interact with the atmosphere through evapotranspiration and precipitation and is available to vegetation growth), the estimating of soil moisture is important for the initialization of land surface schemes. However, *in situ* measurements are, as mentioned earlier, scarce both spatially and temporally, especially for deeper soil moisture.

As reviewed by Kostov and Jackson (1993), conventional methods of direct observations are time and labor consuming and frequent observations over large areas are nearly impossible. Based on the reasoning that there is a strong dependence of the soil's dielectric properties on its moisture content due to the large contrast between the dielectric constant of water and that of soil (i.e., water has a dielectric constant of ~80 at L-band of 1.4GHz, whereas bare soil has a dielectric value of ~3.5), satellite based passive remote sensing is believed to be able to provide near-surface soil moisture for a global coverage. However, the accuracy of such measurements is a constant concern and general methods for inferring the deeper soil moisture are not mature to date. These kind

of approaches get good results for less vegetated surfaces because the uncertainties introduced by variations in surface temperature and, surface roughness are smaller for bare soils.

Climate networks for soil temperature exist (Karl *et al.* 1990; <http://cdiac.esd.ornl.gov/epubs/ndp019/ndp019.html> at the time of writing), with coverage of about 100 km by 100 km and most of them perform observations at least daily. However, most of these observations are not disseminated routinely at the time of measurement, limiting their usefulness for real time numerical prediction and some other applications.

Properly initialized land surface parameters may also contribute to shortening the spin-up time for numerical weather forecast models (Bennett *et al.* 1993). The following is a summary of the literature on land surface data assimilation.

### *1.2. Existing Methods for Soil Moisture Initialization*

Several different approaches to perform land surface data assimilation exist: the land data assimilation system (LDAS), antecedent precipitation index method (API), and variational method. On the basis that the quality of the land surface model output is closely related to the meteorological forcing used to drive it (e.g., radiative fluxes, precipitation), LDAS, a multi-institutional effort to produce land-surface hydrology simulations over the continental US for use in weather and climate models (Schaake *et al.* 2002), performs forced (with meteorological forcing provided) runs of a land surface model to assimilate atmospheric information to obtain an estimate of the land surface states. One example of this approach for application in mesoscale meteorological modeling was described in Xiu and Pleim (2001). With this approach, a long enough period (week-long) preceding the real forecasting period is set aside for forced land



surface model run. The soil moisture is initialized according to climatological rainfall patterns and taking the soil texture into consideration. The model is then run for a long enough period to allow the soil hydrology to adjust to micro-meteorological conditions, especially precipitation.

In the same spirit that Antecedent Precipitation Index (API) is used in catchment hydrology for runoff/infiltration distribution, API is also used to initialize soil moisture content for a land surface model (Linsley *et al.* 1949; Wetzel and Chang 1988; Ziegler *et al.* 1997). Both approaches enjoy the advantage of easy implementation, however, their moisture analyses depend entirely on the land model skill (Henderson-Sellers *et al.* 2002; Qu *et al.* 1998). Their retrieved “optimal” soil moisture usually deviates from the truth. Also, this kind of approach (e.g., retrospective method (Nijssen *et al.* 2001)) is generally case sensitive to and depends on location and time period.

Aside from the lack of routine soil moisture and temperature measurements, for land surface modeling, the use of classical data assimilation tools is further complicated by the fact that significant variability had been observed in both soil moisture and soil properties in small spatial scales (Basara 2001; Wetzel and Chang 1988). Although not all scales are of relevance for the atmosphere, the assimilation method should take this issue into consideration. The statistical-dynamical approach (Avissar 1992) and the fractal models (Marshak *et al.* 1998) for describing heterogeneity are endeavors in this direction.

Variational data assimilation methods try to minimize the misfits between observations distributed over a period of time and the prediction of a forward forecast model. They are mathematically more demanding and require extra adjoint code and a set

of optimization codes. We chose this method in this study because it is an effective approach in retrieving soil prognostic variables and it guarantees that the model is consistent with the assimilated data. The literature (e.g., Xu and Qiu 1997; Grunmann *et al.* 1999; Callies *et al.* 1998; Margulis and Entekhabi 2001; Mahfouf 1991) in this research direction is relatively new and in the initial stage of development. Systematic documentation seems in need.

Existing work on land surface data assimilation can also be grouped into the following three major categories according the relationship between observations and the land surface parameters to be inferred: assimilation of ground surface variables for estimation of surface energy balance components, estimation of profile soil moisture/temperature through assimilation of surface measurements, and estimation of land surface properties by assimilating screen-level atmospheric observations.

#### ***1.2.1. Assimilation of Ground Surface Variables for Estimation of Surface Energy Balance Components***

This type of approach usually chooses to use a simplified land surface scheme (e.g., force-restore description of surface temperature and moisture content) and simplified PBL scheme. Due to this limitation, the target parameters are few. Using Southern Great Plain 1997 (SGP97) hydrologic field experiment measurements and a model formulation for bare ground, Boni *et al.* (2001) discussed the feasibility of assimilating ground surface temperature to estimate superficial soil moisture availability and hence the surface latent and sensible heat fluxes. They found that, under temporally incomplete observations, the most informative periods are those measurements near the peak of the diurnal oscillation. In estimating the superficial soil moisture availability

index, what they actually did is a retrieval of a dynamic parameter. Limited by the data availability (only ground temperature measurements), they could only retrieve a daily average value of this index. Retrieval at lesser aggregating levels may be undetermined.

### ***1.2.2. Estimation of Profile Soil Moisture/Temperature through Assimilation of Surface Measurements***

Much research for remote sensing applications in hydraulic modeling belongs to this category. Pioneering research includes that done by Milly and Kabala (1986), Jackson *et al.* (1987), Entekhabi *et al.* (1995), and Grunmann *et al.* (1999). Kostov and Jackson (1993) reviewed four basic approaches: regression, knowledge-based, inversion, and combination of remotely sensed data with a water balance model. The first two approaches are relatively easier to be placed into operational environments. Their success depends upon *a priori* information on the hydrological properties of soil. As far as we know, few studies include the vegetation factors. The inverse method as reviewed is the inverse solution of a Childs' equation (as in radiative transfer schemes). A similar approach can also be applied to estimate the soil structural properties. For a numerical model, remotely sensed surface soil moisture can be used as input, to update, or to calibrate the model. The model, when it includes a more realistic description of the water budget physics, is expected to give a better description of the profile soil moisture/temperature.

Entekhabi *et al.* (1995) investigated theoretically the assimilation of passive microwave data for the retrieval of profile soil moisture for bare soil. Using a multilayer model of heat and water transfers for a bare soil (based on Milly 1980), they investigated the signal propagation from the deepest layers to the soil surface. They asserted the

feasibility of using passive microwave data (at frequencies less than 10 GHz) for retrieving the soil water content. More recently, Galantowicz *et al.* (1999) tried a Kalman filter based sequential optimal estimation method by assimilating directly radio-brightness for the estimation of soil moisture profiles within the top one meter of less vegetated surfaces. Using eight days in July for a bare ground site, they found that during the subsequent updating (using the Kalman gain, which is a balance between forecasting skill and observational accuracy, to obtain new analyses), the bad effects from wrong initial guess states can be successfully removed and accurate soil states can be reconstructed as a result. The required update frequency is quite low (daily).

Recently, Jones *et al.* (2004) performed profile soil moisture retrieval using a 4DVAR assimilation system with passive remote sensing observations (L-band thermal infrared at 6~10 GHz). They found that the (remote sensing) data are sensitive to the surface soil moisture content, and the soil profile temporal evolution can propagate the information vertically within the entire soil column, thus making the profile soil moisture retrieval practical. To augment the capabilities of the remote sensing data set, the 4DVAR system can also assimilate conventional surface observations. Their sensitivity analysis and retrieval experiments indicate that the 4DVAR method is of significant utility for initializing soil moisture for numerical weather prediction models.

### ***1.2.3. Estimation of Land Surface Properties by Assimilating Screen-Level Atmospheric Observations***

Indirect methods have been proposed to retrieve information on soil moisture from atmospheric information and conventional land use data. Mahfouf (1991) pioneered the attempt of retrieving surface moisture from observations of screen-level air

temperature and relative humidity (10m wind and 2m temperature and humidity as SYNOPs). Using the Interactions Soil Biosphere Atmosphere (ISBA, Noilhan and Planton 1989, NP89 henceforth) land surface scheme, he obtained positive conclusions for a crop area and clear sky conditions. He described two possible approaches: a variational algorithm where a cost function is minimized over an assimilation period, and a sequential assimilation scheme that consists of a set of predictions and in-static correlations of soil moisture. He validated both methods against *in situ* data collected during the HAPEX-MOBILHY (Andre *et al.* 1986) field experiment, using a one-column model to represent the interactions between surface processes and the planetary boundary layer structure. Bouttier *et al.* (1993a&b) further argued for the feasibility of estimating both superficial and deep/bulk layer soil moisture using the time evolution of atmospheric temperature and relative humidity near the surface. They emphasized also that this method requires a close relationship between the near surface atmospheric conditions and the soil moisture.

Calvet *et al.* (1998) also applied the inverse estimation of the bulk soil moisture content using surface variables (either surface soil moisture or temperature). They argue that knowing the atmospheric forcing (especially precipitation) and four to five surface soil moisture measurements over two weeks are adequate to retrieve the bulk soil moisture by inverting ISBA scheme. Because there is a strong relationship between the deeper layer soil moisture and surface soil moisture, especially when the vegetation are in full growth, it is feasible to infer the bulk soil moisture by minimizing error in predicting surface soil moisture. For assimilating surface temperature, they also realized that good

retrievals are obtainable for only relatively dry conditions (maybe because the weaker sensitivity for moist periods).

Based on the same forward model as used by Calvet *et al.* (1998), Bouyssel *et al.* (1998) did a series of variational surface analysis from screen-level atmospheric parameters. Their tangent linear analysis pointed out several interesting topics that inspire this study. Their study, however, was based solely on synthetic data (identical twin experiments).

Recently, Santanello and Carlson (2001) reiterated a phenomenon called decoupling (Gillies and Carlson, 1995), which occurs when rapid surface soil drying takes place under intense sunshine. The decoupling phenomenon, as they argued, occurs more frequently for less vegetated or bare soil surface. Once it occurs, the decoupling, accompanied by a sharp vertical soil water gradient, renders/reduces the usefulness of techniques using, i.e., remotely sensed surface soil moisture to infer the column-averaged/bulk soil moisture. Thus, the method used by Calvet *et al.* (1998) may not be applicable under this condition.

All these demonstrate the desires for retrieving land surface prognostic variables and the challenges facing the researchers. It is generally not possible to produce a direct analysis of soil moisture and/or temperature because direct observations are not available on a routine basis. However, since they have influences on surface fluxes, it may be possible to indirectly estimate these land surface quantities using atmospheric measurements that are available at the lowest atmospheric model level.

At the same time, the indirect connection may be contaminated by other processes such as strong large scale advection (a problem only with column models), cloud cover

that dampen the evapotranspiration signal, and certain numerical bounds inside the scheme that remove the sensitivities of surface fluxes to soil or vegetation properties (it usually is not the fault of numerical bounds, they are only a representation of the physical processes). For example, in ISBA, for bare ground, the evaporation can proceed at potential rate when soil moisture content lies between field capacity and saturation. In this situation, the evolution of relative humidity may not reflect the surface soil moisture condition. Rather, it only reflects the atmospheric forcing parameters. Even in this case, soil moisture content plays a role in the prediction of ground temperature through its influence on soil heat capacity. Near wilting point, the canopy resistance is similarly bounded in the ISBA scheme, which causes a differentiation problem around the wilting point and thus poses a hindrance for adjoint-based methods. Thus, the relationship between soil property and screen-level measurements may be rather weak under some situations hence makes it difficult for an universally successful retrieval.

This study focuses on variational methods of the optimal data assimilation techniques, which are suitable for more indirect observations of land surface related properties and have an inherent flexibility to adapt to temporal and spatial requirements of the applications (Talagrand and Courtier 1987; Jones *et al.* 2004). The variational data assimilation methods would also necessarily depend on land model skill, however, the model strong constraint can be readily relaxed through adding an extra forcing term to represent the model error (Zupanski 1997). Although both Kalman Filter method and 4D variational data assimilation method enjoy the flexibility to include a variety of observations and work with any level of model complexity, we chose variational method over other optimal methods such as those based on the Kalman Filter (Mitchell *et al.*

2002; Reichle *et al.* 2002) because we believe variational method is more computationally efficient, due to its separate treatment of background covariance and optimization (Kalman gain applied to innovation vector depends on error covariance matrix, which evolves in time and is also not easy to save).

One inherent feature of the variational method is that it requires the availability of adjoint model. This is both an extra burden (adjoint models have to be developed for all model components involved in the assimilation algorithm) and a benefit (easiness to conduct sensitivity experiments to provide insight into the forward model). Also, adjoint sensitivity analysis is inherently independent of the data assimilation problem and the associated specification of background covariance because it does not require pre-specification of forward perturbations in the control parameter space. But when one is interested in understanding a specific perturbations' impact, one realization of the space of the perturbations are used to drive adjoint model.

This research is organized as follows: In Chapter 2, we first discussed the dataset used for both assimilation and verification, then the forward land surface scheme and atmospheric planetary boundary layer scheme are described and verified, followed by a rather general description of the variational formalism, while the construction of the adjoint model on the basis of the forward system is presented in Chapter 3, focusing on the technical aspects of verification of the tangent linear and adjoint system. Chapter 4 gives several nonlinear sensitivity experiments and proposed several methods for tangent linear and sensitivity experiments. Chapter 5 covers a set of retrieval experiments based on the data availability of only surface temperature; whereas Chapter 6 address the retrieval experiments assuming data availability of screen-level atmospheric parameters. Both synthetic observations and real OASIS measurements are used. Chapter 7 summarizes this study.



## Chapter Two

### *Data, Forward Model and General Framework for 4DVAR*

#### *Retrieval*

4DVAR data assimilation and/or retrieval systems seek to minimize the misfit between observations distributed over a period of time (called the assimilation window) and the prediction of a forward forecast model (Le Dimet and Talagrand 1986; Talagrand and Courtier 1987; Xu 1996a&b). A cost function, typically of a quadratic form, measures such a misfit. The initial condition of the forecast model is adjusted, starting from an initial guess, so as to minimize the cost function. When the variables defining the initial conditions are not directly measured, such variables are said to be retrieved (from the observed quantities) and the entire procedure is often referred to as retrieval.

Efficient minimization algorithms, such as the conjugate gradient method (Navon and Legler 1987; Fletcher and Reeves 1964) used in this study, require the gradient of the cost function with respect to the variables to be adjusted in the initial condition (called control variables), and the gradient can be efficiently obtained by a backward-in-time integration of the adjoint model. Here, the adjoint is mathematically defined as the transpose of the tangent linear approximation to the nonlinear forward prediction model (Le Dimet and Talagrand 1986). In a more general system, the control variables can include other parameters such as those found in the formulation of the forward model.

In the standard 4DVAR procedure, the forward prediction model is used as a strong constraint, i.e., it is strictly satisfied during the assimilation period. For this reason,

the accuracy of the forward model does affect the accuracy of the retrieval. An additional requirement for a successful retrieval is the existence of a strong connection between the variables that are measured and those to be retrieved. This is referred to as the sensitivity of the cost-function to the control variables, and the sensitivity is measured by the gradient of the cost function with respect to the particular control variable.

There are two prerequisites for a successful variational retrieval: *a)* Accurate (in terms of physical mechanisms, numerical schemes and coding) forward model and high quality data; and *b)* Cost function (a quadratic metric of data-model forecast mismatch) must be sensitive to the control variables (model input or parameters that can be adjusted to better fit model into data). If the uncertainty in the retrieved variable contributes little to the model-data misfit as measured by the cost function, this variable simply cannot be effectively retrieved. Thus, endeavors must first be made to verify and fix any problems related to soil temperature/moisture estimation. During the forward model calibration and backward model inversion, the high quality and high-frequency OASIS measurements will be used as the ground truth and as input for retrieval experiments. The second requirement as applied to the retrieval of soil moisture and temperature from atmospheric forecasting errors is that the impact of soil moisture/temperature on near-surface observations dominates the impacts of other error sources (Bouttier *et al.* 1993a&b).

We organize this chapter as follows. Subsection 2.1 is dedicated to the OASIS dataset description; Subsection 2.2 and 2.3 are devoted to the discussion of the coupled land surface-atmosphere system (forward system) and its verification. A general framework for variational data assimilation is provided in Subsection 2.4. The cost-

functions as used in this study are given and their structures are analyzed in this subsection.

### 2.1. OASIS Data

Directly measured surface fluxes and soil state variables provide the best baseline values for model evaluations. In contrast to the soil moisture and flux measurements during short, intensive observing periods for several well-known field experiments (e.g., FIFE, Sellers *et al.* 1992; HAPEX-MOBILHY, Andre *et al.* 1986), the OASIS provides year round continuous and direct measurements of soil moisture (using the 229-L sensors every half an hour, Basara (2001)) at four different depths (5, 25, 60 and 75 cm) and temperature at three different depths (5, 10 and 30 cm), and all four components of the surface energy fluxes (Net radiation  $R_n$ , latent heat flux  $LE$ , sensible heat flux  $H$  and ground heat flux  $G$ ). Thus OASIS provides the opportunity for rigorously validating the dynamic framework of land surface models (LSMs). The data are also well suited for testing data assimilation techniques and for objective determination of most uncertain soil and vegetation parameters.

Due to their high initial cost and high maintenance, sonic anemometers for direct flux measurements are equipped at only 10 of the 90 OASIS sites. These 10 sites are called super sites, and Norman, Oklahoma (NORM) site is one of them. Super sites are distinguished from the standard sites in that all components of the surface energy budget are directly measured, while at the standard sites, the latent heat flux is the residual term required to close the surface energy budget (Brotzge 2000). The OASIS dataset (provided by Jerry Brotzge) at Norman super site (Elevation: 360 m; Latitude: 35 15' 20"; Longitude: 97 29'; Slope: 0.0; Shrub with dynamic roughness of 0.004 m) are used in this

study. They have been used for model calibration purposes (e.g., Brotzge and Weber 2002; Ren and Xue 2004). The routinely available measurements that can be used to force the land-surface model include air temperature (K), water vapor mixing ratio ( $\text{kg kg}^{-1}$ ), wind speed and direction, surface pressure (mb), and precipitation rate ( $\text{m s}^{-1}$ ). At the OASIS sites, an infrared sensor measures surface skin temperature at 5 minutes intervals. Details of the measurements, including theory, sensor calibration and data manipulation are described in Basara (2001). The recorded vegetation parameters include vegetation type, leaf area index (LAI), vegetation coverage, and NDVI index.

Data from two periods in year 2000 are used in this study. The selected dry period (00Z, 4-28 August, 2000) signifies a synoptically quiescent period with clear sky and wind speed generally less than  $5 \text{ m s}^{-1}$ . Forced by periodical (daily) radiative heat flux, air pressure, air temperature (maximum temperature of  $42^\circ \text{C}$ ), mixing ratio and soil temperatures within 25 cm all show apparent daily cycles. This period shows a drying down process of the surface soil moisture. The volumetric soil water content at 5 cm ( $\sim 0.253 \text{ m}^3 \text{ m}^{-3}$ ) did not drop sharply during the first 48 hours starting from 00Z, August 4, indicating that the drying process enters stage II (Idso *et al.* 1974). The soil moisture measurements at the remaining three depths show little changes on daily basis ( $\sim 0.278 \text{ m}^3 \text{ m}^{-3}$ ).

During this period, vegetation is at a slightly stressed stage of growth, although with a rather high vegetation coverage (0.75, estimation based on the study of Brotzge and Weber (2002)) and  $\text{LAI}=0.72$ . The vegetation is slightly stressed because  $\text{NDVI} = 0.5$ . The soil moisture contents at the top measurement depth (5 cm) fall near the wilting point value (22% for silty clay soil) at the driest hours of a day. This is also shown by the

Halstead coefficient, which is around 0.06 for this period. Considering that the dew formation is insignificant, hence the stomatal resistance is nearly 20 times that of aerodynamic resistance.

We will also test our retrieval using a moist period (6-8 July 2000). Compared with the dry period, this is also a synoptically quiescent period but with much moist soil resulting from antecedent precipitation. The 00Z July 6 surface soil moisture is 0.379, above the field capacity (0.36 for silty clay soil). Vegetation is also more active for this period. We than use  $veg=0.8$ ,  $LAI=0.6$  and  $NDVI=0.55$  for these period.

## 2.2. Forward Model

The forward model used for this study is based on the Advanced Regional Prediction System (ARPS, Xue *et al.* 1995; 2000; 2001). All of our experiments, including forward prediction and 4DVAR retrieval, will be conducted in 1-D column mode. This is necessary because, otherwise, a full 3-D adjoint code will be required for the atmospheric component of model, and we will be running a full blown 4DVAR data assimilation system. This is a major undertaking that is beyond the scope of this study primarily because the associated computational cost would preclude routine implementation.

Almost all land surface models used in atmospheric prediction systems are column based, namely, they do not include horizontal transport of heat or moisture. This is also true of the land-surface model in the ARPS that we use. For our study, the vertical boundary layer mixing process is of the foremost importance in the atmospheric model, particularly, for the periods when weather is inactive so that horizontal advection is less

important. In fact, for our real data experiments, we intentionally choose the periods when the atmosphere is quiescent, so that our 1-D assumption is valid.

The core of the forward model involves solving the coupled energy and water budget equations of the land surface and of the overlying atmospheric boundary layer. Because of the 1-D assumption, the hosting system (ARPS) is trimmed to keep a minimum number of relevant components. In all prognostic equations of the atmospheric model, the advection terms are neglected, so are horizontal mixing terms. For momentum equations, the Coriolis terms are retained, and the horizontal pressure gradient terms are expressed in terms of geostrophic winds. For potential temperature equation and the water vapor equation, only vertical mixing term is kept. Within the atmospheric boundary layer, the turbulent eddy coefficients for momentum, heat, and moisture are diagnostically prescribed using the PBL model of Hong and Pan (1996).

The land surface component of the model consists of prognostic equations for two soil temperature variables (surface/skin temperature and deep layer temperature), a canopy intercepted water reservoir, and two soil moisture variables (superficial soil moisture and deep soil moisture). The land surface model includes the effects of vegetation on surface energy and water budgets, through their effects on radiative and turbulent fluxes. We also implemented some modifications to the original scheme of Noilhan and Planton (1989).

In the following is a description of the relevant components of the land surface and atmospheric models. The general philosophy for land surface modeling and PBL parameterization is available in Appendix 1. The first three subsections in the following

focus on specific parameterization schemes used in this study, and subsection 2.3 presents a series of numerical experiments that verify our forward modeling system.

### *2.2.1. Land Surface Components*

The land surface component of our forward model is based on ISBA of NP89, but also includes significant enhancements based on later work (e.g., Pleim and Xiu 1995; Xiu and Pleim 2001; Ren and Xue 2004). The prediction of both soil moisture and temperature is based on the force-restore approach pioneered by Deardorff (1977, 1978, D77 and D78 henceforth).

With the force-restore approach, two variables are used to describe both temperature and moisture, with one representing that of the skin or near surface layer and the other that of a deeper layer. The surface layer variable is forced by fluxes at the surface and restored at a certain rate to a much more slowly varying state of the deep layer. Such an approach avoids solving equations for multiple soil layers and is generally very efficient. Deardorff (1978) showed that the two-layered force-restore scheme is better than bulk scheme in describing the surface soil moisture content because it contains the mechanism by which a deeper soil layer can influence the thin and fast responding surface layer. This thin and sensitive surface layer gives the flexibility and advantages in surface moisture prediction especially when there is precipitation and/or very active evaporation from the ground surface.

The original paper of Bhumralkar (1975) laid the foundation for the force-restore method when applied to the soil temperature prediction. Deardorff (1977) extended the method to the prediction of soil moisture. Blackadar (1976) also contributed significantly to this method, Dickinson (1988) and Noilhan and Planton (1989) further extended the

system for general applications. Despite its relatively simplistic approach, the force-restore method remains widely used in many disciplines in geosciences (e.g., Boni *et al.* 2001; Adrie *et al.* 2000), and often gives adequate solutions. Compared with multi-layer model, one shortcoming of force-restore method is that it assumes that the surface forcing be sinusoidal. However, the non-sinusoidal behavior mainly affects deep temperature prediction and the effect of the assumption on surface temperature prediction is smaller than what one would intuitively expect (see, e.g. comparison with observations in Ren and Xue 2004). In the following we present the actual prediction equations in the land-surface model that we will use.

*a. The soil temperature prediction equations.*

The soil temperature equations used in this study read:

$$\begin{cases} \frac{\partial T_{sfc}}{\partial t} = C_T (R_{net} - LE - H) - \frac{2\pi}{\tau} (T_{sfc} - T_{dp} - \pi\gamma d), \\ \frac{\partial T_{dp}}{\partial t} = -\frac{(T_{dp} - T_{sfc} + \pi\gamma d)}{\tau}. \end{cases} \quad (2.1)$$

where  $T_{sfc}$  is surface temperature,  $T_{dp}$  is mean surface temperature,  $C_T$  is thermal conductivity, and  $\tau$  is the period of oscillation (equals to 24 hours for daily cycle). In the ISBA, a single mixed heat budget is considered for the bare ground and the vegetation.  $C_T$  represents the average conductivity of bare ground and vegetation, and

$$C_T^{-1} = [(1 - veg)C_G^{-1} + vegC_V^{-1}]. \quad (2.2)$$

Here  $veg$  is the fractional vegetation coverage,  $C_V$  is the inverse vegetation heat capacity, and the inverse of volumetric ground heat capacity  $C_G$  is parameterized using its value at saturation  $C_{Gsat}$  as  $C_G = C_{Gsat} (w_{sat} / w_{dp})^{\frac{b}{\ln 100}}$ , with  $b$  being the Clapp-Hornberger (1978)



parameter. Net radiation flux  $R_n$  is parameterized as  $R_n = R_{sw}(1 - \alpha) + \varepsilon_g(LWD - \sigma T_{sfc}^4)$ . Here  $R_{sw}$  is the solar radiation flux and  $LWD$  is the atmospheric downward longwave radiation reaching the ground. Here  $\alpha$  is the zenith angle and surface soil moisture dependent albedo and  $\varepsilon_g$  the emissivity. The  $\sigma T_{sfc}^4$  term is the emitted longwave radiation from the Earth's surface and  $\sigma$  is the Stefan-Boltzman constant. A sophisticated radiation package developed at the NASA/Goddard Space Flight Center (Chou and Suarez 1994) is used to estimate  $LWD$  as well as the profile of atmospheric short- and long-wave heating/cooling.

Sensible heat flux at the surface is expressed as  $H = \bar{\rho}_{air} C_H C_p |\bar{V}_1| (T_{sfc} - T_{air})$ . Here  $\bar{\rho}_{air}$  is the air density at the surface level;  $C_H$  is the thermal stability-dependent heat exchange coefficient whose definition and estimation will be further discussed at the surface- and boundary-layer section (Subsection 2.2.2);  $C_p$  is the specific heat at constant pressure for dry air; and  $|\bar{V}_1|$  and  $T_{air}$  are wind speed and air temperature taken at the first model level above ground, respectively.

Latent heat flux  $LE$  in Eq. (2.1) has three components: that from the bare ground moisture evaporation ( $E_g$ ), that from the wet part of vegetation evaporation ( $E_v$ ) and that from dry part of canopy transpiration ( $E_{tr}$ ).  $LE = L_v (E_g + E_v + E_{tr})$ , and  $L_v$  is the latent heat for evaporation ( $2.50078 \times 10^6$  Joule/kg). The three soil moisture reservoir are parameterized respectively as  $E_g = (1 - veg) \bar{\rho}_{air} C_H |\bar{V}_1| (h_u q_{sat}(T_{sfc}) - q_{air})$ , and  $h_u$  is a ground surface water deficit factor as defined in Eq. (15) of Mahfouf (1991),  $q_{air}$  is the water vapor mixing ratio taken at the first model level above ground, and  $q_{sat}(T_{sfc})$  is the

saturation mixing ratio at temperature  $T_{sfc}$ ;  $E_v = veg \frac{\delta}{R_a} [q_{sat}(T_{sfc}) - q_{air}]$ , and the wet

fraction of canopy  $\delta = \left(\frac{W_r}{W_{rmax}}\right)^{2/3}$  (D78) and aerodynamic resistance  $R_a = \frac{1}{C_H |\bar{V}_1|}$ ;

and  $E_{tr} = veg \frac{1-\delta}{R_a + R_s} [q_{sat}(T_{sfc}) - q_{air}]$ , where stomatal resistance

$$R_s = \frac{R_{smin}}{LAI} F_1 F_2^{-1} F_3^{-1} F_4^{-1}. \quad (2.3)$$

Here  $F_1 = \frac{1+f}{f + R_{smin}/5000}$ , with  $f = \frac{0.55 R_{sw} \times 2}{R_{GL} LAI}$ .  $R_{GL}$  is a vegetation species-dependent

limit value for global (all-spectrum) radiation ( $30 \text{ W m}^{-2}$  for forest and  $100 \text{ W m}^{-2}$  for crop, according NP89),  $R_{smin}$  is minimum stomatal resistance under free transpiration environmental conditions, and  $LAI$  is leaf area index. Hence  $F_1$  parameterizes the photosynthetically active radiation (assumed to be 0.55 times the solar radiation). The form of  $F_1$  was originally given by Dickinson (1984). In Eq. (2.3),

$$F_2 = \begin{cases} 1, & w_{dp} > w_{fc} \\ \frac{w_{dp} - w_{wilt}}{w_{fc} - w_{wilt}}, & w_{wilt} < w_{dp} < w_{fc} \\ 0, & w_{dp} < w_{wilt} \end{cases}. \quad (2.4)$$

Here root zone or deep layer soil moisture content  $w_{dp}$  is a prognostic variable as will be discussed soon,  $w_{fc}$  is field capacity soil moisture content, which can be used as the threshold for bare soil evaporation (as in the parameterization of  $h_u$  factor, see, e.g., Wetzel and Chang 1987), and  $w_{wilt}$  is the wilting point value of soil moisture content.  $F_2$  describes availability of water in root zone for transpiration.  $F_3 = 1 - \Gamma [e^*(T_{air}) - e_{air}]$ , here  $\Gamma$  is an empirical parameter,  $e^*(T_{air})$  is the saturation vapor pressure at temperature

$T_{air}$  and  $e_{air}$  is the vapor pressure evaluated at the first atmospheric model level above ground. Thus,  $F_3$  represents the effect of the vapor pressure deficit in air.  $F_4$  allows for a temperature dependence of the stomatal resistance and  $F_4 = 1 - 0.0016(298 - T_{air})^2$ .

Compared with NP89, the seasonal soil temperature lapse rate term  $\gamma d$  is added to Eq. (2.1) for the follows. In Ren and Xue (2004), the temperature prediction by NP89 is compared with the OASIS soil temperature measurements. A significant drift is found in the deep layer temperature prediction in the first one to two days in the summer and winter time periods when it is initialized using deep soil temperature measurements. The drift in the summer is of different sign as in winter. In Ren and Xue (2004), the ignorance of the difference in seasonal-mean temperature between the skin layer and deep layer was identified as the cause and the prediction equations of the force-restore model were re-derived taking into account of the temperature change of seasonal-mean temperature with depth. Most of the drift in the forecast temperature is thereby removed and a much better agreement is found between the prediction of the improved model and the observations calibrated to the right depths.

Here we define the seasonal mean soil temperature as the running mean of temperature over 1-2 weeks, a period long enough to remove diurnal temperature changes while retain longer term variations. In general, this temperature increases downward in winter and decreases with depth in summer. Seasonal mean temperature profile can be looked upon as the background upon which the diurnal oscillation is superimposed.

Suppose the seasonal mean temperature profile into the soil is given by  $\widetilde{T}_z = \widetilde{T}_{sfc} + \gamma z$ , where  $\widetilde{T}_{sfc}$  is the mean temperature at the surface, and  $\gamma$  is the “lapse rate” of the mean temperature (positive as temperature decreases with depth). Thus, under

sinusoidal surface forcing with single dominant period, the soil temperature as a solution to Eq. (A1.1) in Appendix A with constant thermal diffusivity can be found to be

$$T(z,t) = \widetilde{T}_{sfc} + \gamma z + A e^{\frac{z}{d}} \sin(\omega t + \phi_0 + \frac{z}{d}), \quad (2.5)$$

where  $A$  is the amplitude of the daily cycle in surface temperature,  $\omega$  is the frequency of oscillation ( $\omega = 2\pi/\tau$ , with  $\tau$  the period of oscillation and equals to 24 hours for daily cycle),  $\phi_0$  is the initial phase delay between surface forcing and soil temperature.

$d = \sqrt{K_T \tau / \pi} = \sqrt{2 \lambda_T / C \omega}$  is the damping depth at which the amplitude of surface temperature oscillations is reduced by a factor of  $e$ .

According to Ren and Xue (2004), we define  $T_{dp} = T(-\pi d, t) + AB' \sin(\omega t + \phi_0 + \alpha')$ , the final equations for soil temperature are:

$$\begin{cases} \frac{\partial T_{sfc}}{\partial t} = C_T (R_{net} - LE - H) - \frac{2\pi}{\tau} (T_{sfc} - T_{dp} - \pi d \gamma) - \frac{2\pi}{\tau} AB'' \sin(\omega t + \phi_0 + \alpha''), \\ \frac{\partial T_{dp}}{\partial t} = -\frac{1}{\tau} [T_{dp} - T_{sfc} + \gamma \pi d]. \end{cases} \quad (2.6)$$

where  $\alpha'' = \tan^{-1} \frac{AB' \sin \alpha'}{AB' \cos \alpha' - Ae^{-\pi}}$ ;  $B'' = \sqrt{(e^{-\pi} - B' \cos \alpha')^2 + (B' \sin \alpha')^2}$ , and

$$B' = \frac{2\pi}{\sqrt{4\pi^2 + 1}} B \approx 0.99B, \quad \alpha' = \alpha + \tan^{-1}\left(\frac{1}{2\pi}\right) \approx -0.37\pi, \text{ and}$$

$$\alpha = \tan^{-1}\left[\frac{-(1+e^{-\pi})}{2\pi e^{-\pi}}\right] \approx -0.42\pi, \text{ and } B = \left[\left(\frac{1+e^{-\pi}}{2\pi}\right)^2 + e^{-2\pi}\right]^{0.5} \approx 0.17.$$

Equation (2.6) is formally similar to NP89, whereas the latter lacks the seasonal temperature trend term ( $\gamma d$ ) shown in both surface and deep temperature equations. There exists also a sinusoidal term in the modified surface soil temperature equation. For

warm season, the relative importance of the forcing terms on the right hand side of the surface temperature equation (first equation in Eq. (2.6)) is in a decreasing order.

The main results from this paper are:

- Among the modifications to NP89 as given in Eq. (2.6), the removal of the seasonal temperature trend is found to be the single most effective revision to the original land surface scheme. The sinusoidal terms are unimportant and hence can be neglected for real applications.
- The importance of the modifications to deep soil temperature prediction is significant whereas that to surface temperature is less although still discernable. This is because for the surface temperature, forcing from the surface energy balance usually dominates (especially during daytime heating period). When this term is smaller, the improvement due to modification to the restore term becomes more evident, and it usually occurs in winter and when the soil is wetter.
- The modifications are not case sensitive and valid for all seasons.
- Considering that the land surface process is more important for the warm season forecasting (Mintz 1984), the modifications are even more relevant because the improvements are most apparent during the summer times.

We believe the revision is valuable also because the improved description to deep layer temperature can give better parameterizations to vegetation transpiration. Consensus of the modeling community is that “the root zone temperature must be included in any skillful model parameterization (Roger Pielke Sr., personal communication)”. This will be especially relevant when the land surface scheme is

coupled with the atmospheric components because there will be more feedback from the calculations of heat and moisture fluxes.

Prior to our modification, there are efforts to remove spurious drift of  $T_{dp}$  toward too low temperatures for polar region during winter period by including an additional relaxation term (e.g., Mahfouf *et al.* 1995), or simply enlarging the time constant  $\tau$  (Brotzge and Weber 2002). These empirical methods are done without starting from the first principle and usually require that the climatological values of deep layer temperature as well as the relaxation rate to be known before hand.

*b. Soil moisture prediction equations.*

The force restore soil moisture equations are essentially unchanged from ISBA as described in NP89. They are,

$$\left\{ \begin{array}{l} \frac{\partial w_{sfc}}{\partial t} = \frac{C_1}{\rho_w d_1} (P_g - E_g) - \frac{C_2}{\tau} (w_{sfc} - w_{geq}), \\ \frac{\partial w_{dp}}{\partial t} = \frac{1}{\rho_w d_2} (P_g - E_g - E_{tr}), \\ \frac{\partial w_r}{\partial t} = vegP - (E_v - E_{tr}) - R_v. \end{array} \right. \quad (2.7a)$$

$$\left. \begin{array}{l} \frac{\partial w_{dp}}{\partial t} = \frac{1}{\rho_w d_2} (P_g - E_g - E_{tr}), \\ \frac{\partial w_r}{\partial t} = vegP - (E_v - E_{tr}) - R_v. \end{array} \right\} \quad (2.7b)$$

$$\left. \begin{array}{l} \frac{\partial w_r}{\partial t} = vegP - (E_v - E_{tr}) - R_v. \end{array} \right\} \quad (2.7c)$$

Here the three prognostic variables include the soil surface wetness ( $w_{sfc}$ ), the bulk/deep-layer soil moisture ( $w_{dp}$ ), and the canopy interception ( $w_r$ ). These time-dependent parameters are forced by precipitation reaching the ground ( $P_g$ ), bare soil evaporation ( $E_g$ ); dew evaporation ( $E_v$ ); evapotranspiration ( $E_{tr}$ ); and vegetation dripping ( $R_v$ ).  $P_g$  equals the total precipitation (per unit surface area,  $P$ ) reaches the ground ( $P(1-veg)$ ) plus those possibly dripped from the canopy ( $R_v$ ). The surface moisture is restored to equilibrium by moisture sources from the thick soil layer by the second term on the right hand side of Eq. (2.7a). The time scales at which these variables act are prescribed *a*

*priori* in the form of a time constant  $\tau$  (set to one day) and the two soil-layer depths for soil moisture ( $d_1$  and  $d_2$ ). The simulations of thermal and hydrological regimes are connected by latent heat flux, the energy form of evaporation and evapotranspiration.

Thus, the interaction between the soil and atmosphere varies as a function of the vegetation shielding factor (*veg*), vegetation type, soil type, and hydraulic conductivity. These properties are specified by diagnostic variables  $C_1$  (hydraulic property of the soil affecting the infiltration at the surface),  $C_2$  (the subsurface conductivity) and  $C_T$  (defined earlier). These parameters are formulated in terms of basic soil parameters such as soil moisture at field capacity ( $w_{fc}$ , filled reservoir capacity), wilting point ( $w_{wilt}$ , below which the plant transpiration stops), saturation soil water content ( $w_{sat}$ , the maximum possible water content),  $w_{geq}$  (the surface volumetric moisture at the balance of gravity and capillary forces), and various other thermal and hydraulic properties of the soil as described in Appendix A.3 of Noilhan and Mahfouf (1996). Since all soil properties are specified according to the 11 soil types of the U. S. Department of Agriculture (USDA) soil textural classification (Clapp and Hornberger 1978), the only soil data required for this scheme are the soil types by textural classifications.

### *c. Discussion on the land surface model*

After examining the parameterization as described by Mahfouf *et al.* (1995), we can summarize the relationship among the five prognostic variables in the following (see 2.1). The bulk/deep soil temperature acts only as a restore constraint of the surface soil temperature and is not directly related to any of the soil moisture reservoirs. Situations for the surface soil temperature are quite different because it is essentially related to all three soil water reservoirs ( $w_r$ ,  $w_{sfc}$  and  $w_{dp}$ ) through the latent heat flux as a bond. The

effect of  $w_{dp}$  on  $w_{sfc}$  is analogous to, but not as direct as that of  $T_{dp}$  on  $T_{sfc}$ , since it is through the parameterizations of restore coefficient  $C_2$  and the balanced (gravity and capillary forces) volumetric moisture  $w_{geq}$ .

The conditionally existence of canopy intercepted water  $w_r$  (rainfall or dew) can affect the two soil water sources because: (a) dripping  $R_v$  can be one component of  $P_g$ , when the accumulated amount surpasses the maximum amount as parameterized by Dickinson (1984), and (b) vegetation transpiration is affected when there are canopy intercepted water as parameterized by Eq. (26) of D78.

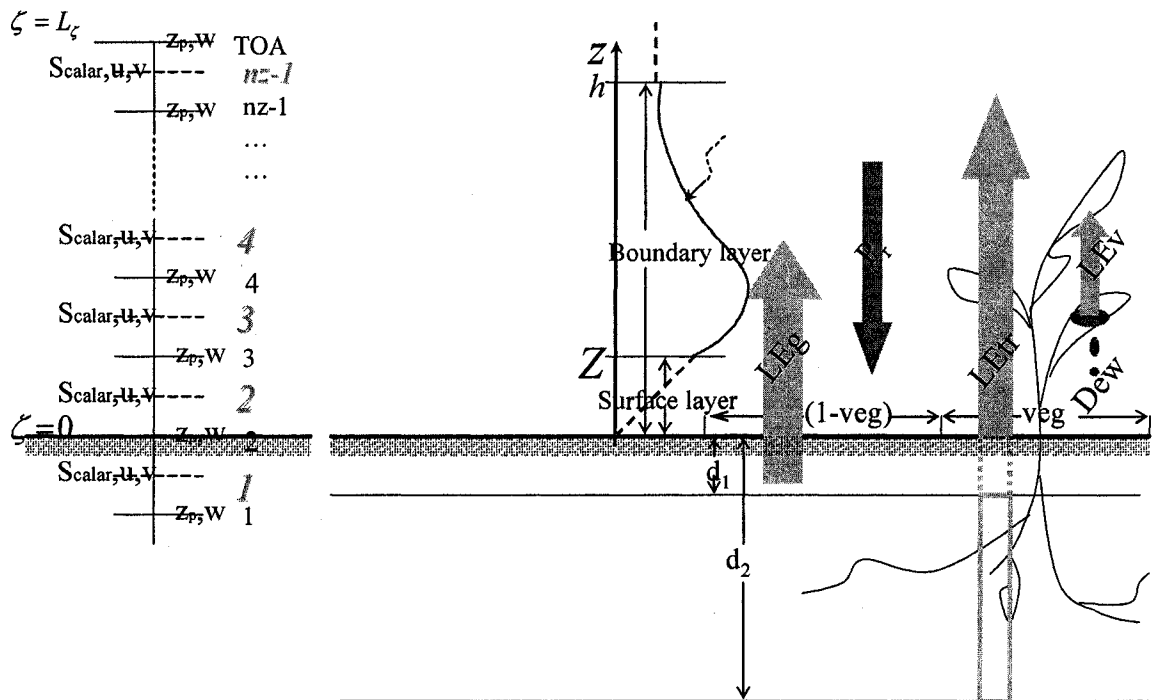


Figure 2.1. Diagram illustrating the LSM-PBL (Reduced ARPS) model structure and vertical grid stencil. *TOA* is top of atmosphere, *S* signifies scalar quantity,  $z_p$  is physical height, and all other symbols are as defined in the text. This figure is partially adapted from Bouyssel *et al.* (1998).



Here we would like to clarify some less frequently discussed points about the ISBA scheme. First, this two layered model does not mean the two layers considered are physically one overlying the other. In ISBA, the nested two layers both start from the surface and extend to two different depths:  $d_1$  and  $d_2$ , for soil hydrology. Thus, unlike the multiple-layer LSMs, the ISBA does not need a root distribution. The  $w_{dp}$  is the volumetric soil moisture associated with a bulk layer of thickness  $d_2$  which supports the vegetation transpiration, whereas evaporation extracts water from the soil surface, estimated using  $\alpha$  method (surface soil moisture availability as a function of  $w_{sfc}$ , Mahfouf and Viterbo (2001)). The second point to emphasize is that parameters  $w_{will}$ ,  $w_{fc}$ ,  $w_{sat}$  depend on soil texture only, whereas  $C_T$ ,  $C_1$ ,  $C_2$ ,  $w_{geq}$  depend on both soil texture and soil moisture. Yet another less frequently discussed aspect is the canopy vegetation reservoir for water or vegetation interception ( $w_r$ ). Dew formation and precipitation contribute to this water reservoir. If the intercepted water exceeds the maximum retainable amount ( $w_{rmax}$ ), canopy dripping ( $R_v$ ) will occur and remove water from  $w_r$  to  $P_g$ . Thus, during the precipitating period,  $P_g$  is not always merely the  $P(1-veg)$  term.

Another problem concerns the selection of  $d_1$  and  $d_2$ , which directly affect the choice of  $C_{1sat}$  and  $C_{2ref}$  (their roles in parameterize  $C_1$  and  $C_2$  follow). The  $d_1$  is the depth to which the diurnal soil moisture cycle extends, when diffusion process dominates the water distribution of soil moisture. It ( $d_1$ ) cannot be set too thick to sacrifice the prompt responses of this thin layer, which directly interacts with atmosphere, to abrupt changes in the atmospheric forcing. The property of prompt response is actually the very reason for introducing force-restore scheme for ground surface (D77).

In ISBA, vegetation transpiration does not extract water directly from the surface layer rather it directly adjusts the soil moisture content of the bulk layer of depth  $d_2$ . This requires that  $d_2$  should at least include most of the root zone of the vegetation cover. Another implied requirement for the choice of  $d_2$  is that the moisture fluxes should be negligible (for all the processes considered) below this depth. This made the choice of  $d_2$  also soil-moisture-vertical-profile-dependent. The value of  $C_1$  and  $C_2$  must be specified after the determination of  $d_1$  and  $d_2$ . They two are also soil type and soil moisture content dependent in ISBA.

In ARPS,  $C_1 = C_{1sat} \left( \frac{w_{sat}}{w_{sfc}} \right)^{b/2+1}$ , and  $C_2 = C_{2ref} \left( \frac{w_{dp}}{w_{sat} - w_{dp} + w_l} \right)$ . Here  $w_l$  is a small number ( $10^{-10}$ ) for numerically purpose only.  $C_{1sat}$  is estimated from the value of hydraulic parameters at saturation, and  $C_{2ref}$  represents the dependency of the restoration coefficient on root zone soil moisture contents. In NP89, it is evaluated from an ensemble perturbation the initial soil moisture profile of a multiple layer reference model (a value that best fits this formulation is taken as  $C_{2ref}$ ). Also, the three water reservoirs are of quite different strength. For example, the interception reservoir has a very small capacity and contains water only a few hours after a rainfall (similarly for dew formation). Its influence on surface fluxes is very short in time. For this reason, we determined not to analyze its water content in this study.

As a summary, the ARPS land-surface scheme used in this study describes the interactions between soil, vegetation and atmosphere. The land surface scheme simulates the surface fluxes ( $LE$ ,  $H$ , and  $G$ ) and predicts the evolution of the surface state variables. It includes the treatment of soil heat content, soil water content, water interception by

vegetation and aerodynamic transfer processes in the atmospheric surface layer. The scheme uses force-restore model (D77 and D78) for soil heat and water content and the  $\alpha$  method (see e.g., Mahfouf and Viterbo 2001) for evaporation. Snow processes are also included in the model but are not activated in this study. Initial values of the five prognostic variables on the left hand side of Eqs. (2.1)&(2.7) compose the control variables in our retrieval experiments.

The static land surface parameters used in this study for Norman site are listed in Table 2. 1. In the model, the three prediction equations for moisture and two equations for temperature are integrated using a 2<sup>nd</sup>-order Runge-Kutta technique.

**Table 2. 1** Static soil and vegetation parameter setting at Norman site (Lat. 35 15' 20"; Lon. 97 29' 0"; characterized by flat terrain, and dynamic roughness of 0.004 m)

$C_{1sat}$	$C_{2ref}$	$R_{smin} / R_{smax}$ (s m <sup>-1</sup> )	$w_{wilt}(m^3 m^{-3})$	$w_{fc}(m^3 m^{-3})$	$w_{sat}(m^3 m^{-3})$
0.132	1.8	200/5000	0.22	0.36	0.435
$d_1$ (m)	$d_2$ (m)	$C_{g_{sat}}(K m^2 J^{-1})$	$C_{G_{veg}}(K m^2 J^{-1})$	$R_{GL}(W m^{-2})$	$b$
0.1	1.0	$3.56 \times 10^{-6}$	$1.5 \times 10^{-3}$	100	4.90

### 2.2.2. PBL Scheme Used in this Study

The planetary boundary layer (PBL) is the layer of atmosphere that directly interacts with the land surface. For the retrieval of soil state variables using surface atmospheric observations, the soil model will be coupled with the atmosphere model and the PBL mixing is the most important process. The governing equation, as described in Appendix 1, reads:

$$\left\{ \begin{array}{l} \frac{\partial \bar{u}}{\partial t} = -\frac{\partial \overline{u'w'}}{\partial z} + f(\bar{v} - v_g), \\ \frac{\partial \bar{v}}{\partial t} = -\frac{\partial \overline{v'w'}}{\partial z} - f(\bar{u} - u_g), \\ \frac{\partial \bar{\theta}}{\partial t} = -\frac{\partial \overline{\theta'w'}}{\partial z} - \overline{R_{radiative}}, \\ \frac{\partial \bar{q}}{\partial t} = -\frac{\partial \overline{q'w'}}{\partial z} + \overline{C_{condensation}}. \end{array} \right. \quad (2.8a)$$

$$\left\{ \begin{array}{l} \frac{\partial \bar{u}}{\partial t} = -\frac{\partial \overline{u'w'}}{\partial z} + f(\bar{v} - v_g), \\ \frac{\partial \bar{v}}{\partial t} = -\frac{\partial \overline{v'w'}}{\partial z} - f(\bar{u} - u_g), \end{array} \right. \quad (2.8b)$$

$$\left\{ \begin{array}{l} \frac{\partial \bar{\theta}}{\partial t} = -\frac{\partial \overline{\theta'w'}}{\partial z} - \overline{R_{radiative}}, \\ \frac{\partial \bar{q}}{\partial t} = -\frac{\partial \overline{q'w'}}{\partial z} + \overline{C_{condensation}}. \end{array} \right. \quad (2.8c)$$

$$\left\{ \begin{array}{l} \frac{\partial \bar{\theta}}{\partial t} = -\frac{\partial \overline{\theta'w'}}{\partial z} - \overline{R_{radiative}}, \\ \frac{\partial \bar{q}}{\partial t} = -\frac{\partial \overline{q'w'}}{\partial z} + \overline{C_{condensation}}. \end{array} \right. \quad (2.8d)$$

where  $t$  is time,  $z$  is altitude,  $u$  is the zonal velocity component (eastward positive),  $v$  is the meridional velocity component (northward positive),  $w$  is vertical velocity, and  $\theta$  is virtual potential temperature, which is defined as  $\theta = \theta_d(1 + 0.61q)$ , here  $\theta_d$  is the potential temperature for dry air, and  $q$  is the mixing ratio of water vapor. Here  $u_g$  is the eastward component of the geostrophic wind,  $v_g$  is the northward component of the geostrophic wind,  $f$  is the Coriolis parameter,  $\overline{R_{radiative}}$  is the radiative cooling/heating rate, and  $\overline{C_{condensation}}$  is the sink term due to condensation (vanishes for clear boundary layer). Here the overbar '—' denotes the grid resolvable, or mean quantity while the superscription prime "'" indicates sub-grid quantity or perturbation. The vertical turbulent flux of a quantity ( $q, \theta$ , or momentum) is expressed as the covariance between its perturbation and the vertical velocity perturbation. Specifically,  $\overline{u'w'}$  and  $\overline{v'w'}$  are components of the Reynolds stress tensor in the east and north directions, respectively; and  $\overline{\theta'w'}$  and  $\overline{q'w'}$  are the components of the turbulent heat and moisture fluxes, respectively.

The Reynolds stress term, for example,  $\overline{u'w'}$  in Eq. (2.8a) is usually parameterized as proportional to the vertical gradient of the mean flow  $\frac{\partial \bar{u}}{\partial z}$  in order to close the system.

The key to a turbulent closure is the determination of the mixing coefficient  $K$ , which is usually parameterized using PBL parameterization scheme inside the convective boundary layer, and is estimated using sub-grid scale turbulent scheme above the convective boundary layer. In this study, for simplicity,  $K$  is a diagnostically obtained profile following the work of Hong and Pan (1996). In comparison with the general forms as shown in equations (A1.11)-(A1.13), boundary layer depth ( $h$ ) takes the place of the Monin-Obukhov length  $L$ . The following is a description of the Hong and Pan (1996) non-local PBL parameterization scheme we implemented into ARPS. The choice of the MRF scheme over the original ARPS TKE-based scheme is also because the adjoint coding is easier without the prognostic equation for TKE.

For any quantity  $c$  (can be  $u$ ,  $v$ ,  $\theta$ , or  $q$ ), the non-local approach for vertical mixing, based on Troen and Mahrt (1986) can be expressed as

$$\frac{\partial \bar{c}}{\partial t} = \frac{\partial}{\partial z} \left[ K_c \left( \frac{\partial \bar{c}}{\partial z} - \gamma_c \right) \right] \quad (2.9)$$

This equation is a form of closure of the diffusion (first term) term in Eqs. (2.8a-d). Since local mixing uses  $K_c \frac{\partial \bar{c}}{\partial z}$  to estimate vertical turbulent fluxes, under conditions that the mean quantity are same for the two selected level, zero flux will result. Chances are actual bulk fluxes are not zero (may flip signs between the two levels). Eq. (2.9) is proposed also to deal with this shortcoming with local schemes. This also suggested that parameter  $\gamma_c$  should be a bulk property of the total convective boundary layer not that of a quantity represents a sub-domain of it. As in Troen and Mahrt (1986), Holtslag and Boville (1993), Holtslag and Moeng (1991), and Hong and Pan (1996), the diffusivity coefficient for momentum is formulated as

$$K_m = \kappa w_{s,m} z \left(1 - \frac{z}{h}\right)^2, \quad (2.10)$$

where  $\kappa$  is Karman constant,  $w_{s,m}$  is a characteristic turbulent velocity scale for scalar transport, and  $h$  is the depth of the PBL. The mixed-layer velocity scale is represented as

$$w_{s,m} = \frac{u_*}{\phi_m} \quad (2.11)$$

Following Dyer's (1974) formulation (Eqs. A1.9&10), here  $\phi_m$  is evaluated at the top of the surface layer  $z=Z$ , with the stability criteria expressed as the covariance of virtual potential temperature perturbation and vertical velocity evaluated at the surface. For example,  $\left(\overline{w'\theta'_v}\right)_{sfc} \leq 0$  signifies unstable condition. The PBL depth  $h$  in Eq. (2.10) is iteratively obtained through

$$h = R_{B,cr} \frac{\overline{\theta_{v,1}} |\overline{u}(h)|^2}{g (\overline{\theta_v}(h) - \theta_{vs})}, \quad (2.12)$$

where  $R_{B,cr}$  is critical Richardson number (set to 0.3 in this study),  $\overline{\theta_{v,1}}$  is the virtual potential temperature at the lowest model level, and should be taken consistent with the  $\Delta z$  in the following definition of bulk Richardson number:

$R_B = g \Delta \overline{\theta_v} \Delta z \left\{ \overline{\theta_v} \left[ (\Delta \overline{u})^2 + (\Delta \overline{v})^2 \right] \right\}^{-1}$ . Here  $\overline{\theta_{vs}}$  is the appropriate temperature near the surface (about 10m, or near the top of the surface layer as in Holtslag and Boville 1993), defined as:

$$\overline{\theta_{vs}} = \overline{\theta_{v,1}} + B \frac{\overline{(w'\theta'_v)_{sfc}}}{w_{s,m}} \quad (2.13)$$

The right hand side of Eq. (2.13) is the scaled virtual temperature excess near the surface, usually bounded (3 K in Hong and Pan 1996) in case surface wind is very weak. Here  $B$  is a coefficient of proportionality (taken as 7.8 in Hong and Pan 1996), which is used in describing the non-local enhancement effects from large-scale eddies to total flux.

$$\gamma_c = B \frac{\overline{w' \theta'_v}}{w_{s,m} h} \quad (2.14)$$

Finally, we take the Obukhov length  $L$  as the second expression in Eq. (A1.16), with the virtual potential temperature evaluated at the surface level.

Similarly, the dimensionless vertical temperature gradient given by Dyer (1974) is

$$\phi_h = \begin{cases} \left(1 - 15 \frac{Z}{L}\right)^{-0.5}, & \left(\overline{w' \theta'_v}\right)_{sfc} \leq 0 \\ \left(1 + 5 \frac{Z}{L}\right), & \left(\overline{w' \theta'_v}\right)_{sfc} > 0 \end{cases} \quad (2.15)$$

The eddy diffusivity for temperature ( $K_h$ ) and moisture ( $K_q$ ) is estimated from the relationship of the turbulent Prandtl number:

$$P_r = \frac{\phi_h}{\phi_m} + \kappa B \frac{Z}{h} = \frac{K_m}{K_h} \quad (2.16)$$

Following Hong and Pan (1996), for the free atmosphere, a local- $K$  approach (Louis 1979) is utilized:  $K = l^2 f_{stb} \left| \frac{\partial \bar{u}}{\partial z} \right|$ , where the mixing length  $l = \frac{\kappa z \lambda_0}{(\kappa z + \lambda_0)}$ , here  $\lambda_0$  is the asymptotic length scale, and  $f_{stb}$  is the stability function. The stability function  $f_{stb}(Ri_g)$  is represented in terms of the local gradient Richardson number

$$Ri_g = \frac{g}{\theta_v} \frac{\partial \bar{\theta}_v}{\partial z} \left\{ \left[ \left( \frac{\partial \bar{u}}{\partial z} \right)^2 + \left( \frac{\partial \bar{v}}{\partial z} \right)^2 \right] \right\}^{-1} \text{ at a given level. Here } \theta_v \text{ is the virtual potential}$$

temperature. Computed  $Ri_g$  is usually numerically bounded to prevent unrealistically unstable regimes (-100 in Hong and Pan 1996).

Implementation of this PBL scheme in ARPS framework is not straightforward because the ARPS equations are first written in a Cartesian coordinate projected onto a plane tangent to or intercepting the earth's surface. A coordinate transformation into curvilinear coordinate system is then performed to put the governing equations into an equally spaced computational domain. The special curvilinear coordinate system that ARPS applies is

$$\zeta = x, \quad \eta = y, \quad \text{and} \quad \zeta = \zeta(x, y, z). \quad (2.17)$$

Equation (2.17) represents a transformation that maps a domain with vertically stretched grid and irregular lower boundary to a regular rectangular domain with equal grid space in each direction. We call the latter the computational domain. The dynamic equations are discretized in the computational space. However, the wind components are Cartesian wind speed. Our column run voids the horizontal coordinate transform and makes the map projection transformation irrelevant, or the map projection factor equals unity. With the definition of  $J_3 = \frac{\partial z}{\partial \zeta}$ ,  $\rho^* = J_3 \bar{\rho}$ ,  $u^* = \rho^* u$ , and  $v^* = \rho^* v$ , the governing equations for atmospheric components become (c.f. Equations (A1.7a-d) expressed in a more general form):



$$\left\{ \begin{array}{l} \frac{\partial \bar{u}^*}{\partial t} = f \bar{\rho}^* (v - v_g) + \frac{\partial}{\partial \zeta} \left( -\bar{\rho} K_{mv} \frac{1}{J_3} \frac{\partial \bar{u}}{\partial \zeta} \right), \end{array} \right. \quad (2.18a)$$

$$\left\{ \begin{array}{l} \frac{\partial \bar{v}^*}{\partial t} = -f \bar{\rho}^* (u - u_g) + \frac{\partial}{\partial \zeta} \left( -\bar{\rho} K_{mv} \frac{1}{J_3} \frac{\partial \bar{v}}{\partial \zeta} \right), \end{array} \right. \quad (2.18b)$$

$$\left\{ \begin{array}{l} \frac{\partial \bar{\rho}^* \theta}{\partial t} = \frac{\partial}{\partial \zeta} \left( -\bar{\rho} K_{Hv} \frac{1}{J_3} \frac{\partial \theta}{\partial \zeta} \right) + f r, \end{array} \right. \quad (2.18c)$$

$$\left\{ \begin{array}{l} \frac{\partial \bar{\rho}^* q}{\partial t} = \frac{\partial}{\partial \zeta} \left( -\bar{\rho} K_{Hv} \frac{1}{J_3} \frac{\partial q}{\partial \zeta} \right), \end{array} \right. \quad (2.18d)$$

$$\left\{ \begin{array}{l} \frac{\partial \bar{p}}{\partial \zeta} = \bar{\rho}^* g \left[ \frac{\theta}{\theta} - \frac{p}{\rho C_s^2} + \frac{q}{\varepsilon q} \right]. \end{array} \right. \quad (2.18e)$$

where  $C_s$  is the sound speed,  $\varepsilon = R_d / R_v \approx 0.622$  is the ratio of the gas constants for dry air and water vapor, and  $f_r$  is radiative forcing and will be further discussed in Subsection 2.2.3.

In ARPS, wind components and the state variables are defined as the sums of base-state variables (those with an over-bar in Eq. (2.18)) and the deviations from the base state (with primes removed). The base state is typically constructed using an external sounding and is assumed horizontally homogeneous, time invariant and hydrostatically balanced.

The  $J_3$  is fixed once the elevation and vertical grid setting is set. For all the following numerical experiments, 80 grid points are used in the vertical direction. The vertical grid is stretched from 4 m at the bottom to 396 m at the top, according to the hyperbolic tangent function given by Eq.7.3.6 in Xue *et al.* (1995). The vertical dimension of the simulated domain is  $\sim 32$  km, deep enough for assuming zero pressure perturbation at the top of atmosphere (TOA). This is actually the top boundary condition for numerically solving the hydrostatic perturbation pressure equation (2.18e).

For a description of the full-fledged 3D ARPS grid stencil setting, the reader is referred to Xue *et al.* (2000 and 2001). For our discussion, we care about only its vertical grid setting (see left side of Fig. 2.1). It is a reduced Arakawa C-grid (Arakawa and Lamb, 1977), where all prognostic scalar variables are defined at the center of the grid box (Figure 2.2), while the normal velocity components are defined on their respective box surfaces. Other derived variables are evaluated at locations that minimize spatial averaging in the difference operations. From 2.1, we understand the variable arrangement relative to the physical boundary. The second level of scalar variables is the first level above ground surface. The vertical gradient of a quantity as evaluated using the first and second layer is centered at the land surface, where the vertical turbulent heat flux,  $H_3$ , is defined. Thus, the surface fluxes as predicted by the land surface scheme provide the lower boundary value for the PBL mixing of the atmosphere.

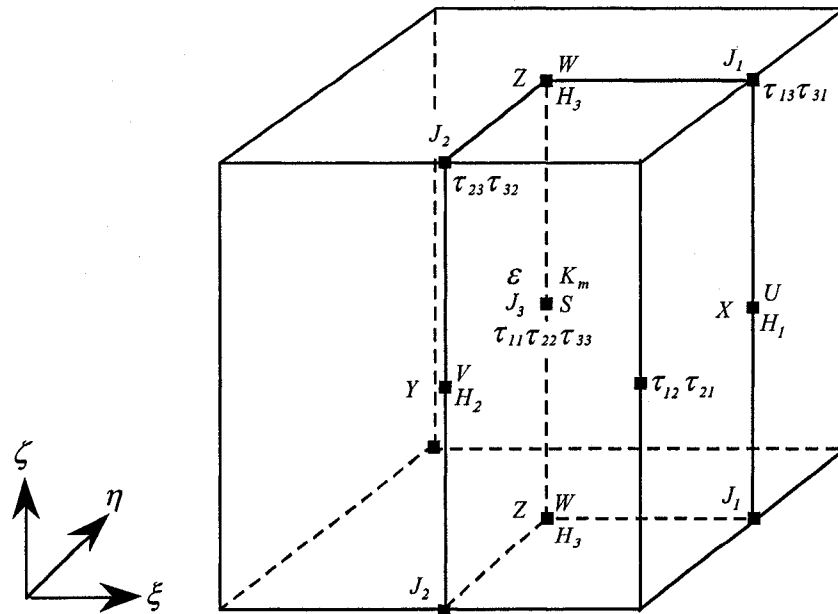


Figure 2.2. A grid box depicting the staggering of the coordinate and placement of dependent variables. Adapted from Xue *et al.* (1995).

Since our column supports no gravity wave, the pressure perturbation equation is further reduced to the hydrostatic equilibrium form. The separation of acoustically active and inactive modes as appeared in the split-explicit time integration scheme of 3D ARPS is unnecessary. The horizontal processes (i.e. Coriolis' force and the pressure gradient force) can be treated explicitly without stability constraint. The leap-frog scheme (with respect to the pressure gradient term and coriolis terms, which are evaluated at central time level) is used for the time integration. However, for the often large vertical mixing coefficients used by the PBL scheme, vertical turbulent mixing often results in a linear stability constraint on the time step size when treated explicitly, especially when the vertical resolution is high. To overcome this potentially severe restriction on the time step size, the implicit Crank-Nicolson type scheme is used for the vertical mixing so that the time integration is absolutely stable for the mixing terms (Xue *et al.* 2000).

In ARPS, the atmospheric and land surface components use different conventions. For example, the equation for potential temperature (Eq. (2.18c)) is not in the energy form (the heat capacity factor is not shown). Hence the sensible heat flux as output of the land surface model is not the same quantity as the potential temperature flux at the lower boundary. Similarly, the equation for specific humidity  $q$  (Eq. (2.18c)) is written in mass flux form (vapor mass per unit time per unit area), whereas the land surface model provides latent heat flux (energy per unit time per unit area) at the lower boundary. Due to these specific features of the atmospheric model, proper adjustments must be made before surface fluxes provided by land surface model could be used by the atmospheric component. In addition, the formulation of the land surface model uses the difference in

temperature, while the eddy turbulent mixing term is expressed in potential temperature

form, a transform factor  $\left(\frac{P_0}{P}\right)^{(1-0.23q_v)^*0.2856}$  should also be taken into account, so that

$$\bar{\rho}K_{Hv} \frac{1}{J_3} \frac{\partial \theta}{\partial \zeta} \Big|_1 = \bar{\rho} \left( \overline{w' \theta'} \right)_{sfc} = \bar{\rho} C_H |\bar{V}_1| (\theta_{sfc} - \theta_1) = \frac{H}{C_p} \left( \frac{1000}{P} \right)^{0.2856(1-0.23q)} \quad (2.19)$$

$$\bar{\rho}K_{Hv} \frac{1}{J_3} \frac{\partial q}{\partial \zeta} \Big|_1 = \bar{\rho} \left( \overline{w' q'} \right)_{sfc} = \bar{\rho} H_u C_H |\bar{V}_1| (q_{v,sfc} - q_{v,1}) = \frac{LE}{L_v} \quad (2.20)$$

Here  $C_H$  is surface layer exchange coefficient,  $\bar{V}_1$  is the horizontal velocity vector at the lowest model layer, and subscript 'sfc' and '1' represent surface and the first atmospheric model layer, respectively.

The kinematic surface fluxes are given by

$$\bar{\rho} \left( \overline{w' u'} \right)_{sfc} = -\bar{\rho} C_M |\bar{V}_1| \bar{u}_1 \text{ and } \bar{\rho} \left( \overline{w' v'} \right)_{sfc} = -\bar{\rho} C_M |\bar{V}_1| \bar{v}_1, \quad (2.21)$$

where  $u_1$  and  $v_1$  are zonal and meridional components of the vector wind  $\bar{V}_1$ . Note also that all fluxes are defined as positive when pointed upward in the atmospheric model, whereas it is defined positive when contributing to ground substrate.

In ARPS, the parameterization scheme in estimating  $C_H$  and  $C_M$  as proposed by Byun (1990), together with the original TKE scheme for estimating  $K$  in PBL layer and the force restore type of soil scheme was tested as in the framework of ARPS against several field experiment data sets. We follow the same practice by using Byun scheme to estimate  $C_H$  and  $C_M$  rather than using those in the original MRF code because we believe the consistency of the original soil scheme with the surface layer parameterization is more important than the consistency with the  $K$  profile in PBL layer.

ARPS diagnoses the PBL depth  $h$  (Eq. 2.12) based on the virtual potential temperature profile. The PBL top is assumed to be at the level where the environmental virtual potential temperature exceeds that of the first level above ground. If the atmosphere is stable right above ground, the PBL depth is set to the thickness of the layer below the first scalar point above ground. In this study, the iteratively obtained  $h$  in MRF is used instead, which includes further adjustment to the height of the inversion by thermal and non-local processes. The parameterizations of the drag coefficients for the surface layer and the land surface model are from ARPS and modified significantly. For the 1-D column setting of the atmospheric model, the advection effect, if significant, can be estimated from a corresponding 3D reference run. This is not a major concern for high pressure controlled synoptically quiet conditions. With a companion 3D run, the geostrophic wind components can be evaluated from the 3D pressure field. For our 1D model run, for simplicity, the geostrophic winds for atmosphere levels above the PBL are interpolated from the two subsequent soundings about 12 hours apart and the winds are linearly interpolated to the corresponding vertical model levels. For the layers within the PBL, a constant geostrophic wind profile is assumed which assumes the wind speed values at the top of the boundary layer. The radiation heating/cooling processes and the microphysics are kept as they are in ARPS (they represent the radiation and condensation terms in Eqs. 2.8c&d). The upper boundary Rayleigh dumping is not used because 1D column run does not support gravity wave mode in the system.

### *2.2.3. Radiative Heating/Cooling*

The electromagnetic radiation emitted from the earth-atmospheric system concentrates on infrared (*IR*) region (long wave radiation), while that from the sun's

photosphere, having an equivalent blackbody temperature of about 600 K peaks at about  $0.47 \mu\text{m}$ , according to Wien's displacement law. The solar and thermal *IR* spectra may be separated into two independent regions at about  $4 \mu\text{m}$ . The overlap of these two spectra is relatively insignificant. This distinction makes it reasonable to treat the transfer of solar radiation independent of the transfer of *IR* radiation in terms of source function, except for a water vapor window near the  $3.7 \mu\text{m}$ . Contributions from both should be accounted for during daytime in case this wave length is used for remote sensing purposes.

In the discussion of the *IR* transfer in terrestrial atmosphere, it is commonly assumed that, in localized portions, the atmosphere is in thermodynamic equilibrium and being plane-parallel. The former allows us to use Plank intensity for the source function by virtue of the Kirchhoff law whereas the latter implies that the variations in the intensity and atmospheric parameters such as temperature and components profiles are allowed only in the vertical direction. In the governing equation (e.g., eq. (2.1.5) of Liou (1992)), the source term is approximated using Plank intensity. However, the determination of the absorption coefficient in stratified atmosphere consisting of a variety of radiatively active gases is complicated. In the lower atmosphere, the absorption line shape takes the Lorenz profile (a line profile directly proportional to pressure) because molecular collisions caused pressure broadening dominates. Line coupling (especially for  $\text{CO}_2$ ) and the line width uncertainty caused by much frequent collision with foreign molecules than with like molecules (because all radiatively active gases are of low concentration), modifications to Lorenz profiles are usually introduced. In the upper atmosphere ( $>40 \text{ km}$ ), the spectral lines are broadened by Doppler effects because the molecular velocities increase with temperature. The Doppler profile is also called square

root temperature profile. For the altitude in between ( $20 < z < 50 \text{ km}$ ), Voigt profile is assumed to combine the effects from both collision- and Doppler-broadening. Line by line methods or more conveniently statistical band methods are used to estimate the spectral transmittance. Then broad band methods (in formally solving the radiative transfer equation, temperature is used in terms of Stefan-Boltzmann law instead of Plank function) may be used to calculate infrared fluxes and heating rates.

Absorption of solar radiation in the atmosphere is primarily due to atomic and molecular oxygen ( $\text{O}_2$ ) and nitrogen ( $\text{N}_2$ ), ozone ( $\text{O}_3$ ), water vapor ( $\text{H}_2\text{O}$ ) and carbon dioxide ( $\text{CO}_2$ ). Absorption spectra due to electronic transitions of molecular and atomic oxygen, nitrogen and ozone occur chiefly in the *uv* region, while those due to vibrational and rotational transitions of triatomic molecules such as  $\text{H}_2\text{O}$ ,  $\text{CO}_2$ , and  $\text{O}_3$  are found in the *ir* region. Absorption of the solar energy in the visible region is very minor. Thus, as solar radiation penetrate the earth's atmosphere, most of its energy in the *uv* region is absorbed by oxygen and nitrogen species in the upper atmosphere. A large portion of solar energy in the near-*IR* region is absorbed by water vapor in the troposphere. The Rayleigh scattering of molecules (mainly  $\text{O}_3$ ) also contributes to the redistribution/attenuation of solar radiation traveling through atmosphere. The scattering intensity is proportional to scattering cross section (depend on incident wave length and volumetric number density of species) and phase function (a special form of the general Legendre polynomial expression as defined by Rayleigh in 1871). As a matter of fact, solar heating is produced mainly by absorption of  $\text{H}_2\text{O}$  below  $\sim 10 \text{ km}$  (less than  $0.6 \text{ K}/12 \text{ hrs}$ ), by absorption by  $\text{CO}_2$  between  $10\text{-}15 \text{ km}$  (less than  $0.1 \text{ K}/12 \text{ hrs}$ ), and exclusively by  $\text{O}_3$  absorptions above  $15 \text{ km}$  ( $< 1 \text{ K}/12 \text{ hrs}$ ). Cloud appearance significantly complicates

the radiative transfer for shortwave (through the scattering effects of raindrops) as well as for *IR* radiation.

In ARPS, The short wave heating/cooling is calculated using the radiative transfer scheme of Chou (1990, 1992) which divides solar spectrum into ultraviolet region where ozone absorption and Rayleigh scattering are considered and visible region where cloud scattering is considered. The cloud and atmospheric infrared cooling/heating are calculated according Chou and Suarez (1994). The scheme had been used for a cloud ensemble model (Tao *et al.* 1996).

### *2.3. Verification of Forward Nonlinear Model*

In this study, forward model is used as a strong constraint. For this reason the accuracy of the forward model affects the accuracy of the retrieval. This section contributes to verify the forward coupled land surface-atmospheric model. For the land surface quantities, i.e., soil temperature and moisture, *LE* and *H*, model output will be checked against corresponding OASIS measurements. Atmospheric profiles of potential temperature and specific humidity will be compared with soundings that are available every 12 hours. Our verification experiments are done for a variety of situations and desirable results are obtained. In the following we present results from two clear sky periods, one from August (a dry period) and one from July 2000 (a wet period). These periods were introduced in section 2.1 when discussing the OASIS data. The fit of model prediction to observations is judged relative to the magnitude of instrument error and daily cycle magnitude for the specific variables. For both periods, model forecasts continuously for two days, with time step of 1 minute for both atmospheric and soil components.



The setting of the atmospheric model is described above. Putting into the framework of the 3D ARPS stencil ( 2.1 and 2.2), it is apparent that the first atmospheric layer above ground is actually the second count of the atmospheric model. Due to this grid staggering, the first scalar point is half a grid interval above ground. Eighty vertically stretched grid levels are used and the minimum vertical grid interval is 4 m. The first scalar point is therefore 2 m above ground. The 4 m layer depth is chosen so that the model data level matches that of the OASIS data level.

The atmospheric model parameters used in this study are listed in Table 2. 2. The leap-frog time integration used in treating the four atmospheric quantities require an Asselin time filter to be applied regularly to damp the computational modes.

Table 2. 2 Atmospheric model parameter setting

<i>Symbol</i>	<i>Meaning</i>	<i>value</i>
$\Delta z_{\min}$	Minimum vertical grid interval	4 m
$\kappa$	Karman constant	0.4
$nz$	number of atmosphere layers (ARPS physical layers= $nz-3$ )	80
$B$	a coefficient of proportionality, which is used in describing the non-local enhancement effects from large-scale eddies to total flux	7.8
$\Delta t_{big}$	large time step for model integration	60 s
$\Delta t_{rad}$	interval for updating radiation process	1800 s
$\Delta t_{sfc}$	time step for land surface processes	60 s
$\lambda_0$	the asymptotic length scale for mixing length (free atmosphere)	30 m
	<i>Flux mixing depth</i>	200 m
$Km_{min}/$ $Km_{max}$	lower/upper bounding for turbulent eddy coefficients	0.01/1000.0
$Pr_{min}/$ $Pr_{max}$	lower/upper turbulent Prandtl number	0.5/4.0

### *2.3.1. Verification for August 6-8 period*

We compared model predictions and observations for surface variables through the selected dry period and good agreements are obtained. However, due to some missing soundings, the comparisons of profile atmospheric quantities are impossible for some periods, including August 4-6, the period used for our first set of retrieval experiments. For the coupled run, we here present results for August 6-8, 2000, a synoptically quiescent summer period characterized by warm temperatures (maximum surface temperature of 45° C), and a soil dry-down period and stressed vegetation (NDVI = 0.5). A vegetation cover of 75% was estimated for this period following Brotzge and Weber (2002). Table 2. 1 gives a detailed description of the parameter settings.

The surface and deep soil moisture values at 12Z, August 6, 2000 are initialized using the measurements at 5 and 25 cm, respectively. For the selected period, the respective values for superficial and deep soil moisture are 0.253 and 0.278, respectively. The surface temperature is initialized using measurement by an infrared instrument while the deep soil temperature is initialized using the preprocessed value according the procedure described in Ren and Xue (2004). The latter takes the seasonal temperature trend into account for the force-restore model. This data processing procedure and the modifications to the original force-restore equations together help improve the soil temperature prediction. Considering the rather stressed growing conditions for the vegetation, the minimum stomatal resistance is set to  $200 \text{ m s}^{-1}$ , significantly larger than the original value of NP89. Similarly, the inverse of the vegetation (unit area and a depth of  $d_1$ ) heat capacity is reset to be  $1.5 \times 10^{-5} \text{ K m}^2 \text{ J}^{-1}$  according the reasoning of more recent papers (Pleim and Xiu 1995; Xiu and Pleim 2001), rather than  $2.0 \times 10^{-3} \text{ K m}^2 \text{ J}^{-1}$  as used

in NP89 and Noilhan and Mahfouf (1996). This significantly lower value of  $C_V$  signifies higher heat storage of the vegetation than previously thought.

With these settings, rather satisfactory descriptions of the soil temperatures are obtained with our model (Figure 2.3). The surface temperature is predicted accurately, with maximum errors generally less than 2 K. There lacks apparent phase error and a slight warm bias is present in the prediction that is less than 1K. Our modification to the soil equations (Eq. (2.6)) systematically improved the nighttime surface temperature prediction (Figure 2.3). The time series for deep soil temperature ( $T_{dp}$ ) indicate that revisions to the force-restore temperature equations are very necessary. Otherwise, the deep soil temperature will drift upward and finally assumes a same daily average temperature as that of the surface temperature. We are most satisfied by the accurate prediction of the surface and deep soil temperatures primarily because that the maximum model-data differences of 2 K and 0.5 K respectively fall well within the measurement error range. Without the modifications introduced to the model by Ren and Xue (2004), the errors would be much larger.

The out-of-phase behavior in the simulated surface soil moisture with respect to diurnal atmospheric forcing is believed to be due to more complicated vegetation activity and the hydraulic displacement of the soil water potential (Caldwell *et al.* 1991; Caldwell 1990; Herman 1997; Horton and Hart 1998; Ishikawa and Bledsoe 2000; Song *et al.* 2000; Ren *et al.* 2004). It is beyond the capacity of the current force-restore model, which does not include the effects of hydraulic lift. Without implementing the effects of hydraulic lift, the simulated surface soil moisture shows phase error compared with the observations. However, the absolute differences in forecasts and observations are

generally small, generally around the order of magnitude of measurement error. We emphasize that the magnitude of the daily cycle is rather accurately modeled and so is the deep soil moisture.

The measured and predicted specific humidity is not the same from the starting time, due to the fact that the model is initialized using a 12Z sounding and the 2m value is interpolated from the sounding which is 2 g/kg larger than the corresponding measurement. The evolution sometimes deviates from the measurements. The downward wiggles (15Z and 21Z) corresponding to a switch on/off of the stability measured by the bulk Richardson number. Using a value of bulk Richardson number  $<0.5$  helps to remove these wiggles. It is interesting that the measured specific humidity increases during heating period and decreases during nighttime. The out of phase feature of the simulation is connected with the surface soil moisture simulation. The absolute difference is generally less than 3 g/kg and the simulation is satisfactory on daily basis. Whether or not the out-of-phase feature affects our retrieval based on OASIS screen level observations depends critically on the sensitivity of specific humidity to soil moisture content (to be addressed in Section 4.1). The retrieval scheme can perform at best to reduce the initial guess errors in initial soil moisture values within the perturbation range that can cause specific humidity bifurcating as large as 3g/kg, for this relatively dry case.

A satisfactory description of the surface energy fluxes is obtained (Figure 2.4). For this period of simulation, during daytime, our model suffers some overestimation to both latent ( $LE$ ) and sensible ( $H$ ) heat fluxes. The peak value difference as large as  $50 \text{ W m}^{-2}$  for 18-24Z August 7 corresponds the inaccurate surface soil moisture. During nighttime, model overestimates sensible heat flux while underestimates latent heat flux.

However, both magnitudes are small (less than  $15 \text{ W m}^{-2}$ ) and well within the instrument error ranges for such variable measurements.

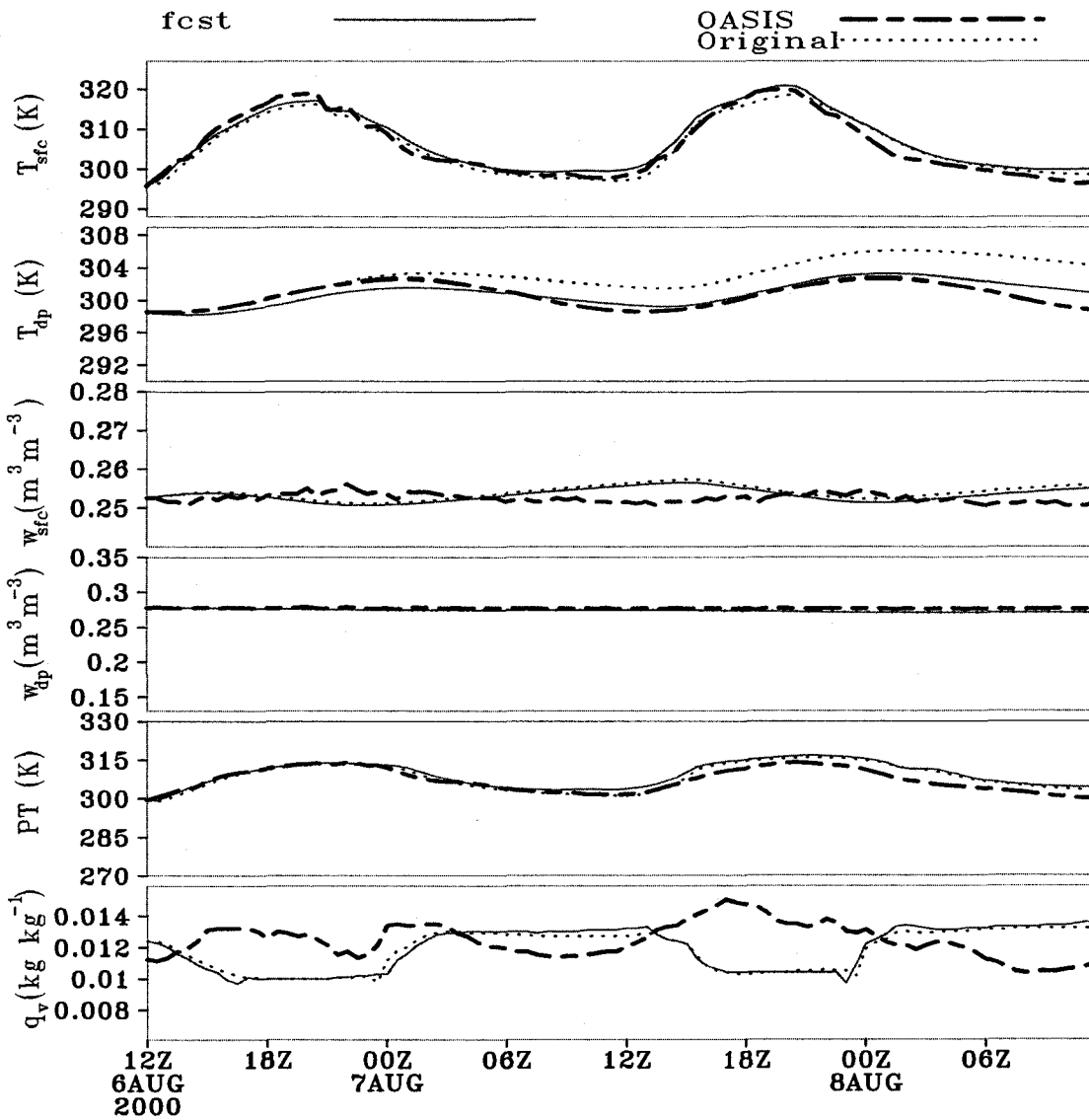


Figure 2.3. Comparisons between modeled (solid line for revised scheme and dotted line for original land surface scheme) and observed (thick dot dashed lines) soil temperatures, soil moistures, screen-level potential temperature and specific humidity for 6-8 August 2000.

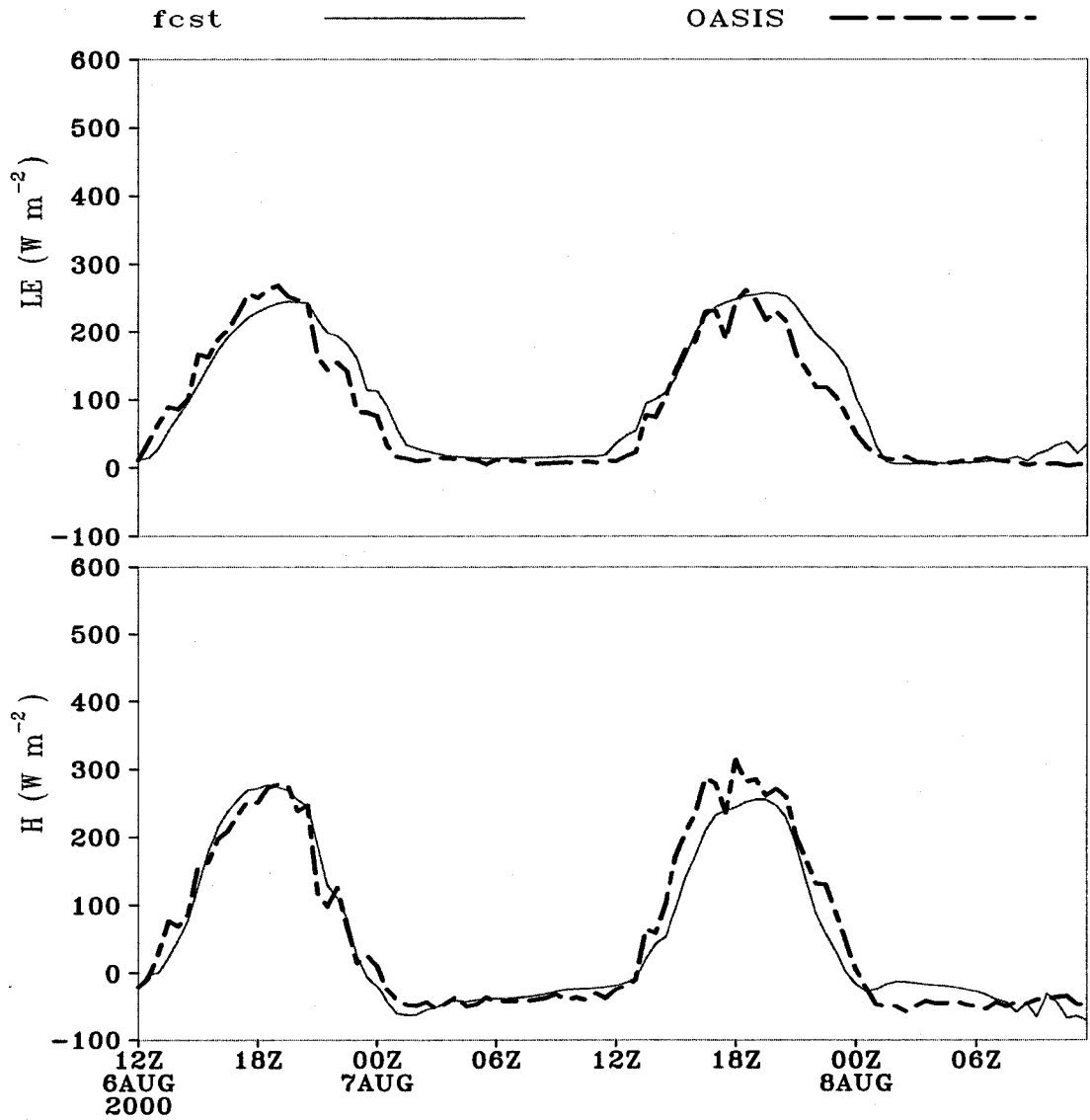


Figure 2.4. The comparisons between modeled (solid lines) and observed (dot dashed lines) latent and sensible heat fluxes for 6-8 August 2000.

Accurate prediction of the atmospheric condition is also critical for our retrieval experiments. We compare the vertical profiles of atmospheric potential temperature and specific humidity with the corresponding soundings (figures not shown). The model integration starts from 12Z sounding. 12 hours later (00Z August 07), the modeled and observed potential temperature profiles are close to each other (modeled is slightly warmer) and the difference is generally less than 2K. 24 hours later, the profiles are still quite similar as to the PBL height, whereas the difference can be as large as 5K.

Most of the errors in the specific humidity profile are near surface, whereas the prediction is pretty accurate higher up. Although the detailed structures in the profile are not predicted after 24 hours, the general trend is pretty accurate ( $<2\text{g/kg}$ ). The 00Z, 08 August 2000 sounding is missing, making it impossible to verify the forecast profiles at the end of the two days. We however feel confident that the forecasting will be still loyal as long as atmospheric fields are horizontally uniform.

Our first set of retrieval experiments involves only the stand-alone (oneway forcing) mode of the forward system. Unlike the coupled state (only specify the initial conditions, the surface energy fluxes are coordinated by model rather than refreshed by observations), where the soil moisture and temperature simulations are depended upon both the soil schemes and the PBL schemes, for the one-way forcing, it suffices to examine only the soil scheme accuracy. Because we use observations for meteorological forcing as input to the 1D ARPS and compare the results with OASIS observed soil moisture content and temperature.

A systematic refinement and verification study had been performed for this 1D land surface scheme using OASIS data (Xue and Ren 2001, unpublished material). Here

we highlight some of the findings of model validation. Whereas the surface skin temperature, superficial and deep soil moisture values are initialized with OASIS observations, the deep soil temperature is initialized according to Ren and Xue (2004). The time step for LSM integration is 30 minutes. Figure 2.5 is produced with continuous atmospheric forcing variables for a 6 day period starting at 00Z, August 4, 2000.

The surface temperatures are predicted accurately, with peak value differences generally less than 2 K. There lacks apparent phase error and the warm bias in the prediction is less than 1 K. The  $T_{dp}$  time series indicate that revisions to the force-restore temperature equations (Eq. (2.1)) are very necessary. Otherwise, the  $T_{dp}$  will be dragged upward and finally assumes a same daily average temperature as the  $T_{sfc}$ . We must admit that, for superficial soil moisture estimation, there is apparent phase error. However, the difference is generally negligible for most study purposes. The deep soil moisture prediction is rather satisfactory because the model-measurement difference is less than  $0.01 \text{ m}^3 \text{ m}^{-3}$ . For this period of simulation, during daytime, our model systematically overestimates  $H$  with peak value difference as large as  $50 \text{ W m}^{-2}$ . During nighttime, model-measurements differences are small for both  $H$  and  $LE$  (less than  $15 \text{ W m}^{-2}$ ), and well within the instrument error ranges for such variable measurements. As expected, without model error bouncing within the coupled system, the agreements with the observations are generally better than the coupled run case.



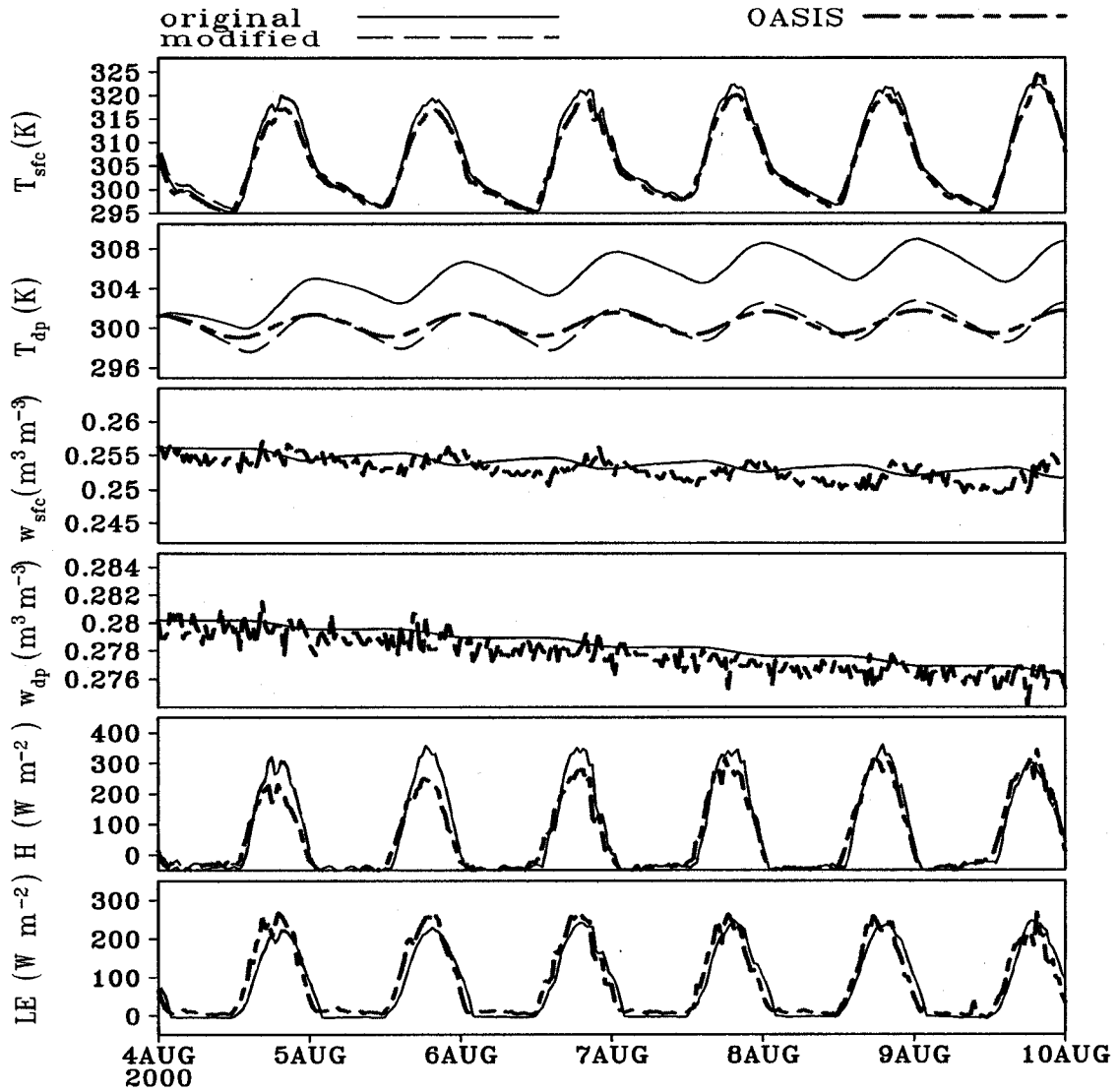


Figure 2.5. Model predicted vs. observed (OASIS) soil temperature ( $T_{sfc}$  and  $T_{dp}$ ), moisture ( $w_{sfc}$  and  $w_{dp}$ ), and surface energy fluxes ( $H$  and  $LE$ ). The curve labeled as 'original' is the model predictions before our revision as in section 2.2.1a).

### 2.3.2. Verification for July 6-8 period

The soundness of the atmospheric components of the forward model can also be seen from another test run for 06 July 2000 period. Similar to the 6-8 August 2000 period, this is also a synoptic quiescent period but with much more moist soil resulting from antecedent precipitation. We show results for this period mainly for the purpose of attesting to the versatility of our forward model. For this period, the soil water content is near the field capacity value and the vegetation is more active, we therefore specify a vegetation coverage as 0.8 and LAI=0.6. The heat capacity for vegetation is increased to  $1.12 \times 10^{-5}$  ( $\text{K m}^2 \text{ J}^{-1}$ ). Under this condition, the minimum stomatal resistance is a critical parameter in determining the surface energy partition. The role of vegetation coverage is mainly to provide the shielding effects.

The model is initialized using sounding of 00Z 6 July 2000 and OASIS measurements at the same time. As before, we compare the surface and deep soil moisture and temperature as well as the screen-level air temperature and mixing ratio with OASIS data (Figure 2.6). All agree very well except for 2m air humidity during daytime period with the difference being as large as  $5 \text{ g kg}^{-1}$ . The  $LE$  and  $H$  time series are close to the observed ones (Figure 2.7). The differences are generally less than  $50 \text{ W m}^{-2}$ , the usual instrument error for flux measurements. Figure 2.8 shows the evolution of the vertical profiles of air potential temperature (Figure 2.8a) and mixing ratio (Figure 2.8b). The time-height cross sections as plotted in Figure 2.9 illustrates the daily cycle of eddy diffusivities ( $a$  for momentum and  $b$  for vapor and thermal) calculated using the non-local scheme as implemented in our model.

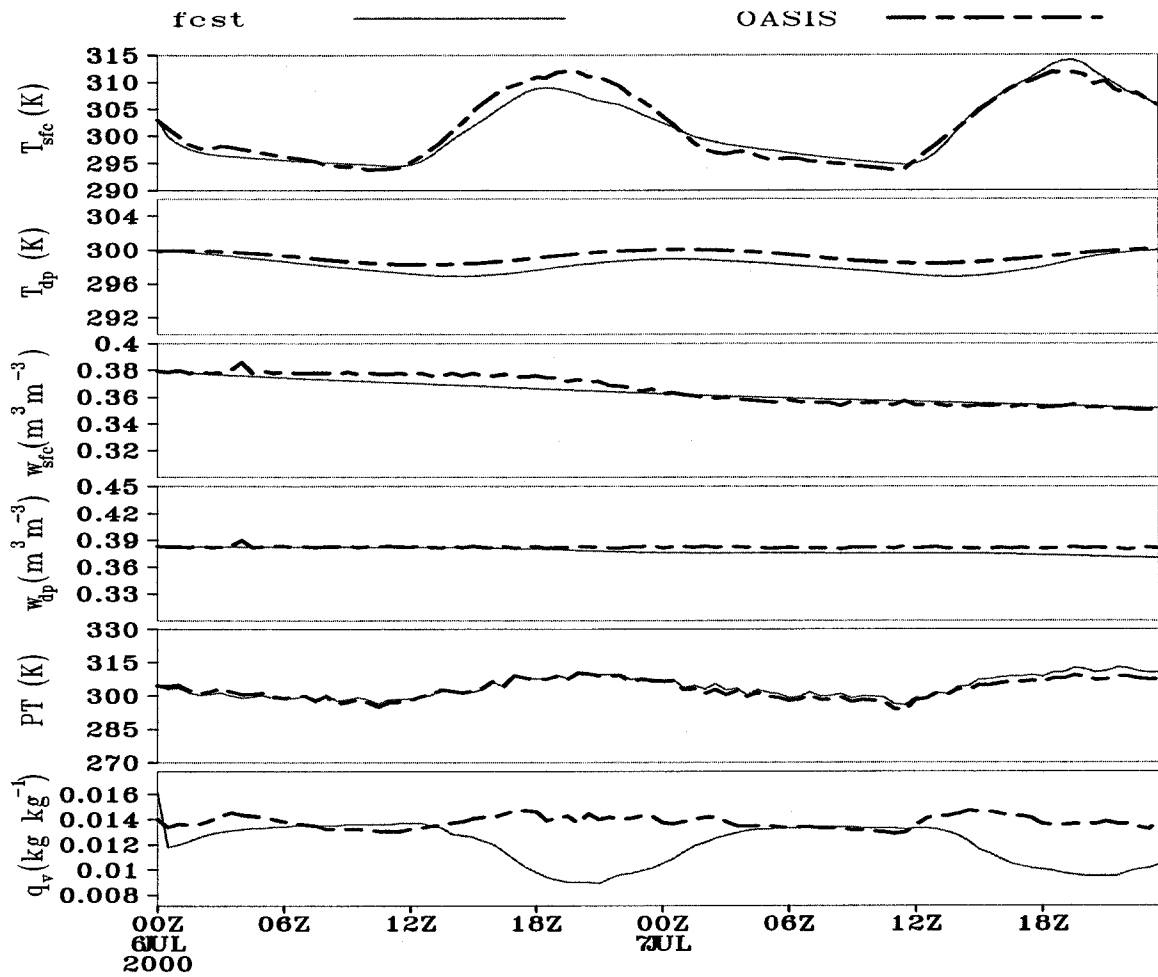


Figure 2.6. Comparisons between modeled (solid lines) and observed (thick dot dashed lines) land surface and screen-level atmospheric model parameters for July 06-07, 2000 moist period.

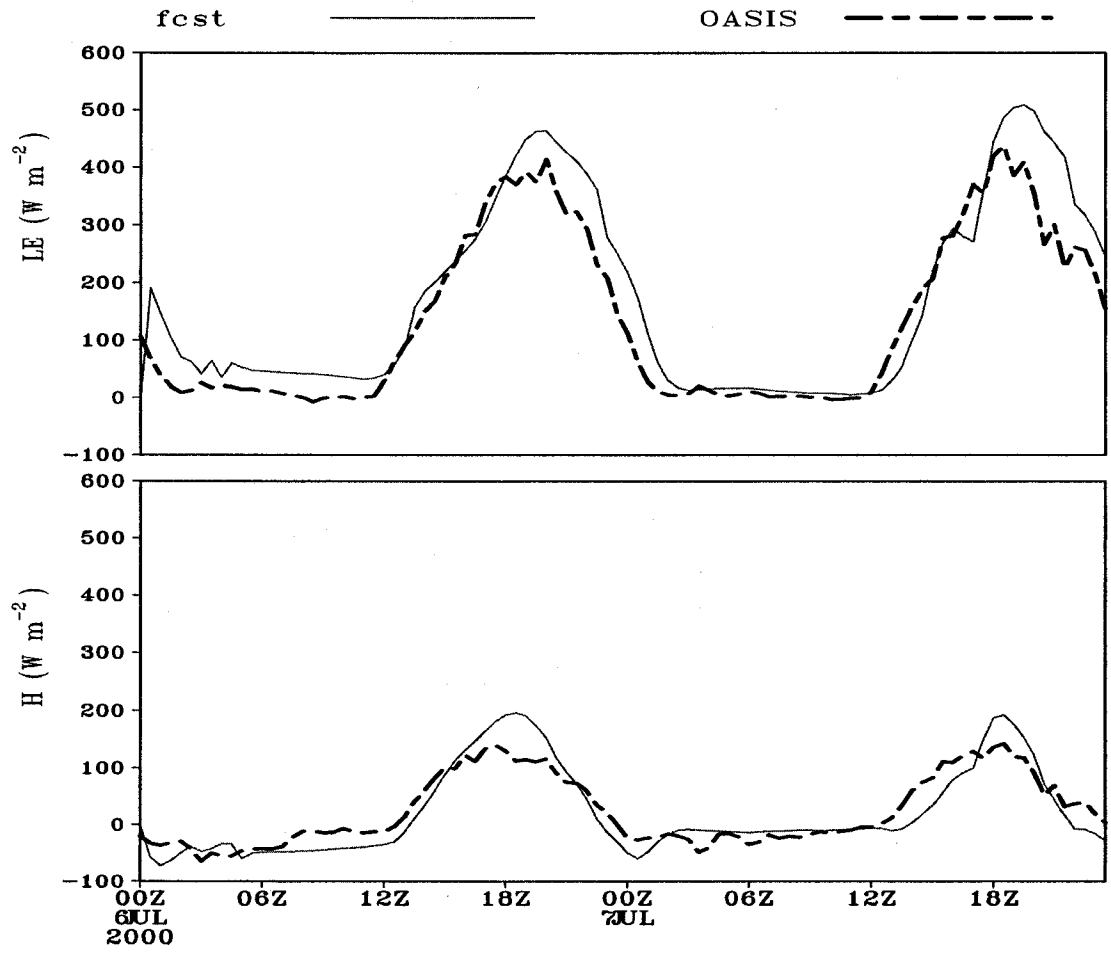


Figure 2.7. The comparisons between modeled (solid lines) and observed (dot dashed lines) latent and sensible heat fluxes for the 00Z, July 06-07, 2000 period.

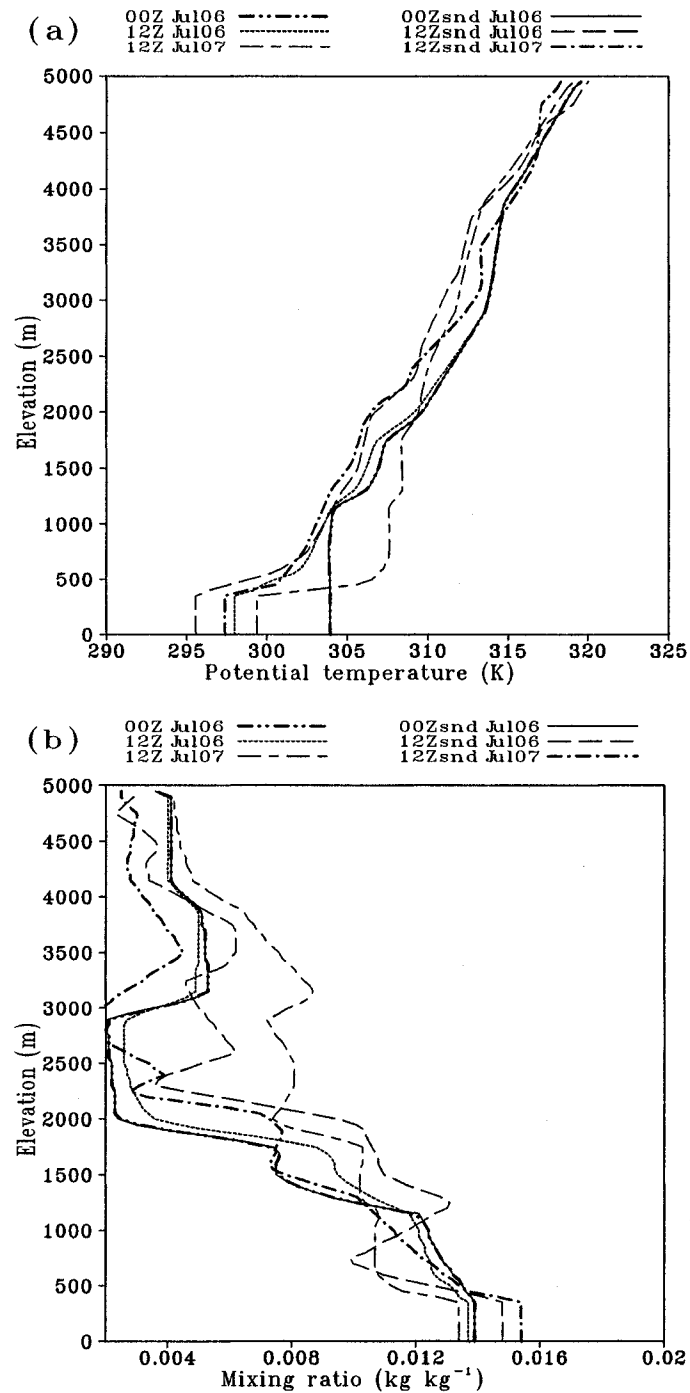


Figure 2.8. The evolutions of atmospheric potential temperature (a) and specific humidity (b) for the moist period (July 06-08). The 00Z and 12Z soundings are provided for comparison with the corresponding model predictions. Note that Norman's elevation is about 360m, thus the constant part at the bottom is an artifact of plotting.

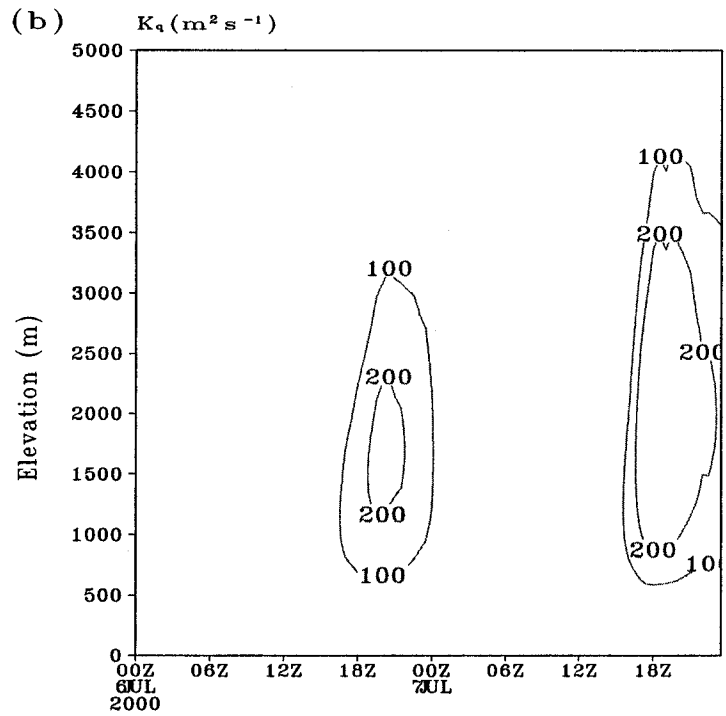
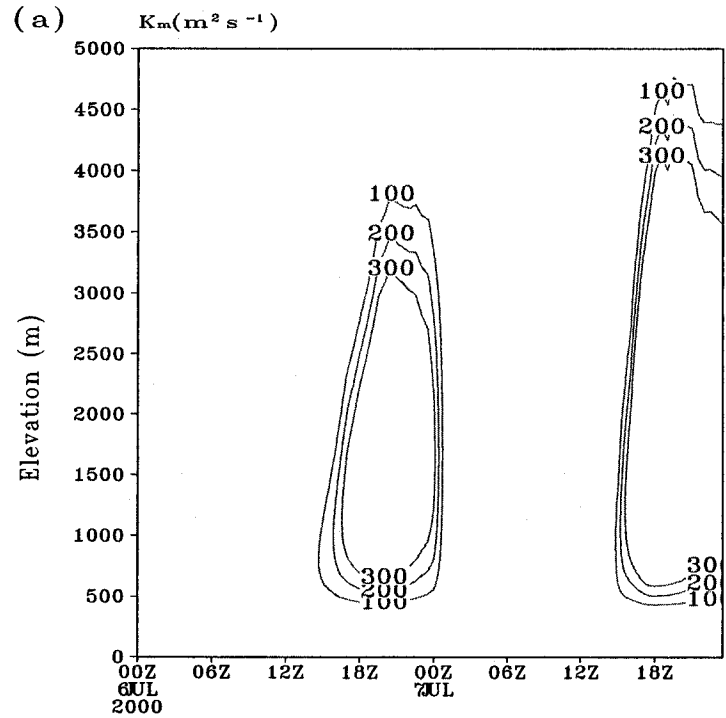


Figure 2.9. Time-elevation cross sections of the eddy diffusivity calculated with the non local scheme for (a) momentum and (b) thermal.

The daily variations/cycles for potential temperature (10K), mixing ratio (0.005), and the eddy coefficients for momentum ( $300 \text{ m s}^{-2}$ ) and heat/moisture ( $200 \text{ m s}^{-2}$ ) are all apparent and reasonable for Norman site and the selected season. For potential temperature and mixing ratio, the comparisons with the corresponding 00Z sounding give very satisfactory agreements. As shown in Figure 2.8a&b, the still accurate profiles one day later are attributable to the successful nighttime restore back mechanism in the ARPS treatment of flux distribution.

A sequence of hourly plots (not shown) shows that a mixed boundary layer is fully developed by 17 Z. Due to the vegetated ground surface, the superadiabatic layer near the surface is not apparent, whereas the negative  $\theta$  perturbation at the top of the boundary layer resulting from entrainment are clearly seen. The depth of the planetary boundary layer is accurately predicted. The nighttime very cold and dry spikes which appear for the potential temperature and mixing ratio simulations, respectively, are successfully eliminated by implementing the flux distribution scheme of ARPS, which distribute the estimated surface radiative cooling caused near surface air potential temperature drops during nighttime into a certain depth. The depth for swapping flux redistribution was set to 200 m, which is clearly shown in the 3Z profiles. We are pretty sure that the development and collapse of the planetary boundary layer are accurately described by the model because, on 12Z 8August (the ending time of forward integration), the soundings for mixing ratio and potential temperature are rather close to our modeled profiles.

To verify that our implementation of the MRF PBL scheme works as expected, we plot the time-height contours of vertical eddy diffusivity coefficients for potential

temperature and water vapor mixing ratio in Figure 2.9a&b. It can be seen that both diffusivity coefficients for mass and momentum gradually increase from sunrise up to mid-afternoon, and then decrease relatively quickly near sunset. Such results are in concert with those of Hong and Pan (1996, see their Figure 2). The centers of the contours of the eddy coefficients and the relative magnitude between that for heat and that for momentum are all consistent with published results (Hong and Pan 1996). Labeled using the height as vertical coordinate, the location of the maximum  $K_m$  and  $K_h$  are about 1/3 of the overshoot height. The shapes of  $K$ 's profiles experience a transition from like-one side distribution to biased two-sided distribution and to normal distribution as vertical stratifications transits from stable to neutral and to convective.

The accurate description of daytime growth and nighttime collapse of the PBL as well as the evolution of the PBL height are important not only because PBL height exhibits a strong daily cycle driven by the surface heating, but also because it grows in conjunction with the entrainment of the warm (higher in potential temperature) and dry air from the overlying free atmosphere. The entrainment fluxes, which serve as the main connection between the coupled land surface PBL system and the overlying free atmosphere, warm and dry the mixed layer. Considering that the similarity theory is applied on the mixed layer property and the corresponding surface property, this process of entrainment not only directly affects the PBL energy and moisture distribution but ultimately the surface energy and moisture budget as well.

The results confirm the accuracy of the forecast prediction model, which is essential for the retrieval experiments to be conducted based on this forward model and its adjoint. Also, the reader is cautioned that due to technical difficulties in adjoint



coding, some parameterizations in PBL component as well as in land surface component will be altered. However, all such modifications are acceptable only when they do not alter the overall forecasting performance as shown in this section.

Finally, on the basis of the simulations, we would like to make a comparison between the wet period and the moist period in order to illustrate the role of vegetation and soil conditions on the development of PBL structure and possible implication for convective initiation.

The solar and atmospheric radiation at the Earth's surface is distributed very differently on dry and wet surfaces. On bare dry land, the absorption of this energy results in a relatively strong heating of the surface (resulted from weak latent heat flux, i.e., evaporation), which usually generates high sensible and ground heat fluxes. On wet surfaces, however, the incoming radiation is used mainly for evaporation, and the sensible heat flux transferred into the atmosphere and conducted into the soil is usually much smaller than the latent heat flux. When the ground is covered by dense and active vegetation, water is extracted mostly from the plant root zone soil by transpiration. This case is usually characterized by strong latent heat flux even if the soil surface is dry. To illustrate this mechanism, we make a comparison between the diurnal variation of the profiles of potential temperature and specific humidity up to a height of 5000m in the atmosphere obtained for the dry period and the moist period.

Clearly, the surface heat fluxes and temperature, during the daytime hours, are extremely sensitive to the ability of the earth's surface to evaporate and transpire water. At peak hours of the noon, for instance, the sensible, latent and ground surface temperature differences between the two simulated cases are as large as  $185 \text{ W m}^{-2}$ , 100

$W\ m^{-2}$ , and 10 K, respectively. The faster heating rate of the dry case generates a vigorous turbulent mixing and an unstably stratified PBL, as shown by the profile of potential temperature in Figure 2.10a. On the contrary, the slower heating rate of the wet period limits the development of the PBL to a height of about 1300m (Figure 2.10c and *d* for the first day), but the vigorous evapotranspiration during the wet period provides a supply of moisture which significantly increases the amount of water in the shallow PBL, as evident from the profile of specific humidity in Figure 2.10d. For the following days, the previous day accumulated moisture help moisten the lower troposphere atmospheres.

On the average, during the afternoon hours, the temperature of the PBL during the dry period is 5K warmer than that of the PBL during the wet period. During the nighttime hours, the cooling for the dry period is slightly more significant than the wet period, as indicated by the profiles of temperature before sunrise in Figure 2.10*a* and *c*. The relatively small differences of surface energy fluxes, temperature, humidity and PBL height are mainly due to differences in top layer heat capacity (as indicated by  $C_{Gv}$ ). However, the nighttime remoistening is more apparent for the wet period (Figure 2.10*b* and *d*).

Obviously, these results are specific to the particular conditions that have been selected for the simulations (day of year, initial profile of atmospheric and soil temperatures and humidities, synoptic conditions). Whereas different results are obtained for different combinations of such conditions, the general trends hold for a broad range of conditions.

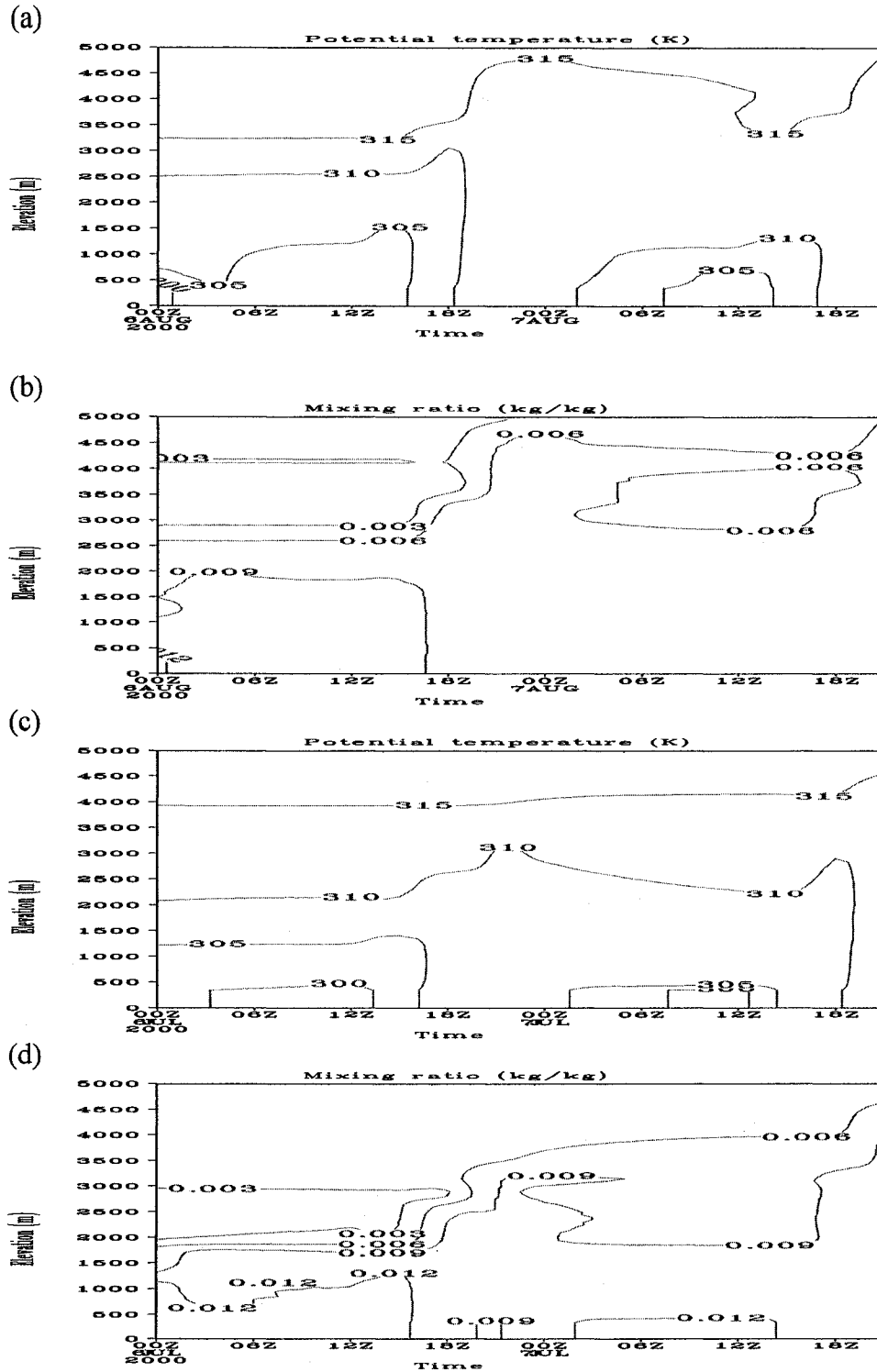


Figure 2.10. Diurnal variation of profiles of (a and c) potential temperature and specific humidity (b and d) in the atmospheric planetary boundary layer for (a and b) a dry period and for (c and d) a moist period, simulated for a cloudless mid-summer period at Norman (a vegetated site).

## 2.4. Adjoint sensitivity and Variational Data Assimilation

Sensitivity studies and data assimilation may at first sight seem like rather different subjects. Using a variational optimization approach, adjoint model can however be developed for use by both (Errico 1997). In the following, a general variational framework is described, of which the adjoint sensitivity and variational data assimilation are special applications.

### 2.4.1. A General Statement of Sensitivity Study and Data Assimilation Using Adjoint

Consider a physical model that is represented in vector form by the following system of coupled nonlinear differential equations:

$$\frac{\partial U}{\partial t} = F(U, \alpha), \quad (2.22)$$

where  $U(t)$  is an  $N_s \times 1$  state vector (where  $N_s$  is the number of state variables augmented to include all spatial locations for a distributed physical system) and  $F$  is an  $N_s \times 1$  nonlinear vector operator that is a function of the states themselves and the  $N_p \times 1$  vector of time invariant spatially distributed model parameters  $\alpha$ . Forcings such as the observed meteorological inputs are included in  $F$ .

We next define a scalar “measurement importance functional” (Backus and Gilbert 1970; Marchuk 1981 & 1994) as

$$J = \iint_{\Sigma} \phi(U, \alpha) dx dt, \quad (2.23)$$

where  $\phi$  is a nonlinear function of the state variables and model parameters,  $x$  is the spatial variable, and  $t$  is time. In sensitivity study  $J$  may represent a quantity of interest (e.g., diurnally averaged evaporation), whereas for data assimilation it would represent

the cost function, which is generally a least square performance metric that indicates the difference between model predictions and measurements. In either case, we are generally interested in obtaining sensitivity derivatives (Errico 1997). For sensitivity studies, these derivatives give the sensitivity of the model response to various model parameters. This gives insight into the relative sensitivities to different parameters as well as which physical processes are most important in the system. In data assimilation we generally need the derivatives of the least square cost function with respect to target parameters (also called control variables) as input to an optimization scheme.

With the above general task in mind, we first adjoint the model to the “measurement importance functional” using a vector of Lagrange multipliers (Yu and O’Brien 1991)  $\lambda^T$ :

$$L = J + \iint_{\Sigma} \lambda^T \left[ \frac{\partial U}{\partial t} - F(U, \alpha) \right] dxdt, \quad (2.24)$$

where  $T$  represents transpose operator, and  $L$  is the Lagrangian which transforms a constrained minimization problem into an unconstrained problem.

We now take the first order variation of  $L$  with respect to  $U$  and  $\alpha$ .

$$\delta L = \iint_{\Sigma} \left\{ \left[ -\frac{\partial \lambda^T}{\partial t} - \lambda^T \frac{\partial F}{\partial U} + \frac{\partial \phi}{\partial U} \right] \delta U + \left[ \frac{\partial \phi}{\partial \alpha} - \lambda^T \frac{\partial F}{\partial \alpha} \right] \delta \alpha \right\} dt dx + \lambda^T \delta U \Big|_{t_0}^t, \quad (2.25)$$

where we assumed that the time period under consideration is  $[t_0, t_f]$ . If we denote the

values of the Lagrange multiplier at the initial and final time as  $\lambda_0$  and  $\lambda_f$ , and

assume  $\lambda_f = 0$  (Thacker 1988), Eq. (2.25) can be simplified as

$$\delta L = \iint_{\Sigma} \left\{ \left[ -\frac{\partial \lambda^T}{\partial t} - \lambda^T \frac{\partial F}{\partial U} + \frac{\partial \phi}{\partial U} \right] \delta U + \left[ \frac{\partial \phi}{\partial \alpha} - \lambda^T \frac{\partial F}{\partial \alpha} \right] \delta \alpha \right\} dt dx - \lambda_0^T \delta U(t_0). \quad (2.26)$$

A minimization of  $L$  requires that

$$\begin{cases} -\frac{\partial \lambda}{\partial t} - \frac{\partial F^T}{\partial U} \lambda + \frac{\partial \phi}{\partial U} = 0, & (2.27a) \\ \frac{\partial L}{\partial \alpha} = \int \left[ \frac{\partial \phi}{\partial \alpha} - \lambda^T \frac{\partial F}{\partial \alpha} \right] dt = 0, & (2.27b) \\ \frac{\partial L}{\partial U(t_0)} = -\lambda_0 = 0. & (2.27c) \end{cases}$$

The equation (2.27a) is called adjoint system (of Eq. (2.22)) because the Lagrange multipliers are called the adjoint variables. The adjoint model must be integrated backward in time as a terminal value problem. Note that the homogeneous part of the linear differential equation (the first two terms on the left hand side of Eq. (2.27a)) is totally determined by the Jacobian of the forward model with respect to  $U$  (i.e.,  $\frac{\partial F^T}{\partial U}$ ), while the forcing  $\frac{\partial \phi}{\partial U}$  is dependent on the gradient of the model response. It is clear that the homogeneous adjoint model (so called adjoint system) can be constructed separately (see Chapter 3) and then used in conjunction with different measurement importance functionals.

Our ultimate goal is that  $\frac{\partial L}{\partial \alpha}$ , and  $\frac{\partial L}{\partial U(t_0)}$  approach zero. However, once  $\lambda$  is

known by integrating of the adjoint model, (2.27b) and (2.27c) do provide the way to find the gradient of  $L$  with respect to parameter  $\alpha$  and initial condition of the control variable  $U(t_0)$  during the minimization process. Herein exists one of the primary benefits of the adjoint method in that, once the adjoint model is developed, all of the derivatives can be obtained efficiently through a single forward model run and a single adjoint model run.

This is possible by the fact that the adjoint model is developed from the forward model and propagates the sensitivity information backward in time over the model integration.

Closely related to the adjoint model is tangent linear model (TLM, will be defined in Eq. (2.29)). For the convenience of the following discussion, the forward system is written in discrete integration form (evolution form) rather than in differential form as in Eq. (2.22). The conception of small perturbation, which forms the basis for the following derivation, can be found in Marchuk (1994), among other sources.  $M$  is designated as the discrete system of  $F$  and  $x$  is designated as model control variable  $U$ . The remaining notational explanations are available in Appendix 2, except otherwise explicitly defined in the context.

Pick a control vector  $c \in R^n$  and let  $\bar{x}(0) = c$ , here over bar means base state. The orbit/trajectory can be computed using  $x(k) = M(x(k-1), \alpha) = \dots = M^{(k)}(c + \delta c, \alpha)$ . The actual evolution of the perturbation is given by

$$x(k) - \bar{x}(k) = M^k(c + \delta c, \alpha) - M^k(c, \alpha). \quad (2.28)$$

Since the computation of  $M^k(x, \alpha)$  is very difficult in general, this quantity is usually approximated using the first order Taylor series expansion:

$$M(x(0), \alpha) = M(\bar{x}(0) + \delta c, \alpha) \approx M(\bar{x}(0), \alpha) + J_M(\bar{x}(0), \alpha) \delta c.$$

Here  $J_M$  is the Jacobian of  $M$  with respect to  $x$ .

Similarly  $\bar{x}(1) + \delta x(1)$  is an approximation to  $x(1)$  to a first order accuracy. Thus,

$$M(x(1), \alpha) = M(\bar{x}(1) + \delta x(1), \alpha) \approx M(\bar{x}(1), \alpha) + \delta x(1) J_M(\bar{x}(1), \alpha).$$

By denoting  $\delta x(2) = \delta x(1) J_M(\bar{x}(1), \alpha)$ ,  $\bar{x}(2) + \delta x(2)$  is thus an approximation to  $x(2)$ .

Continuing this argument, inductively defining

$$\delta x(k+1) = \delta x(k) J_M(\bar{x}(k), \alpha), \quad (2.29)$$

results in  $\bar{x}(k+1) + \delta x(k+1)$  as an approximation to  $x(k+1)$ .

Note that Eq. (2.29) is a non-autonomous linear dynamic system where the one step transition matrix  $J_M(\bar{x}(k), \alpha)$  is evaluated along the base state. Equation (2.29) is known as the tangent linear system (TLM). For convenience, introducing the following notation  $J_M(k) = J_M(\bar{x}(k), \alpha)$ , then Eq. (2.29) can be rewritten as

$$\delta x(k+1) = \delta x(k) J_M(k) = J_M(k) J_M(k-1) J_M(k-2) \dots J_M(1) J_M(0) \delta c.$$

If one further defines, for  $i \leq j$ ,  $J_M(i:j) = J_M(j) J_M(j-1) \dots J_M(i)$ , Eq. (2.29) can be further reduced to  $\delta x(k+1) = J_M(0:k) \delta c$ , or  $\delta x(k) = J_M(0:k-1) \delta c$ .

The iterative scheme that defines the TLM as in Eq. (2.29) can also be written in a matrix-vector form:

$$F \delta x = b, \quad (2.30)$$

where  $F$  is an  $N$  by  $N$  block partitioned matrix given by

$$F = \begin{bmatrix} I & O & O & & \\ -J_M(1) & I & O & & \\ & -J_M(2) & I & O & \\ O & & -J_M(3) & I & O \\ \dots & \dots & & & \\ & O & & -J_M(N-1) & I \end{bmatrix},$$

$$\delta x = (\delta x(1), \delta x(2), \delta x(3), \dots, \delta x(N))^T,$$

and  $b$  is a block partitioned vector given by

$$b = (J_M(0) \delta c, 0, 0, \dots, 0)^T.$$



Interestingly, homogeneous adjoint model is formally a transpose of the TLM model. For detailed derivations and explanations of the relationship between TLM and adjoint model (ADM), the reader is suggested to read Appendix 2 (Eqs. (A2.3-2.7)).

#### 2.4.2. 4DVAR Procedure and Definitions of Two Cost Functions Used in this Study

For simplicity and ease of illustration, here consider a synthetic initialization problem in which the objective is to estimate the initial conditions that minimize the model-measurement misfit, where we assume no model error and perfect model parameters (i.e., model is a strong constraint, see e.g., Zupanski (1997)).

For the stand-alone or forced run of the land surface model, all the sensitivity channels (adjoint variables corresponding to the atmospheric quantities) of atmospheric parameters will be locked. For example, for the assimilation of observed ground surface temperature, the cost-function is defined as:

$$J(T_{sfc}) = 0.5 \sum_{i=1}^N \left( \frac{T_{sfc,i}^o - T_{sfc,i}^f}{\sigma_T^o} \right)^2. \quad (2.31)$$

The forcing term in the adjoint equation is then  $-(\sigma_T^o)^{-2} (T_{sfc,i}^o - T_{sfc,i}^f)$  and the gradient of the objective function with respect to the initial conditions can then be computed as  $\frac{\partial L}{\partial U(t_0)} = -\lambda_0$ . Here  $U(t_0)$  is control variables that are connected to  $T_{sfc}$  through model dynamics.

For the soil-state variable retrieval problem using screen-level atmospheric observations as the constraint, the cost function is constructed as quadratic function of

screen-level atmospheric forcing variables. They are related through model dynamics to the land surface model variables. Define  $U(t_0) = (T_{sfc}^0, T_{dp}^0, w_{sfc}^0, w_{dp}^0, w_{canop}^0)^T$ ,

$$J(U) = \sum_{i=1}^N \left[ \left( \frac{T_{air,i}^o - T_{air,i}^f(U)}{\sigma_T^o} \right)^2 + \left( \frac{q_{air,i}^o - q_{air,i}^f(U)}{\sigma_q^o} \right)^2 \right] + (U - \bar{U})^T \sigma_a^{-2} (U - \bar{U}), \quad (2.32)$$

where  $N$  is the number of observations during an assimilation period,  $T$  represents temperature (superscript  $T$  means matrix transpose), with subscripts  $air$ ,  $sfc$ ,  $dp$  indicating that for the air, surface soil and deep layer soil, respectively. Here  $q$  is for water vapor specific humidity, with the notational conventions as those for temperature  $T$ . The  $\sigma^o$ 's represent the relative confidence accredited to each observation and prediction pair, which are typically the standard deviation of the observational error.  $\bar{U}$  is the prior estimate of the initial condition vector and  $\sigma_a^{-2}$  is the prior error covariance. The three  $\sigma$ 's weight the model-measurement misfit and prior estimate misfit, respectively, based on the uncertainty involved in each component. For example, if the measurement error was very small and the prior knowledge of the initial conditions was poor, then we would expect the estimation procedure to change greatly the initial guess or prior estimate in an effort to fit the model output to the measurements. When many observations are available in the assimilation period or assimilation window, the background term, i.e., the last term in Eq. (2.32), is less valuable since the situation of retrieval problem tends to be over-determined. This tends to be the case for our 1-D problem because of the relatively small degree of freedom. Also, for land surface variables we usually lack proper background analyses *a priori* (e.g., usually no *a priori* soil moisture information).

Following the treatment in Subsection 2.4.1, one obtains the adjoint model as

$$\frac{\partial \lambda}{\partial t} = -\frac{\partial F}{\partial U} \lambda - 2 \frac{\partial T_{air}}{\partial U} \sigma_{air}^{o-2} (T_{air,i}^o - T_{air,i}^f) - 2 \frac{\partial q_{air}}{\partial U} \sigma_{air}^{o-2} (q_{air,i}^o - q_{air,i}^f). \quad (2.33)$$

The adjoint model is integrated backward in time to obtain  $\lambda$ , the gradient of the objective function with respect to the initial conditions can then be computed as

$$\frac{\partial J}{\partial U(t_0)} = -\lambda_0 + 2(U - \bar{U})\sigma_a^{-2}. \quad (2.34)$$

Using this framework, the estimation procedure, or the procedure of optimally retrieving the initial state  $U$ , is as follows.

- 1) Based on the prior guess of the initial conditions  $U(t_0)$ , integrate the forward model over a chosen assimilation window in which observations are used. This forward integration yields  $U(t)$ , which is saved for use by the adjoint model integration.
- 2) Using the model-measurements misfit as forcing, integrate the adjoint equation (2.33) backward in time to obtain adjoint vector  $\lambda_0$ .
- 3) Compute the gradient of the objective function with respect to each initial condition according to Eq. (2.34).
- 4) Using certain optimization algorithm, such as the quasi-Newton methods (Shanno and Phua 1980; Gill and Murray 1979; Liu and Nocedal 1989; Buckley and Lenir 1983) or the conjugate gradient method (Shanno 1978; Navon and Legler 1987) as used in this study, determine an optimal increment  $\delta U$ , which is added to the prior guess of  $U$  to obtain a new  $U(t_0)$ . This procedure is repeated until a convergence is reached. A forward model run with the obtained initial conditions will give quantities other than the control or analysis variables. Figure 2.11 is a flow chart of the 4DVAR data assimilation scheme.

Because of linearization involved in formulating the adjoint model (Eq. (2.29)), an anticipated difficulty lies with the fact that land surface models usually contain threshold processes that can induce discontinuities in the cost function (Xu 1996a; Bao and Warner 1993). These threshold processes, and the chaotic character of the land surface system, can also have the effect of resulting in multiple minima (Talagrand 1991).

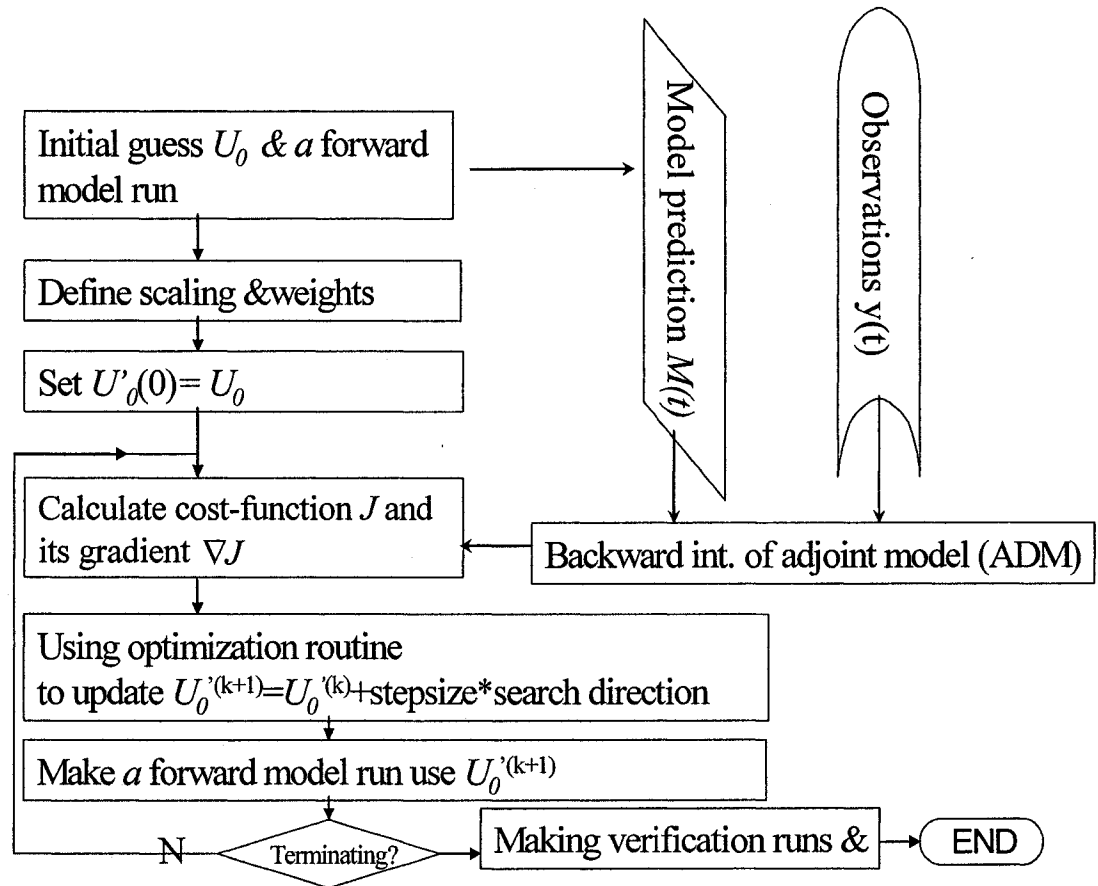


Figure 2.11. Flow chart of the main minimization routine.

The 4DVAR data assimilation procedure can be summarized as follows (e.g., Le Demet and Talagrand 1986, Courtier and Talagrand 1987a&b): Applying a minimization procedure that make use of the adjoint, a model trajectory is brought as close as possible

to the data by varying control variables. The closeness of model trajectory to data in a period is quantified by a cost function. An iterative algorithm is used to minimize the cost function. Starting from a first guess, the value of the cost function and its gradient with respect to the control variables are used to improve the estimation of the vector of the control variables. Under a series of forcing composed of the model-data misfits, a backward integration of the adjoint model provides the gradient vector of cost function with respect to control variables.

Adjoint sensitivity studies and data assimilation are closely related because both use the gradient information provided by the adjoint model. McLaughlin (1995) generalized a framework that includes the cases of control variables (variables that have influence to cost function and usually is the objective of retrieval) are initial conditions, model parameters, and even model error (see also, Zupanski 1997). The adjoint (backward) method is a powerful tool for studying sensitivity. Using a nonlinear forward model and the adjoint of its tangent linear model (TLM), one can calculate the sensitivity of a chosen forecast metric (e.g., precipitation rate, accumulated precipitation, average temperature) to all model input variables at all grid points simultaneously (see, e.g., Errico 1997; Rabier *et al.* 1993). The sensitivity is expressed in terms of the gradient of the metric with respect to the input variables, and thus a single run of the forward model and its adjoint can reveal the sensitivity to different variables as well as the regions of maximum sensitivity.

Sensitivity studies using an adjoint model are not without limitations, the most important being the necessity of linearization. The adjoint based on the TLM may

become invalid when the time period studied is long and/or when the initial perturbation is large so as to cause solution bifurcation.

#### 2.4.3. Analysis of the topology of the Cost Function

The data assimilation problem is in fact an optimization problem. The major goal here is to find suitable initial land surface parameters (two soil temperatures and two soil moisture variables) so that the model predicted screen-level temperature and relative humidity come close to the corresponding observations. Feasibility study needs to be performed first. The structure of the cost-function is informative to this end because it indicates the overall (temporal domain) sensitivity of the measurement to the perturbations on the control variables. Different cross-sectional images also indicate the relative sensitivity of the two involved control variables. In the following numerical experiments, for the dry case, a reference run (coupled run of our forward system as described in Subsection 2.2) starting from 12Z 6 August 2000 is made and the model output of  $T_{air}$  and  $q_{air}$  series are looked upon as observations. While keeping the forward model settings as described in the forward model verification section (Subsection 2.3), perturbations on  $T_{sfc}$ ,  $T_{dp}$ ,  $w_{sfc}$  and  $w_{dp}$  are made for each forward model run. For each forward model run, the value of the cost function can be obtained according to Eq. (2.32), with observational error standard deviations estimated to be  $\sigma_{T_{air}}^o = 1K$  and  $\sigma_{q_{air}}^o = 1g/kg$ , respectively. The  $w_{sfc}$ - $w_{dp}$  cross section of the cost function is shown in Figure 2.12a, which is produced by using forward model run starting from ( $w_{sfc}=0.247m^3 m^{-3}$ ,  $w_{dp}=0.278$ ) as reference. The two soil moisture contents are varied from 0.15 to 0.35  $m^3 m^{-3}$  for  $w_{sfc}$  and from 0.17 to 0.37  $m^3 m^{-3}$  for  $w_{dp}$ , respectively, keeping all remaining parameters (Table 2. 1 and Table 2. 2) intact. For each forward model run, the

observations and forecasts are compared every 10 large time step ( $\delta t = 60s$ ) over the 24-hour assimilation period. For Norman site, the vegetation growth is somewhat stressed during this soil dry-down period,  $veg=0.75$ , and  $NDVI = 0.5$ . The soil hydraulic properties are specified as  $w_{fc}=0.36$ ,  $w_{wilt}=0.114$ , and  $w_{sat}=0.435$ .

For the one day simulation period (12Z 6-7 August 2000), the shape of the cost function shows the strong nonlinearity of the problem. The minimum is located in a narrow U-shaped valley around the point (0.247; 0.278) in Figure 2.12a. The exact location of the minimum is of little significance because the variation of  $J$  inside the valley is small. As long as  $w_{sfc}$  and  $w_{dp}$  are chosen inside the valley the response to the atmosphere remains almost the same. In fact, the value of  $w_{sfc}$  is undetermined between  $w_{dp}=0.35$  and  $0.37 \text{ m}^3 \text{ m}^{-3}$ , and  $w_{sfc}$  may be anywhere between  $0.2$  and  $0.4 \text{ m}^3 \text{ m}^{-3}$ . This suggests that some additional information has to be used in order to retrieve the initial soil moisture in both layers unambiguously. Remember that the shape of the cost function is the result of the relative strengths of the evaporation from bare soil from layer 1 and 2 and the transpiration from layer 2. With our parameter setting of  $veg=0.75$  and root-layer depth=1.0 m, the magnitude of the evaporation is slightly larger than transpiration (from layer 2).

Thus, the axis of the valley of about 135 degree measured from the horizontal axis. The results are equally sensitive to  $w_{dp}$  and to  $w_{sfc}$ . For another set of parameters, for instance if the wilting point rises to 0.22,  $w_{dp}$  could be more accurately determined while the information on  $w_{sfc}$  would be degraded. That is because sharp gradients exist near the wilting point value for  $w_{dp}$ . Also, the exact value of  $w_{sfc}$  is actually undetermined simply because there are many (three isolines of 450 shown on Figure 2.12b) local minima





upper corner, indicating the screen-level atmospheric variables do not response sensitively to soil moisture variations any more.

Figure 2.13 is the shape of cost function as a function of the initial soil temperatures. Unlike the case for soil moistures, where the cost function has a rather irregular shape as also found in Callies *et al.* (1998), the influence of the initial soil temperatures on the cost function is more regular, with the field showing one minimum (unimodal property). It shows similar dependency of the cost function on the surface and deep layer soil temperatures. However, as must be emphasized that the shape of the cost-function contour does not tell the absolute sensitivity. As we will discuss in Subsection 4.1, the atmospheric fields are actually less sensitive to the initial soil temperature error for this relatively dry period. Thus, from Figure 2.13, we can only claim that there is no essential difference in retrieving the two soil temperature values. We performed parallel experiments for the wet period. In addition to the features discussed for the dry case, we will also investigate the structure of the cost function and its variation with assimilation window length.

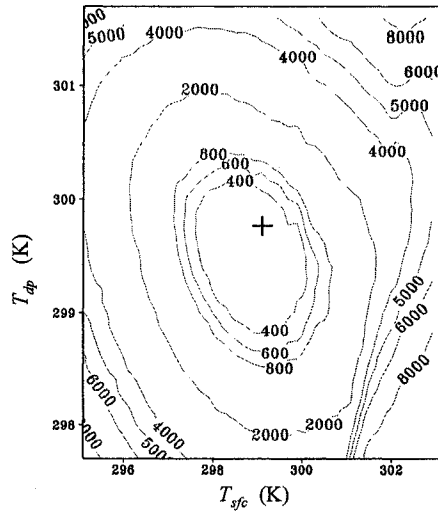


Figure 2.13. Variation of the cost function with respect to different values of initial soil moisture for 12Z, 6-7 August 2000 at Norman site. The cross is the searched state.

In Figure 2.14, with an assimilation window of 3-hour, we calculated the value of the cost function for  $T_{sfc}$  varying down from 301.02 K and up to 306.02 K, with an increment of 0.5 K;  $T_{dp}$  varying down to 299.5 K and up to 300.5 K, with an increment of 0.1;  $w_{sfc}$  varying down to  $0.339 \text{ m}^3 \text{ m}^{-3}$  and up to  $0.439 \text{ m}^3 \text{ m}^{-3}$ , with an increment of 0.01  $\text{m}^3 \text{ m}^{-3}$ ; and  $w_{dp}$  varying down to  $0.363 \text{ m}^3 \text{ m}^{-3}$  and up to  $0.413 \text{ m}^3 \text{ m}^{-3}$ , with an increment of  $0.005 \text{ m}^3 \text{ m}^{-3}$ . The forecast and the observations (from the reference run, labeled with a cross in the figures) are compared every minute. We plotted different cross-sections of it containing  $U^T$  for all possible couples among  $T_{sfc}$ ,  $T_{dp}$ ,  $w_{sfc}$ , and  $w_{dp}$ .

For the 3 hour assimilation window and this relatively moist period, we can see that analysis of soil temperatures and soil moistures are mainly uncoupled. The most important variations of the cost functions are related with  $T_{sfc}$  and  $w_{sfc}$ , showing the sensitivity of 2m atmospheric parameters to the surface soil conditions. Similar to the dry case, the influence of soil temperatures on the cost function is mainly quadratic and unimodal, indicating that linearity dominates this 3-hour period (Figure 2.14a). The most

interesting cross-section corresponds to the  $(w_{sfc}, w_{dp})$  couple. The cost function has indeed an irregular shape as found in Callies *et al.* (1998). It is bordered by flat zones corresponding to dried or saturated reservoirs. There is a valley of low values inside of which the gradient is very small. This indicates an ambiguity for the repartition of water in the two reservoirs. As long as the values of  $(w_{sfc}, w_{dp})$  remain in the valley the response of the atmosphere at 2m is alike within the assimilation window.

We repeated this experiment with 6 hour assimilation window (Figure 2.15). Similar to 3-hour window case, the cost function is not sensitive to  $w_{dp}$  (Figure 2.15c&e) and not to  $w_{sfc}$  for a wide range of  $T_{sfc}$ ,  $T_{dp}$ , and  $w_{sfc} > 0.3 \text{ m}^3 \text{ m}^{-3}$  (Figure 2.15b&d). However, the unimodal quality is fading, indicating that nonlinearity is gaining an upper hand. For example, if searching starts from two locations in the  $T_{sfc}$ - $T_{dp}$  couple (X1 and X2 on Figure 2.15a), the final searched results may be different. Retrieval under this circumstance may be difficult. Figure 2.15f indicates that the U shaped valley is narrowed and the retrieval may be even ambiguous.

We further enlarged the assimilation window to 24 hours (Figure 2.16). However, neither the shapes nor the magnitudes of the cost function contours change significantly from those corresponding ones in Figure 2.15. This indicates that the sensitivity may be well within one day. And all the previous assertions are still valid quantitatively.

The discussion of Chapter 2 was centered on 4DVAR retrieval of initial soil prognostic variables. First, the forward model system was constructed and verified against OASIS measurements. General 4DVAR formalism was reviewed which include the linearization of the forward model to get the tangent linear model and adjoint model. In addition to sensitivity analysis, the adjoint model can be used as an estimation tool.

State estimation posed as a variational data assimilation problem fits naturally within the general framework shown in Subsection 2.4.1. The basic idea of variational data assimilation is that given some measurement of the system, which may be nonlinearly related to model states and parameters, one wish to obtain optimal estimates for a set of control parameters that minimize a weighted least squares cost function.

The function of adjoint model in the 4DVAR optimization system was thoroughly discussed. Although the homogeneous part of the adjoint system can be constructed disregard of the actual form of the cost function, the backward integration of the adjoint model in a 4DVAR optimization system need to be forced by model-data misfit. The actual form of the forcing depends on the definition of the cost function. As specific instances (of the general formalism) in this study, two specific forms of cost function were then introduced. For the one defined on purpose of retrieval land surface prognostic variables through assimilating screen-level atmospheric variable measurements, the structure of the cost function was analyzed for both dry and moist periods. It was found that the dependency of the cost function on soil moistures has rather complex structure. The relative difficulties of retrieval superficial and deep soil moisture depend, among other possible factors such as soil moisture profile distribution, on the vegetation coverage and the growth conditions. The dependency on soil temperature is more regular. More nonlinear sensitivities will be discussed in Chapter 4, preceding TLM and ADM sensitivity experiments.

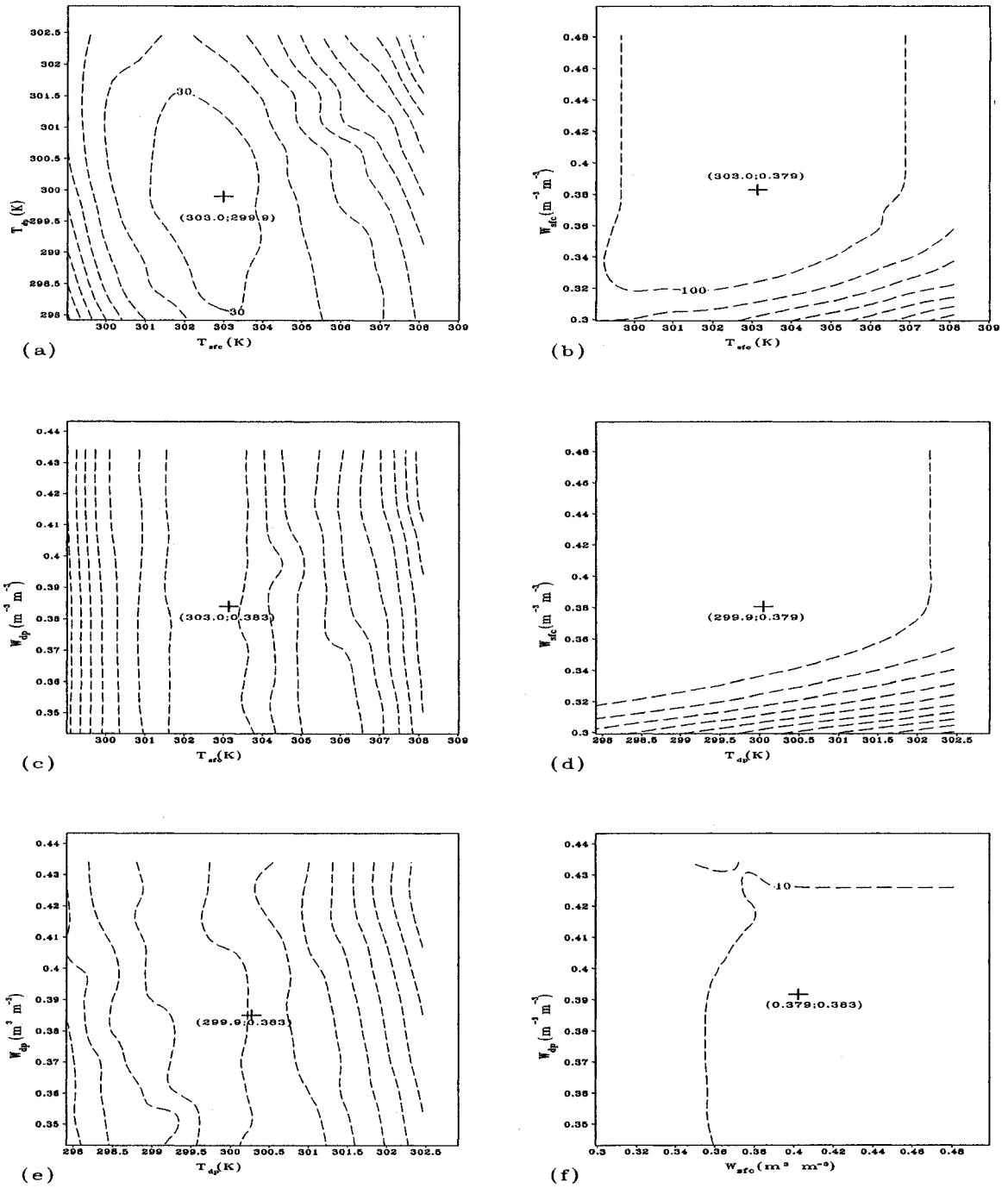


Figure 2.14. Representation of several cross-sections of the cost function for simulated observations every 1 minutes and an assimilation window of 3 hours. The variation of the cost function with surface and deep soil temperature (a), the couple between  $T_{sfc}$  and  $w_{sfc}$  (b),  $T_{sfc}$  and  $w_{dp}$  (c),  $T_{dp}$  and  $w_{sfc}$  (d),  $T_{dp}$  and  $w_{dp}$  (e), and the couple between  $w_{dp}$  and  $w_{sfc}$  (f). Searched state (reference) labeled with a cross sign.  $\sigma_T = 1.0K, \sigma_{qv} = 1g/kg$ .

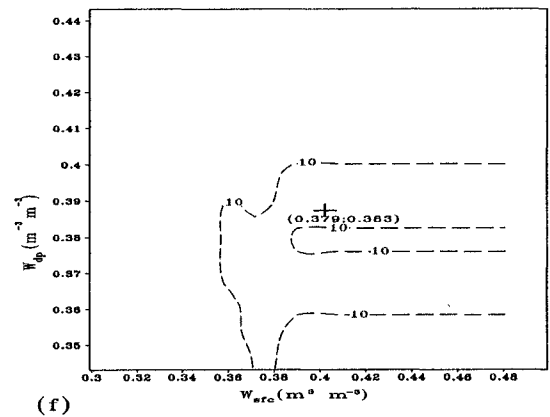
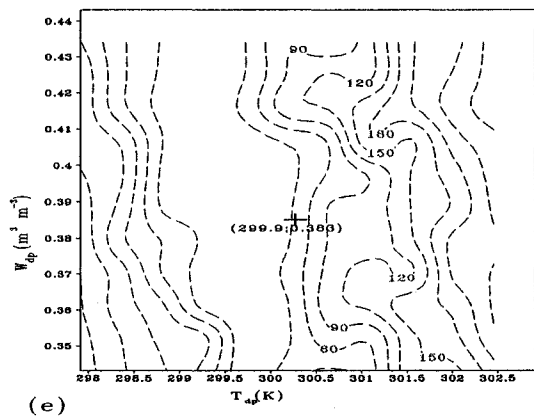
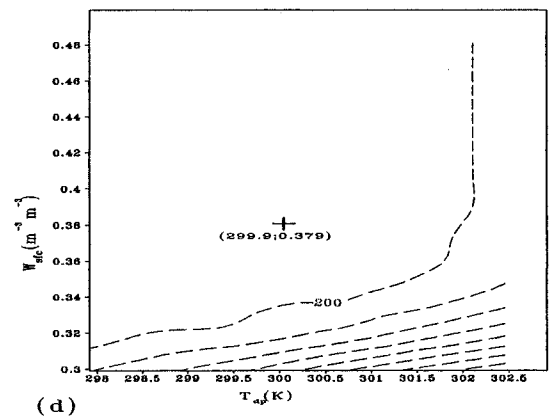
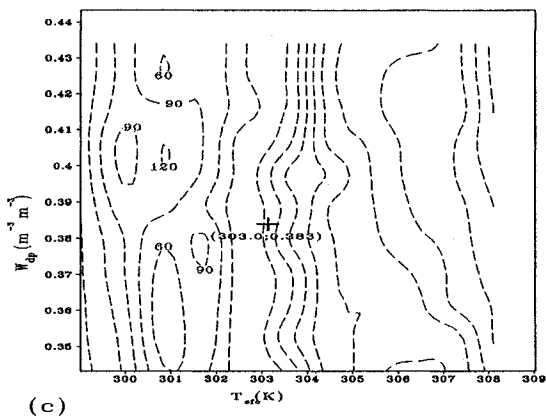
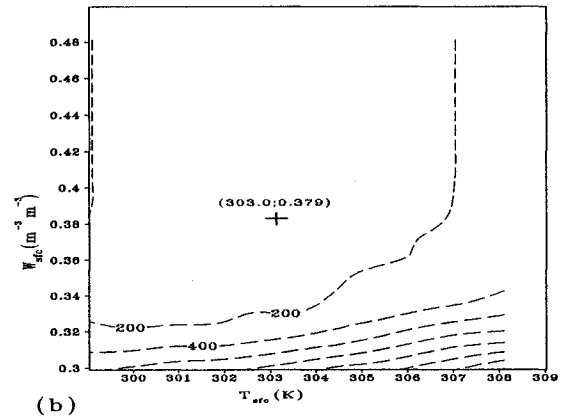
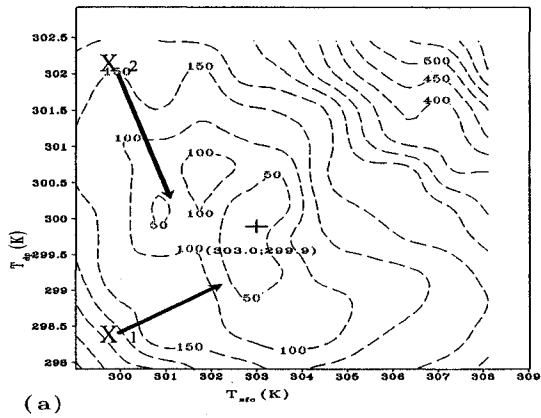


Figure 2.15. Same as Figure 2.14 but with an enlarged assimilation window of 6 hours.

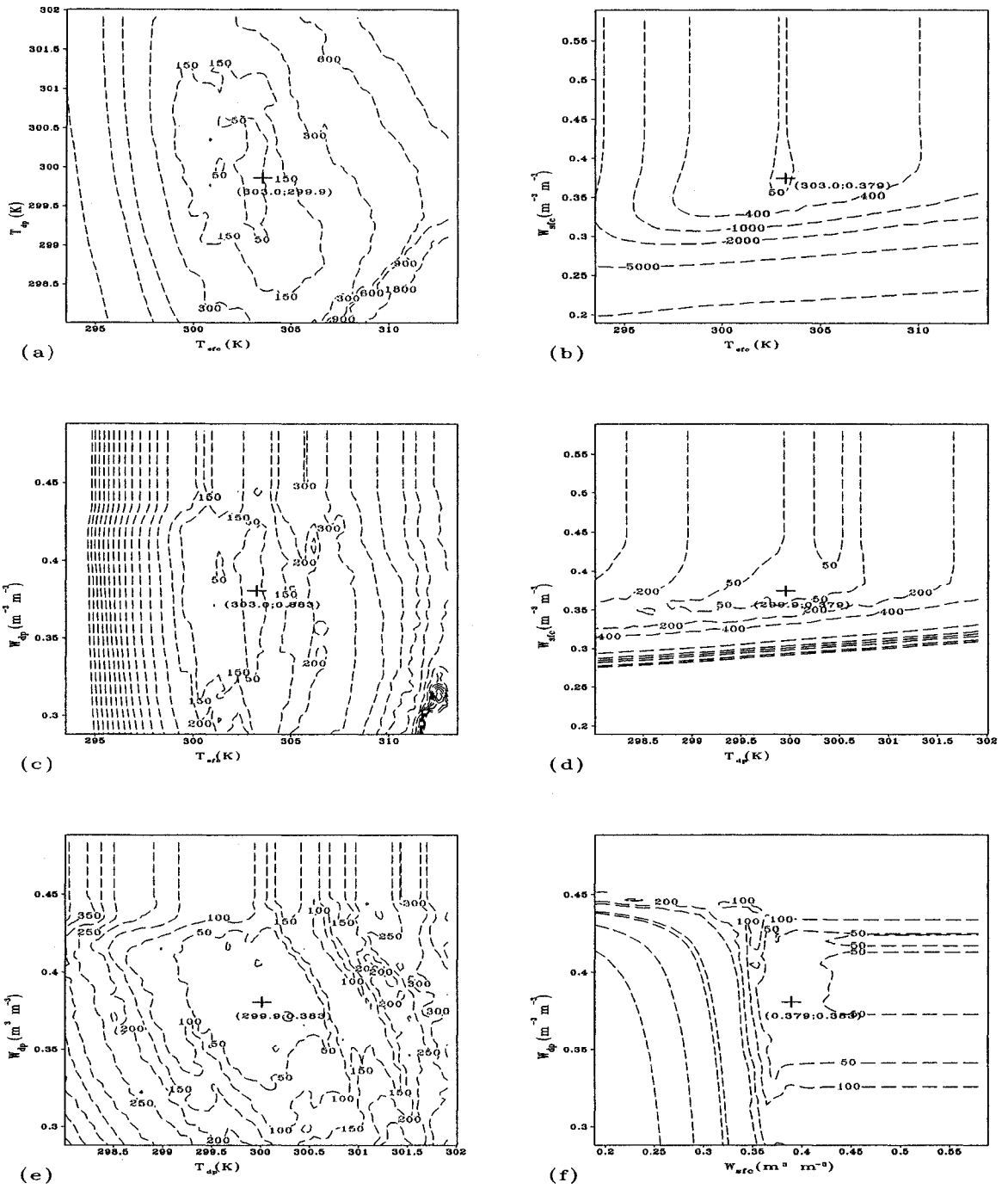


Figure 2.16. Same as Figure 2.14 and Figure 2.15 but with an enlarged assimilation window of 24 hours.

## Chapter Three

### *Development of Tangent Linear (TLM), Adjoint Models (ADM), and 4DVAR retrieval systems*

This chapter contributes to the technical aspects of constructing TLM and ADM models. We chose to hand-code the TLM and ADM because hand-coded adjoint is more humane and more efficient than machine produced one. More importantly, it helps the researcher to become more familiar with both the forward and backward system, which comprises the prerequisite for good research.

#### *3.1. Construction and Verification of the Tangent Linear and Adjoint Models*

Backward modeling (adjoint model construction), unlike the forward modeling (forecasting model and its tangent linear model), has no direct physical laws to guide the researcher, thus, finishing the adjoint code is merely half way from finishing the adjoint system. Thorough and objective testing of the components is indispensable.

##### *3.1.1. Techniques for Coding Tangent Linear and Adjoint Models*

The development of a numerical simulation program is usually done in three steps. First, the analytical differential equations are formulated. Then a discretization scheme is chosen, and the discrete difference equations are constructed. Finally, an algorithm that solves the discrete equations in a programming language is implemented. The construction of the tangent linear model (TLM) and adjoint model (ADM) may be implemented after any of these three steps. For example, Thacker 1987; Long and Thacker 1989a&b constructed the adjoint system separately (from the forward model) by



deriving an Euler-Lagrange equation set. For less complicated model, its analytical form of adjoint system may be directly discretized to form the adjoint code (Schroter 1989). What we will present here is a code-to-code approach (Giering and Kaminski 1998), which is especially suitable for sophisticated models with complicated boundary conditions and on/off switches. ADM constructed this way is also strictly consistent with the forward model.

A numerical model is an algorithm that can be viewed as a composition of differentiable functions as represented by a series of statements in numerical code. The order of evaluation of the individual functions is imposed by the algorithm. The TLM and ADM models can be developed directly from the numerical code by applying the chain rule.

TLM model is a first order linearization along a non-linear trajectory resulting from the evolution of the unperturbed state. Operating in forward mode, the intermediate derivatives are computed in the same order as the model computes the composition. Thus the TLM model can be constructed by a linearization of each forward model statement. The base state calculation immediately follows the linearization statements. The linearization is only for the active input and output variables, not for those constants or diagnostic (from inactive variables) variables that act as coefficients. Compared to the adjoint coding (will be detailed soon), TLM coding is more straightforward. However, caution should be paid to avoid re-computation when subroutines are called.

Mathematically, the adjoint model is simply a transposition of the TLM. For a large computer code written in higher level languages (e.g., FORTRAN), the transpose of the TLM has to be obtained by translating the TLM line by line into a sequence of

computer code which realizes the transpose operation of TLM. In contrast to TLM, ADM operates in reverse mode, i.e., the intermediate derivatives are computed in reverse order. Accordingly, the required base states (the nonlinear trajectory of the TLM) are also needed by ADM in reverse mode. This poses the major difficulty for adjoint model construction.

With a global familiarity of the forward model, hand coding tends to produce high efficient adjoint system. The process tends to be very tedious, however. In recent years, automatic tools for generating TLM and adjoint codes, based on forward model code have gradually improving, with the most mature system being that TAF (Transformation of Algorithms in Fortran) system (Giering *et al.* 2003; Kaminski *et al.* 2003, unpublished material), a commercial version of the more widely used TAMC (Tangent-linear and Adjoint Model Compiler), developed by the same authors.

Thus, hand-coding of adjoint should generally follow the following procedure:

- 1) In each statement, enhancements to the right hand side adjoint variables are measured by the adjoint perturbation of the left hand variable. The adjoint perturbation disappears as the corresponding variable is refreshed by assignment.
- 2) Draw a flow chart first, then take notes of the reused variables and do a global analysis of dependency.
- 3) Constructing the adjoint codes. A distinct adjoint model code fragment corresponds to each model code statement. The adjoint code fragments are composed in reverse order compared to the forward model code. For each kind of statement, simple rules can be formulated for constructing adjoint statements, as stated in 1).

- 4) Lastly, consider the arrangement of required base states. As we stated earlier, 70% of the work lies in providing the required variables, i.e., variables computed by the model code and used by the adjoint code. Confliction occurs due to redefinition of required variables.
- 5) Special techniques are required to treat situations such as hidden reuse in recursive loops (Giering and Kaminski 1998), iterative procedures and nonlinear implicit functions (Zou *et al.* 1997).

An example for hand coding adjoint system of Lorenz system is presented in Appendix 3. The 4DVAR system used in this study was similarly constructed. Here we show the flow chart for the land surface model, which is one core part for assimilating surface ground temperature for retrieving initial land surface prognostic variables. The flow chart of the forward scheme is shown in Figure 3.1. Note that in the forward scheme, the second order Runge-Kutta method requires two calls of the subroutine *tendency*, which provides the right hand side of Eqs. (2.1 & 2.7). In the adjoint coding, the synchronizing of these two half time step (for soil model integration) is necessary. We solved this dilemma by storage.

Also, in the adjoint coding (not shown for clarity), several continuous alternatives for Eq. (2.4) parameterization are available, to cope with the above mentioned differential problems. Similar problem exists for the PBL parameterization for bulk Richardson number. In calculating the bulk Richardson number, the convective contribution to the wind speed is omitted when virtual potential temperature difference between air and surface is less than 0.1K. We did this mainly because there is a singular point in the adjoint of the PBL component resulted from the parameterization of the convective

component of wind speed. The gradient becomes infinity when PBL experience a transition from stable to unstable regime. We do not calculate the gradient for a temperature difference less than 0.1 K between the two temperatures used for parameterization. This treatment is relevant for the set of experiments assimilating screen-level atmospheric measurements and retrieving initial land surface prognostic variables.

As above mentioned, the thorough and objective verification of the adjoint code is an indispensable step for creating an effective 4DVAR data assimilation system. We now investigate the verification of the adjoint code and then the entire 4DVAR system.

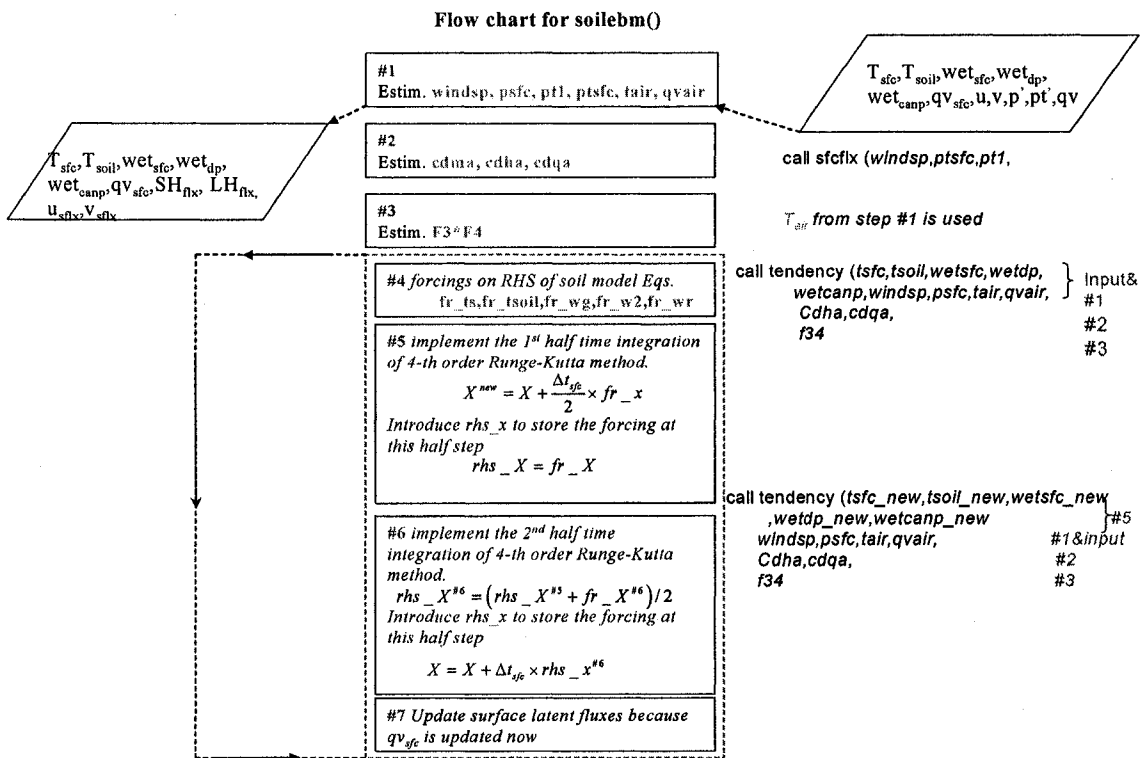


Figure 3.1. Flow chart of subroutine soilebm

### 3.1.2. Verifications of TLM and ADM

Because ADM is based on TLM, or the former is the matrix transform of the latter, the error sources of TLM are also the error sources of ADM. However, functions of TLM and ADM models are essentially different. TLM is used to approximate the evolution of a small perturbation on forward model. The time integration is forward. However, the backward integration of ADM is to unveil the sources of the perturbation. The adjoint variables corresponding to output of the forward model is actually input in the backward integration. Reflected on the hand coding, for each statement, the perturbation of the right hand terms are expressed in the form of perturbation on left hand side term.

Generally, we have the following two methods to verify the correctness of the adjoint model, all based on the definition of adjoint operator. The first method uses the inner product of the solutions to the direct and adjoint equations, a time invariant quantity [LeDimet and Talagrand, 1986, Eqs. (4.4) and (4.8)]. For tangent linear model R,

$$a) \quad \langle R(t_0, t_n) \delta X(t_0), R(t_0, t_n) \delta X(t_0) \rangle = \langle R^*(t_n, t_0) R(t_0, t_n) \delta X(t_0), \delta X(t_0) \rangle.$$

Here the notations agree with those in Appendix2. The left hand side of (a) is the inner product of tangent linear perturbation vector at the ending time, and should equal to the inner product of adjoint variable at the initial time. Note that the right hand side is the inner product of perturbation at initial with a vector that is produced by adjoint integration starting from the ending point value of tangent linear model.

Considering that the magnitudes of different control variables are quite different. For example, soil moisture is less than 1.0 whereas soil temperatures are around 300. If all variables are perturbed simultaneously, the small quantities (consider only the

numbers, not the units) tends to be overshadowed by the larger quantities in the inner product. Therefore, component-by-component verification may be more trust-worthy.

b) Using the  $i$ th base vector  $e_i = (0, 0, 0, \dots, 1, 0, \dots, 0)$  as initial perturbation to TLM, after integration to time level  $t_n$ , one gets the following relationship  $\langle R^*(t_0, t_n), e_i \rangle_j = \langle R(t_n, t_0), e_j \rangle_i$ .

These two methods are especially suitable for hand-coded adjoint with TLM kept for verification purpose. The verification of the adjoint code for the Lorenz system is presented in Appendix 3 (Fig. 3A.2&3).

### 3.2. Verification of The 4DVAR Data Assimilation System

The function of ADM in a 4DVAR system is to estimate the gradient of cost-function with respect to control variables. It is thus critically important to verify the correctness of the 4DVAR assimilation system. The correctness of the gradient value is verified against the Taylor expansion of cost function around control variables (p32. in Wang 1993)

$$I(\alpha) = \frac{J(U(t_0) + \alpha h) - J(U(t_0))}{\alpha h^T \nabla J(U(t_0))} = 1.0 + o(\alpha). \quad (3.1)$$

Where  $\alpha$  is a small scalar (real number),  $h$  is a random perturbation vector which can be generated by using the Fortran library function, and  $h^T$  is the transpose of  $h$ .

For values of  $\alpha$  which are small but not very close to the machine zero, one should expect a value of  $I(\alpha)$  approaching 1 linearly for a wide range of magnitudes of  $\alpha$ . The experiment was performed using forced run of the land surface model with cost function defined as Eq. (2.31). The micrometeorological forcing variables are those of

00Z, 04-06 August 2000 OASIS measurements at Norman super-site (as discussed in detail in Subsection 2.1 and also Chapter 5). The results are shown in Figure 3.2. It is clearly seen that for values of  $\alpha$  between  $10^1$ - $10^{-4}$  unit values for  $I(\alpha)$  are obtained. The correctness of the gradient of the cost function and the correctness of the vector product have therefore been verified.

In this chapter, we systematically illustrated the procedures of ADM and TLM model construction and verification. The application of these general rules to our model system is discussed. Our ADM and TLM are proved error free and laid the solid foundation for real data assimilation. Also, the optimization routines are constructed with reference to ARPS data assimilation system.

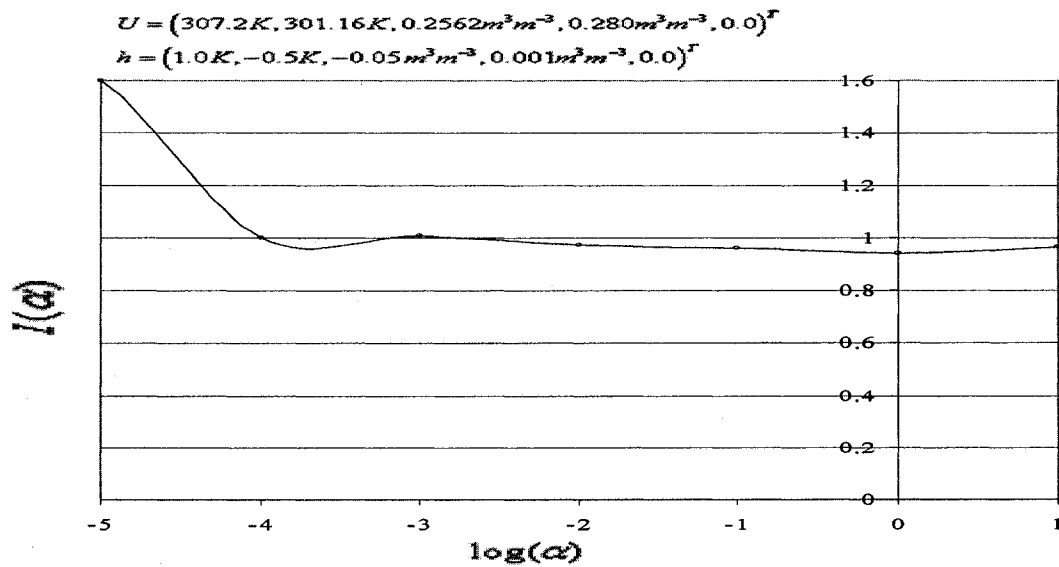


Figure 3.2. Verifications of the correctness of the gradient calculation by ADM. This experiment is done with the micrometeorological observations of 00Z, 04-06 August 2000 at Norman OASIS super site. Function  $I$  as defined in Eq. (3.1) is plotted. The curve deviates from unity for different reasons as  $\alpha \rightarrow 10^{-5}$  and  $\alpha \rightarrow 10^2$ . The former is due to truncation error while the latter is because the small perturbation assumption is violated.

## Chapter Four

### *Initial Condition and Model Parameter Sensitivity Experiments*

One important aim of this study is to assimilate the screen-level atmospheric variables for the estimation of soil moisture and temperature. To this end, sensitivity experiments should be performed to see if the screen-level atmospheric parameters are sensitive to the variation of surface soil moisture/temperature.

Compared with finite difference technique (which perform two forward run with slightly perturbed value on one control variable to estimate the gradient of the cost function with respect to this control variable), an important superiority of adjoint technique lies with its ability to efficiently trace the origins of these sensitivities (Giering and Kaminski 1998). Diagnostic insight into the relative sensitivities and estimation of the influence functions for different parameter can be obtained through tangent linear sensitivity study. Pathways of sensitivity can also be obtained by decomposing the adjoint sensitivities.

As a benchmark for the tangent linear sensitivity and the ensuing data assimilation experiments, Subsection 4.1 discusses some results from the nonlinear sensitivity experiments. Subsections 4.2 and 4.3 are respectively dedicated for tangent linear sensitivity and adjoint sensitivity studies.



#### 4.1. Nonlinear Sensitivity Experiments

In a non-linear system, the model sensitivity to a perturbation on a certain prognostic variable at a certain time depends sensitively on the values of the remaining variables. It is not possible to conclude the sensitivity at all circumstances. Our results in this subsection should be viewed just as case studies. The first reference run configuration is set exactly the same as the dry case for verification study in Subsection 2.3. We will examine the model sensitivities to each control variable (except canopy water because it is insignificant for this study period), measured by the departures from the reference run by atmospheric potential temperature and vapor specific humidity. In the following nonlinear forward model based sensitivity experiments, the perturbations made to the initial values of prognostic variables are all comparable with the usual model forecasting error magnitudes and also significantly larger than instrument uncertainties.

Sensitive or not is based on the comparison with the daily cycle magnitude of the quantity of interest, i.e., relative importance. We use three statistical indices to quantify the difference between each forward model run with the reference run: maximum difference between two time series (*MAE*), mean bias error (*MBE*) and root mean squared error (*rms* or *RMSE*). For easier comparisons, they are listed inside the figures except for those of profiles.

Before discussing the model sensitivity to a perturbation on soil moisture, an examination of the relative importance of the three latent heat flux components is informative because the relative contribution from the three components (defined in Subsection 2.2.1) is indicative of water moisture depletion distribution among soil slab. Figure 4.1 shows the percentages of the latent heat fluxes relative to the total latent heat

flux. Dew is insignificant at night and there is no canopy interception at this period of two days. Figure 4.1 reveals the fact that, during this drying down period, the vegetation is rather stressed. Even with a vegetation-coverage as high as 75%, less than 40% of the latent heat flux is from the transpiration ( $E_{tr}$ ) in this case. More than 60% of the water vapor is evaporated from the 10 cm surface soil layer. An interesting phenomenon under this condition is that, an increase in vegetation-cover raises the daily cycle amplitude of the skin temperature, resulting from a reduced latent heat flux thus more heat is used to heat the ground. This assertion is further confirmed by numerical experiments use different vegetation coverage while keep the remaining parameter setting the same as the reference configuration.

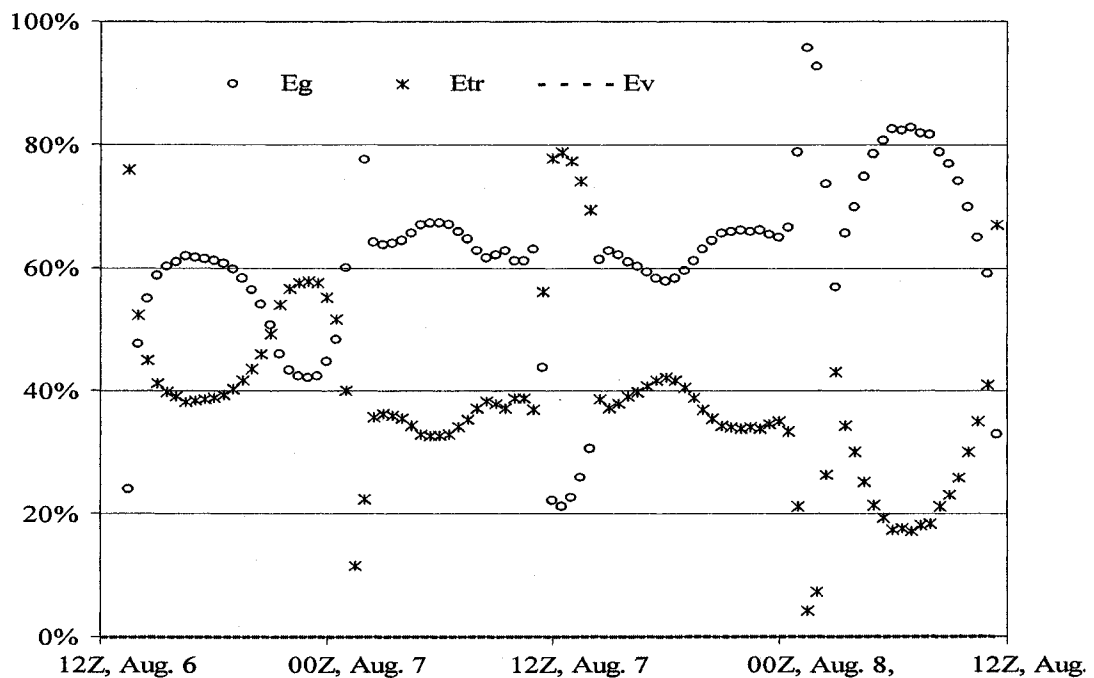


Figure 4.1. The relative contributions to the total latent heat flux from the three reservoirs ( $E_g$ ,  $E_{tr}$ , and  $E_v$ ). With vegetation cover as high as 75%, the bulk of latent heat flux is still from the ground  $E_g$  (over 60% during peak hours during daytime), showing a stressed vegetation growth during this period.

The sensitivity of surface state variables and fluxes to initial superficial soil moisture contents is shown in Figure 4.2 and 4.3. The initial superficial soil moisture is varied down to 0.2026 and up to 0.4026 with increment of  $0.05 \text{ m}^3 \text{ m}^{-3}$ . The one starts with  $0.3026 \text{ m}^3 \text{ m}^{-3}$  is actually the reference run. From Figure 4.2*c, e, & f*, for surface soil moisture and surface fluxes, the difference in initial surface soil moisture disappears within 1.5 days. However, the effects on soil temperatures and deep soil moisture last much longer time (Figure 4.2*a, b&d*). For this magnitude of uncertainty ( $0.2 \text{ m}^3 \text{ m}^{-3}$ ), all land surface states and surface fluxes are sensitive to the perturbation in surface soil moisture.

Figure 4.3 shows the sensitivity of atmospheric potential temperature and specific humidity to initial surface soil moisture. The influence at 12 hours later can propagate as high as 730 mb. At the surface the perturbation can be over 50% of its daily cycle amplitude. Figure 4.3a indicates that high surface soil moisture contents result in lower atmospheric potential temperature within the whole planetary boundary layer. The physical explanation is that surface net radiative energy balance is mainly used for evaporating soil water and less is spent for heating the ground. Thus, turbulent mixing is weaker and the lower potential temperature profile is resulted. Figure 4.3b indicates that the mixing ratio profile has a positive response to increased surface soil moisture content, indicating more moisture is transferred and mixed into the atmosphere although the daytime mixing is weaker.

For the two quantities to be assimilated (screen-level air potential temperature and specific humidity), we calculated the *rms*, *MAE* and *MBE*. The *rms* difference can be 4.3K for  $T_{air}$  and 4 g/kg for  $qv_{air}$ , for  $0.1 \text{ m}^3 \text{ m}^{-3}$  changes in initial  $w_{sfc}$ .

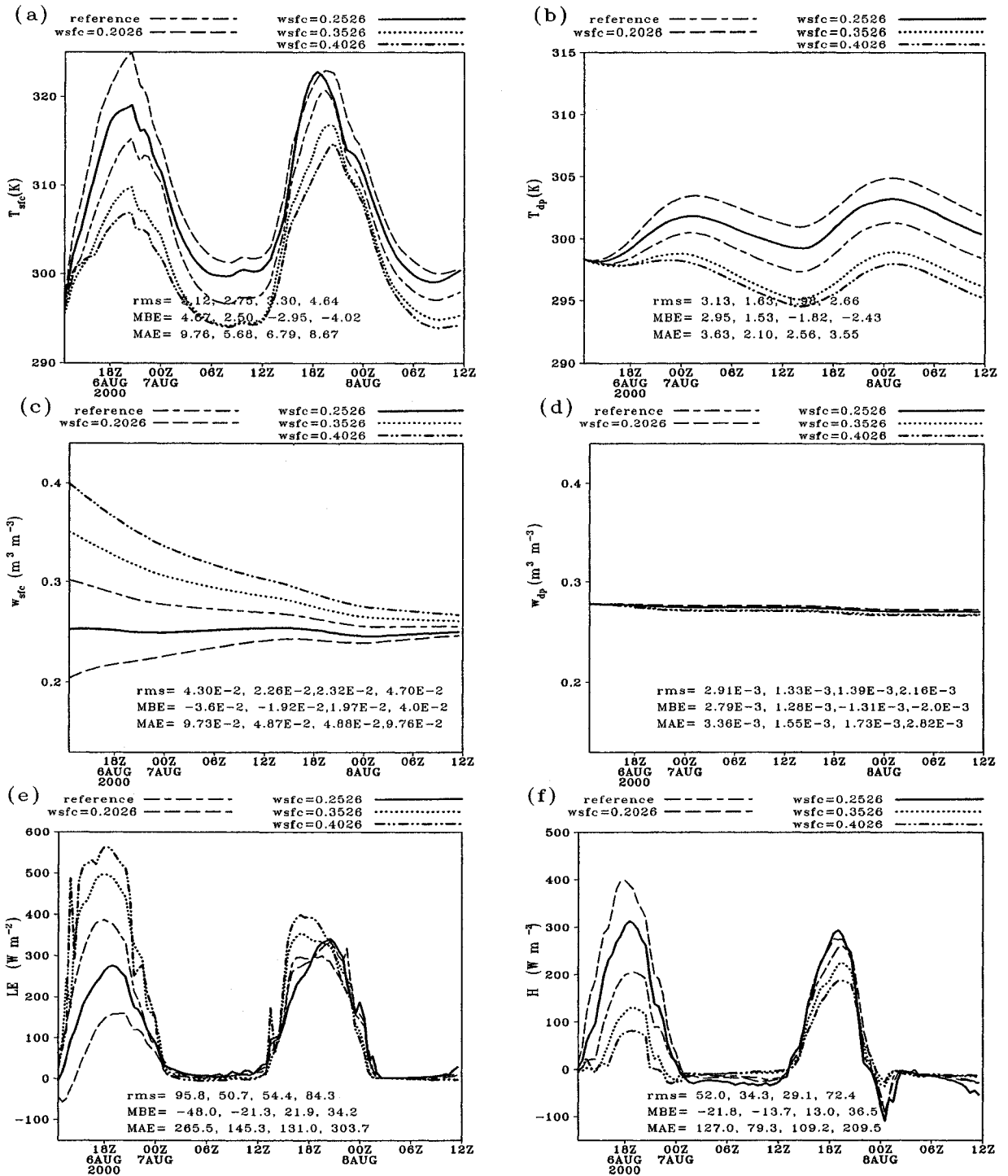


Figure 4.2. Sensitivity of surface variables and surface fluxes to  $w_{sfc}$ , for a magnitude of uncertainty of  $0.2 m^3 m^{-3}$ .

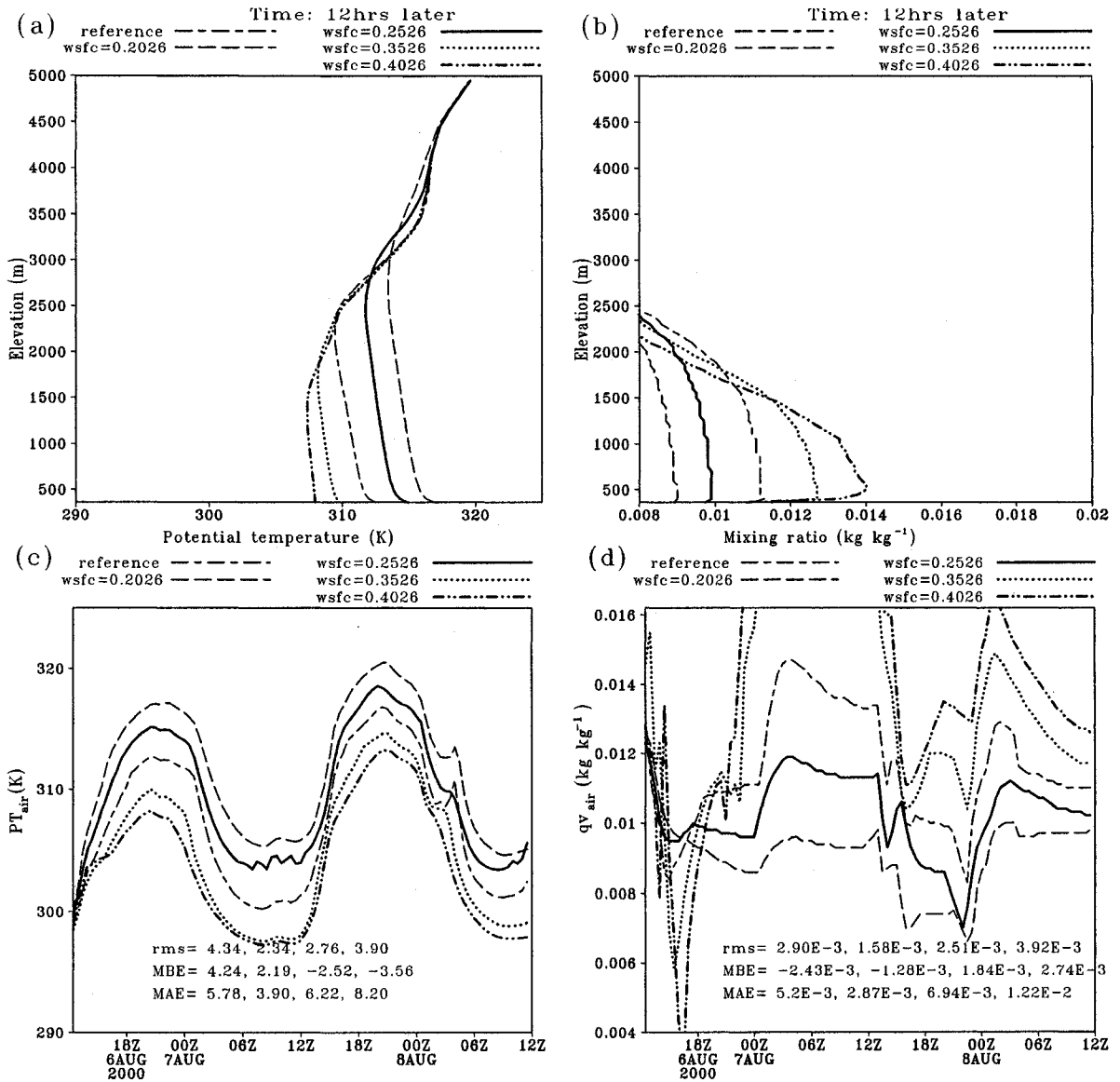


Figure 4.3. Variations in profile air potential temperature and mixing ratio in response to changes in initial  $w_{sfc}$ . The atmospheric properties are sensitive to surface soil moisture uncertainty. The influence at 12 hr later can propagate as high as 2000 m (*a* and *b*). At the surface the uncertainty can be over 30% of its daily cycle amplitude (*c* and *d*).

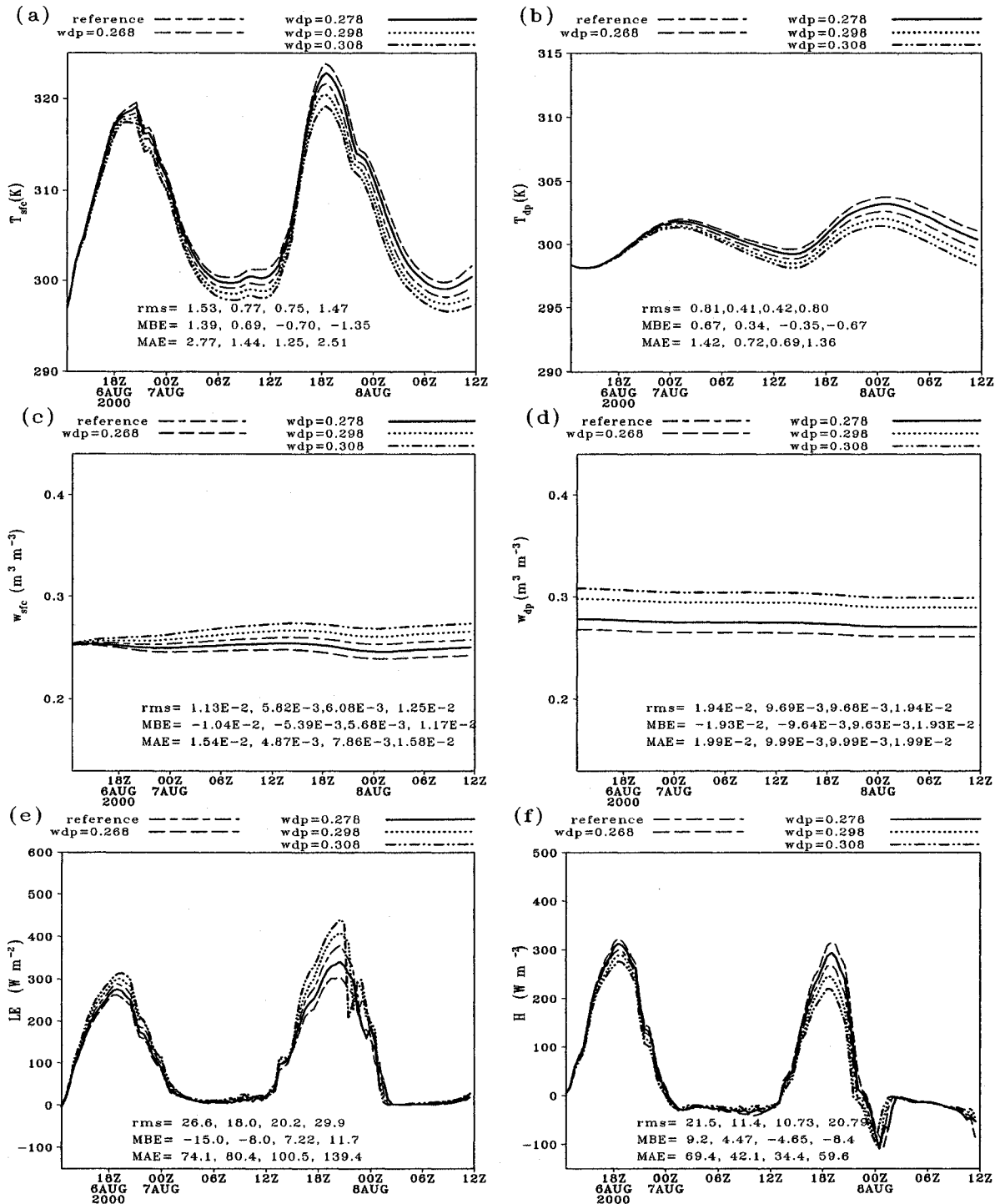


Figure 4.4. Sensitivity of land variables (a-d) and surface fluxes (e and f) to initial deep soil moisture uncertainty of  $0.04 m^3 m^{-3}$ . The difference in initial surface soil moisture is long lasting, resulting from the fact that the deep soil layer is a much larger reservoir than the surface layer.

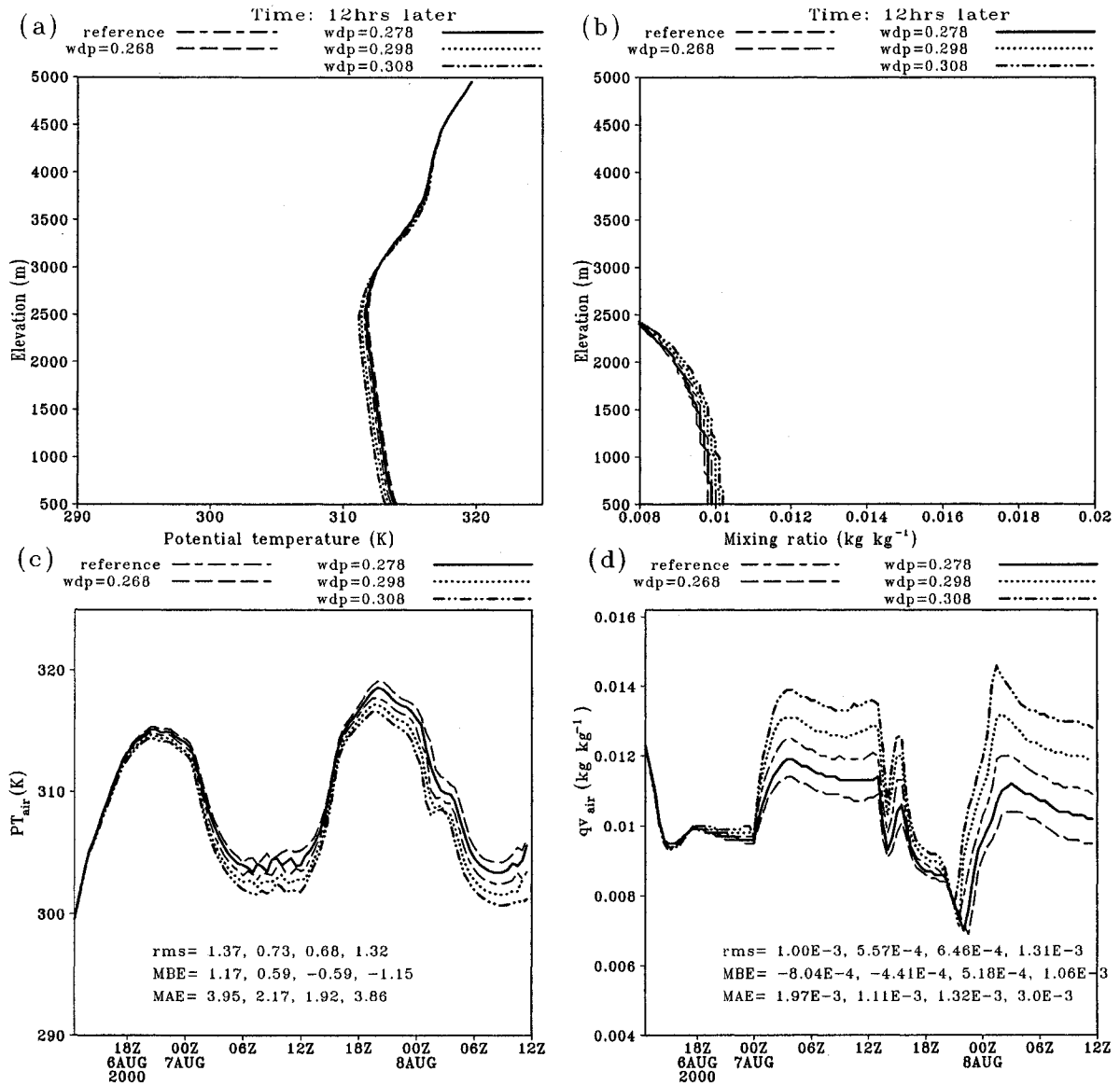


Figure 4.5. The atmospheric properties such as potential temperature (a) and specific humidity (b) are also rather sensitive to deep soil moisture uncertainty. In comparison to Figure 4.3, the effects of deep soil moisture perturbation are far less direct, though. The time series at 2m are plotted (c and d) to show the most sensitive periods.

Because the deep soil is 9 times thicker than the surface layer, the water holding capacity is an order of magnitude larger. That is why perturbations of an order of magnitude smaller ( $\pm 0.05$  in Figure 4.4 and 4.5) on initial deep soil moisture can cause

similar sensitivity (e.g., *rms* error  $\sim 30 \text{ W m}^{-2}$  for *LE* and *H*). Also, its effects on all other components are persistent.

From Figs. 4a&c, different initial values of  $w_{dp}$  result in very distinct evolutions of the simulated  $w_{sfc}$  and  $T_{sfc}$ . It is based on this fact that Calvet *et al.* (1998) asserted the possibility of obtaining information of  $w_{dp}$  from observing surface ground temperature ( $T_{sfc}$ ) and superficial soil moisture ( $w_{sfc}$ ).

A difference from the case of perturbing surface moisture is that the atmospheric responses to deep soil moisture changes are less direct (cf. Figure 4.5a&b with Figure 4.3a&b). The maximum difference at 18Z is at the surface level, where the maximum departure from the reference run is only 20% the corresponding amount in Figure 4.3b. Similar situations exist for potential temperature (cf. Figure 4.5a with Figure 4.3a).

It is a quite different scenario for the model sensitivity with respect to soil surface temperature as indicated in Figure 4.6 and 4.7. Even with an error in initial surface temperature as large as 5 K (instrument error is usually about 1K) inserted at this time of a day (12Z, or early morning hours), the only land surface component that is sensitive to this perturbation is deep soil temperature. This strongly suggests that, during the solar insolation quickly increasing period, error on the initial surface soil temperature is not an important issue for model predictability. The insensitivity (e.g., *rms* error  $< 10 \text{ W m}^{-2}$  for *LE* and *H*) of atmospheric components to initial deep soil temperature error, as shown in Figure 4.8 and 4.9, is also due to the fact that there is no direct contact between the deep soil and the atmosphere.



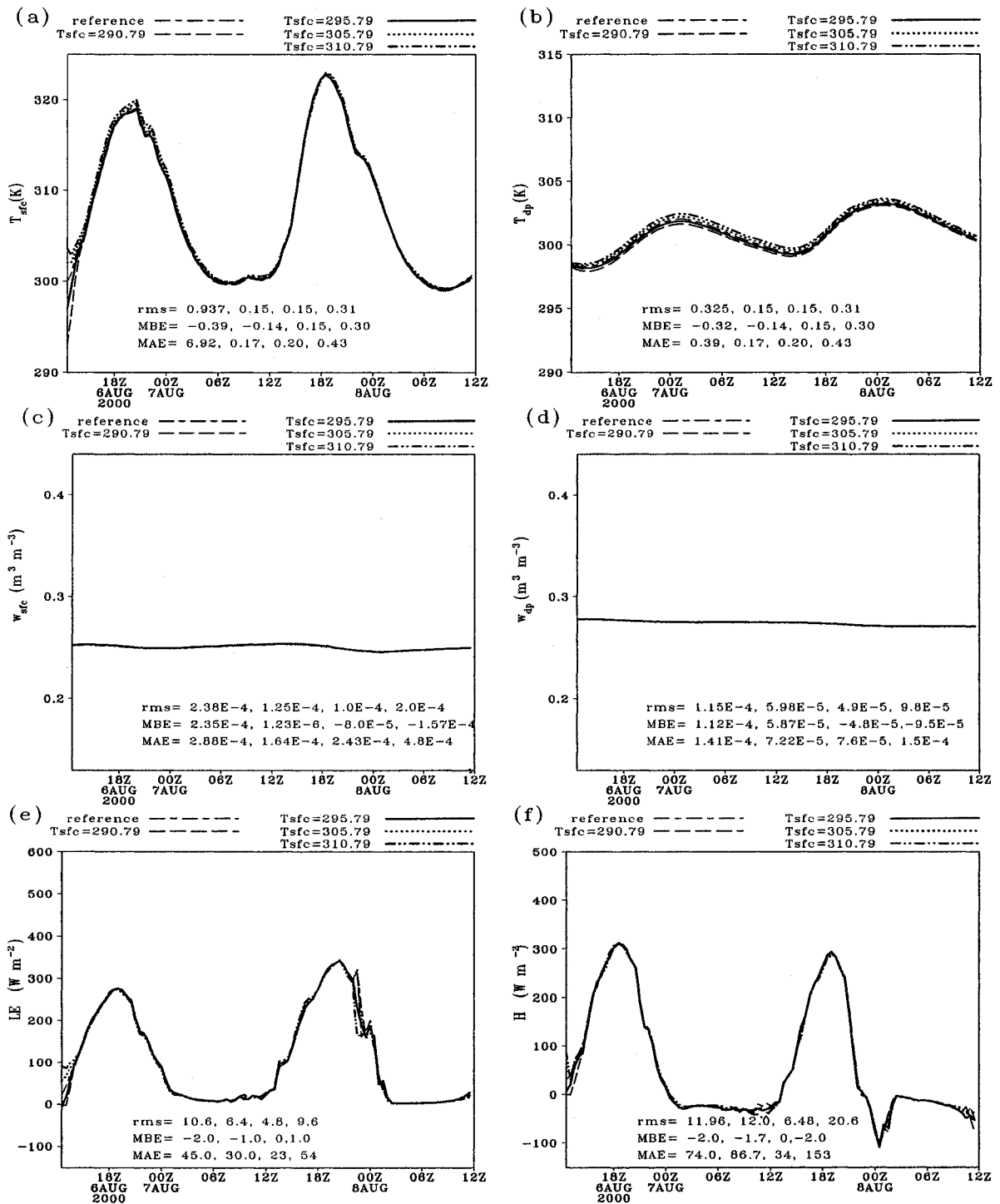


Figure 4.6. Same as Figs. 4.2 and 4.4 but for sensitivities of land variables (a-d) and surface fluxes (e and f) to initial  $T_{sfc}$ .

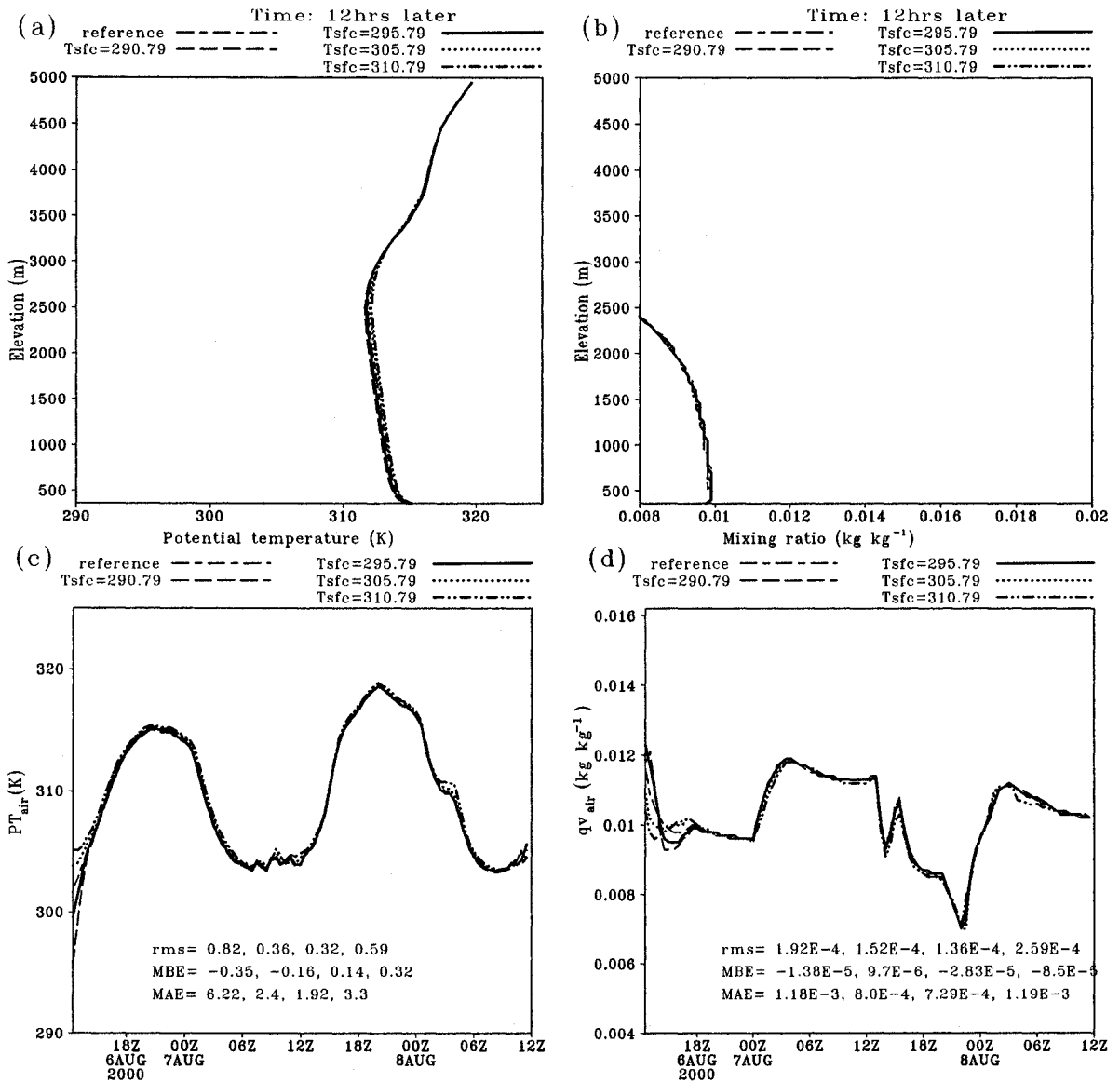


Figure 4.7. The effects of perturbing  $T_{sfc}$  on atmospheric components.

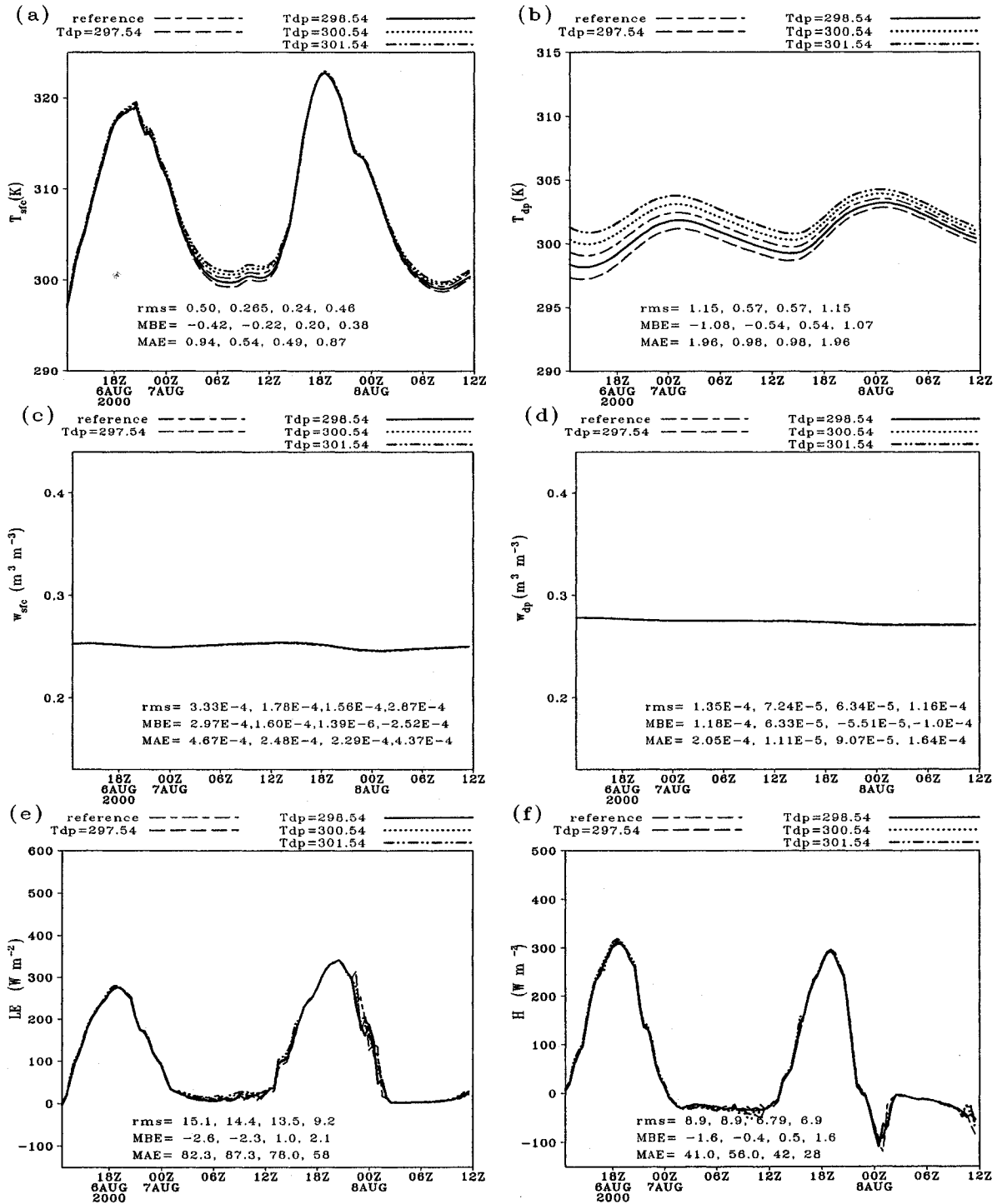


Figure 4.8. Sensitivities of land variables (a-d) and surface fluxes (e and f) to perturbation on deep soil temperature.

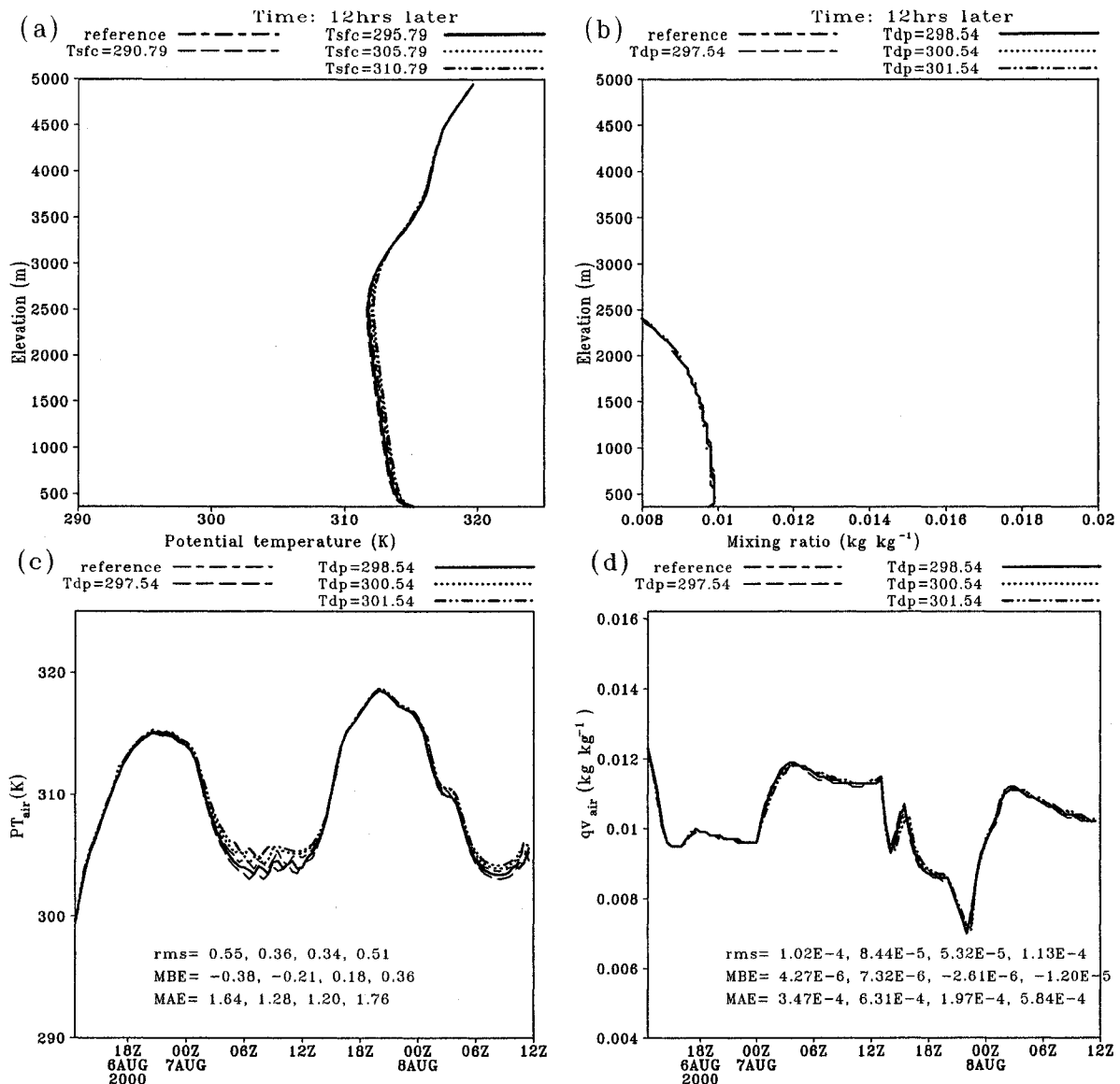


Figure 4.9. Sensitivities of atmospheric components to variations on initial deep soil temperature. Not sensitive to the uncertainty in deep soil temperature of 1K.

Exactly parallel sensitivity experiments are performed for the selected wet period. The reference run is the verified wet period (July 06-08, 2000) in Chapter 2. We then perturbed the initial  $T_{sfc}$  five times down from 298K and up to 318 K with increment value of 5K;  $T_{dp}$  five times down from 299K and up to 303K with increment of 1K each time. The statistics of differences (as compared with the reference run) such as *MBE* (Mean Bias Error); *rms* (root mean squared error) and *MAE* (Maximum Absolute Error) are summarized in Table 4. 1 and Table 4. 2.

The influence for perturbing initial value of  $T_{sfc}$  is most significant on sensible heat flux. The maximum difference can be as large as  $205 \text{ W m}^{-2}$  for  $\Delta T_{sfc} = -10\text{K}$ . The duration of the sensitivity period is the first 18 hours. At twelve hours later, the air potential temperature profile changed most between 100-1400m, rather than near surface level. The effects on mixing ratio are similar but manifest mostly near surface. The sensitivity to  $T_{dp}$  is most apparent during nighttime, most apparent on air potential temperature and  $T_{sfc}$  time series. The sensitivity lasts  $\sim 40$  hours for our chosen perturbation range. From Table 4. 1 and Table 4. 2, it seems that the sensitivities to both  $T_{sfc}$  and  $T_{dp}$  scale linearly within our perturbation ranges.

For this wet period, except for the curve corresponds the driest end ( $0.329 \text{ m}^3 \text{ m}^{-3}$ ), there is nearly no sensitivity from the surface variables and surface fluxes to initial values of  $w_{sfc}$ , as indicated by Figure 4.10. Same assertions can be made for the air potential temperature and mixing ratio (Figure 4.11). This is because as soil moisture near field capacity, the latent heat flux is no longer sensitive to its variation. Thus variational retrieval may not be effective in retrieving the exact initial surface soil moisture value. For the driest curve, the effects on all the land surface quantities last long,

though. For our selected perturbation range, there is nearly no sensitivity to initial deep soil moisture variations (Figure 4.12 and 13), drastically different for the drying period case. The emphasis of soil moisture content on NWP, as indicated by many studies (see Introduction section) should be viewed as for the relatively dry period.

Table 4.1 Sensitivity to  $T_{sfc}$

	$PT(K)$	$q_v(kg/kg)$	$T_{sfc}(K)$	$T_{dp}(K)$	$w_{sfc}(m^3m^{-3})$	$w_{dp}(m^3m^{-3})$	$H(Wm^{-2})$	$LE(Wm^{-2})$
<b>RMSE</b>								
$\Delta T_{sfc} = -10K$	0.40	$8.73 \times 10^{-4}$	0.32	0.11	$1.42 \times 10^{-5}$	$5.0 \times 10^{-4}$	7.1	24.0
$\Delta T_{sfc} = -5K$	0.17	$3.56 \times 10^{-4}$	0.14	0.0488	$6.97 \times 10^{-6}$	$2.41 \times 10^{-4}$	3.45	8.25
$\Delta T_{sfc} = 5K$	0.19	$2.64 \times 10^{-4}$	0.13	0.0587	$6.66 \times 10^{-6}$	$2.25 \times 10^{-4}$	3.94	11.29
$\Delta T_{sfc} = 10K$	0.33	$4.26 \times 10^{-4}$	0.27	0.135	$1.23 \times 10^{-5}$	$4.23 \times 10^{-4}$	6.2	13.60
<b>MBE</b>								
$\Delta T_{sfc} = -10K$	-0.22	$4.9 \times 10^{-4}$	-0.11	-0.11	$1.11 \times 10^{-5}$	$4.98 \times 10^{-4}$	1.24	-5.54
$\Delta T_{sfc} = -5K$	-0.094	$1.73 \times 10^{-4}$	-0.05	-0.047	$5.68 \times 10^{-6}$	$2.39 \times 10^{-4}$	0.73	-2.3
$\Delta T_{sfc} = 5K$	0.10	$-1.33 \times 10^{-4}$	0.064	0.058	$-5.79 \times 10^{-6}$	$-2.23 \times 10^{-4}$	-1.06	2.12
$\Delta T_{sfc} = 10K$	0.24	$-2.0 \times 10^{-4}$	0.17	0.13	$-1.04 \times 10^{-5}$	$-4.2 \times 10^{-4}$	-1.66	3.20
<b>MAE</b>								
$\Delta T_{sfc} = -10K$	2.65	$2.7 \times 10^{-3}$	2.5	0.15	$3.64 \times 10^{-5}$	$5.6 \times 10^{-4}$	40	205
$\Delta T_{sfc} = -5K$	0.98	$9.65 \times 10^{-4}$	1.16	0.0725	$1.59 \times 10^{-5}$	$2.61 \times 10^{-4}$	15.7	56
$\Delta T_{sfc} = 5K$	0.84	$7.64 \times 10^{-4}$	0.97	0.0716	$1.43 \times 10^{-5}$	$2.51 \times 10^{-4}$	28.85	100
$\Delta T_{sfc} = 10K$	1.47	$1.24 \times 10^{-3}$	1.85	0.15	$2.83 \times 10^{-5}$	$4.69 \times 10^{-4}$	31	109

Note: MBE means Mean Bias Error; and MAE means Maximum Absolute Error.

Table 4.2 Sensitivity to  $T_{dp}$

	$T_{air}(K)$	$q_v(kg/kg)$	$T_{sfc}(K)$	$T_{dp}(K)$	$w_{sfc}(m^3m^{-3})$	$w_{dp}(m^3m^{-3})$	$H(Wm^{-2})$	$LE(Wm^{-2})$
<b>RMSE</b>								
$\Delta T_{dp} = -2K$	0.44	$8.11 \times 10^{-5}$	0.46	1.17	$1.83 \times 10^{-5}$	$3.25 \times 10^{-4}$	2.84	9.24
$\Delta T_{dp} = -1K$	0.20	$6.44 \times 10^{-5}$	0.22	0.58	$8.87 \times 10^{-6}$	$1.61 \times 10^{-4}$	1.60	6.93
$\Delta T_{dp} = 1K$	0.19	$7.05 \times 10^{-5}$	0.20	0.57	$9.42 \times 10^{-6}$	$1.74 \times 10^{-4}$	1.64	4.99
$\Delta T_{dp} = 2K$	0.35	$1.08 \times 10^{-4}$	0.36	1.12	$2.02 \times 10^{-5}$	$3.69 \times 10^{-4}$	3.32	9.65
<b>MBE</b>								
$\Delta T_{dp} = -2K$	-0.38	$-1.26 \times 10^{-5}$	-0.39	-1.10	$1.67 \times 10^{-5}$	$2.95 \times 10^{-4}$	-0.19	-7.59
$\Delta T_{dp} = -1K$	-0.17	$-2.82 \times 10^{-5}$	-0.19	-0.54	$8.20 \times 10^{-6}$	$1.47 \times 10^{-4}$	-0.27	3.95
$\Delta T_{dp} = 1K$	0.16	$1.98 \times 10^{-5}$	0.18	0.53	$-8.85 \times 10^{-6}$	$-1.60 \times 10^{-4}$	0.44	2.92
$\Delta T_{dp} = 2K$	0.28	$5.32 \times 10^{-5}$	0.31	1.04	$-1.90 \times 10^{-5}$	$-3.4 \times 10^{-4}$	0.52	6.67
<b>MAE</b>								
$\Delta T_{dp} = -2K$	0.76	$3.85 \times 10^{-4}$	0.76	1.96	$3.48 \times 10^{-5}$	$5.07 \times 10^{-4}$	7.32	24.87
$\Delta T_{dp} = -1K$	0.37	$3.10 \times 10^{-4}$	0.37	0.98	$1.61 \times 10^{-5}$	$2.43 \times 10^{-4}$	5.75	52.8
$\Delta T_{dp} = 1K$	0.42	$1.84 \times 10^{-4}$	0.33	0.98	$1.35 \times 10^{-5}$	$2.36 \times 10^{-4}$	3.34	17.36
$\Delta T_{dp} = 2K$	0.67	$2.45 \times 10^{-4}$	0.57	1.96	$2.92 \times 10^{-5}$	$5.0 \times 10^{-4}$	9.24	28.4

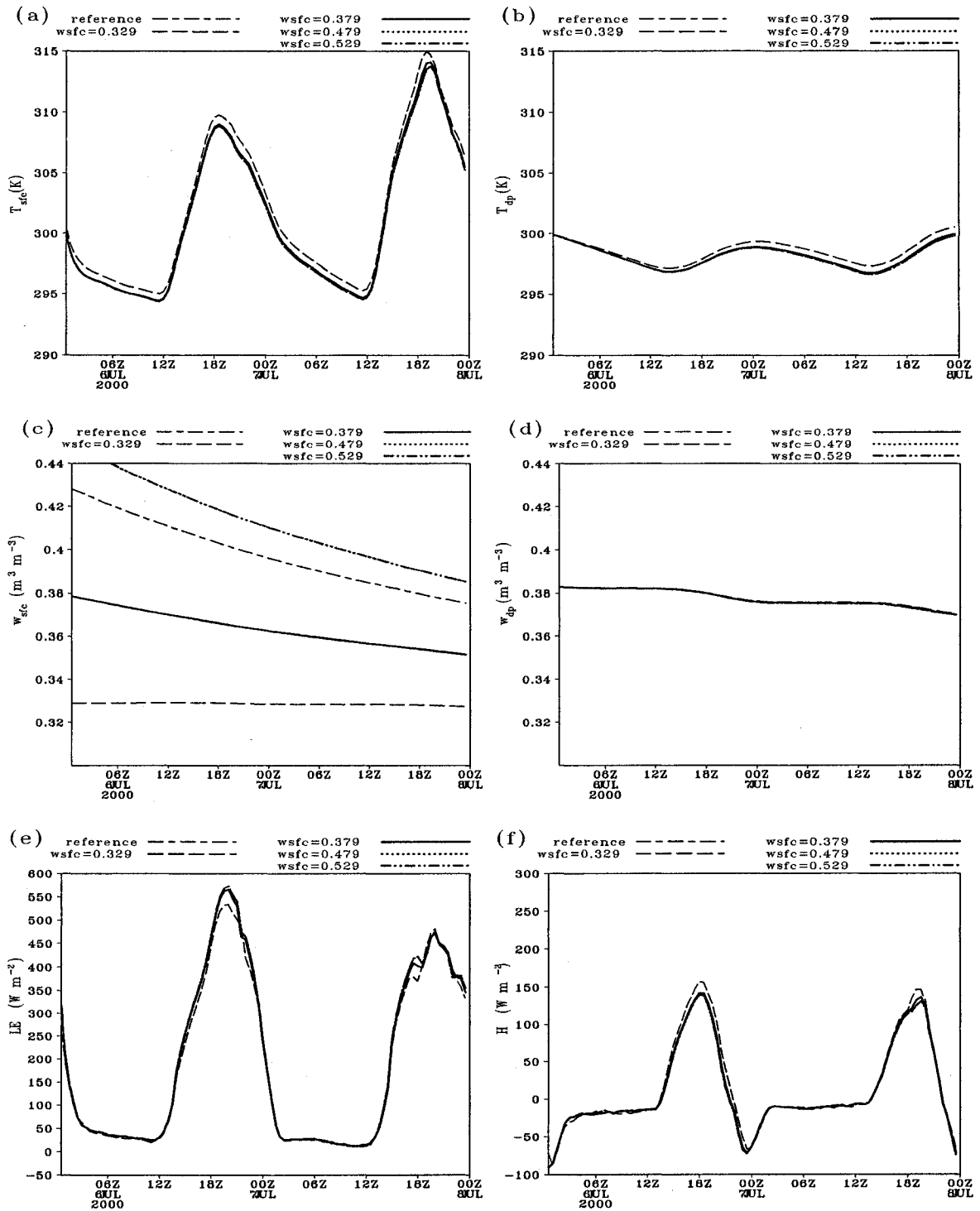


Figure 4.10. Sensitivity of surface variables and surface fluxes to initial value of  $w_{sfc}$ .



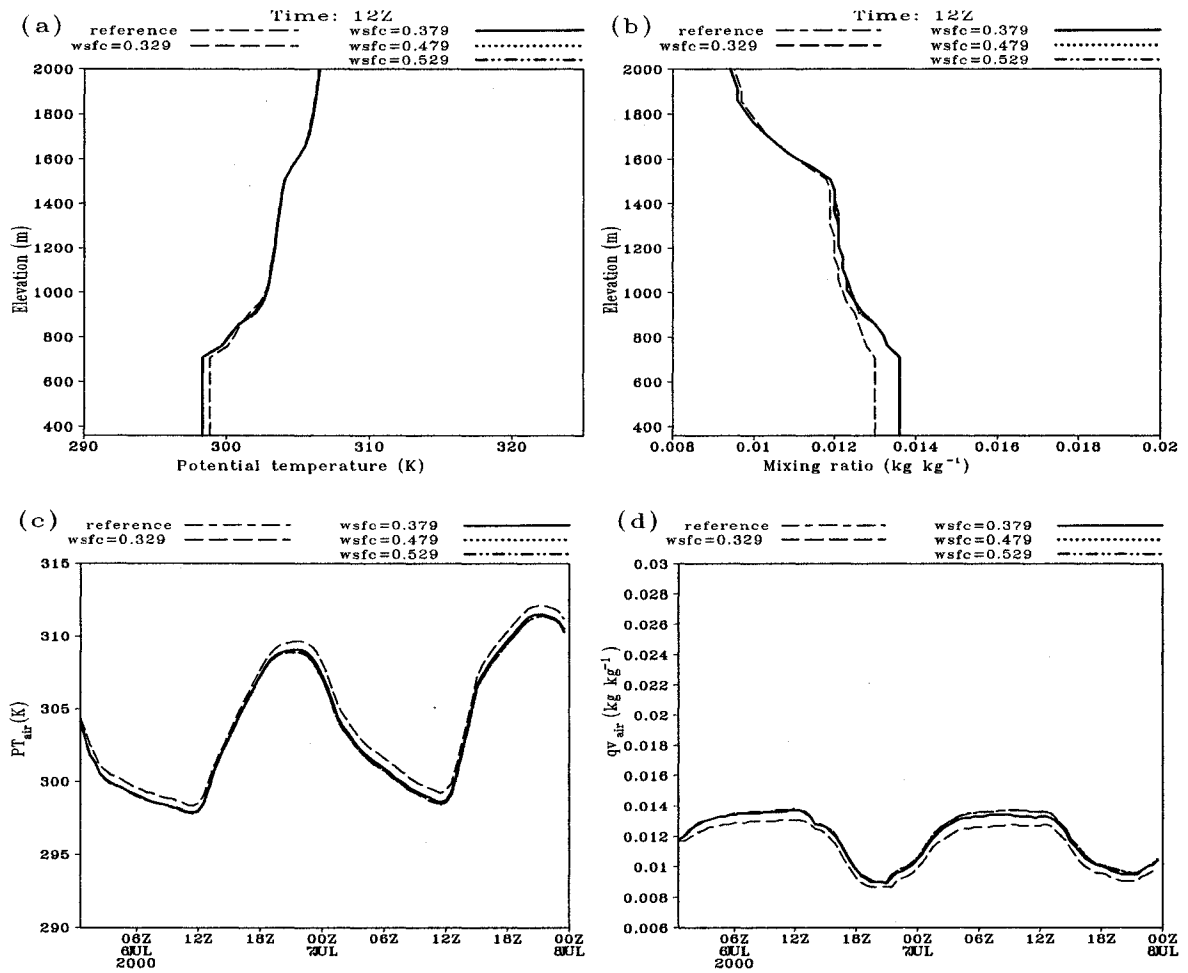


Figure 4.11. Sensitivity of air potential temperature and mixing ratio to initial value of  $w_{sfc}$ . Those at screen-level are also plotted.

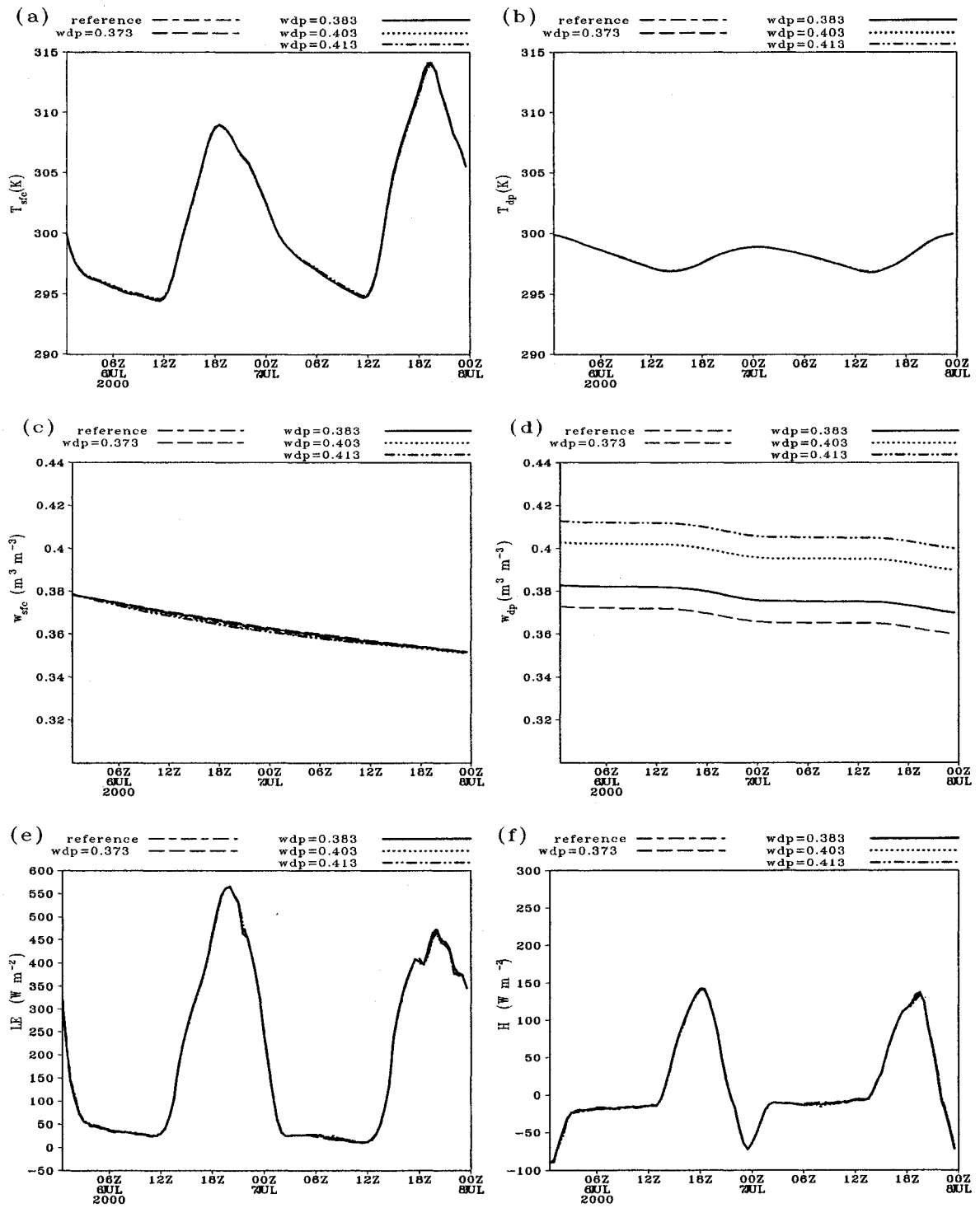


Figure 4.12. Sensitivity of surface variables and surface fluxes to initial value of  $w_{dp}$ .

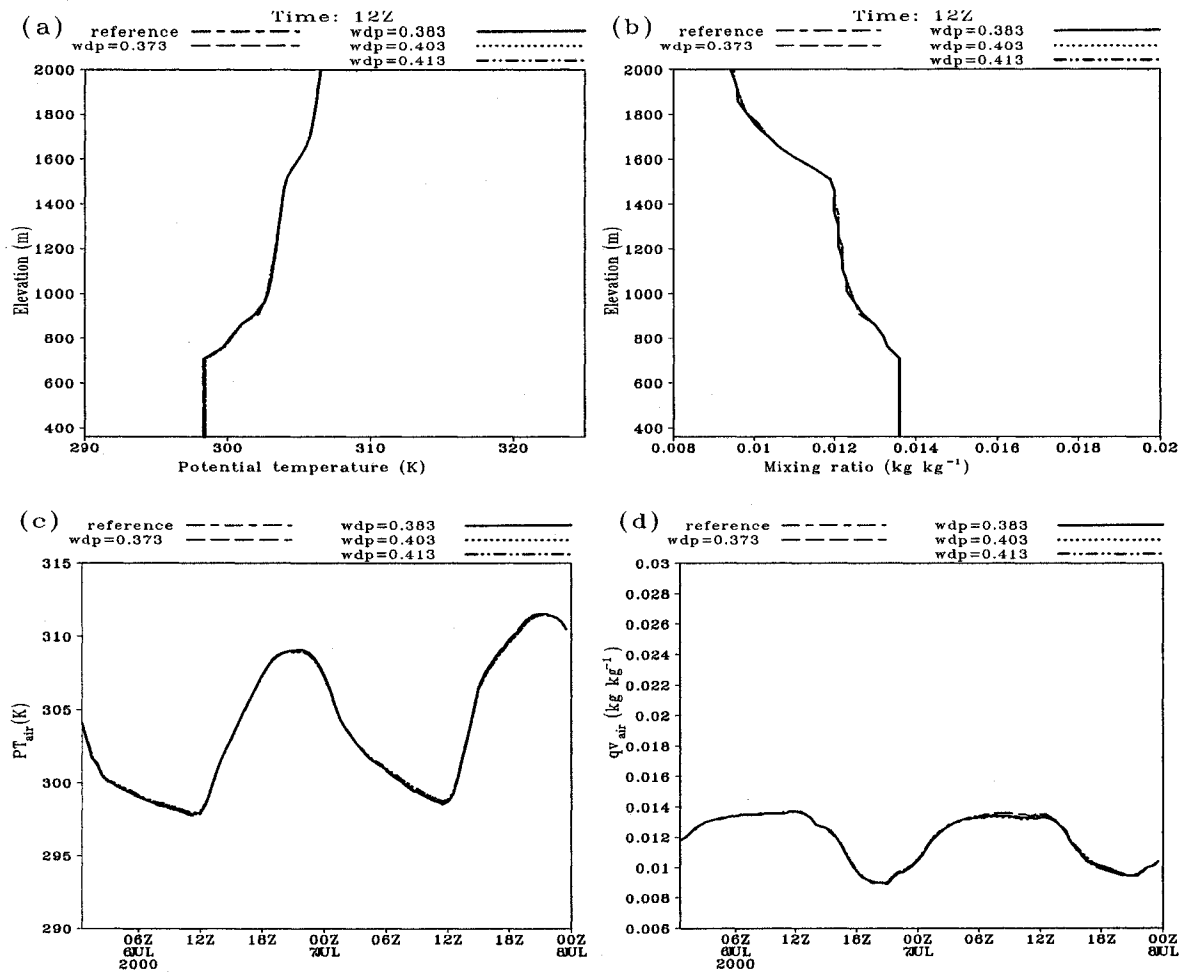


Figure 4.13. Sensitivity of air potential temperature and mixing ratio to initial value of  $w_{dp}$ . Those at screen-level are also plotted.

In this subsection, we want to evaluate the influence of each surface parameter on the surface fluxes and the screen-level parameters. We presented the results of four experiments realized with an initial perturbation on  $T_{sfc}$ ,  $T_{dp}$ ,  $w_{sfc}$  and  $w_{dp}$  separately and respectively. Through analyzing these figure, we observed the consequences of the surface perturbations on the surface fluxes as well as the evolution of the atmospheric components. For the dry period, these quantities are very sensitive to the soil water contents. An augmentation of the soil moisture increases the latent heat flux and reduces

the sensible heat flux. The influence of a perturbation on the deep soil water content lasts longer than the impact of the perturbation on the superficial reservoir moisture content, because of the small capacity of the superficial reservoir. The influence of the mean temperature on surface fluxes is very low whereas the one of the surface temperature is quite unnoticeable. During the strong solar insolation time period, the screen-level parameters are forced by the surface fluxes and thus depend sensitively on the soil water contents. The soil moistures have an impact during night inasmuch as the air at 2m does not reach the saturation point. When it does happen, the soil humidity becomes independent of the 2m specific humidity. As a conclusion to the nonlinear sensitivity experiments for the dry period, we think the soil moisture will be retrievable with a rather high confidence whereas the soil temperature will be harder to retrieve. A parallel series of sensitivity experiments performed during a wet period yield drastically different scenarios: nearly no sensitivity for deep soil moisture.

#### *4.2. Tangent Linear Sensitivity*

The tangent linear model is the linearization of the forward model around a nonlinear state (Eq. 2.30). The adjoint is formally a transpose of the tangent linear model (Eqs. A2.3-A2.7). Thus the issue of nonlinearity is relevant for adjoint and tangent linear model. Verifying the validity of tangent linearization is a necessary step preceding adjoint retrieval exercises. In this subsection, we discuss first the validation of the tangent linear hypothesis, secondly we will use the tangent linear model to evaluate the influence of the surface parameters on surface fluxes and screen-level parameters.

The tangent linear model describes the impacts on the forecast of an initial perturbation. It corresponds well with the real forecast done with the perturbed state as

long as the initial perturbation is small. We want here to evaluate if the tangent linear hypothesis is still valid for a mean perturbation. The magnitude of the chosen perturbation is of the same order as the *rms* forecast errors on soil variables:  $\delta T_s = +2^\circ K$ ,  $\delta T_2 = +0.5^\circ K$ ,  $\delta w_g = 0.05$ , and  $\delta w_2 = 0.01$ .  $U$  represents the initial surface state,  $\delta U$  the perturbation,  $M$  the direct model and  $M'$  the tangent linear model. We will plot a 48 hour forecast of the different curves  $M(U)$ ,  $M(U + \delta U)$  (*long dashed*) and  $M(U) + M'(U)\delta U$  (*dotted*).

#### 4.2.1 Tangent Linear Verification for Forced Land Surface Model Runs

Figure 4.14 is the case for selected period starting from 00Z 04Aug. The forward model run ( $M(U)$ ) starts from control variable state  $U = (307.16K, 301.2K, 0.2562m^3m^{-3}, 0.28m^3m^{-3}, 0.0)^T$ . The control variable state was perturbed by  $\delta U = (2K, 0.5K, 0.05m^3m^{-3}, 0.01m^3m^{-3}, 0.0)^T$  and the curve labeled  $M(U + \delta U)$  was then produced by another forward model run. With this perturbation vector, we run the tangent linear model around a nonlinear base produced by forward model run with  $U = (307.16K, 301.2K, 0.2562m^3m^{-3}, 0.28m^3m^{-3}, 0.0)^T$  to get time series  $M'(U)\delta U$ . The time series labeled as  $M(U) + M'(U)\delta U$  are produced by combining  $M(U)$  and  $M'(U)\delta U$ . As expected, the long dashed and the dotted lines are not exactly the same. They are relatively close, however.

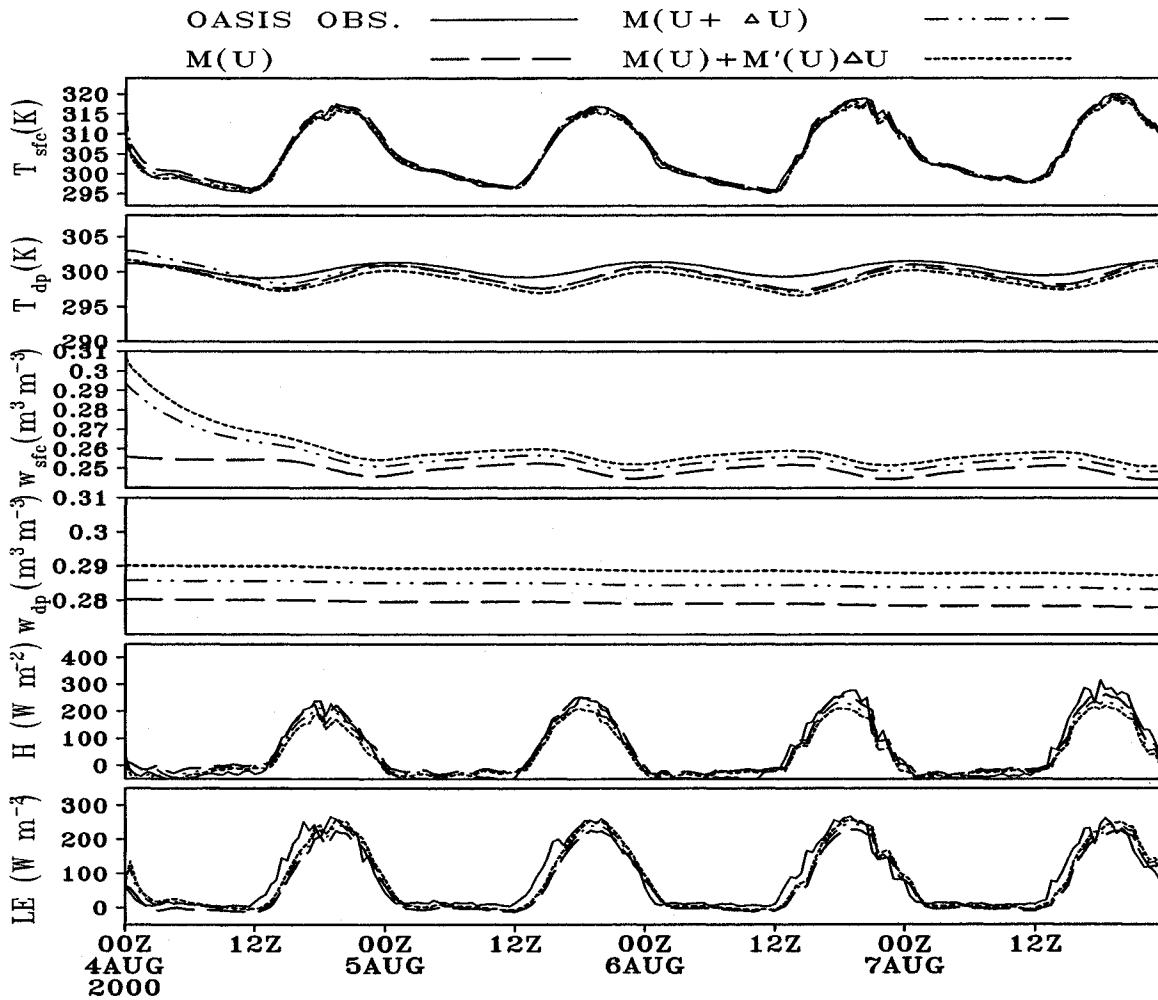


Figure 4.14. Tangent linear verification for forced land surface model runs. The control variables are  $U = (307.16K, 301.2K, 0.2562m^3m^{-3}, 0.28m^3m^{-3}, 0.0)^T$  while the perturbations are  $\delta U = (2K, 0.5K, 0.05m^3m^{-3}, 0.01m^3m^{-3}, 0.0)^T$ .  $M(U)$  (dashed),  $M(U + \delta U)$  (dot dashed) and  $M(U) + M'(U)\delta U$  (dotted) are shown. For the verification of the forward model, in the first four panels, OASIS corresponding observations are also shown.

This experiment was repeated several times with different initial perturbations and we obtained the same results showing that the tangent linear hypothesis is globally well satisfied on 48 hours. Actually, under observed atmospheric forcing, the longer the period, the smaller the differences among the three curves and finally the differences

disappear, first the surface temperature, followed by deep soil temperature and surface soil moisture content and by deep soil moisture.

#### *4.2.2 Tangent Linear Verification for Coupled Model Runs*

Similar to the forced run case, we see that the long-dashed and the dotted lines are relatively close (Figure not shown for clarity). We repeated this experiment several times with different initial perturbations and obtained the same results showing that the tangent linear hypothesis is globally well satisfied on time span of two days. We do not evaluate this hypothesis on a longer period because then the 1D model forecasts are less and less accurate. The discrepancies on the 2 m relative humidity (long dashed and the dotted lines) is from the non-linearities of the model. Note that the formulation of the drag coefficients are modified in the tangent linear model because the derivative became very big when the Richardson number approaches zero (neutral stability) and create strong oscillation in the tangent linear model. This situation occurs twice daily when the stability of the atmosphere is changing. However, the TLM is not apparently affected elsewhere of the day.

#### *4.3. The Evolution of the Adjoint Variables and Period of Most Sensitivity*

Physical insight into the behavior of the system comes once we have integrated the adjoint model backward in time, yielding  $\lambda(t_i)$ . Recall that each adjoint variable corresponds to a state variable and we showed (Eq. (2.27)) that the adjoint variable at  $t=0$  directly relates the sensitivity of the model response to the initial condition of the state variable. Hall and Cacuci (1983) formally derived the physical meaning of the adjoint variables, they conclude that, analogously, the adjoint variable at any time  $t_i$  is directly

related to the sensitivity of  $L$  to a perturbation in its corresponding state variable at that particular time. Because there is an adjoint function corresponding to each state variable, we can thus foresee which states are most important at different times of the simulation period through the comparison between states. For example, if one curious how an observation of dew temperature will be the influence by a soil temperature perturbation inserted at any other time between the starting (integration) time and the observation time, an adjoint model run from this measurement to the insertion period will tell the answer.

#### 4.3.1. Decomposition of Adjoint Sensitivities

Following Margulis and Entekhabi (2001), we decompose Eq. (2.26) according to parameters and each components of the state vector into

$$\begin{aligned} \delta L &= \iint_{\Sigma} \left\{ \left[ \frac{\partial \phi}{\partial \alpha} - \lambda^T \frac{\partial F}{\partial \alpha} \right] \delta \alpha \right\} dt dx - \lambda_0^T \delta U(t_0) \\ &= \delta L_1 + \delta L_2 + \delta L_3 + \delta L_4 + \dots + \delta L_{N_p} + \delta L_{N_p+1} + \delta L_{N_p+2} + \dots + \delta L_{N_p+N_s}, \end{aligned} \quad (4.1)$$

where each term represents the individual contribution of a perturbation of a particular parameter to the total model response. Note that once the adjoint variables are determined, each of the above term can be computed because the derivatives are only functions of the forward model solution and model parameters. Embedded in this equation is information about the relative sensitivity of model response to each parameter (initial conditions are also considered as model parameters), as well as the temporal distribution of variation in model response to a given parameter. This equation will serve as the theoretical basis for one numerical experiment in Chapter 5.



### 4.3.2. Relative Parameter Sensitivities

The relative sensitivities (Errico *et al.* 1997) are a measure of the percentage change in model response from a percent change in a given parameter. We define a cross comparable nondimensional adjoint variable similar to Eq. (42) of Margulis and Entekhabi (2001) to quantify the model relative sensitivity  $r_k$  to parameter  $\alpha(k)$ :

$$r_k = \frac{\delta L_k / L}{\delta \alpha_k} = \frac{\partial L / L}{\partial \alpha_k}, \quad (4.2)$$

where the derivative can be computed once the adjoint variables are available. Note that this is a nondimensional measure of the relative importance of each parameter in determining the model response.

## Chapter Five

### *Retrieval of Soil States Using Soil Skin Temperature Observations*

As stated before, we perform two sets of retrieval experiments, assuming different data availabilities. The first one uses skin temperature and is designed to operate with a micrometeorological data stream provided for the stand-alone forward model run by observations, simulations, or NWP analyses. The only needed adjoint code is that of land surface model (i.e., two layer soil model and the estimation of surface drag coefficients, as shown in Figure 3.1). Considering that surface skin temperature measurements are widely available from remote sensing platforms, this approach is of practical importance for numerical weather prediction. The second set of experiments ingests screen-level atmospheric potential temperature and specific humidity measurements and thus needs a coupled land-atmospheric model and its adjoint code. The second approach assumes only the availability of atmospheric observations which is usually the case in reality. This chapter is dedicated to the first approach while the second approach will be discussed in Chapter 6.

Since this chapter tries to unveil the mechanism in land surface processes, to avoid the model imperfection in atmospheric components, we provide the land surface model with micrometeorological variables including precipitation, surface atmospheric pressure, screen-level air temperature, relative humidity, wind speed, and net radiation. Only ground temperature information is used in the retrieval system in order to estimate the land surface control of surface fluxes. In practical applications of this scheme, the required atmospheric variables can be derived using objective analysis methods.

### 5.1. Data

The possible assimilation period, August 4-28, a total of 24 days, is divided into three consecutive periods of 8-day each. The surface ground temperature to be assimilated can be inferred from soil profile measurements by an extrapolation technique (Jackson 1997; Ren and Xue 2004). The extrapolation scheme needs a soil thermal diffusivity  $K_T$  ( $\text{m}^2 \text{s}^{-1}$ ), which is related to soil thermal conductivity  $\lambda_T$  ( $\text{W m}^{-1} \text{K}^{-1}$ ) by soil heat capacity, i.e.,  $K_T = \lambda_T / C_v$ , to estimate the scale depth for daily cycle. For a given site,  $\lambda_T$  can be estimated using the phase-amplitude method as described in the appendix of Ren and Xue (2004). This kind of methods tends to work best under periodic diurnal forcing. The result of applying phase-amplitude methods shows that the scaling depth is 14.4, 13.56 and 14.8 cm, respectively, for the three selected periods. Other basic daily cycle soil parameters are shown in Table 5.1. The *A priori* determined  $K_T$ , especially when applied to different soil moisture situations, gives systematic error in the inferred ground temperature. For our selected period, using surface temperature extrapolated from measured 5 cm deep soil temperature tends to give much lower surface temperature amplitude due to an overestimation of the scaling depth. In this study, we use directly measured infrared surface temperature rather than the extrapolated surface temperature. The seasonal temperature trends (Column 3 in Table 5.1) are estimated using the method described by Ren and Xue (2004) and used in Eq. (2.1). The soil and vegetation properties are listed in Table 2. 1.

**Table 5. 1** Parameters used in the selected period (August 4-27, 2000)

Infrared surface temperature data are used in calculating the following soil temperature parameters (Notations follow Ren and Xue 2004)

	$\overline{T}_{sfc}$	$\overline{T}_{sfc} - \overline{T}_{dp}$ (K)	$A_0$ (K)	$A_{dp}$ (K)	$d$ (m)
(08/04-08/11)	306.04	5.49	9.7	0.51	0.144
(08/12-08/19)	306.70	4.70	13.5	0.96	0.135
(08/20-08/27)	307.60	5.46	13.8	1.20	0.148

For short-range weather prediction purpose, the assimilation periods may be much less than 28 days. However, we processed land surface observations thus long from the following considerations. For estimation of the  $\gamma d$  term in Eq. (2.1), the best way is to use weeklong time series of measurements. For the sparse sampling scheme to obtain enough information, longer assimilation period may be necessary. Even the required assimilation period is much shorter than 28 days, to test the robustness (i.e., if the scheme is case sensitive) of the assimilation scheme, we may also need several different time periods. This month-long observation period allows us to choose different assimilation windows.

## 5.2. Numerical Experiment Design

The numerical experiments performed in this chapter are listed in Table 5. 2. We will first perform Observing Simulation System Experiments (OSSEs, Arnold and Dey 1986; Lord *et al.* 1997) to investigate the feasibility and robustness of the retrieval scheme. Parallel real data assimilations follow. The first OSSE experiment (OSSE1) assumes initial guess error in only one control variable ( $w_{dp}$ ). The second OSSE experiment (OSSE2) assumes initial guess errors (all being significantly larger than typical forecast error for such quantities) exist in all control variables. For the third

experiment (OSSE3), the error magnitudes in OSSE2 are doubled. Comparisons between OSSE2 and OSSE3 show the scheme's robustness to initial guess error magnitudes. Equally important is the scheme resistance to Gaussian noise. We thus designed OSSE4 to see the effects of magnitudes of Gaussian noise on the quality of the retrievals. Finally, we designed an experiment to point out a shortcoming which has not yet been widely realized for retrieval using oversimplified land surface schemes.

For real data assimilation, we show one case with wilting point initial guess on soil moisture contents (OASIS1). Based on this case, the issues of data sampling strategy (OASIS2) and the effects of assimilation window length (OASIS3) are discussed.

In real application, the initial guess errors are carried over from previous cycle of forward model prediction. Therefore, it is a natural requirement for our retrieval scheme to tolerate initial guess errors larger than model inaccuracies. For quantifying our initial guess errors, the forward model inaccuracies in temperature and soil moisture content are specified as 2 K and  $0.01 \text{ m}^3 \text{ m}^{-3}$  respectively, the same order as the measurement uncertainties for these quantities.

**Table 5. 2** Numerical experiment design for retrieval with stand-alone land surface model and its adjoint

August 4- dry period	OSSE	A 2-day nature run of LSM starting from 00Z August 4 <sup>th</sup> , 2000, forced by the OASIS measured surface atmospheric variables; Synthetic (simulated) observations of ground temperature sampled every 30 minutes and used by the retrieval experiments
		OSSE1: Initial guess error exist in $w_{dp}^0$ only. $\delta U=(0.0,0.0,0.0,0.035 \text{ m}^3 \text{ m}^{-3},0.0)^T$
		OSSE2: Initial guess error exist in all control variables: $\delta U=(5\text{K}, -2.5\text{K}, +0.015\text{m}^3 \text{ m}^{-3}, +0.0175\text{m}^3 \text{ m}^{-3}, 0.0\text{m}^2 \text{ m}^{-2})^T$
		OSSE3: Initial guess errors in OSSE2 doubled.
		OSSE4: Resistance to Gaussian noise
	OSSE5: Consequence of severance the deep soil connection	
	OASIS	OASIS observations of ground temperature available every 30 minutes and used by the retrieval experiments
		OASIS1: Initial guess error exist on soil moisture contents: Wilting point guess $U^f=(307.16\text{K}, 301.25\text{K}, 0.2\text{m}^3 \text{ m}^{-3}, 0.2\text{m}^3 \text{ m}^{-3}, 0.0\text{m}^2 \text{ m}^{-2})^T$
		OASIS2: Effects of Data Availability 1.Using the same setting as control run OASIS1; 2.Three sampling strategies: Full (complete continuous data availability), daytime (data availability at a 3-hr wide window centered on local noon, i.e.18Z for Norman site) and nighttime (local midnight 06Z for Norman site)
		OASIS3: Effects of Assimilation Window Length 1. $U^f=(308.2\text{K}, 300.75\text{K}, 0.226 \text{ m}^3 \text{ m}^{-3}, 0.29\text{m}^3 \text{ m}^{-3}, 0.0)$ 2.For each experiment, using retrieved initial conditions, a forward model run is made to produce an extra forecasting 2 days long

### 5.3. Observing Simulation System Retrieval Experiment (OSSE)

OSSEs are commonly used to test new data assimilation systems or new observation network or platform (see, e.g., Arnold and Dey 1986; Lord *et al.* 1997). With OSSE experiments, simulated observation data are created by model runs. For future observing instruments or platforms, OSSE is the only way to examine the potential impact of their observations. To examine the effectiveness of new data assimilation techniques or systems, OSSE is also a very effective tool because the modeler has full control over the entire system, include data availability and quality. One also knows the truth about the

state to be analyzed or retrieved because it is given by the simulation model. Using OSSE, one does not have to worry about any possible error with the simulation model, at least initially, so as to be able to focus on the correctness and quality of the assimilation and/or retrieval system that is developed. For these reasons, we will first present in this chapter results from OSSE experiments. Results from real data will be presented in the next one.

The aim of this section is to discuss the feasibility of retrieval of initial values of the five prognostic variables (i.e., two soil temperatures, two soil moistures, and a canopy reservoir for intercepted water) through merely minimizing the trajectory difference between modeled and observed surface temperature  $T_{sfc}$ . Our optimization system can perform all the retrievals simultaneously, inasmuch as the small perturbation and over-determination requirements are satisfied. Small perturbation requirement demands that our initial guesses should not be too wild to violate the tangent linear assumption. Over-determination requires the observations of ground temperature outnumber the total control/retrieved variables, which is not a major concern for retrieval of initial conditions for a column model (or spatially low resolution models).

We created the synthetic trajectory ground temperature and other model states and fluxes (which are not assimilated but can be used for model verification purposes) through a forward run of the LSM for two days starting from 00Z, 4 August 2000, forced by the OASIS measured atmospheric variables. The true initial land surface states are  $(T_{sfc}^0, T_{dp}^0, w_{sfc}^0, w_{dp}^0, w_{canopy}^0) = (307.16\text{K}, 301.16\text{K}, 0.2562 \text{ m}^3 \text{ m}^{-3}, 0.2802 \text{ m}^3 \text{ m}^{-3}, 0.0 \text{ m}^2 \text{ m}^{-2})$ . Here, superscript '0' means initial value.

The first retrieval experiment was done by assuming a positive error of  $0.035 \text{ m}^3 \text{ m}^{-3}$  in the initial deep soil moisture  $w_{dp}^0$ . We chose an assimilation window of 2 days, starting from 00Z, 4 August 2000. From analyzing the adjoint variable time series, we want to gain insight into how perturbations in each state variable affect the cost function defined as Eq. (2.31). Just as the state variables are of variant scales (e.g.,  $Ts' \sim O(10^2)$  and  $ws' \sim O(10^{-1})$ ) so are the corresponding adjoint variables that have dimensions of  $1/[u_i]$  (here  $u_i$  is the  $i$ th component of the control vector  $U$ ). To gain insight into their relative sensitivities, we define a cross comparable nondimensional adjoint variable (Subsection 4.3.2). However, unlike Margulis and Entekhabi (2001), we used the daily cycle magnitude (12.8K here) instead of temperature values themselves in normalizing the corresponding adjoint time series. Similarly, soil moisture was subtracted by the wilting point value before being multiplied to the adjoint variables of soil moistures.

The time series (indicated by a prefix ‘ $ad\_$ ’) of the normalized adjoint variables are plotted in Figure 5.1, for the first iteration in the minimization process. Except for the adjoint variable corresponding to canopy interception (which is constantly zero because there was no precipitation or dew formation during this period), adjoint variables are plotted from the least influential (top panel  $ad_{T_{sfc}}$ ) to the most influential variable (bottom panel  $ad_{w_{dp}}$ ). Except for  $ad_{T_{sfc}}$ , which holds the last time level difference between the predicted and synthetically “observed” surface temperature due to initial deep soil moisture error, all of the remaining adjoint variables are equal to zero at the end of the assimilation window of two days.



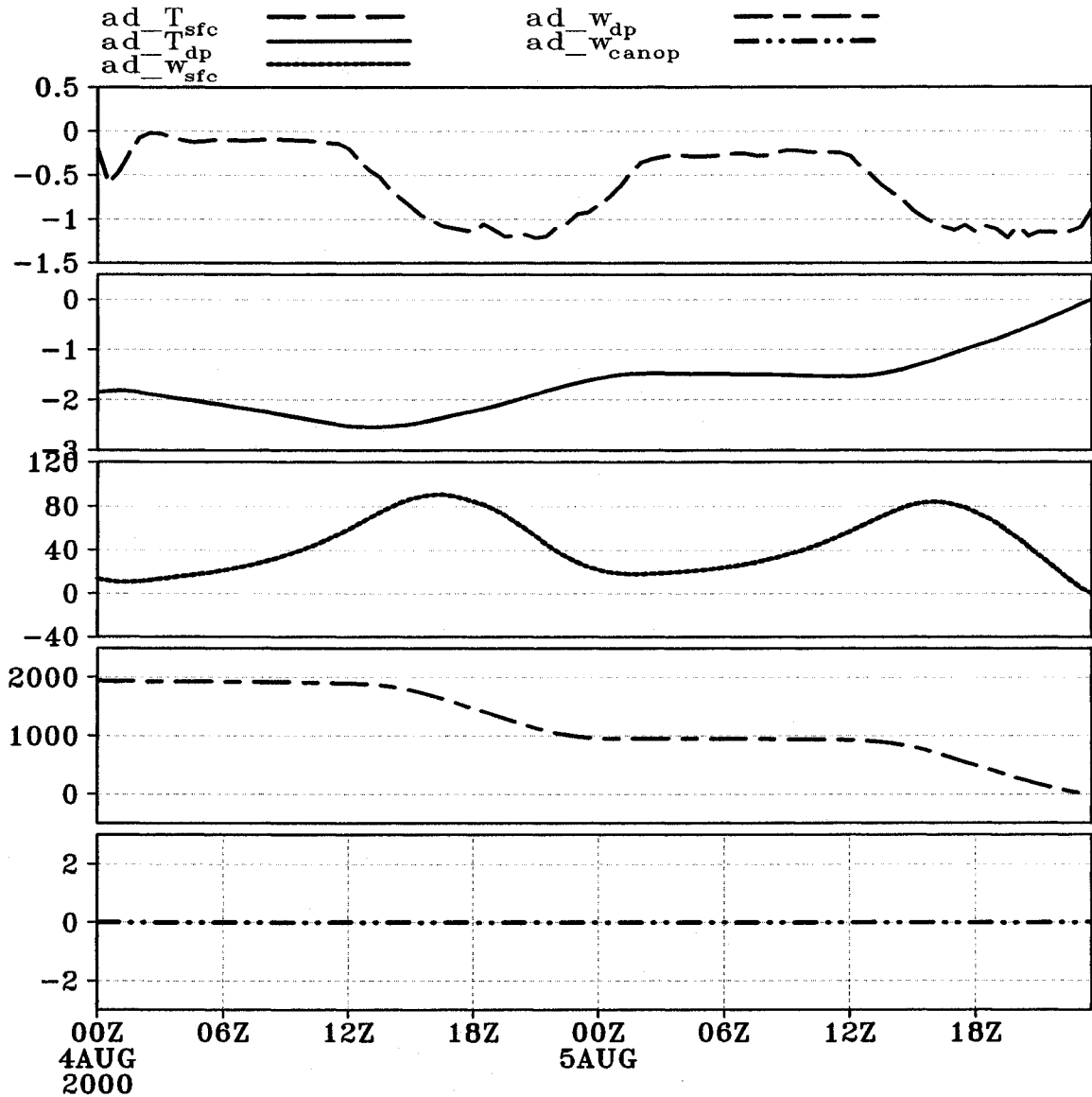


Figure 5.1. The time series of adjoint variables from  $w_{dp}+0.025$  at the first iteration of minimization. Each adjoint variable is marked by its corresponding state variable with an  $ad\_$  prefix.

Mathematically, this is a direct result of the terminal condition placed on the adjoint model (Eq. (2.25)). Physically, this represents the deterministic causal nature of the system, in that perturbations in the state variables beyond the assimilation window have no influence on the cost function (model response, which is the ground surface temperature in this study). As the adjoint model proceeds backward in time toward the

initial condition, each adjoint variable will accumulate information that influences the cost function in different ways depending on their respective roles in the forward dynamic system. In a sense, the backward marching of the adjoint model signifies an information collection process that marks the influence of each state on the trajectory fitness of  $T_{sfc}$  over this assimilation period. Thus, the first usage of this diagram is to identify the relative sensitivity among different variables.

The second goal is to identify the positive or negative feedback that is triggered by the introduced initial condition error. For example, in Figure 5.1, we see that the most sensitive adjoint variable is the one corresponding to deep soil moisture. The positive feedback is accumulated all the way to about 25 (at the initial time), and is more than two orders of magnitude larger than the adjoint variables for soil temperatures. If the optimization scheme is allowed to vary only one specific variable to minimize the cost function, it will surely pick the initial deep soil moisture. After analyzing the convergence of the corresponding estimated state variable to its actual value (figures not shown), we found that the adjustment to  $w_{dp}$  is the most significant one, while the adjustments to  $T_{sfc}$  and  $T_{dp}$  are insignificant. Similar analysis can be applied to any interim time step using the result of Hall and Cacuci (1983), i.e., the adjoint variable at any time  $t = \tau'$  is directly related to the sensitivity of cost function to a perturbation in its corresponding state variable at that particular time  $\tau'$ . Thus, we can cross compare between states to see which is most important at different times during the model integration.

Figure 5.1 indicates also the feedback (to the innovation in  $w_{dp}$ ) from  $T_{sfc}$  is a negative one, which is especially significant during daytime heating period. Thus,

increased deep soil moisture increases  $LE$  and reduces the energy used for heating the ground. The feedback from deep soil temperature is similar but with phase shift resulted from the larger heat inertia of the deep soil layer. The feedback from  $w_{sfc}$  is positive, since it may gain (or loss less) soil moisture from the capillary effects through exchanging with deep soil reservoir. The most sensitive period (for  $w_{sfc}$ ) is also during daytime, indicating that the soil moisture exchange is passively forced by the evapotranspiration process.

Without model error and with complete surface temperature measurements, the minimization is very efficient, after three iterations, the cost function is only 0.1 percent of its initial value. The minimization was carried out 5 iterations before terminating, satisfying the smallness of the criteria, which is defined as the cost function difference between two adjacent iterations. Upon convergence, the initial guess error was minimized to insignificant amount ( $\sim 2 \times 10^{-4} \text{ m}^3 \text{ m}^{-3}$ )

With the retrieved initial states, we integrated the forward model for one more time to obtain the state estimates. Figure 5.2 illustrates how much improvement is gained in predictions by assimilating merely ground temperature observations. Once the convergence is reached, the assimilated  $T_{sfc}$  trajectory nearly coincidences with the observed one as expected. Although no corresponding observations for them are assimilated, the two soil moisture values and the deep temperature values are also successfully updated, through the model dynamics as a constraint. Their trajectories resulting from erroneous initial  $w_{dp}$  are all deviate from the corresponding true trajectories, with the deviations for both  $w_{sfc}$  and  $w_{dp}$  being about  $0.02 \text{ m}^3 \text{ m}^{-3}$  during

much of the two days period. Consequently, the surface fluxes are also significantly improved by more than  $50 \text{ W m}^{-2}$  at the peak hours.

We must emphasize that  $T_{sfc}^0$  is the least sensitive one in this experiment. If the sensitivity channels of  $w_{sfc}$  and  $w_{dp}$  are closed, however, initial value of ground temperature experiences large and proper adjustment to its true value. Unfortunately, the simulation of  $LE$  and  $H$  using the retrieved temperature values ( $T_{sfc}^0$  &  $T_{dp}^0$ ) are both poor (Figure 5.3), because the initial guess errors associated with soil moistures (panels c&d) cannot be effectively removed by merely adjusting initial soil temperatures.

Because the LSM is run in stand-alone mode, the effects on PBL structure by soil moisture error cannot be shown here. In reality, because of the slow rate at which the deep soil moisture evolves and the limited number of *in situ* observations that can be anticipated, the start-up bias is likely to persist for weeks. Refinements to current LSMs should emphasize the process uncertainty in soil moisture description. The relative importance of superficial and deep soil moisture contents depends on site-specific land-cover conditions. For less vegetated area, surface soil moisture may play a more important role than shown here based on Norman site characteristics.

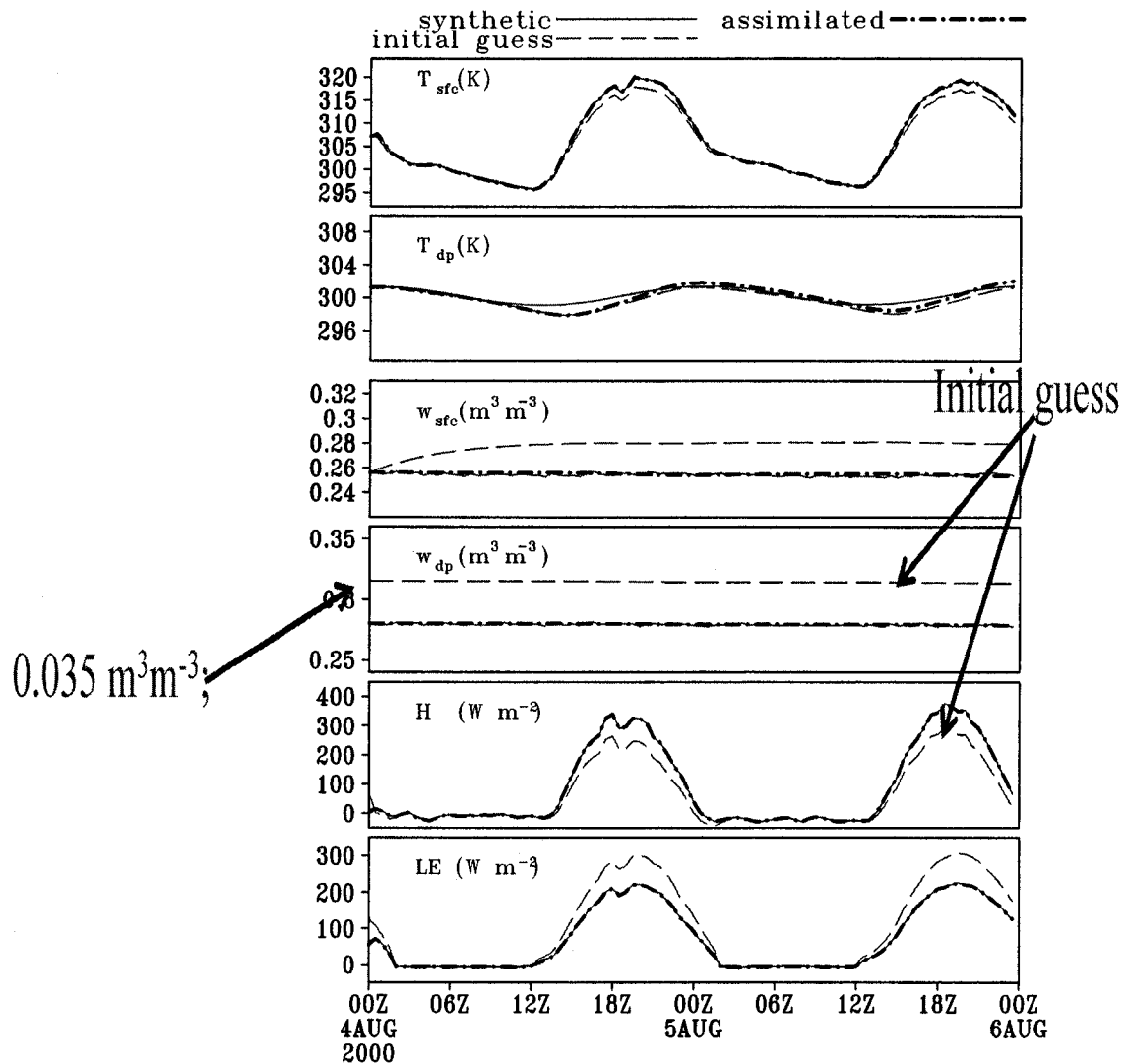


Figure 5.2. Comparison of actual state variables and latent and sensible heat fluxes (synthetic) with those prior (initial guess) and estimated using retrieved values (assimilated). Only ground surface temperatures are assimilated.

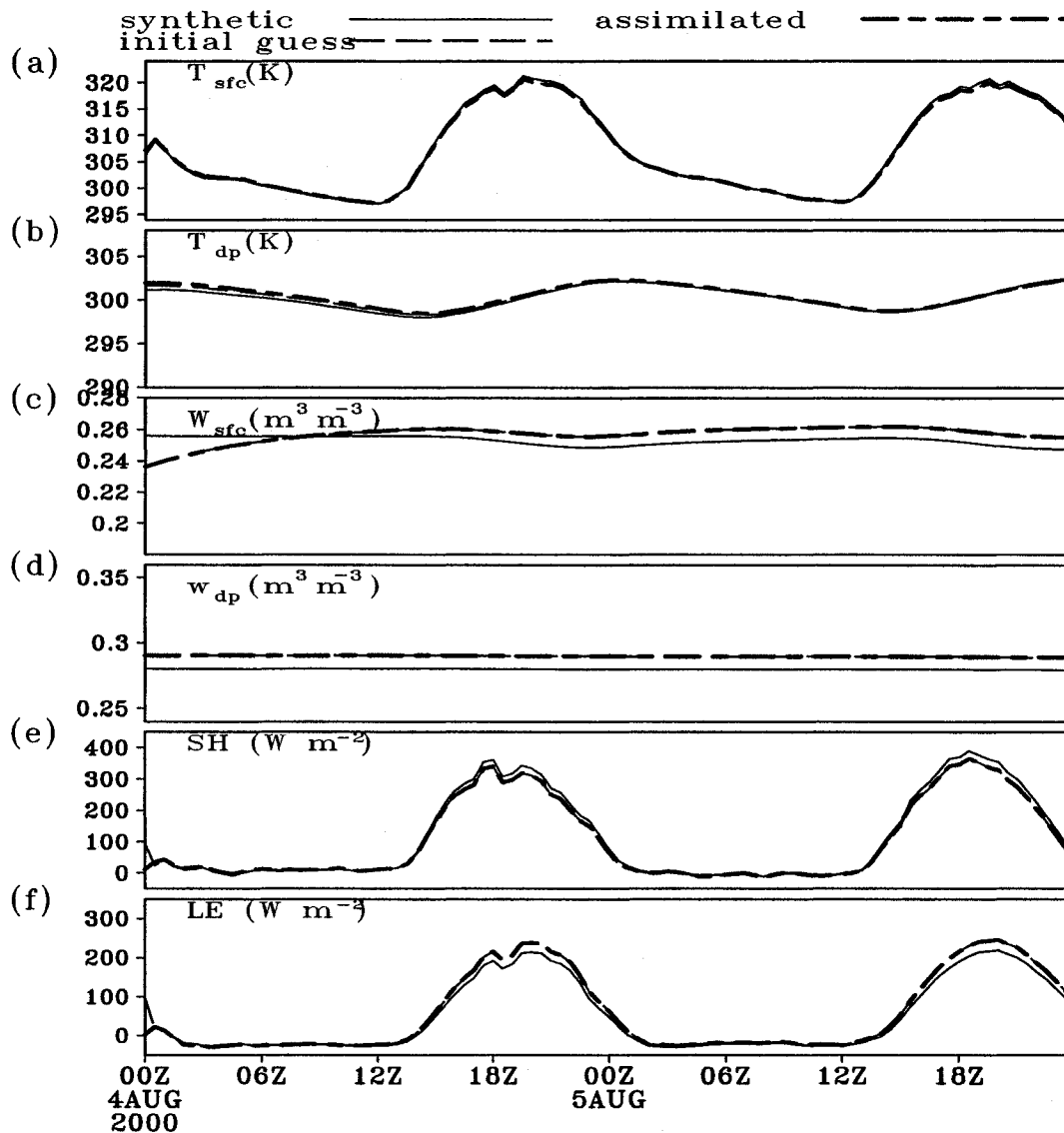


Figure 5.3. As Figure 5.2 but with only temperature sensitivity channels opened for the assimilation. Although surface temperature time series are accurately retrieved, the surface fluxes are at systematic errors.

Similar experiments are repeated in which errors are added to  $T_{sfc}^0$ ,  $T_{dp}^0$ , and  $w_{sfc}^0$  in turn. The results are summarized in Table 5.3. Because the uncertainty in initial surface temperature has least influence on the ensuing surface temperature evolution, it is most difficult for the minimization scheme to pinpoint its exact initial value. On the contrary,

the deep soil moisture has the strongest influence on the surface temperature evolution, thus is the easiest one to retrieve. This is also consistent with our nonlinear sensitivity experiments evaluating the influence of each surface parameter on surface fluxes and ground surface temperature. We found that  $LE$ ,  $H$  and  $T_{sfc}$  are very sensitive to the soil water contents, and the influence of deep soil moisture error lasts longer than ten days, whereas the influence of superficial soil moisture lasts barely one day. For the evolution of  $T_{sfc}$ , the influence of initial value uncertainty of deep temperature is much smaller and the one of  $T_{sfc}$  itself is quite insignificant.

Viewing from another angle, the initial guess error associated with surface temperature is least important and the initial errors in soil moisture are far more important in affecting the surface temperature evolution. Assimilation scheme for initial condition, if applied to land surface models, should concentrate on the better estimation of soil moisture conditions.

Table 5.3 Initial states retrieval using synthetic data

Control variable	Initial rms error	$J_{\text{final}}/J_0$	# iterations needed	Retrieved initial condition			
				$T_{sfc}$	$T_{dp}$	$w_{sfc}$	$w_{dp}$
$T_{sfc}+3.0K$	0.310	0.153	17	306.76	301.23	0.25	0.280
$-3.0K$	0.315	0.65	40	305.80	301.14	0.25	0.280
$T_{dp}+2.0K$	0.154	0.25	12	307.16	303.16	0.29	0.280
$-2.0K$	0.157	0.3	11	307.16	299.16	0.23	0.280
$w_{sfc}+0.01$	0.042	9.7E-5	7	307.16	301.16	0.256	0.280
$-0.008$	0.035	3.4E-7	8	307.16	301.16	0.256	0.280
$w_{dp}+0.025$	1.2	8.7E-11	4	307.16	301.16	0.256	0.280
$-0.01$	0.94	2.4E-10	4	307.16	301.16	0.256	0.280

We now assume initial guess errors exist on all control variables. In the following experiment, we use

$\delta(T_{sfc}^0, T_{dp}^0, w_{sfc}^0, w_{dp}^0, w_v^0)^T = (5.0K, -2.5K, 0.015m^3m^{-3}, 0.0175m^3m^{-3}, 0.0m^2m^{-2})^T$ , or the initial guess vector is  $U^i = (312.16K, 298.5K, 0.271m^3m^{-3}, 0.297m^3m^{-3}, 0.0m^2m^{-2})^T$ .

It takes the optimization scheme 15 iterations to converge to  $U^r = (307.18K, 301.22K, 0.259m^3m^{-3}, 0.2803m^3m^{-3}, 0.0m^2m^{-2})^T$ , as shown in Figure 5.4. The root mean squared error (*rms*) in surface temperature prediction was reduced by over 5 orders of magnitudes from its initial amount (Figure 5.4a). The ultimate retrieved initial land variables are all close to the true values, as indicated by the fact that the initial guess errors are all reduced to insignificant amount:  $\delta U = (0.03K, 0.06K, 0.013m^3m^{-3}, 0.0001m^3m^{-3}, 0.0m^2m^{-2})^T$ . However, the process of finding these true values is not monotonous (in this case for  $T_{dp}$ ). The undershoots (after iteration 4, see Figure 5.4b) drag the ground surface temperature time series from overriding to under the true trajectory (reduced the previous cost-function value, though). However, optimization scheme is clever enough to make corrections for following iterations (because the adjoint integration produces correct guidance to the adjustments by providing the direction of the gradient vector).

Using assimilated initial land surface parameters, we integrated the forward model for one more time to obtain the state estimates. Figure 5.5 illustrates how much improvement is gained in representing the states by assimilating merely the ground temperature observations. Upon convergence, errors for  $T_{sfc}^0$  and  $T_{dp}^0$  are less than 0.6K, for  $w_{sfc}^0$  less than  $0.013m^3m^{-3}$  and even accurate for  $w_{dp}^0$  ( $\sim 0.0001m^3m^{-3}$ ). As a result, the assimilated  $T_{sfc}$  trajectory nearly coincidences with the observed one as expected. The two soil moisture values and the deep temperature values, although no corresponding



observations for them are assimilated, can also be successfully updated, through the model dynamics as a bond. Although their initial guess trajectory are all apparently deviant from the corresponding true trajectories, the retrieved trajectories are nearly indiscernible from the “true” ones. As a result, the surface fluxes are correctly reproduced.

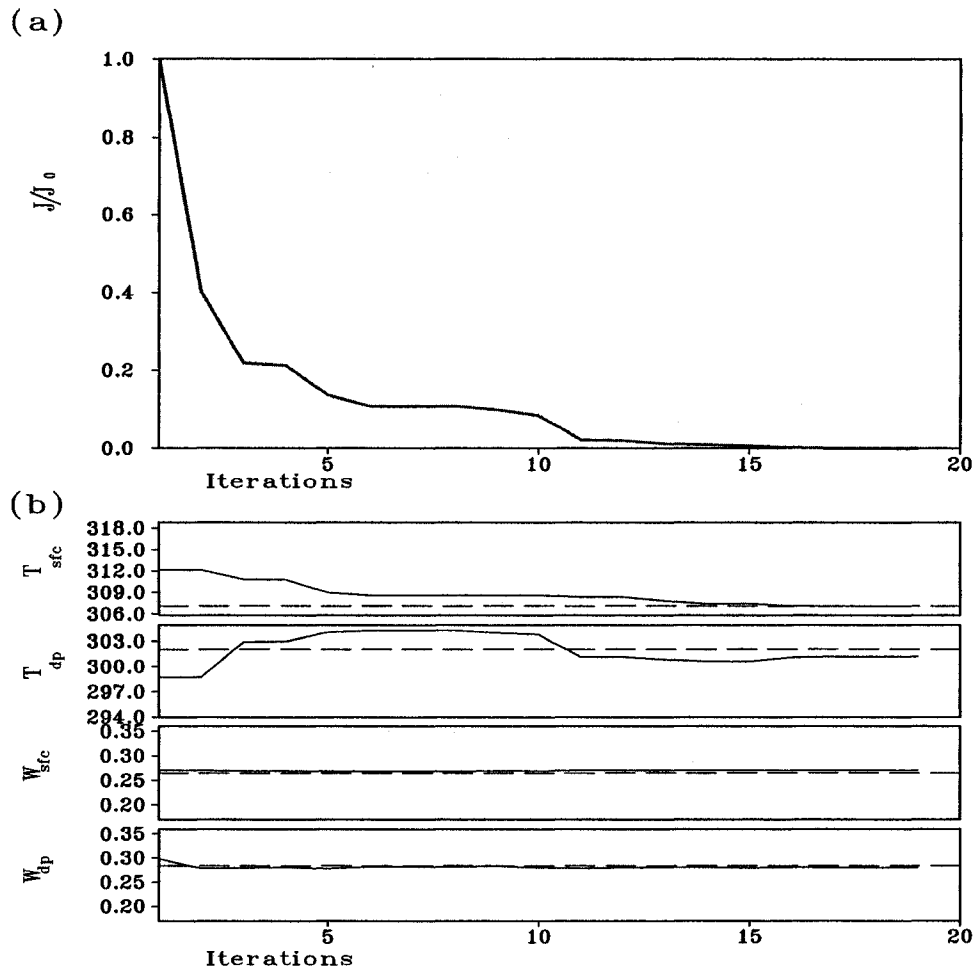


Figure 5.4. Retrieval experiments with initial guess errors on all control variables. Reduction in cost function (a); and the convergence of the control variables to the “true” (dotted lines) values (b).

We double the initial guess error magnitude and find the retrieval is still pretty successful. However, it takes more iteration to converge (Figure 5.6&5.7). In addition to the case shown in Figure 5.4-5.7, other scenarios were tested with different initial guess error magnitudes. In general, the retrieval procedure is robust for reasonable perturbations in the prior guess values. If the perturbations are too large, however, there can be other estimates that reproduce the measured ground temperature but are different from the actual state of the system (i.e., solution bifurcation). This ambiguity can be reduced in actual application for coupled runs by introducing other observations to the cost function, i.e., surface atmospheric measurements. Specifically, the initial guess errors on surface soil temperature can be as large as 35K, or we can just put the initial guess at 320K or 275K without apparent effects on the performance of the optimization scheme.

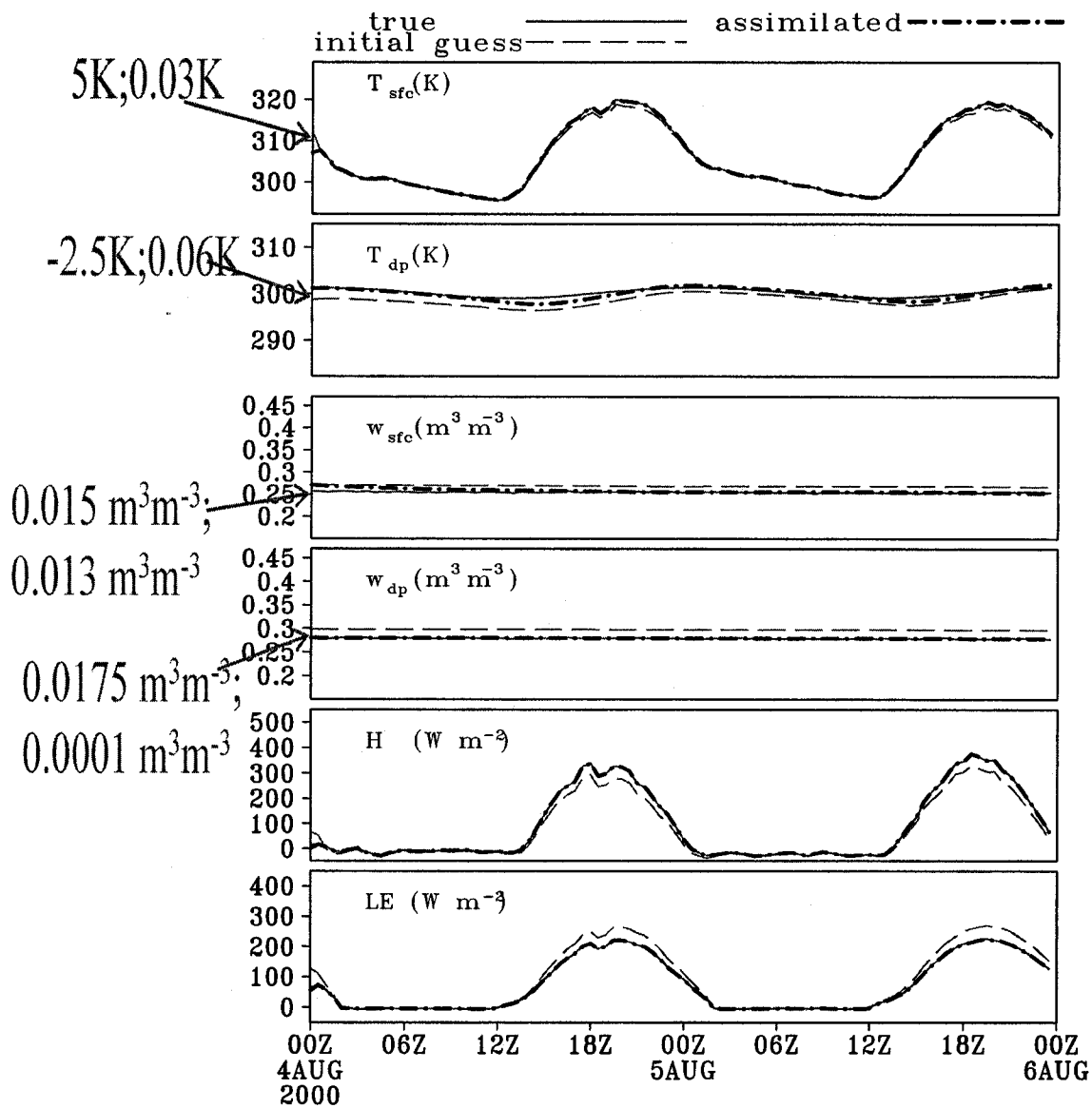


Figure 5.5. Comparison between trajectories resulted from prior guess initial conditions (long dashed lines) and retrieved values (dot dashed lines). The true trajectories are shown as solid lines. Retrieval experiments with initial guess errors on all control variables.

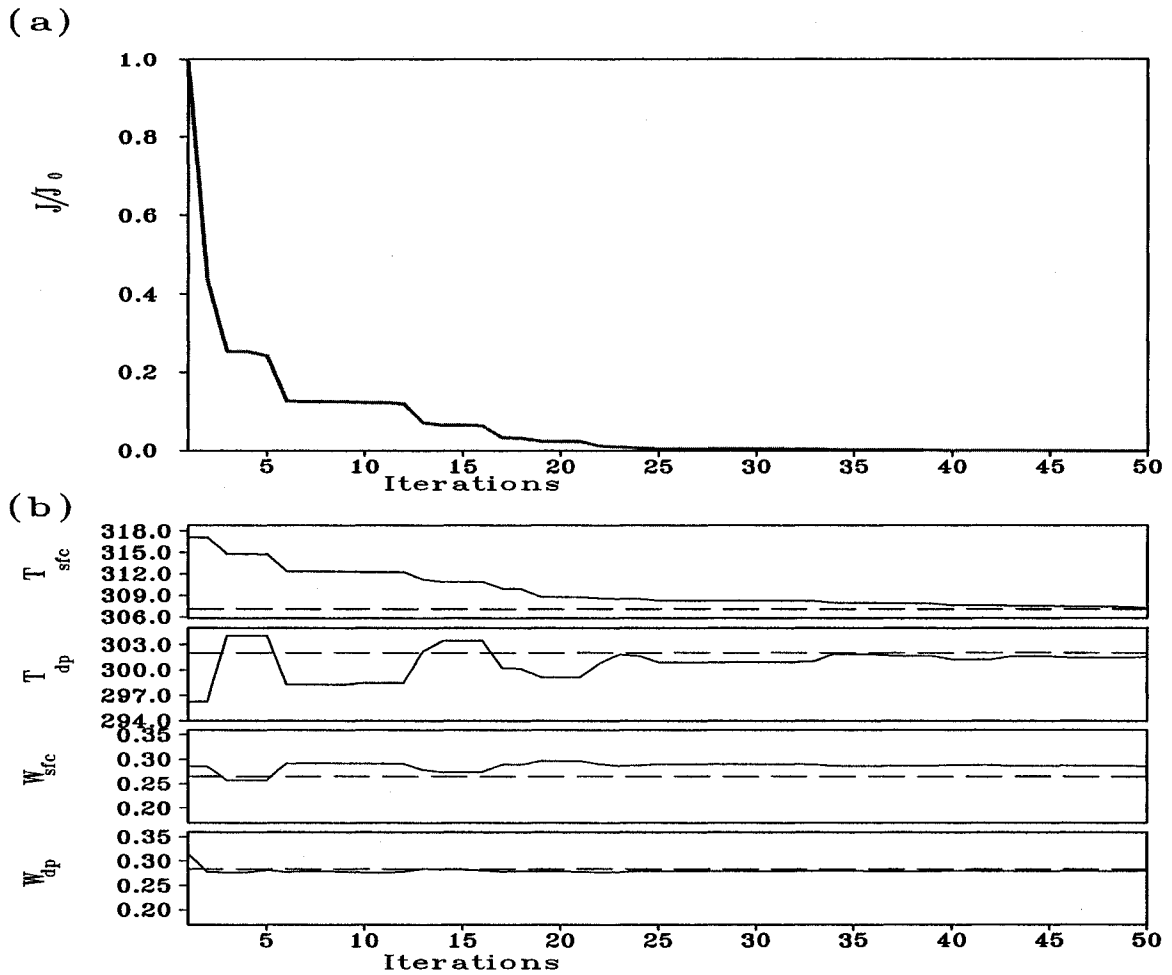


Figure 5. 6. As Figure 5.4 but with doubled initial guess errors

However, due to the way ground heat capacity is parameterized (Eq. (8)) and the numerical bounding in parameterizing ground surface water deficit factor  $h_u$ , initial guess of deep soil moisture value must lie within the range of wilting point and saturation. We found that our scheme works as long as the initial guess soil moistures lie between  $0.23\text{m}^3 \text{m}^{-3}$  and  $0.4\text{m}^3 \text{m}^{-3}$ . This range is large and practical considering that soil moisture usually lies within that range year round for Norman site and instrument error is only  $0.05\text{m}^3 \text{m}^{-3}$ .

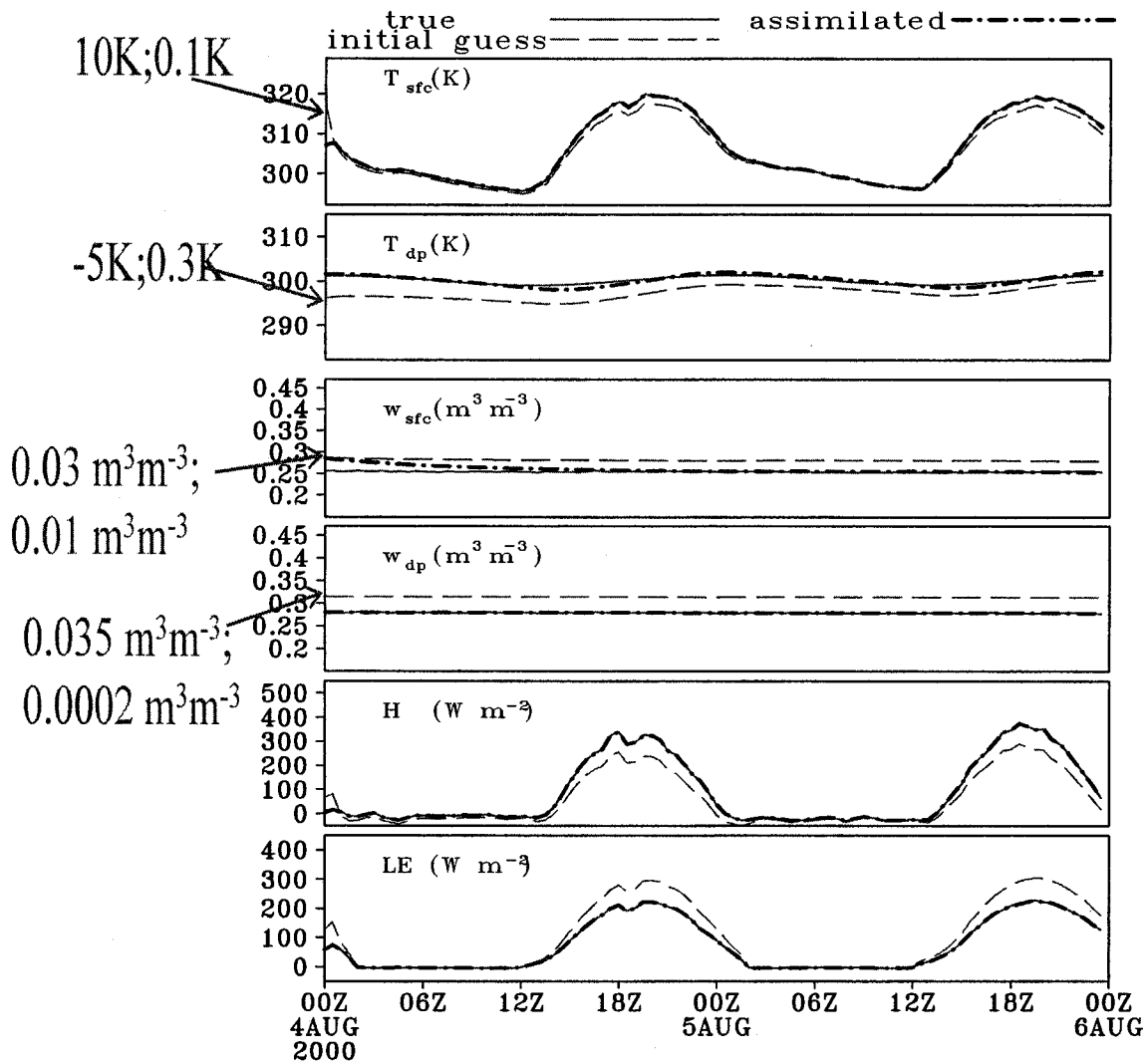


Figure 5.7. As Figure 5.5 but with doubled initial guess errors

For some simplistic land data assimilation systems that do not involve soil moisture evolution, it is some times difficult for them to differentiate the error sources. To illustrate this situation, we repeated the above retrieval experiment (for inaccurate guesses on several control variables simultaneously). The initial guess values for  $T_{sfc}^0$ ,  $T_{dp}^0$  and  $w_{dp}^0$  are 330K, 285K and  $0.3\text{m}^3\text{m}^{-3}$ , respectively. This time, however, only sensitivity channels for two soil temperature variables are open and the sensitivity channels of  $w_{sfc}$

and  $w_{dp}$  are closed. Upon convergence, the *rms* error of  $T_{sfc}$  time series was reduced to <5% of its initial value of 2.9K (Figure 5.8a). It takes only two steps for the optimization scheme to find two temperatures ( $T_{sfc}^0=307.13\text{K}$ ,  $T_{dp}^0=302\text{K}$ ) close to the corresponding true values (Figure 5.8b). Although the initial values of  $T_{sfc}$  and  $T_{dp}$  experience proper adjustments to their true values and their time evolutions are hence accurately retrieved (see time series of  $T_{sfc}$  and  $T_{dp}$  in Figure 5.9), the simulations of soil moistures ( $w_{dp}$  &  $w_{sfc}$ ) as well as surface fluxes ( $LE$  &  $H$ ) using the retrieved  $T_{sfc}^0$  and  $T_{dp}^0$  are poor and contain systematic errors (Figure 5.9).

This is because the initial guess errors associated with soil moistures (see time series of  $w_{sfc}$  and  $w_{dp}$  in Figure 5.9) cannot be effectively removed by adjusting initial soil temperatures. Despite the significant adjustment in the temperature values, the trajectories of soil moistures and surface fluxes nearly unchanged. Actually, in our further experiments, we found that the further away the initial guessed  $w_{dp}$  deviates from its true value, the poorer the simulated (using the retrieved initial values of  $T_{sfc}^0$  and  $T_{dp}^0$ ) surface temperature series are.

If we close only the deep soil moisture sensitivity channel, the retrieval scheme tries to adjust mainly  $w_{sfc}^0$  to obtain good  $T_{sfc}$  estimation. When  $w_{dp}^0 < 0.01\text{m}^3\text{m}^{-3}$ , this aliasing of the true causality works good for both  $T_{sfc}$  and  $LE$  and  $H$  time series. However, as initial guess error on  $w_{dp}^0 > 0.025\text{m}^3\text{m}^{-3}$ , retrieval becomes poor. This is also the reason why Li and Islam (2002) disagrees with Boni *et al.* (2001) on whether or not it is sufficient to have an accurate soil moisture profile to yield accurate surface fluxes. Boni *et al.* (2001), limited by their over-simplified forward model, could not establish possible

pathways between ground temperature and the deep soil moisture, and thus attribute all explained mechanisms to the surface wetness indicator or the surface temperature itself. As abovementioned, their different accounts also arise from the characteristic of their respective sites. Specifically, Boni *et al.* (2001) used a less vegetated SGP99 field campaign site (Jackson 1997).

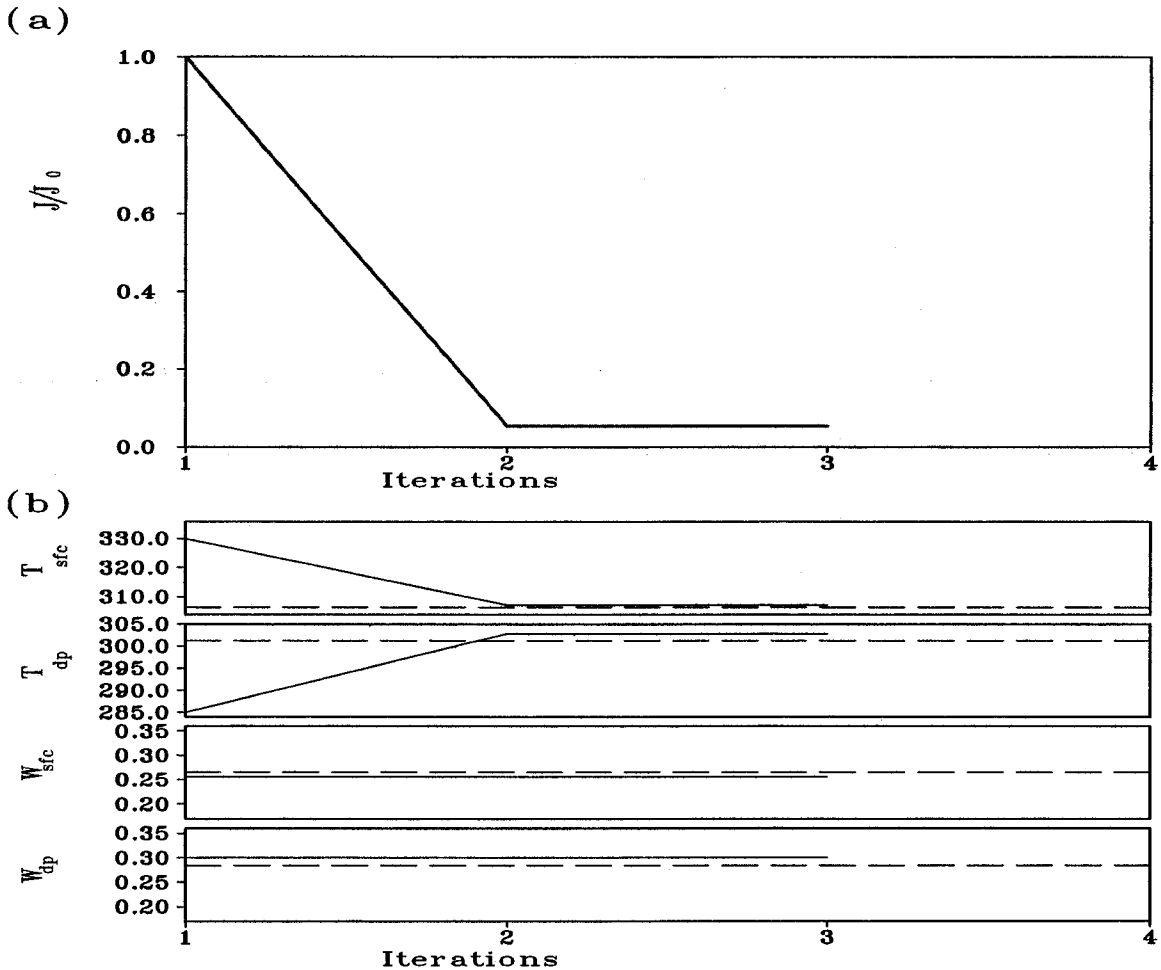


Figure 5.8. Similar to Figure 5.4 but with a reduced control variable set that consists only soil temperature states. (a) the decrease of the cost function (normalized by its initial value), and (b) the convergence of the control variables to their true values. This experiment is done using an initial guess state vector  $U^i = (330K, 285K, 0.2562m^3m^{-3}, 0.3m^3m^{-3}, 0.0m^2m^{-2})^T$ .

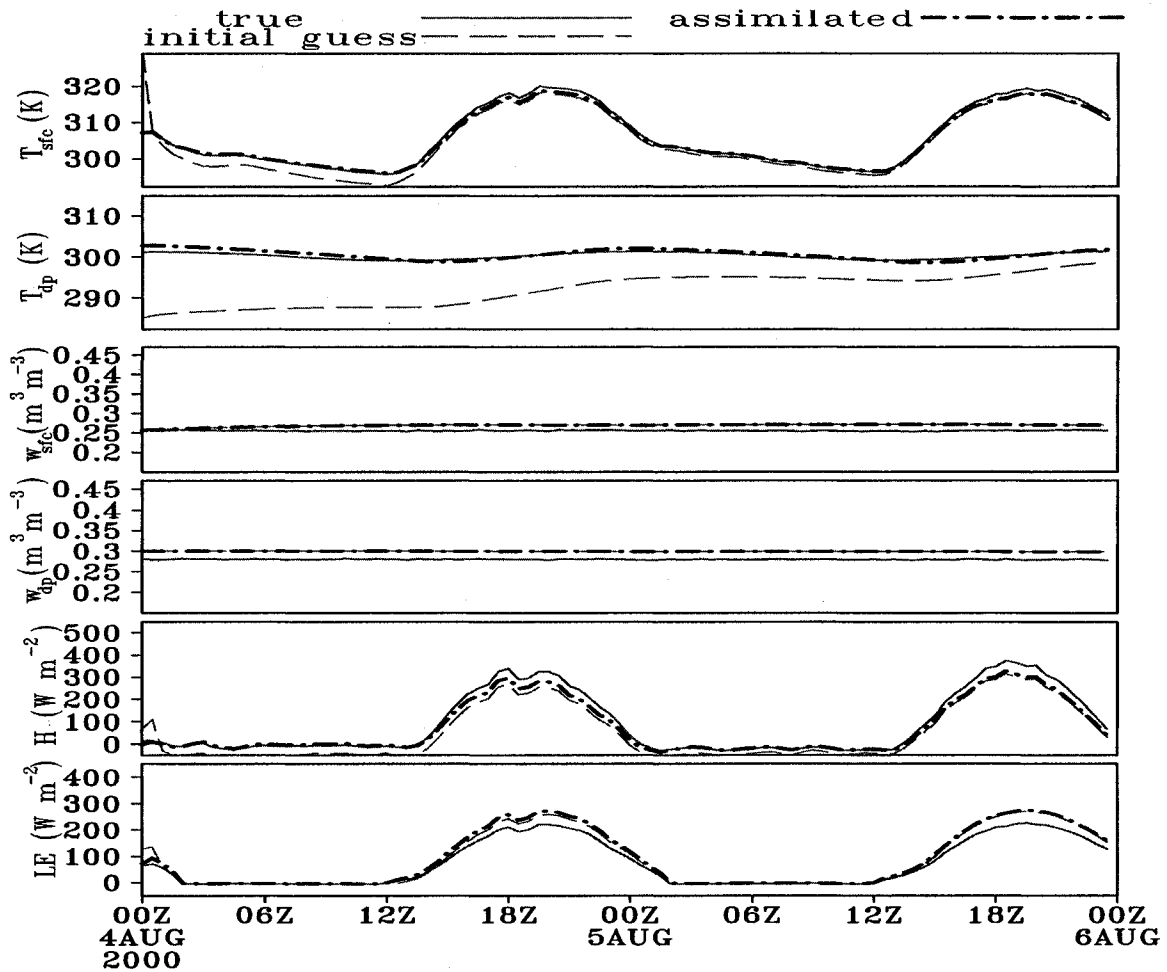


Figure 5.9. Similar to Figure 5.5 but with a reduced control variable set that consists only soil temperature states. Comparison between trajectories resulted from prior guess initial conditions and retrieved values (for state variables and  $LE$  and  $H$ ). This experiment is done using an initial guess state vector  $U^i = (330K, 285K, 0.2562m^3m^{-3}, 0.3m^3m^{-3}, 0.0m^2m^{-2})^T$ .

Robustness is more of an issue when using real data, where model error is usually involved. We tested the robustness of the assimilation scheme by adding zero-mean Gaussian noises of different standard deviations ( $std$ ) to the synthetic observations of  $T_{sfc}$ . The final degree of closeness as measured by the cost-function degrades with increasing



noise level. The larger the noise level becomes, the poorer the retrieval is. In fact, the retrieval does not work effectively when the noise level surpasses  $4.0K \text{ std}$ .

Note also that the canopy interception does not play a role in this set of experiments, because our atmospheric forcing does not produce precipitation and/or dew formation during this assimilation period. We performed another set of artificial experiments where precipitation events of different duration and intensity are artificially added to the assimilation period. The reduction to solar radiation is proportional to the precipitation rate and totally shut down as precipitation rate exceeds  $10^{-5} \text{ m s}^{-1}$ . We find that the sensitivity is milder and rather different from that of soil moisture, especially for small precipitation events that occur during daytime. We suspect that the different behavior is associated with parameterization of stomatal resistance. Raindrops on leaves may on the one hand increase the direct evaporation but also reduced the transpiration rate (from both a reduced radiation and less exposure of stomata).

Using synthetic data, we systematically documented the following basic issues of land data assimilation: robustness of the retrieval scheme as related to information redundancy; temporal measurement sparsity; and the physical implications of the adjoint variables and the usage in sensitivity studies. Through the sensitivity analysis, we are sure that whether initial soil moisture condition that optimizes the superficial soil moisture description leads to optimal estimation of surface fluxes actually depends sensitively on the vegetation coverage and growth conditions.

Synthetic experiments are ideally suited for algorithm performance tests since all of the uncertain inputs are known by design. In particular, synthetic experiments allow us to isolate the effects of the nonlinearities in the hydrological model on the quality of the

estimates. Such experiments are an indispensable first step toward a field application, although they clearly cannot replace tests based on actual observations. Compared with using synthetic data, two more difficulties must be dealt with for real data assimilation, namely, data sparseness and model error.

#### *5.4. Retrieval Experiments with Real Data*

For this set of experiments, the basic experiment setting and the micrometeorological data are exactly the same as those described in Subsection 5.3. This time, the scheme assimilates the OASIS measured instead of the model created surface ground temperature series. We performed the retrieval experiments for soil state variables and verified the results against OASIS. A recently implemented revision to the force-restore soil temperature scheme was found vital for the performance of the retrieval scheme as applied to real data.

##### *5.4.1. Initial value retrieval*

Without proper climate background to initialize, a natural option is to give soil moisture an initial guess of either saturation or wilting point value (partly because the hysteresis phenomenon). We here present a retrieval experiment with initial guess soil moisture at wilting point (Figure 5.10 and Figure 5.11). The wilting point initial guess values are an underestimation of  $0.038 \text{ m}^3\text{m}^{-3}$  to superficial soil moisture and an underestimation of  $0.08 \text{ m}^3\text{m}^{-3}$  for deep soil moisture. The retrieval scheme can reduce the initial guess errors to  $<0.01 \text{ m}^3 \text{ m}^{-3}$  and  $-0.02 \text{ m}^3 \text{ m}^{-2}$ , respectively (Figure 5.10b). The resulted improvements to surface fluxes are significant. For example, the peak value  $LE$  from initial guess can have a difference from the truth as large as  $200 \text{ W m}^{-2}$ , whereas the

retrieved one has maximum difference of only  $40 \text{ W m}^{-2}$ . The cost function is lowered by over one order of magnitude (Figure 5.10a). Improvements in the forecasting time series for the state variables and surface fluxes are shown in Figure 5.11.

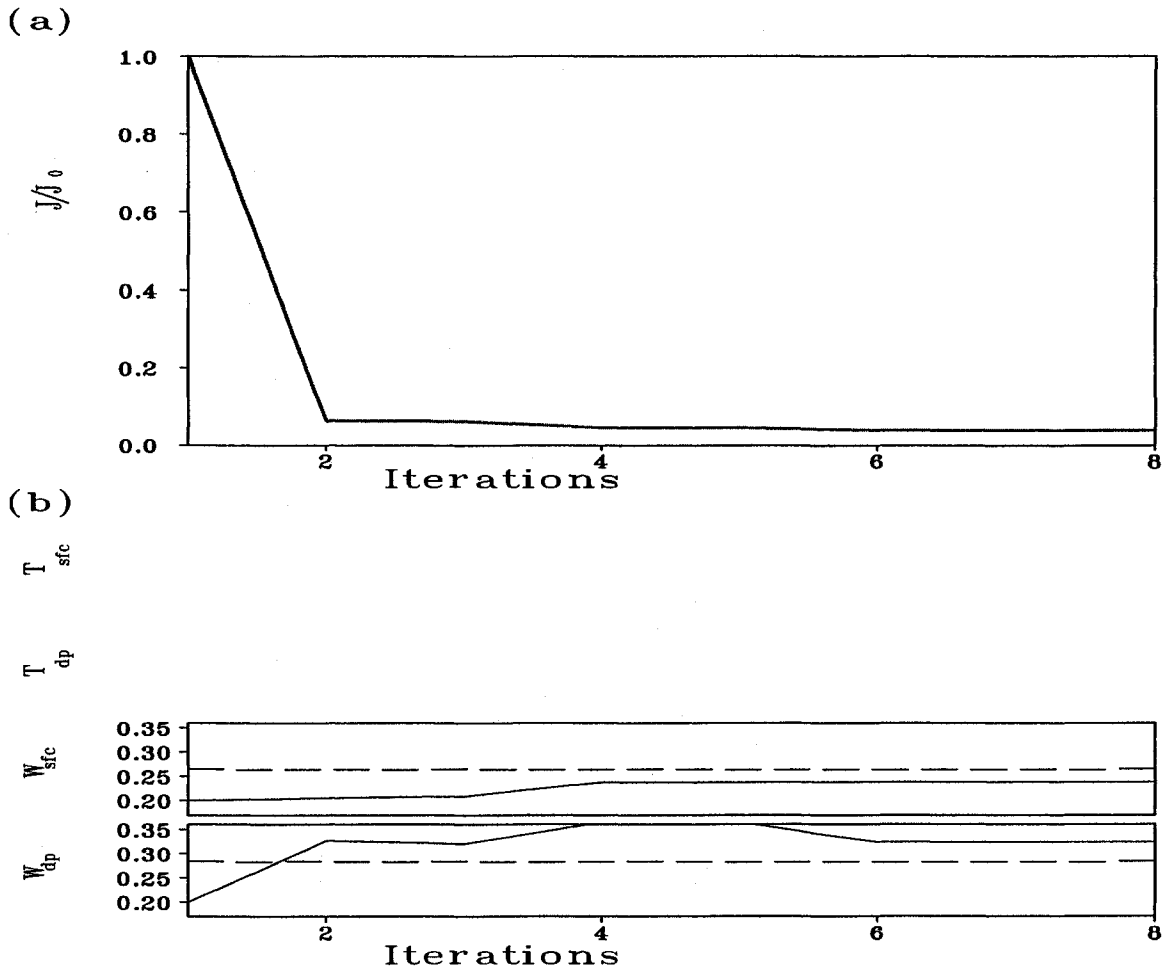


Figure 5.10. Retrieval experiments with initial guess errors on soil moisture variables. (a) Reduction in cost function; and (b) the convergence of the control variables to the “true” (dotted lines) values.

Using this experiment as a reference, we here address two extra issues for 4DVAR data assimilation: sampling strategy, i.e., are different times of day equally informative? And the effects of assimilation window length.

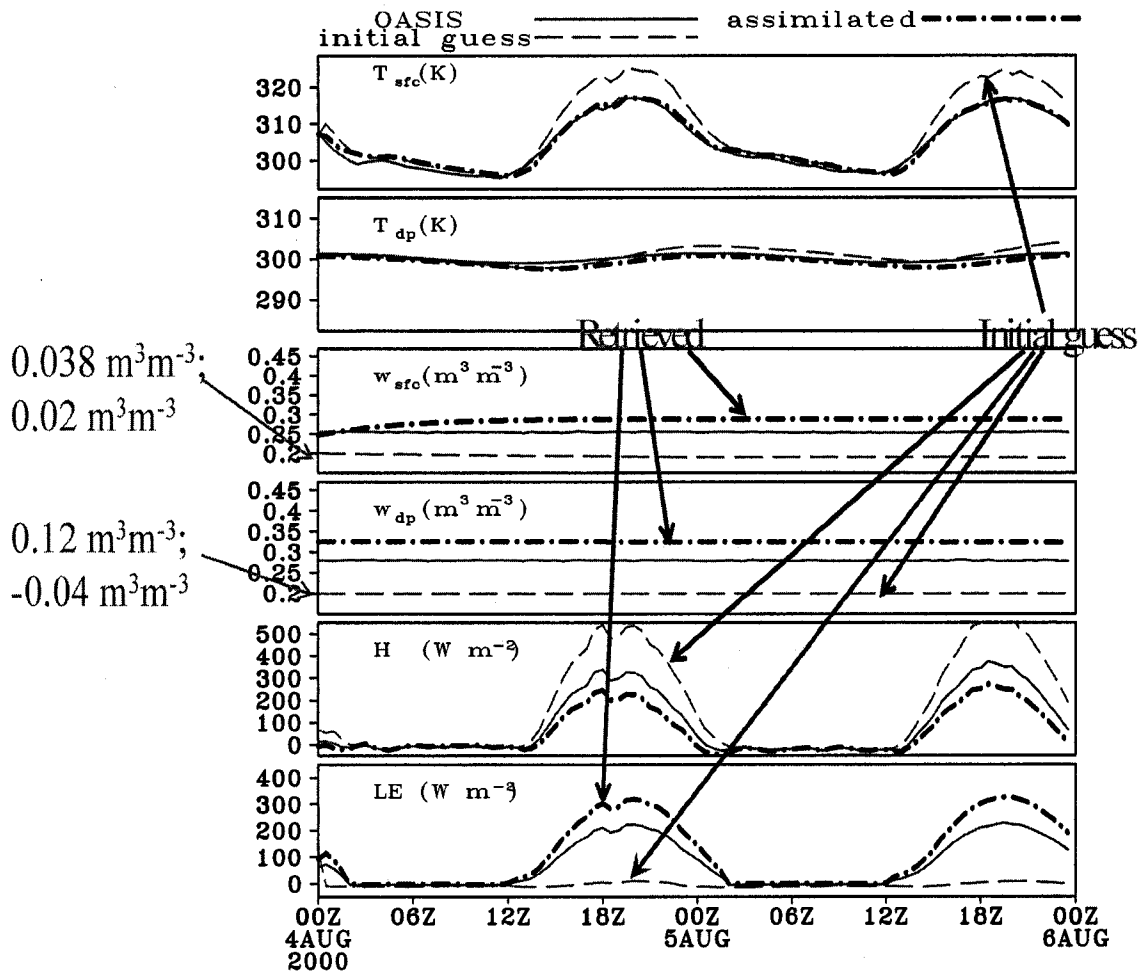


Figure 5.11. Retrieval experiments with initial guess errors on soil moisture variables. Comparison between trajectories resulted from prior guess initial conditions and retrieved values.

#### 5.4.2. Sampling strategy

The ideal case of continuous sampling serves as the basis to evaluate the performance of the assimilation system when it is supplied with sparsely-sampled observations of surface ground temperature. Information (data) from different times of day may be of quite different importance. It is of practical use to study the sampling strategy. For example, when remote sensing from low orbit satellites is used as the source

of such observations, it is expected that only a few observations per day (often no more than two from a single platform) are available.

In addition to the retrieval experiments that assume continuous half-hourly observations (as the reference run), we performed two other experiments assuming half-hourly OASIS data availability at a three-hour wide window centered on local noon (~18Z at Norman site) and a 3-hour window centered on local midnight (06Z). The first is called daytime assimilation and the second called nighttime assimilation.

With complete observations, after 5 iterations, the initial guess errors can be effectively removed, especially that associated with soil moisture. We also performed two other experiments assuming data availability at a 3-hour wide window centered on local noon (18Z at Norman) and a 3-hour wide window centered at local midnight (06Z). The first is called daytime assimilation and the second one nighttime assimilation. We compared the assimilation results of both soil temperatures and surface latent ( $LE$ ) and sensible ( $H$ ) heat fluxes. The nighttime assimilation gives the worse estimation for all the quantities (Figure 5.12). It misrepresented the peak values of surface temperature and hence severely underestimated the sensible heat flux.

However, we notice that the nighttime surface temperature is simulated rather well and the initial guess error decreased by 80% (figures not shown). The readers are cautioned not to compare the convergence rate of the cost function, because, except for the complete assimilation case, only those periods with observations are used in compose the cost function, not the whole period.

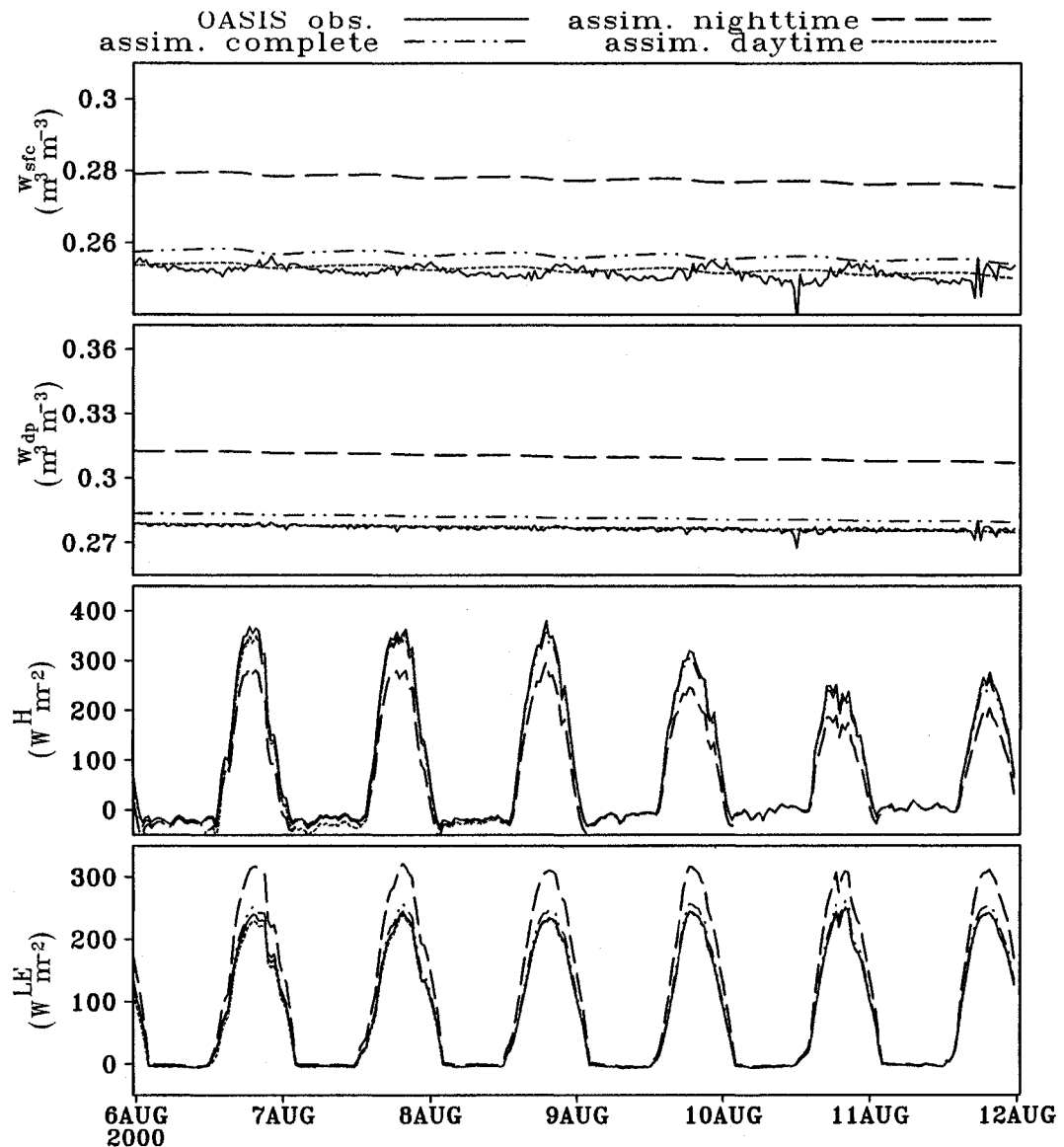


Figure 5.12. The respective accuracy (shown by differences) in estimation soil moistures and surface fluxes of three sampling schemes: continuous sampling (dot dot dash line), daytime (dotted lines), and nighttime sampling (long dashed lines).

We did not find the daytime period especially informative for experiments with synthetic data. The reason why the selected daytime period are more informative for real observations assimilation may be because the information to noise ratio is higher in that period, when the forcings are steadily strong. In other words, the weak signal during

nighttime is easy to be inundated by the instrument error. We tested a series of assimilation windows which are of equal length (3-hour) and adjacent to each other and together cover the whole daily cycle. To our surprise, the quickly heating up period (early morning hours) is the worst assimilation period. We repeated this experiment by varying the window length from 1 hour (2 measurements) to 6 hours (12 measurements). Although there are very noisy periods when the assimilation window is narrow, the general pattern always hold true.

#### 5.4.3. *The Effects of Assimilation Window Length*

The assimilation period should be long enough to let the sensitivities show up and not too long to let the nonlinear effects dominate. Another reason that observations cannot be too few is the over-determination requirement, which is not a major concern for this study. To determine the 'optimal' assimilation period is one goal of this study. Figure 5.13 is presented to show the effects of assimilation period length. Using OASIS measurements and an initial guess control vector of  $U^i = (308.16K, 300.75K, -0.226m^3m^{-3}, 0.2902m^3m^{-3}, 0.0)^T$ , we performed three retrieval experiments with respective assimilation period of 2, 4, and 8 days, all end at 00Z, 12 August 2000. Using retrieved initial conditions, an extra forecasting period of 8 days is made for each experiment.

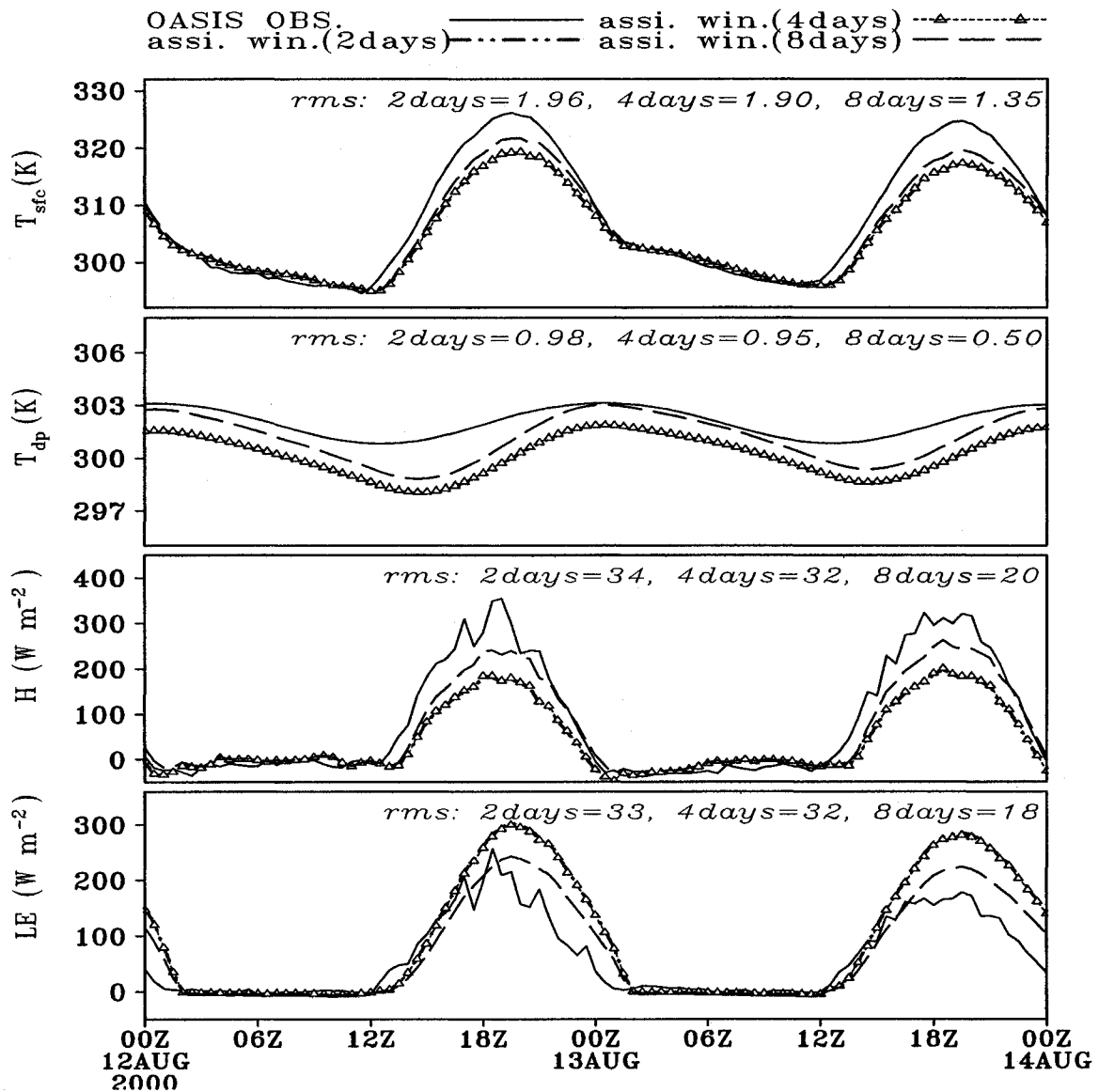


Figure 5.13. The effects of assimilation window length. Three experiments with respective assimilation period of 2 (ass. win. 2 days), 4 (ass. win. 4 days), and 8 days (ass. win. 8 days), all ending at 00Z, August 12<sup>nd</sup>, 2000, are performed. For each experiment, using retrieved initial conditions, a forward model run is made to produce an extra forecasting 8 days long (forecasting periods follows immediately the assimilation periods). The shared forecast period, i.e., 00Z, August 12-14, is shown here. Real OASIS observations are used in these experiments for initial conditions retrieval.

The shared forecasting period, i.e., 00Z, 12 August-00Z, 14 August, is shown here. The forecasts for the prognostic model variables ( $w_{sfc}$  and  $w_{dp}$  are not shown for



clarity) are best from using the initial conditions retrieved from  $T_{sfc}$  contained in 8 days. This agrees with our assertion about the information redundancy. To overcome the noisy signal contained in the observations, the quantity of observation matters. To have a deeper understanding, we also calculated *rms* errors for this 8-day forecasting period. The *rms* errors for using assimilation periods of 2, 4 and 8 days are respectively 1.96, 1.92 and 1.36K for  $T_{sfc}$ ; 0.98, 0.95 and 0.55 for  $T_{dp}$ ; 0.016, 0.015 and 0.0037  $\text{m}^3 \text{m}^{-3}$  for  $w_{sfc}$ ; 0.02, 0.019 and 0.003  $\text{m}^3 \text{m}^{-3}$  for  $w_{dp}$ ; 34, 32, and 20  $\text{W m}^{-2}$  for  $H$ ; and 33, 32 and 19  $\text{W m}^{-2}$  for  $LE$ . With the increased assimilation period, the estimations for the initial conditions of the two soil moistures are most significantly improved, followed by deep soil temperature and by surface temperature, in this order. As a result, the estimations for both latent and sensible heat fluxes are significantly improved.

In Chapter 5, the feasibility of assimilating ground surface temperature for estimating initial soil states is confirmed, first with synthetic data and then real OASIS measurements. Using synthetic data, several outstanding issues are discussed such as robustness of the retrieval scheme as related to information redundancy; temporal measurement sparsity; and the physical implications of the adjoint variables and the usage in sensitivity studies. Through the sensitivity analysis, we found that whether initial soil moisture condition that optimizes the superficial soil moisture description leads to optimal estimation of surface fluxes actually depends on the vegetation coverage and growth conditions.

We explained why the daytime period is the most informative period for the performance of the retrieval scheme. It is also shown that filter-based methods such as fitting an error covariance structure to interpolate model-data misfit at one time level to

other levels is not essential for successful land data assimilation under incomplete measurements. They are especially ineffective for systematic model error. The longer the assimilation period is, the more accurate the retrieved initial soil moisture conditions are. This again points the importance of information redundancy, especially for schemes assimilating noisy observations.

Another finding is that our modification to the force-restore temperature equation (Eq. (2.6)) is important for the scheme performance. The original soil temperature scheme and its adjoint simply do not work for real data assimilation (so no figures are shown). Assimilation system based on both revised and the original scheme works fine for OSSE experiments. However, the assimilation system based on the original forward soil temperature scheme no longer functions to assimilate data produced by the revised forward model. This suggests that, the old system may cause systematic error in the  $T_{sfc}$  estimation, although not necessarily of significant magnitude (small for wet conditions).

Tied by the forced run framework, the bad effects on PBL structure cannot be shown by initial errors in soil states. In reality, because of the slow rate at which the deep soil moisture evolves and the limited number of *in situ* observations that can be anticipated, the start-up bias in deep soil moisture is likely to persist for weeks. Chapter 6 will address the issues about initial land surface states retrieval using coupled land surface-atmospheric model and its adjoint. By then we will have a better understanding the response of planetary boundary layer developments in response to perturbations on initial soil states. The conclusions such as the relative sensitivity of soil moisture and soil temperature will be tested under more general circumstances.

## Chapter Six

### *Retrieval of Soil States Using Atmospheric Observations Only*

In this chapter, we use variational method to determine the land surface model initial states with which the model forecast best fits screen-level atmospheric observations of potential temperature and specific humidity within the assimilation window. This is achieved through minimizing a cost function  $J(U)$  (in the form of Eq. (2.32)) defined as a quadratic difference of the screen-level air temperature and specific humidity. The  $J$  is an implicit function of the control variable  $U$ . As indicated in Eq. (2.1) and (2.7),  $U$  contains the soil temperature ( $T_{sfc}$  and  $T_{dp}$ ), the soil water contents ( $w_{sfc}$  and  $w_{dp}$ ) and the canopy interception/dew  $w_{canp}$ . Because  $w_{canp}$  is insignificant in the selected periods,  $U$  has only four effective dimensions.

We have two more concerns with respect to retrieval of initial soil state variables using screen-level atmospheric observations: The very different sensitivities may cause a separation of soil moisture and temperature analysis; and there may exist an optimal data assimilation window length resulted from the contest between decreasing accuracy of the atmospheric components and increased information redundancy with longer assimilation window. These two concerns all root in the fact that a prerequisite for retrieving soil moisture from atmospheric forecast errors is that the impact of soil moisture on near surface observations dominates the impacts of other error sources (Bouttier *et al.* 1993a).

We have seen (Subsection 4.1) that the most important variations of the cost function are related with  $w_{sfc}$  and  $w_{dp}$  for the dry period, showing the sensitivity of the 2m parameters to the soil moisture condition. During the wet period, however, there is nearly

no sensitivity of the screen-level atmospheric variables to  $w_{dp}^0$ . And most of the cost function variations are associated with surface temperature. Thus, performing retrieval of a control variable of four dimensions ( $w_{sfc}$ ,  $w_{dp}$ ,  $T_{sfc}$ , and  $T_{dp}$ ), we anticipate a separation (uncoupled) of the analysis of soil temperatures and soil moistures.

For coupled land surface-atmospheric model runs, the model error may accumulate more quickly than forced land surface model runs, owing to the inaccuracy resides in atmospheric components and its feedback onto land surface components. Increasing assimilation window length has two competing effects on the performance of the assimilation scheme: Increased number of observations provides more information for the retrieval scheme and; Model predicted trajectories may significantly deviate from the true states, especially for the later stage of forecasting. The model-error differences may then be dominated by the model inaccuracy in the later stage of forecasting. Adjusting initial state variables to minimize the differences may be misleading and the adjusted initial values may start getting away from the true values. Thus, an optimal length for assimilation window may exist.

In atmospheric modeling, specification of soil moisture determines to a large extent the relative magnitudes of sensible and latent heat fluxes (Bowen ratio) and therefore the diurnal evolution of planetary boundary layer (its thermal and moisture structure). It is upon this basis that we want to infer land surface information from the evolution (response) of the near surface atmospheric conditions.

With these issues in mind, we designed a set of numerical experiments (Table 6.1) parallel to what are in Chapter 5 but for the selected wet period. To ease the interpretation of the causality mechanism, we first performed OSSEs. Using OSSEs, we

systematically documented issues such as system robustness to initial guess errors and Gaussian observational noise magnitudes, sampling strategies when observations are corrupted with random noise, and effects of preconditioning for non-circular cost function structures. Possible optimal window length is tackled with an assimilation experiment ingesting real OASIS observations.

**Table 6. 1 Retrieval experiment design for coupled model system**

July 6- wet period	OSSE	A 3-hr nature couple run starting from 00Z, 6 July 2000; Synthetic (simulated) observations of atmospheric potential temperature( $PT$ ) and specific humidity ( $q_v$ ) sampled every 5 minutes and used by the retrieval experiments; $U^{true}=(303.02K, 299.9 K, 0.379m^3m^{-3}, 0.383m^3m^{-3}, 0.0m^2m^{-2})$
		a. Initial guess errors exist in all control variables: $U^i=(310K, 305K, 0.2 m^3m^{-3}, 0.2 m^3m^{-3}, 0.0m^2m^{-2})$ (OSSEa)
		b. other experiments to test the robustness of the retrieval scheme to initial guess errors (OSSEb)
		c. Scheme resistance to Gaussian noise in $PT$ and $q_v$ (OSSEc) <ol style="list-style-type: none"> <li>1. Gaussian noise series of zero mean and different standard deviations are added to obs.</li> <li>2. <math>T_{air}</math></li> <li>3. <math>q_v</math></li> <li>4. Both <math>T_{air}</math> and <math>q_v</math> (guarantee that noise series added on <math>T_{air}</math> and <math>q_v</math> are not correlated)</li> </ol>
	OASIS	OASIS observations of $PT$ and $q_v$ available every 5 minutes are used by the retrieval experiments
		a. control run: Initial guess control variable $U^i$ same as OSSE runs (OASISa)
		b. Effects of Data Availability (OASISb) <ol style="list-style-type: none"> <li>1. Using the same setting as control run (a);</li> <li>2. Three sampling strategies: Full (complete continuous data availability), daytime (data availability at a 3-hr wide window centered on local noon, i.e. 18Z for Norman site) and nighttime (local midnight, i.e., 06Z for Norman site)</li> </ol>
		c. Identify the optimal assimilation window length (OASISc)
		d. Effects of model error in land surface process (OASISd)

### 6.1. Observing Simulation System Experiment (OSSE) Retrieval

We simulated observations of temperature and specific humidity at 2m every minute. The retrieval scheme may use the data less frequently (i.e., every 5 minutes). For

the experiments testing the noise resistance ability of the scheme, a Gaussian noise is applied on the synthetic observational series. For another set of experiments investigating the information content of each period of a day, the assimilation window is designed to cover only some periods of a day (e.g., daytime hours). For yet another set of numerical experiments trying to identify the optimal assimilation window length, the assimilation window length is varied from three hours to two days.

### *6.1.1. Convergence of the minimization*

We want to evaluate whether or not the retrieval method is able to realize a good analysis, i.e. to approach closely the real initial states. The reference run is a coupled 3-hr nature run starting from 00Z, 6 July 2000 (true initial states are  $T_{sfc}^0=303.02\text{K}$ ,  $T_{dp}^0=299.9\text{K}$ ,  $w_{sfc}^0=0.379$ , and  $w_{dp}^0=0.383$ ). Synthetic observations of atmospheric potential temperature and specific humidity are sampled every five minutes and used by the retrieval experiments. The first set of experiments is performed assuming perfect observations (without added noise) (Figure 6.1). The initial guess control variables are  $T_{sfc}^i=310\text{K}$ ,  $T_{dp}^i=305\text{K}$ ,  $w_{sfc}^i=0.2$ , and  $w_{dp}^i=0.2$  (superscript  $i$  means initial). These initial guess errors are significant compared to usually existing model errors for such quantities.

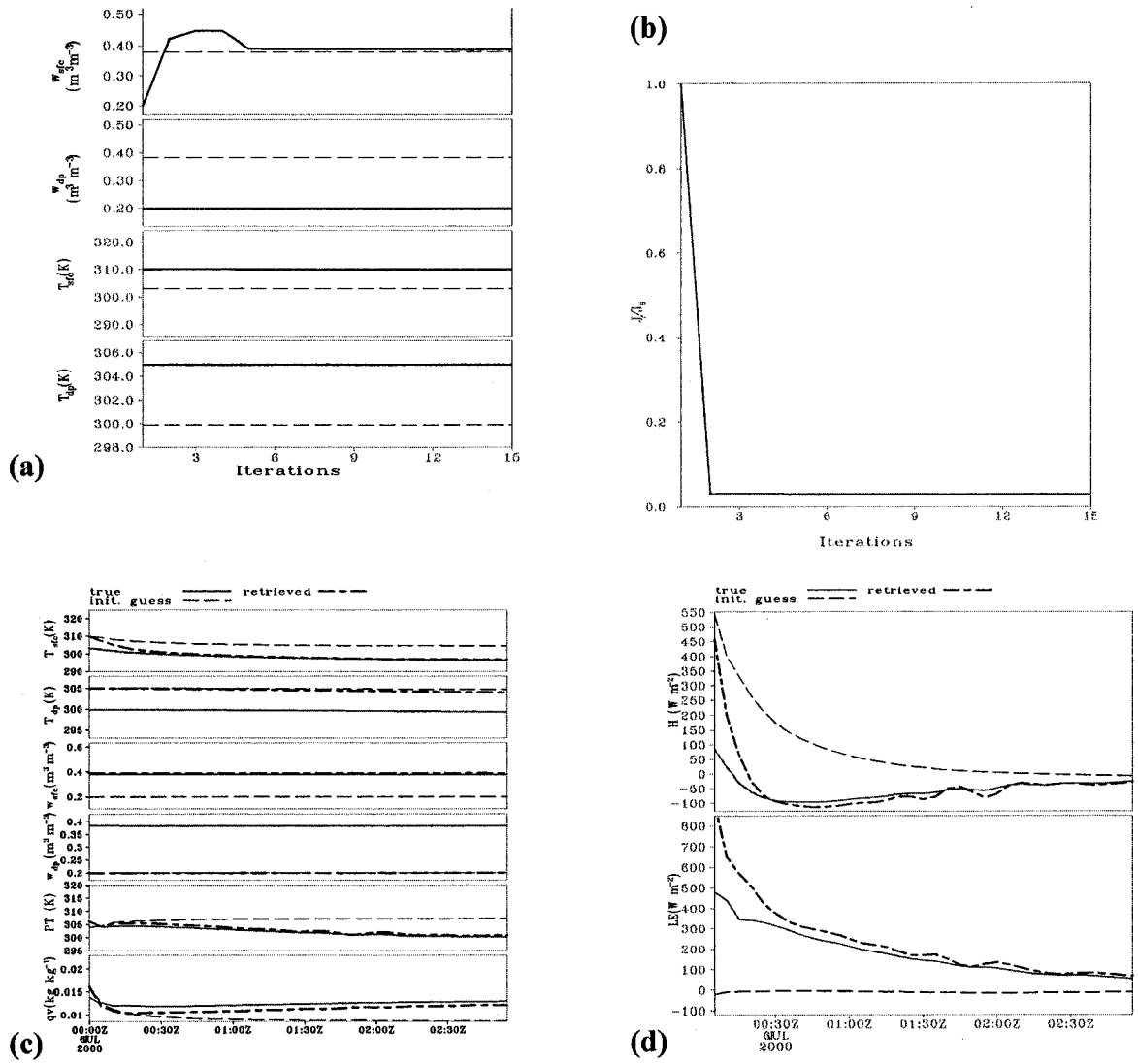


Figure 6.1. Reference OSSE retrieval experiment for assimilating screen-level atmospheric measurements. (a) the convergence of the control variables to the “true” values (dashed lines); (b) Reduction in cost function; (c) comparison between state trajectories resulted from prior guess initial conditions and retrieved values; and (d) is the surface  $LE$  and  $H$  trajectories from initial guess and retrieval as compared with synthetic truth.

Upon convergence, only the initial value of  $w_{sf}$  was successfully adjusted (Figure 6.1a). The cost function, however, was significantly reduced (Figure 6.1b). The trajectory fitness within the assimilation window is overall satisfactory for the state variables (Figure 6.1c) and surface fluxes (Figure 6.1d). The initial dry guess drastically overestimated the  $H$  whereas underestimated  $LE$ . The retrieved curves, after the first 30 minutes, come close to the true trajectories. Using the retrieved initial states, we made an extended forecasting of 21 hours (Figure 6.2). The improvements of using retrieved over using initial guessed states are significant, measured by the statistics as summarized in Table 6. 2 and Table 6. 3. This is especially the case for daytime heating period (12-24Z).



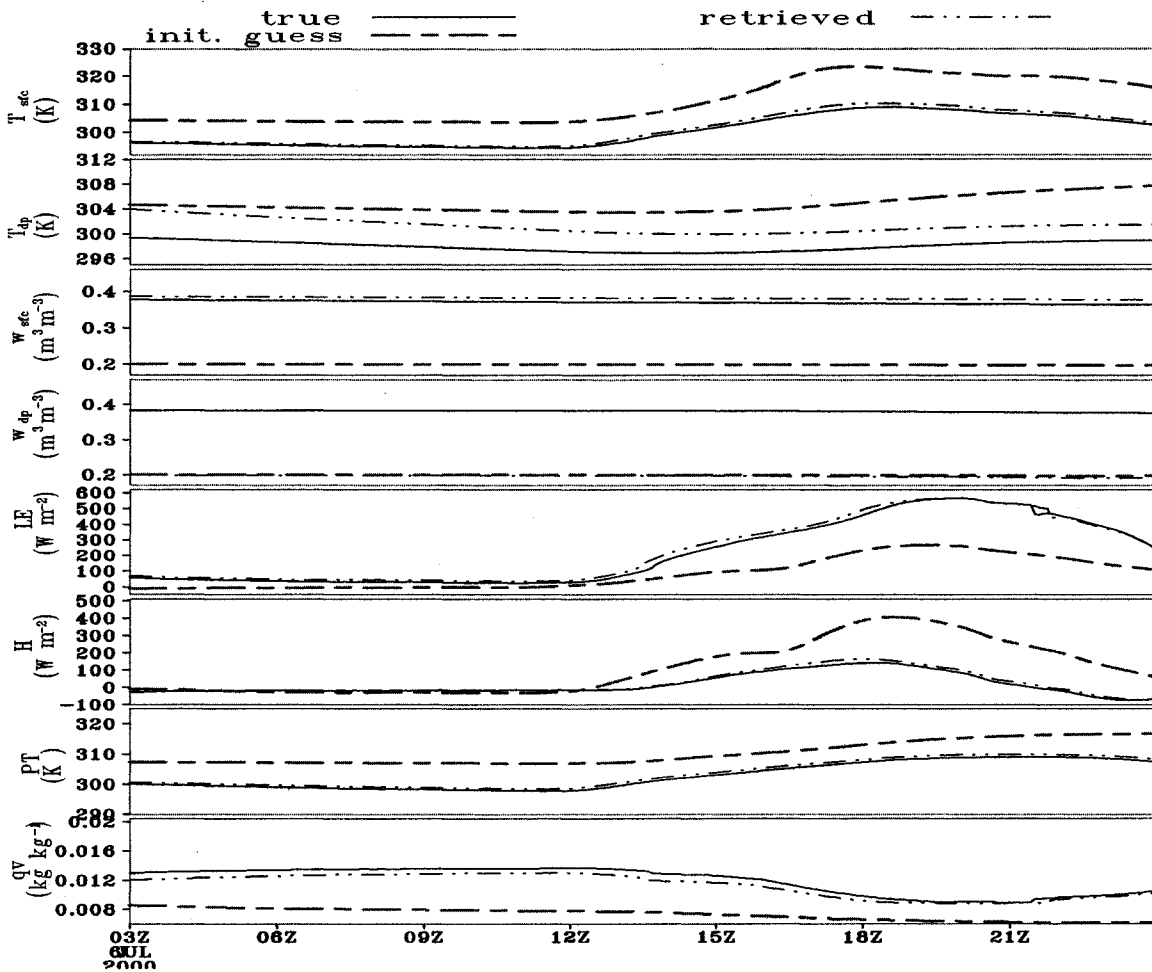


Figure 6.2. Comparison between state trajectories resulted from prior guess initial conditions and retrieved values for the true forecasting period (following the assimilation window).

A comparison between Table 6. 2 and Table 6. 3 shows that the *rms* errors for screen-level air temperature, specific humidity are reduced from 6.83 K to 0.8K and 4.13 g/kg to 0.68g/kg respectively. The latent and sensible heat fluxes are reduced respectively from 130  $W m^{-2}$  to 11  $W m^{-2}$  and from 179  $W m^{-2}$  to 19.33  $W m^{-2}$ . The improvements resulted from using retrieved over initial guess state variables are also shown in the trajectory fitness of the state variables themselves (column 4-7 in Table 6.2 and Table 6.3).

**Table 6. 2** Some statistics between initial guess and observation within the forecasting period

	$T_{air} (K)$	$q_v(kg/kg)$	$T_{sfc}(K)$	$T_{dp}(K)$	$w_{sfc}(m^3 m^{-3})$
<i>RMSE</i>	6.83	$4.13 \times 10^{-3}$	10.0	3.77	0.184
<i>MBE</i>	6.72	$-4.0 \times 10^{-3}$	9.8	3.43	-0.184
<i>MAE</i>	8.52	$5.32 \times 10^{-3}$	13.4	6.28	0.187
	$w_{dp}(m^3 m^{-3})$	$H(Wm^{-2})$	$LE(Wm^{-2})$		
<i>RMSE</i>	0.18	130	179		
<i>MBE</i>	0.18	87	-145		
<i>MAE</i>	0.18	260	309		

**Table 6. 3** Some statistics between retrieved and observation within the forecasting period

	$T_{air} (K)$	$q_v(kg/kg)$	$T_{sfc}(K)$	$T_{dp}(K)$	$w_{sfc}(m^3 m^{-3})$
<i>RMSE</i>	0.80	$6.84 \times 10^{-4}$	1.01	3.37	$1.19 \times 10^{-2}$
<i>MBE</i>	-0.78	$6.33 \times 10^{-4}$	-0.92	-3.32	$-1.18 \times 10^{-2}$
<i>MAE</i>	1.05	$1.16 \times 10^{-3}$	1.80	4.6	$1.36 \times 10^{-2}$
	$w_{dp}(m^3 m^{-3})$	$H(Wm^{-2})$	$LE(Wm^{-2})$		
	0.184	11.06	19.33		
	0.184	-6.31	-14.2		
	0.184	27.44	52.5		

We performed another retrieval experiment starting from  $T_{sfc}^i = 310K$ ,  $T_{dp}^i = 300K$ ,  $w_{sfc}^i = 0.4$ , and  $w_{dp}^i = 0.4$  (saturation soil moisture initial guess as shown in Figure 6.3 and Figure 6.4). For this case, the  $T_{sfc}$  is retrieved with better accuracy for this wet period. The adjustments to soil wetness is insignificant (<0.5%). Without previous knowledge about soil wetness, it is hard to retrieve the exact soil moisture values.

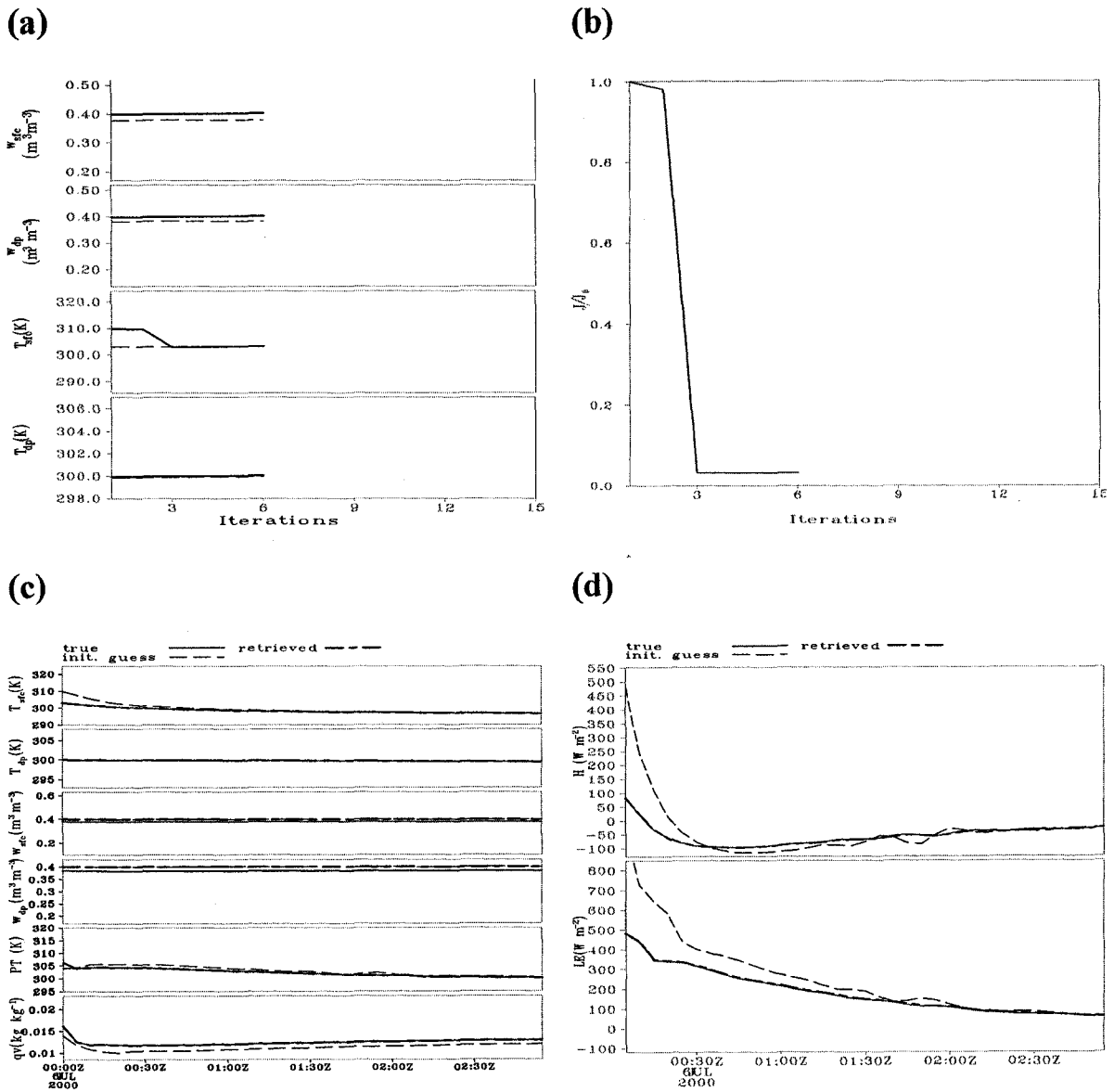


Figure 6.3. As Figure 6.1 but with saturation initial guess.

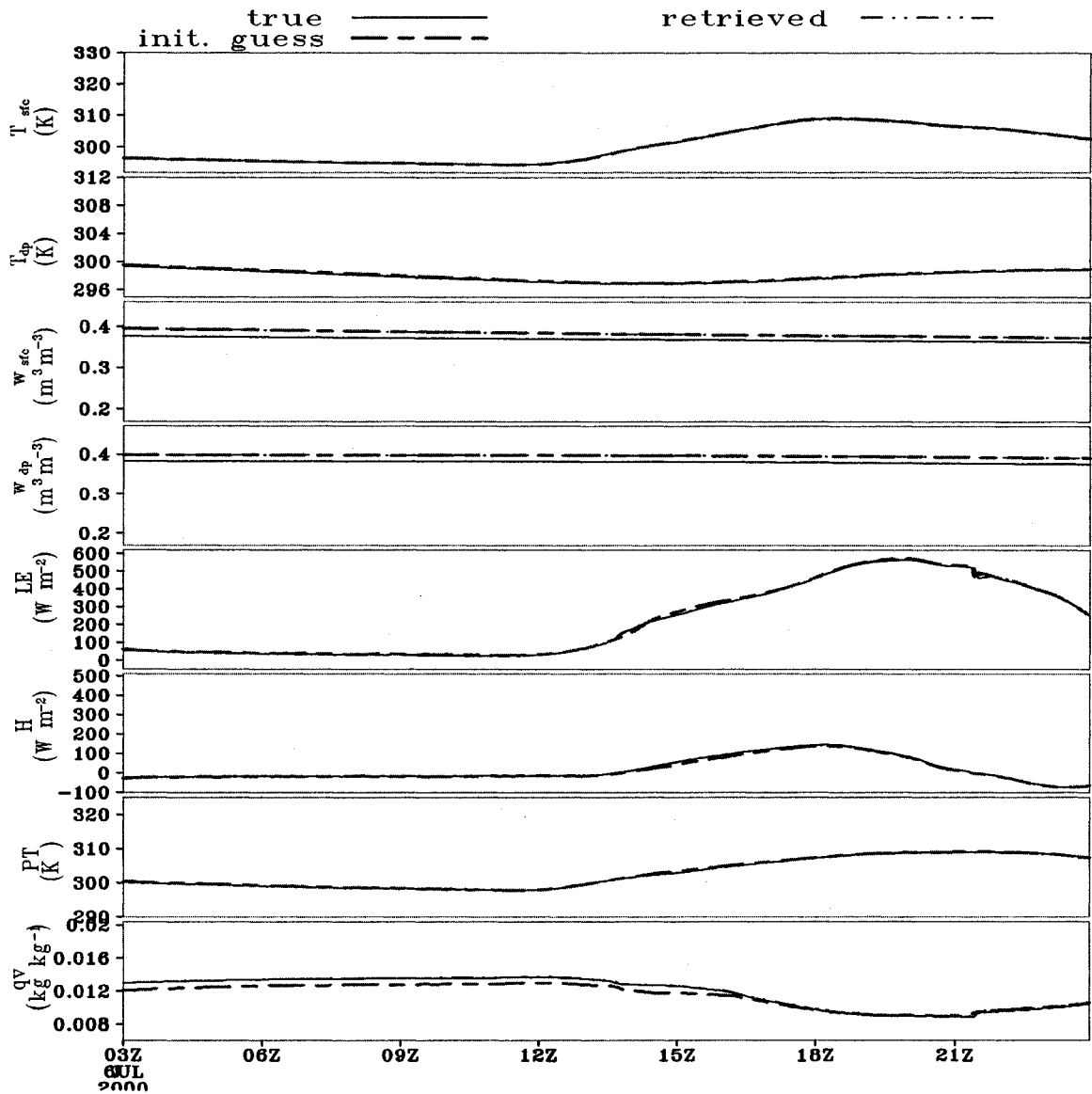


Figure 6.4. As Figure 6.2 but for saturation initial guess for soil moistures.

A comparison between Figure 6.2 and Figure 6.4 indicates that the sensitivity caused by initial guess error of 10K on  $T_{sfc}^0$  causes less sensitivity (measured by the *rms*) than that caused by a  $0.18 \text{ m}^3\text{m}^{-3}$  error on initial  $w_{sfc}^0$ . This can be explained by analyzing the components of the latent heat flux for this period. For this rather moist period, the direct evaporation from the surface layer dominates *LE*. Wilting point guess causes

unrealistically low  $LE$  (Figure 6.1d). Effects from perturbation on  $T_{sfc}^0$ , as shown in the forward sensitivity experiment, are short lasting at best.

For this retrieval experiment, a comparison between Table 6. 4 and Table 6. 5 indicates that the *rms* errors for screen-level air temperature, specific humidity are reduced from 0.2 K to 0.11K and 6.45 g/kg to 0.86g/kg respectively. The latent and sensible heat fluxes are reduced respectively from 4 W m<sup>-2</sup> to 1 W m<sup>-2</sup> and from 5.6 W m<sup>-2</sup> to 4.9 W m<sup>-2</sup>. The improvements are not as significant compared to the wilting point initial guess retrieval experiment.

**Table 6. 4** Some statistics between initial guess and observation within the forecasting period

	$T_{air} (K)$	$q_v(kg/kg)$	$T_{sfc}(K)$	$T_{dp}(K)$	$w_{sfc}(m^3 m^{-3})$
RMSE	0.2	$6.45 \times 10^{-4}$	0.125	$7.06 \times 10^{-2}$	$3.14 \times 10^{-5}$
MBE	0.16	$-5.37 \times 10^{-4}$	$4.05 \times 10^{-2}$	$6.84 \times 10^{-2}$	$2.69 \times 10^{-5}$
MAE	0.49	$9.31 \times 10^{-4}$	0.25	0.1	$4.86 \times 10^{-5}$
	$w_{dp}(m^3 m^{-3})$	$H(Wm^{-2})$	$LE(Wm^{-2})$		
RMSE	$3.30 \times 10^{-4}$	4.187	5.6		
MBE	$-3.29 \times 10^{-4}$	-2.36	2.38		
MAE	$3.66 \times 10^{-4}$	13.4	23.7		

**Table 6. 5** Some statistics between retrieved and observation within the forecasting period

	$T_{air}(K)$	$q_v(kg/kg)$	$T_{sfc}(K)$	$T_{dp}(K)$	$w_{sfc}(m^3m^{-3})$
RMSE	0.11	$8.59 \times 10^{-5}$	0.137	$5.87 \times 10^{-2}$	$1.47 \times 10^{-2}$
MBE	$3.7 \times 10^{-2}$	$-7.05 \times 10^{-5}$	$6.31 \times 10^{-2}$	$-5.03 \times 10^{-2}$	$-1.45 \times 10^{-2}$
MAE	0.235	$4.43 \times 10^{-4}$	0.253	$7.8 \times 10^{-2}$	$1.92 \times 10^{-2}$
	$w_{dp}(m^3m^{-3})$	$H(Wm^{-2})$	$LE(Wm^{-2})$		
RMSE	$1.67 \times 10^{-2}$	1.92	4.96		
MBE	$-1.67 \times 10^{-2}$	1.23	-2.84		
MAE	$1.68 \times 10^{-2}$	4.7	38.26		

Table 6. 6 listed several retrieval experiments starting from different initial conditions. From Table 6. 6, it seems as long as initial guess  $T_{sfc}^0$  lies above its true value and initial guess  $w_{sfc}^0$  lies below its true value, the adjustment to the  $w_{sfc}$  is significant. As long as  $w_{sfc}^0$  is guessed above the true value, the adjustment to  $T_{sfc}^0$  is significant. Scheme is robust for initial surface moisture guess in the range of wilting point (0.24) to saturation (0.45), and even more tolerant for initial surface temperature guess errors. These can be explained by analyzing the contour of the cost function, especially the  $w_{sfc}$ - $T_{sfc}$  crosssection (see Figure 2.14-Figure 2.16). For this moist period, the separation of sensitivity between  $T_{sfc}$  and  $w_{sfc}$  is so strong that it is not easy to get both quantities successfully retrieved without proper preconditioning (to be detailed soon).

Table 6. 6 Initial states retrieval using synthetic data

Initial guess control variable				Initial <i>rms</i> error in $\theta$	$J_{\text{final}}/J_0$	# it. needed	Retrieved initial condition			
$T_{\text{sfc}}$	$T_{\text{dp}}$	$w_{\text{sfc}}$	$w_{\text{dp}}$				$T_{\text{sfc}}$	$T_{\text{dp}}$	$w_{\text{sfc}}$	$w_{\text{dp}}$
308.0	299.5	0.3	0.2	1.6	3.08E-2	5	304.4	300.4	0.40	0.19
300	300	0.4	0.4	0.47	0.26	5	301.1	300.0	0.4	0.39
300	300	0.2	0.2	3.05	9.8E-3	4	300.1	300.0	0.34	0.19
320	320	0.2	0.2	3.5	0.31	5	319.0	319.0	0.38	0.20
308	298	0.35	0.378	0.7	0.76	3	308.0	297.9	0.37	0.378
298	300	0.409	0.403	1.1	8.89E-4	3	303.1	299.8	0.41	0.40
300	300	0.5	0.4	0.49	0.11	4	302.8	300	0.5	0.399
310	300	0.4	0.4	0.49	4.92E-2	4	301.8	300	0.4	0.399
310	300	0.2	0.4	4.0	7.29E-2	3	310.0	300	0.39	0.4
310	300	0.5	0.4	1.1	2.28E-2	4	303.0	300	0.5	0.39

### 6.1.2. Robustness to Gaussian noise

Another important issue is the noise level that the scheme can tolerate. To this end, the observations created with the coupled 1D land surface atmospheric model are corrupted with realizations of a Gaussian noise with different standard deviation magnitudes on  $T_{\text{air}}$  and  $q_{\text{air}}$ . Use the reference retrieval experiment configuration (OSSEa), we performed retrieval experiments with Gaussian noise of different magnitudes (0.1, 0.5 and 2.0 K for temperature and 1, 2 and 5 g/kg for specific humidity) added to the air temperature and mixing ratio time series within the assimilation window, respectively and jointly. In Figure 6.5, we compared retrieval experiments with noise added to screen-level parameters and that without noise corruption. Generally, the higher the noise level, the worse the retrieved trajectory fitness (as measured by the cost function).

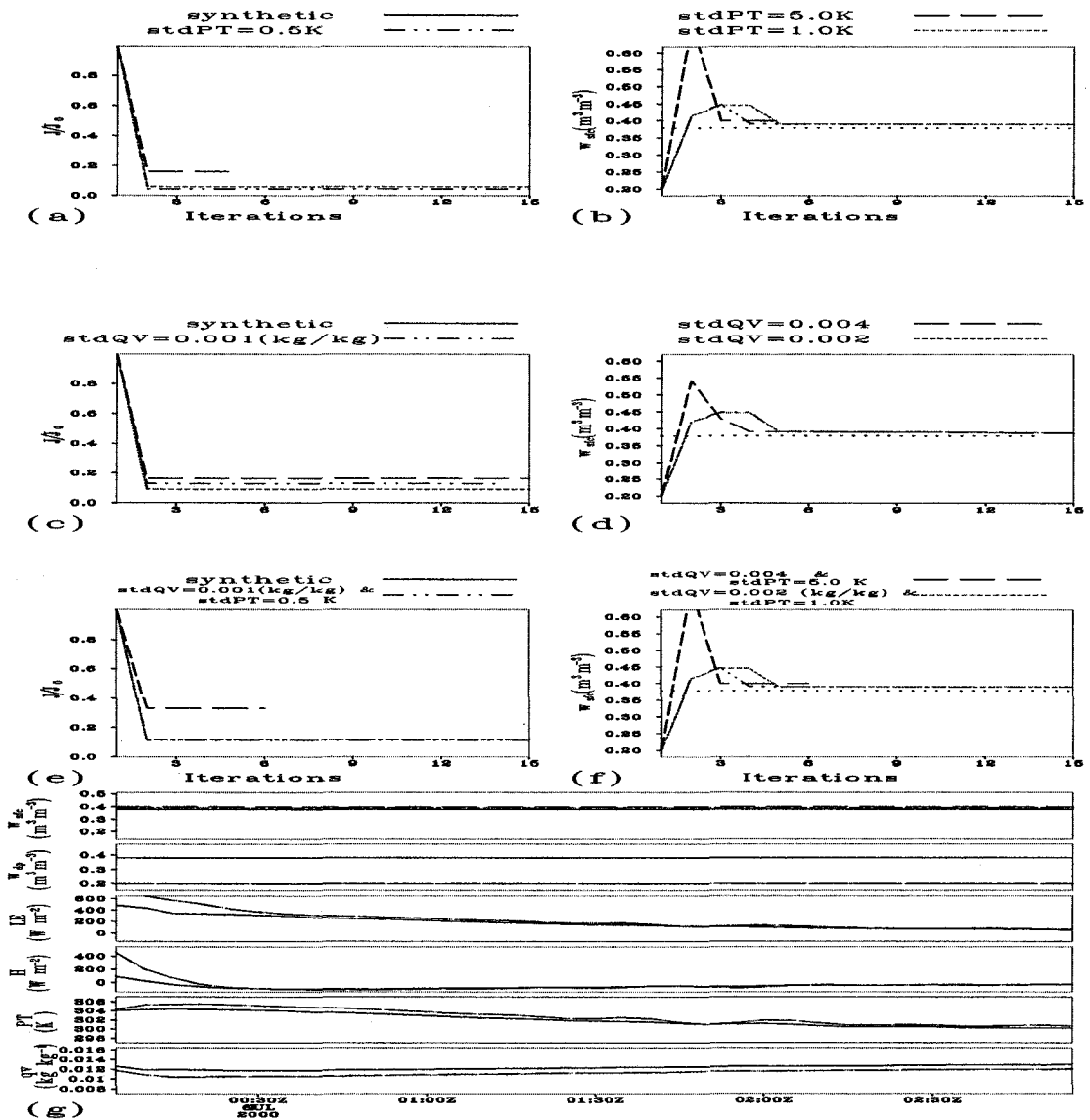


Figure 6.5. Comparison of the retrieval scheme performance under three different Gaussian noise levels added to potential temperature (a and b), specific humidity (c and d) series separately and jointly (e and f). (a), (c) and (e) are reductions of the cost function; (b), (d) and (f) are the approaching of the true surface soil moisture at each iteration, and (g) is the comparison of the atmospheric states ( $w_{sfc}$ ,  $w_{dp}$ ,  $PT$  ( $T_{air}$ ) and  $qv$ ) and surface fluxes ( $LE$  and  $H$ ) assimilated with the retrieved initial states for joint Gaussian noise added to observations of  $PT$  and  $qv$ .

However, for a particular state ( $w_{sfc}$  in Figure 6.5b), the retrieval can be benefited from the added noise. For Gaussian noise added to the 2m air temperature, when the



standard deviation is smaller than 3 K, convergence is not affected. For Gaussian noise added to specific humidity, standard deviation smaller than 4 g/kg has no apparent effects on convergence.

### 6.1.3 Effects of observational accuracy

Without a background term in the cost function, the relative magnitudes of  $\sigma_{qv} / \sigma_T$  matters for the retrieval performance. Use the reference configuration, we tested a series of experiments with  $\sigma_T$  varies from 0.5 to 3 K and  $\sigma_{qv}$  varies from 1 to 4 g/kg. The finally retrieved  $w_{sfc}$  are listed in Table 6. 7.

Table 6. 7 Retrieved  $w_{sfc}$  with different measurement accuracies

$\sigma_T$ (K)	0.5	1.0	2.0	3.0
Retrieved $w_{sfc}$ ( $\text{m}^3\text{m}^{-3}$ )	0.391	0.387	0.800	0.556
$\sigma_{qv}$ (g/kg)	1	2	3	4
Retrieved $w_{sfc}$ ( $\text{m}^3\text{m}^{-3}$ )	0.390	0.389	0.390	0.391

Compared to the true state of  $0.379 \text{ m}^3\text{m}^{-3}$ ,  $\sigma_{Tsfc}=1 \text{ K}$  yields the best retrieval. Generally, the larger the measurement standard deviation, the worse the retrieval is. This is, however, not a monotonic process. In the above,  $\sigma_{Tsfc}=2 \text{ K}$  yields the worst estimation of the initial surface soil moisture (0.8). That the final convergence is sensitive to the chosen of measurement accuracy indicates that the screen-level potential temperature evolution has important control over the retrieval of surface soil moisture for this wet period and partially vegetated surface. From Table 6. 7, it seems for standard deviation less than 4 g/kg, the retrieval seems not sensitive to the measurement accuracy of the specific humidity.

## 6.2. Retrieval Experiments with Real Data

The first real data assimilation experiment (see Figure 6.6) uses exactly the same initial guess as OSSEa but instead assimilate the OASIS observed screen-level air potential temperature and specific humidity. Similar to the corresponding OSSE experiment (Figure 6.1), only  $w_{sf}^0$  gets significantly improved (Figure 6.6a). Primarily due to the model errors, the decrease of the cost function is not as apparent as the corresponding OSSE. There is still ~18% error as measured by the cost function (Figure 6.6b). Whereas the trajectories of the prognostic variables are significantly updated (Figure 6.6c) within the assimilation window, the improvement in surface fluxes are quite limited (Figure 6.6d). We right now are not clear whether the poor surface fluxes are due to spin up or other unknown reasons. What we can see is that significant adjustment in model sensible and latent heat fluxes are made during the first two hours to correct for the dry initial conditions.

We further examine the improvements for the one day long extra forecasting period that follow the assimilation window period. Fortunately, the improvements are all apparent and significant, especially for the daytime heating period. The *rms* error for  $H$  is reduced from  $132 \text{ W m}^{-2}$  to  $<11 \text{ W m}^{-2}$ . For  $LE$ , *rms* error is reduced from  $179 \text{ W m}^{-2}$  to merely  $20 \text{ W m}^{-2}$ . More detailed statistics are given in Table 6. 8 and Table 6. 9. Thus, so long as the initial values of the LSM prognostic variables are correctly retrieved, the surface fluxes will be improved in the long run. Spin up is now suspected to be the reason for limited improvements within the assimilation window for surface fluxes.

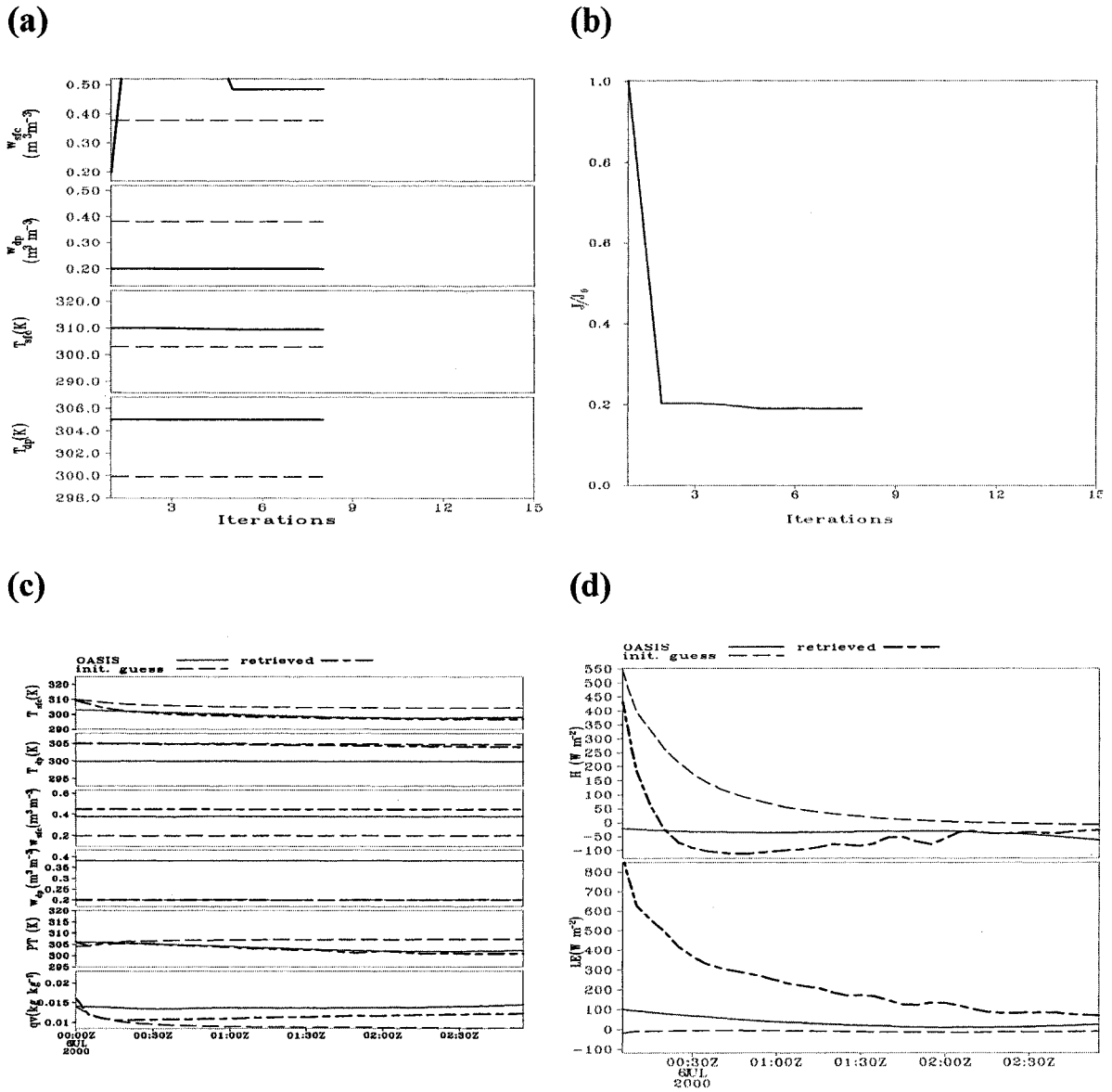


Figure 6.6. Reference OASIS retrieval experiment for assimilating screen-level atmospheric measurements. (a) the convergence of the control variables to the true values (dashed lines); (b) Reduction in cost function; (c) comparison between state trajectories resulted from prior guess initial conditions, retrieved values, and OASIS observations; and (d) is similar to (c) but for  $LE$  and  $H$ .

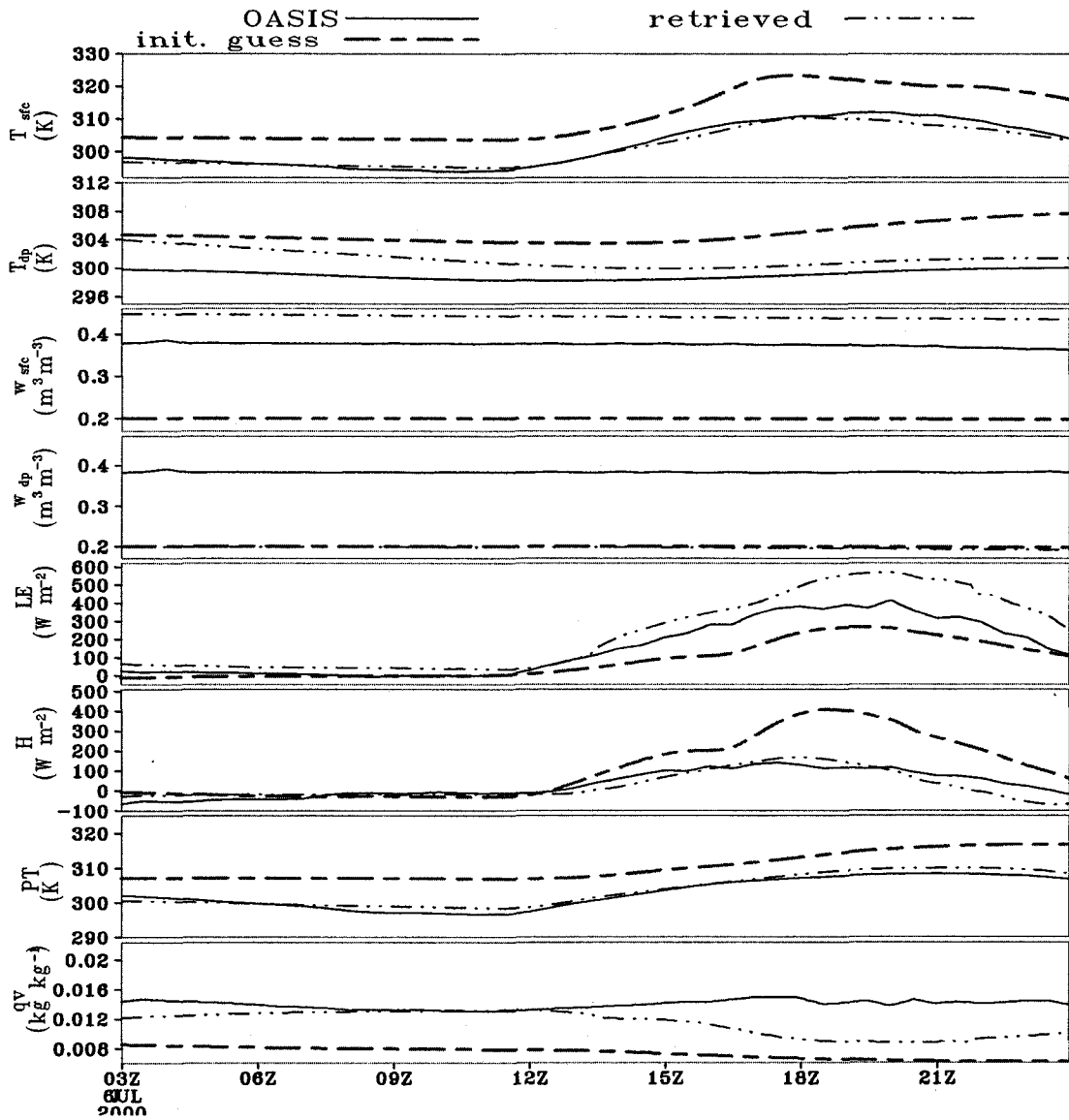


Figure 6.7. Comparison between state trajectories resulted from prior guess initial conditions and retrieved values for the true forecasting period (following the assimilation window).

**Table 6. 8** Some statistics between initial guess and observation within the forecasting period

	$T_{air}(K)$	$q_v(kg/kg)$	$T_{sfc}(K)$	$T_{dp}(K)$	$w_{sfc}(m^3m^{-3})$
RMSE	6.85	$4.19 \times 10^{-3}$	10.06	3.78	0.24
MBE	6.74	$-4.07 \times 10^{-3}$	9.83	3.44	-0.24
MAE	8.53	$5.36 \times 10^{-3}$	13.47	6.30	0.25
	$w_{dp}(m^3m^{-3})$	$H(Wm^{-2})$	$LE(Wm^{-2})$		
RMSE	$2.78 \times 10^{-3}$	132	179		
MBE	$2.45 \times 10^{-3}$	88	-146		
MAE	$5.43 \times 10^{-3}$	261	310		

**Table 6. 9** Some statistics between retrieved and observation within the forecasting period

	$T_{air}(K)$	$q_v(kg/kg)$	$T_{sfc}(K)$	$T_{dp}(K)$	$w_{sfc}(m^3m^{-3})$
RMSE	0.773	$5.92 \times 10^{-4}$	0.976	3.365	$7.25 \times 10^{-2}$
MBE	-0.757	$5.51 \times 10^{-4}$	-0.89	-3.31	$-7.25 \times 10^{-2}$
MAE	1.01	$1.04 \times 10^{-3}$	1.72	4.59	$7.3 \times 10^{-2}$
	$w_{dp}(m^3m^{-3})$	$H(Wm^{-2})$	$LE(Wm^{-2})$		
RMSE	0.184	10.9	19.56		
MBE	0.184	-5.92	-14.9		
MAE	0.184	26.7	55.5		

### 6.2.1. Influence of the assimilation window length

For OSSE experiments without noise corruption to the simulated observations, we did not see apparent benefit in using longer assimilation window length (>6hours). Parallel experiments with Gaussian noise (1K std and 0 mean) on air temperature are performed for several assimilation window lengths: 60, 120, 180, 240, 300, 360, and 720

minutes. We found that except for the general trend of improvement on the retrieved initial  $w_{sfc}$  with increased assimilation window length, including nighttime period in the assimilation window also sacrifices the retrieval somewhat, causing wiggles on the curve of retrieved  $w_{sfc}^0$  versus assimilation window length.

Exactly the same retrieval experiments were performed for assimilating real OASIS observations. The performance of the retrieval system, as measured by the decrease of the cost function, can be seen from Figure 6.8. For assimilation window less than one day, increasing of assimilation window is beneficial. Choosing assimilation window longer than 6 hours can steadily reduce the initial guessed error by more than one order of magnitude (considered significant reduction for real data assimilation). Further increase assimilation window length from 6 to 12 hours is less effective in further reducing the initial guess error. More interestingly, use too long assimilation window (e.g., 24 hours) sacrifices the retrieval. This signifies a contesting between model error and the information content. Another severe hindrance of using too long assimilation window is the computational cost associated with both forward model integration and also the backward model integration of the adjoint. For the sake of efficiency, we suggest assimilation window of about six hours for this relatively moist periods and vegetated surfaces.

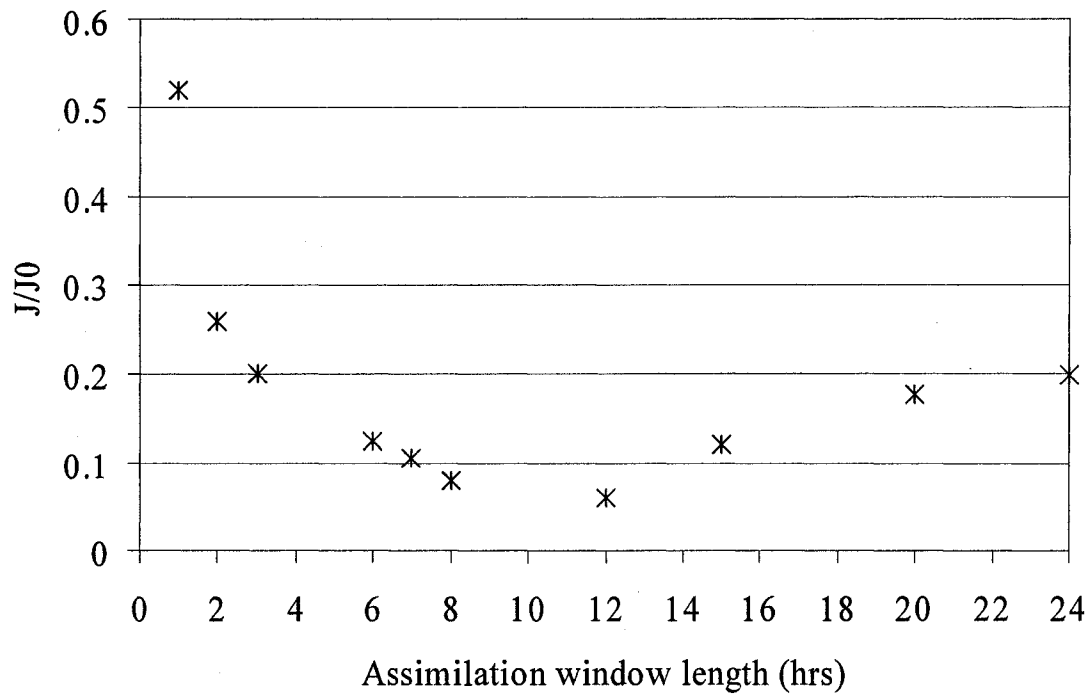


Figure 6.8. Relationship between the accuracy in retrieval and the assimilation window length.

Using an assimilation window of one hour and initial guess control variables:  $T_{sfc}=303\text{K}$ ,  $T_{dp}=300\text{K}$ ,  $w_{sfc}=0.379\text{ m}^3\text{ m}^{-3}$ ,  $w_{dp}=0.38\text{ m}^3\text{ m}^{-3}$ , we addressed another related issue of influence of the assimilation frequency. We tested assimilating the observations every 1, 2, 3, and 4 minutes. As expected, assimilating every 4 minutes is much more efficient than every 1 minute. All retrieval experiments arrive at  $T_{sfc}=303.1\text{K}$ ,  $T_{dp}=300.2\text{ K}$ ,  $w_{sfc}=0.40\text{ m}^3\text{ m}^{-3}$ ,  $w_{dp}=0.383\text{ m}^3\text{ m}^{-3}$ . However, when assimilation frequency becomes too low (<every 5 minutes in this case), the retrieved states will deviate from the true states gradually and become significantly for assimilation frequency of 10 minutes each.

We performed similar experiments for other assimilation window lengths. As we expected, the longer the assimilation window, the more deserving to perform less

frequent assimilation is. For example, 12 hour assimilation window can tolerate assimilating the data every 30 minutes. The apparent benefit for performing assimilation at lesser frequency is for efficiency of the scheme. Updating the forcing every minute makes the scheme less practicable for real application (For some initial guesses, it takes 4 hours for a single column run of the retrieval scheme for a 24- hour assimilation window).

### 6.2.2. *Effects of preconditioning*

Preconditioning is a technique for effectively (robust as well as efficient in both time and space) solve large sparse matrix problems. It is also believed that proper preconditioning can improve the convergence of the optimizer (e.g., Gilbert and Lemarechal 1989; Bouyssel *et al.* 1998). This is still an unsolved problem and general effective preconditioners are lacking.

When using an iterative method to solve a linear system of equations, a good choice of preconditioner can have a dramatic impact on runtime and robustness. Instead of solving a system  $Ax=b$ , you solve a preconditioned system  $M^lAx=M^lb$ , where  $M$  is the preconditioner. A good preconditioner must have a variety of properties. First, the preconditioned system should converge quickly. This generally means that  $M^lA$  has a small condition number (ratio of the maximum to minimum singular value, i.e., square root of the eigen value). Second, it should be easy to solve systems of the form  $My=z$ .

Pre-conditioning may be applied in order to improve the convergence of the minimization. It works best when the selected control vectors are not completely orthogonal. General and case-insensitive approaches for preconditioning are hard to achieve without prior knowledge of the cost function structure. Based on the reference

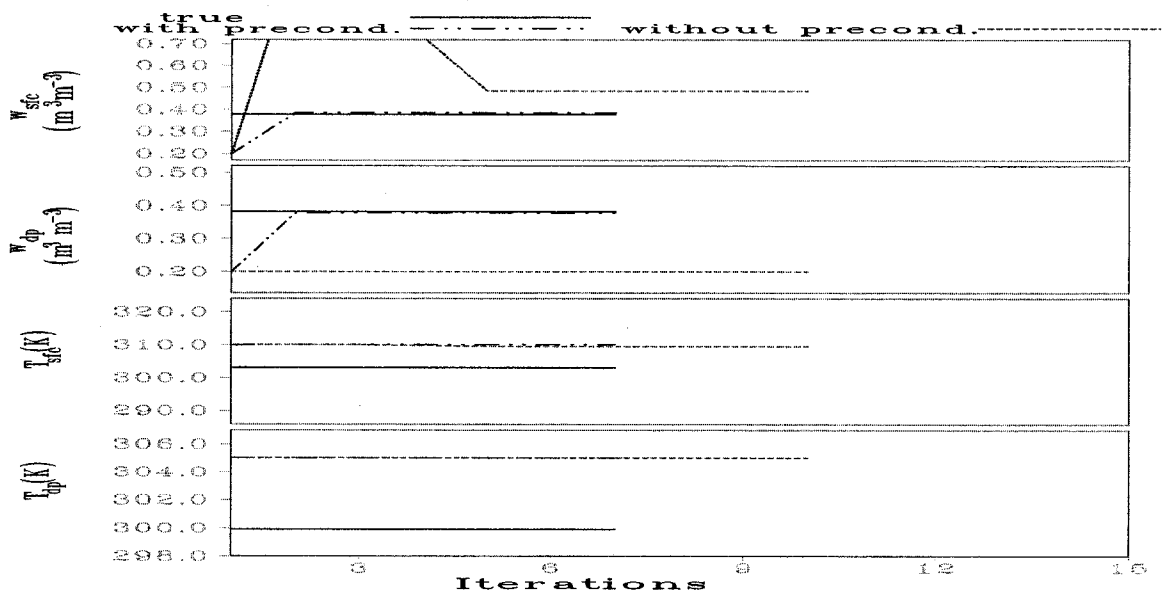


run, we tried by setting the step size ratio of  $w_{sfc}$  and  $w_{dp}$  to be 1:100, according to the analysis of the  $LE$  components (we found that direct evaporation from wet surface dominate during this wet period). We found that both  $w_{sfc}$  and  $w_{dp}$  can be successfully retrieved (Figure 6.9a). The improvement of using preconditioning is best represented by Figure 6.9b for the forecasting period, especially for the evolution of  $w_{dp}$  ( $rms$  errors reduced from 0.17 to 0.0049  $m^3m^{-3}$ ). Improvement on other components are not significant mainly because the land surface are too wet, otherwise, the improvement will be more salient by correct initial value of  $w_{dp}$ .

Here we want to further test if our selected control variable set is proper. To this end, we choose initial guess control variables as  $T_{sfc}=305K$ ,  $T_{dp}=300K$ ,  $w_{sfc}=0.24 m^3m^{-3}$ ,  $w_{dp}=0.4 m^3m^{-3}$  and an assimilation window of 3 hours starting from 00Z, July 06, 2000. The retrieval results are listed in Table 6. 10.

Preconditioning can force adjustment to the corresponding components of the control variable. However, improper preconditioning (e.g., the second experiment) may result in erroneous retrieved states. The last experiment also indicate that the system adjust surface moisture and temperature most significantly. Same amount of adjustment does not affect the convergence of the retrieval. This also some what confirmed our assertion about the separation of sensitivity between temperature and soil moisture.

(a)



(b)

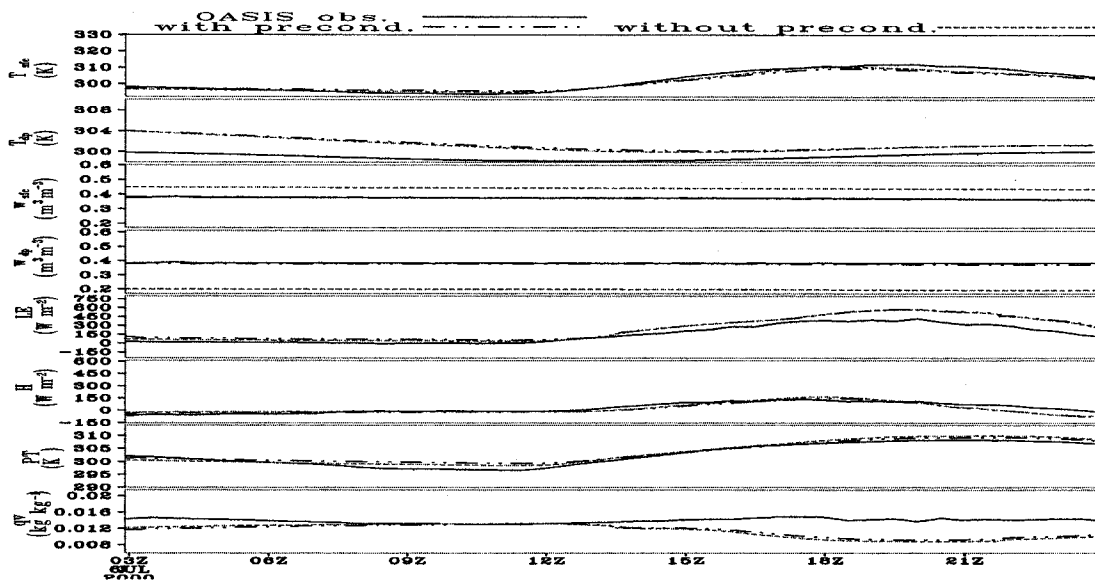


Figure 6.9. Comparison between with and without preconditioning for (a) the approaching of control variables to the true states and (b) the forecasting of land surface and atmospheric state variables and surface fluxes.

Table 6. 10 Preconditioning numerical experiments

$\alpha$	Init. <i>rms</i> in $\theta$ (K)	$J_{\text{final}}/J_0$	# it.	Retrieved initial condition			
				$T_{\text{sfc}}$ (K)	$T_{\text{dp}}$ (K)	$w_{\text{sfc}}$ ( $\text{m}^3\text{m}^{-3}$ )	$w_{\text{dp}}$ ( $\text{m}^3\text{m}^{-3}$ )
$(1.0,1.0,1.0,1.0)^T$	2.55	2.79E-2	4	305.007	300.0	0.377	0.4
$(10.0,1.0,0.001,1.0)^T$	2.55	0.4	4	297.077	299.91	0.233	0.399
$(10.0,1.0,0.1,1.0)^T$	2.55	3.82E-2	4	305.72	299.91	0.369	0.4
$(0.1,1.0,0.1,1.0)^T$	2.55	2.79E-2	4	305.007	299.91	0.377	0.4

The generation of good preconditioners involves as much art as science. The best preconditioners tend to be application-specific, exploiting insight into the precise problem being solved. A number of general purpose preconditioner have been developed which often work well in practice. The most widely used of these are variants on incomplete factorizations and approximate inverses. Unfortunately, these general purpose approaches tend to be poorly understood theoretically, and they sometimes perform badly. New ways of thinking about preconditioning are urgently needed.

### 6.3. Extended Definition of the Cost Function

Model predictions and measurements both provide useful information about the actual state of the soil. The aim of our land surface data assimilation algorithm is to combine these two sources of information. To obtain a systematic viewpoint of the model error, an expansion of the definition of the cost function to include the effects of model error is necessary. Based on Newton's momentum theory (Bers *et al.* 1963; Hopf 1948), the uncertainty in model state can be transformed into errors in forcing. Thus, state equation (2.22) can be written more generally as

$$\frac{\partial U}{\partial t} = F(U, \alpha) + \eta, \quad (6.1)$$

where  $\eta$  is an  $N_s \times 1$  vector composed of a set of model errors that are treated as random forcing terms in the state equation. For convenience, we assume  $\bar{\eta}$  is zero. This assumption could be relaxed if evidence suggested the presence of a systematic bias in the model error. Note that temporal correlations in the model errors can lead to a bias in the state  $U$  even when the model error at a specific time is truly random.

The cost function as defined in (2.24) is now transformed into:

$$\begin{aligned}
L = & J + \iint_{\Sigma} \lambda^T \left[ \frac{\partial U}{\partial t} - F(U, \alpha) - \eta \right] dx dt + \int \lambda_0^T [U(t_0) - U_0 - \varepsilon_0] dx \\
& 0.5 \times \int_x \int_{t_0}^1 \int_{t_0}^1 \eta^T(t') W(t' t''; x' x'') \eta(t'') dt' dt'' dx + \\
& 0.5 \times \int_x \varepsilon_0^T(x') V(x' x'') \varepsilon_0(x'') dx
\end{aligned} \tag{6.2}$$

where  $\varepsilon_0$  is initial guess errors in initial guess control variables,  $W \sigma_{\eta} = \delta(t-t') \delta(x-x')$  and  $\sigma_{\eta}$  is the error covariance of model error. A similar derivation to Eq.(2.27) results:

$$\begin{cases}
\frac{\partial U}{\partial t} - F(U, \alpha) - \eta = 0 & (\text{for } \delta\lambda), & (6.3a) \\
U(t_0) = U_0 + \varepsilon_0 & (\text{for } \delta\lambda_0) \\
-\frac{\partial \lambda}{\partial t} - \frac{\partial F^T}{\partial U} \lambda + \frac{\partial \phi}{\partial U} = 0, & (\text{adjoint equation}) & (6.3b) \\
\frac{\partial L}{\partial \alpha} = \int \int \left[ \frac{\partial \phi}{\partial \alpha} - \lambda^T \frac{\partial F}{\partial \alpha} \right] dt dx = 0, & (\text{for parameter } \alpha) & (6.3c) \\
\frac{\partial L}{\partial U(t_0)} = -\lambda_0 + \lambda_0 = 0, & (\text{for } \delta U_0) & (6.3d) \\
\frac{\partial L}{\partial \eta} = \iiint \eta W dt' dt'' dx' dx'' - \int \int_0^1 \lambda^T(t; x) dt dx = 0, & (\text{for } \delta\eta) & (6.3e) \\
\varepsilon_0 = B \lambda_0, \text{ where } V \times B = I. & (\text{for } \delta\varepsilon_0) & (6.3f)
\end{cases}$$

Eq. (6.3) is the general form for considering the model error for a full-fledged 4DVAR system. For applying to 1D situation, the system can be simplified significantly. In the following, the first section discusses one way of simulating model error. The remaining two sections are expectations for future research in this direction of retrieval with model error.

### 6.3.1. Influence of the soil and vegetation

We simulated land surface model error by producing the synthetic time series of screen-level atmospheric parameters using one land cover type while try to assimilate this measurements using forward and adjoint models using another type of vegetation. Similarly, we rotated soil types. In the same spirit, model parameter errors (e.g., on *veg*) are performed by creating synthetic series using wrong parameters.

#### a.) Role of vegetation

Using a 3-hour long assimilation window and the same setting of the reference run, starting from initial guess control variables:  $T_{sfc}=305\text{K}$ ,  $T_{dp}=300\text{K}$ ,  $w_{sfc}=0.24 \text{ m}^3\text{m}^{-3}$ ,  $w_{dp}=0.4 \text{ m}^3\text{m}^{-3}$ , we tested retrieval using different vegetation coverage (Table 6. 11). As expected, using the 0.83, which is closest to the true coverage, gives the best estimation of the initial surface soil moisture.

**Table 6. 11** Simulating model error in vegetation coverage

Veg	Init. <i>rms</i> in $\theta$ (K)	$J_{\text{final}}/J_0$	# it. Needed	Retrieved initial condition			
				$T_{sfc}$ (K)	$T_{dp}$ (K)	$w_{sfc}(\text{m}^3\text{m}^{-3})$	$w_{dp}(\text{m}^3\text{m}^{-3})$
0.63	3.38	1.29E-2	4	305.020	300.0	0.42	0.4
0.73	3.16	2.60E-2	4	304.975	299.91	0.398	0.399
0.83	2.55	2.79E-2	4	305.008	300.0	0.377	0.40
0.93	1.18	0.112	3	305.008	300.0	0.394	0.40

Using retrieved  $T_{sfc}$  and  $w_{sfc}$  as performance index, the effects of  $Rs_{min}$  on the retrieval is investigated for a variety of vegetation coverage (0.53-0.93) (Figure 6.10). The retrieval can be erroneous, especially for soil moisture, by wrongly specify the vegetation type.

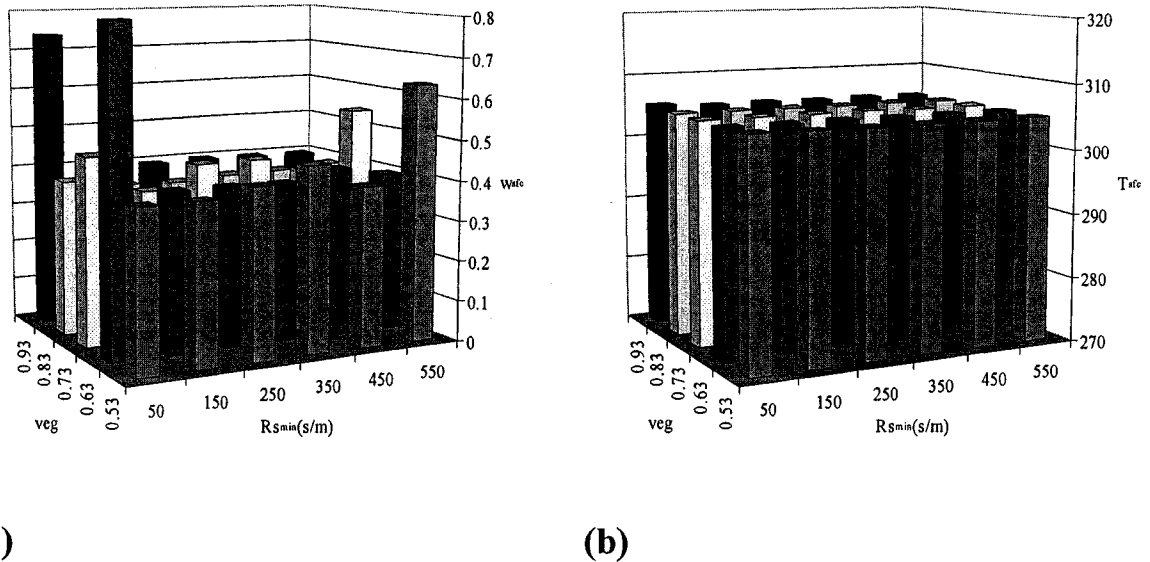


Figure 6.10. Influence of  $Rs_{min}$  on the retrieval of  $W_{sfc}$  (a) and  $T_{sfc}$  (b). Initial guess control variables are:  $T_{sfc}=305K$ ,  $T_{dp}=300K$ ,  $w_{sfc}=0.24 \text{ m}^3 \text{ m}^{-3}$ ,  $w_{dp}=0.4 \text{ m}^3 \text{ m}^{-3}$ . Assimilations are done using a 3-hr assimilation window.

#### b.) Role of soil

Retrieval scheme is very sensitive to the selection of soil type. It easily breaks up if using the wrong soil type data and trying to fit the model to the observations. Or, scheme finds the wrong states lack of physical meaning.

### *6.3.2. Identifying the Most Significant Model Errors*

One significant difference between synthetic experiments and real data assimilation lies in the existence of model imperfection for the later case. Aided by Eqs. 6.3a-d, this study tries to identify model defects in what aspects are most important for successful land surface data assimilation. To successfully deal with this problem, we must exploit our knowledge of the forward model. The proposed work is unique in that we address process uncertainty as well as initial conditions importance. Many outstanding issues and concerns are from our lack of knowledge of the time evolution scales of land surface variables. With this in mind, we will discuss the following two issues: First, did soil moistures response the same way as soil temperatures to atmospheric forcings? Second, the relative importance of accumulated daily mean and peak values of diurnal cycle.

### *6.3.3. Effects of Atmospheric Forcing Conditions and Advection*

Several studies (see Subsection 1.3) show that under intense solar insolation (daytime clear sky conditions during summer season) and weak winds, the connection between land surface process and PBL property is stronger and the causality relationship is easy to be identified. The finished part of our study serves as an effort to well-document these results.

Limited by our 1D structure, the advection effects cannot be included in the forward model run. However, in reality, advection causes significant atmospheric fields deformation and affects the evolution of atmospheric fields. The local linkage between land surface states and above atmospheric properties may be altered and effaced by the advection process. Callies *et al.* (1998) proposed a method to take the advection into

consideration for 1D column model. His 1D assimilation is accompanied by a full-fledged 3D run of a forward model, which provides the reference trajectories of model variables. The 1D stand-alone model trajectories are adjusted by the differences (with the reference trajectories). This is certainly a way to reduced forward model error. However, construction a full fledged 4DVAR system may solve this issue more completely and convincingly. Next phase of our effort will be putting our land surface scheme and its adjoint into a fullfledged atmospheric 4DVAR system. This can be achieved by enrich our PBL model to include three dimensional processes or simply find a parent system for our land surface scheme.



# Chapter Seven

## *Summary and Conclusions*

Modern numerical weather prediction requires the initial conditions of the included land surface/ soil-vegetation model. The lack of routinely available measurements of land surface variables motivated the development of schemes that infer land surface information from routinely measured variables.

Based on 4DVAR strategy, a retrieval system for the initial state of a soil-vegetation model is developed which assimilates either skin temperature (potentially available through satellite remote sensing) or routinely available screen-level atmospheric measurements. In the former case, the cost-function used in the 4DVAR minimization procedure is defined as a quadratic measurement of the model forecast error in ground surface temperature. The soil-vegetation model and its adjoint are run in stand-alone mode with the surface atmospheric state provided as an input to the soil model. When the screen-level atmospheric variables, namely, temperature and moisture, are used in the cost function, coupled soil-vegetation and the atmospheric models have to be solved. To avoid the need for developing a full 4DVAR system of a 3D coupled system, a 1D-column simplifying assumption is made. Radiation and vertical mixing are the main processes in this case. The vertical mixing is handled by the non-local MRF PBL scheme, and soil-vegetation processes are described by a two-layer model implemented in the ARPS.

The sensitivities of the measured variables to the retrieved (control) variables are first studied via forward simulations. Such simulations are verified against Oklahoma

Atmospheric Surface Layer Instrumentation System (OASIS) measurements. An important correction is made to the deep layer temperature prediction equation to enable successful retrieval of deep layer temperature and improve that of others.

Unlike previous studies such as Bouyssel *et al.* (1998) and Boni *et al.* (2001), both OSSE and real data retrieval experiments were performed, assuming two different types (skin temperature or screen level atmospheric variables) of measurements, for one dry and one wet period during 2000 at Norman OK OASIS site. The retrieval systems are able to recover the correct values of soil state variables in most cases. The robustness of the systems is assessed by testing different sizes of initial guess errors and different measurement errors. The impact of assimilation window length and data availability on the retrieval is also examined.

Compared with Entekhabi *et al.* (1995) and some other oversimplified treatment of land surface processes (e.g., Xu and Zhou 2003; Boni *et al.* 2001), our explicit treatment of vegetation processes is critical for the successful real data assimilation for deep soil moisture content for partially vegetated surfaces. In contrast, Xu and Zhou (2003) discussed a linear regression method for retrieving bulk soil moisture contents from soil temperature measurements, based solely on the soil heat capacity dependency on soil moisture contents. Results from Boni *et al.* (2001) are also limited to bare ground case.

The strategy being developed in this work includes a series of refinement of the forward land surface scheme and several creative approaches in applying variational data assimilation techniques for land surface studies. This also lays the basis for successful land data assimilation. Results outline the feasibility of a variety of approaches to retrieve

prognostic land surface variables. Rather than detailed mathematical formulations, this study, however, concentrates on exploring the roles of soil/vegetation characters in data assimilation processes. The methodology in this work may also contribute to the construction of next generation land surface models.

In Chapter 1, the recent studies related to land surface data assimilation are reviewed and put into three general categories (API, LDAS type of atmospheric forcing, and variational). Variational data assimilation works in land surface modeling can also be classified into three approaches, according data availability and retrieval objectives.

This work tried to investigate the feasibility of 4DVAR retrieval schemes in land surface modeling with emphasis on investigating the connections between screen-level observations and the evolution of soil states.

In Chapter 2, the OASIS dataset, which is used for assimilation as well as verification purpose in our retrieval experiments, are discussed. We then discussed in detail the forward models used. The land surface scheme used in this study is based on ISBA as of NP89, which uses simplified land surface and subsurface scheme for mesoscale studies. The general designing philosophy is a compromise between the bucket and multi-layered Richards' equation based methods. That is, a two level force-restore version of surface process models. Our land surface component is improved based on our recent work (Ren and Xue 2004). The resulting land surface scheme was proven vital for successful retrievals with real OASIS observations. The way we concocted the PBL scheme integrated the advantages of ARPS and MRF PBL schemes and also kept the implementation of its adjoint code in mind. The radiative transfer scheme of ARPS is also properly modified. We then introduced a generalized variational framework with

sensitivity study and data assimilation being special cases. The two forms of cost-function are introduced and their basic characteristics briefly discussed based on repeated forward model runs.

In Chapter 3, the coding method of TLM and ADM is summarized. The technique (vector verification) for adjoint verification and 4DVAR system verification are discussed. The flow chart for the adjoint system of our forward model is listed and commented, providing interested user and easier way to understand the physics.

Chapter 4 provides the rational and theory background for the two chapters that follow. In Chapter 4, the pivot upon which the adjoint retrieval is hung, i.e., the validity of TLM is checked and shown to be long enough for medium range weather forecasting. As the basis for analyzing and interpreting the retrieval results, the way of decomposing adjoint sensitivity is illustrated. Previously, nonlinear sensitivity experiments were performed to identify the closeness of the linkage of atmospheric and land state variables, through examining the sensitivity of atmospheric states to perturbations on initial land surface states.

Chapter 5 contains a series of retrieval experiments based on forced land surface model and the adjoint codes of the relevant components. The OSSE experiments enable several important issues be addressed. Retrieval experiments with real observations of ground temperature are also successful. The example addressing sampling strategy indicates that daytime period is more informative for retrieval (the reason is then unveiled). Experiments with different assimilation period lengths and otherwise identical conditions clearly shows that the more observations the more accurate the retrieved initial

soil states tend to be. This is in consistent with the information importance principle and agrees with several recent studies.

Assimilating of ground surface temperature for uncertain land surface parameters is a promising approach mainly because the development of remotesensing technique that makes the surface temperature measurements more widely available on routine basis. However, recent study on land data assimilation by Boni *et al.* (2001) and Li and Islam (2002) give different account about the feasibility of retrieval profile soil moisture content from surface energy balance. Boni *et al.* (2001) proposed a scheme to assimilate ground temperature for the estimation of a surface moisture index. They found that the optimized surface soil moisture index also lead to satisfactory description of the surface energy balance components. Through a series of sensitivity experiments, Li and Islam (2002), however, found that initial soil moisture profile that optimizes the surface soil moisture description does not necessarily lead to optimal estimation of the surface fluxes. The success of model inversion depends, to a large extent, on the successful retrieval of root zone soil moisture instead.

Discussions in Chapter 5 indicate that both claims may be correct since the field site used by Boni *et al.* (2001) is much less vegetated and consequently the ground evaporation overwhelms the transpiration process. For a bare ground surface, the soil moisture availability may be the single most important parameter that affects the simulation of the ground heat flux. For a highly vegetated area, however, the surface moisture flux is generally dominated by evapotranspiration. The key parameters for realistic simulation of transpiration are root zone soil moisture content and the canopy

resistance. It is because the limitation of the over simplified treatment of the Boni *et al.* (2001) scheme that prohibits their further analyses.

Assimilating screen level atmospheric measurements for land surface model variables as performed in Chapter 6 is more demanding also because it involves the coupling between land surface process and the overlying atmospheric components must be significant. We found that results as asserted in the past literatures are generally the situations when land surface is rather dry. To give a complete view of the data assimilation issue, we intentionally reported here a more difficult case for retrieval initial conditions: moist land surface conditions.

For a relatively wet period, a series of retrieval experiments are performed and results analyzed in Chapter 6. The most important finding is that the measurement sensitivity (cost function) is proven insensitive to the value of deep soil moisture (total water content) for this very wet condition. The marked sensitivity separation between  $T_{sfc}$  and  $W_{sfc}$  prevents all control variables be simultaneously retrieved successfully without proper preconditioning. Based on the surface latent heat flux partitioning among two reservoirs, a simple way for proper preconditioning is proposed and found successful for the studied case. Most significantly, the conception for land data assimilation was further extended theoretically in Chapter 6. The points outlined there merit further investigation.

The major findings in Chapter 6 are:

- Under synoptically calm conditions, land surface prognostic variables can also be successfully retrieved from the screen-level atmospheric observations via a 4DVAR procedure

- Using a wet period as an example, our retrieval scheme functions well. It is robust to reasonable magnitudes of Gaussian noise in data
- It can tolerate initial guess error much greater than the measurement error magnitudes
- These successful assimilation is a consequence of explicit inclusion of the vegetation transpiration process and the proper definition of the deep soil temperature in our land surface data assimilation system framework
- For noisy observations, there is an optimal window length of about 6 hours. Compared with the stand-alone run (Chapter 5), where within roughly 10 days, it is identified that the longer the assimilation window the better the retrieved initial states, suggesting that model error does not become significant up to 10 days of assimilation window length for forced run of the land surface model.

In this study, by restricting the application (of our data assimilation system) to only weather situations when impact of soil moisture on near surface atmospheric conditions is dominant, e.g., to situations with clear sky, low wind speed and strong radiative input, we are sure that the analyzed soil moisture/temperature corrections are not caused by an attempt to compensate for model deficiencies in parameterization. For more sophisticated system, the analysis will be more difficult to obtain and significant efforts will be put into that direction in the future.

## References

- Abramopoulos, F., C. Rosenzweig, and B. Choudhury, 1988: Improved ground hydrology calculations for global climate models (GCMs): Soil water movement and evapotranspiration, *J. Climate*, **1**, 921-941.
- Adrie, F., G. Jacobs, and B. G. Heusinkveld, 2000: Force-restore for ground surface temperature and moisture content in a dry desert system. *Water Resour. Res.*, **36**, 1261-1268.
- Andre, J. C., J. P. Goutorbe, and A. Perreir, 1986: HAPEX MOBILHY: A Hydrologic Atmospheric Experiment for the Study of water budget and evaporation flux at the climatic scale. *Bull. Amer. Meteor. Soc.* **67**, 138 – 144.
- Arakawa, A., and V. R. Lamb, 1977: Computational design of the basic dynamical processes of the UCLA general circulation model. J. Chang (ed.), *Methods in computational physics*, New York, Academic Press, pp174-246.
- Arnold, C., and C. Dey, 1986: Observing-system simulation experiments: Past, present, and future. *Bull. Amer. Meteor. Soc.*, **67**, 687-695.
- Avissar, R., 1992: Conceptual aspects of a statistical-dynamical approach to represent landscape subgrid-scale heterogeneities in atmospheric models. *J. Geophys. Res.*, **97**, 2729-2742.
- Backus, G. E., and F. Gilbert, 1970: Uniqueness in the inversion of inaccurate gross earth data, *J. Phil. Trans. Roy. Soc. London, Ser. A*, **266**, 123-192.
- Bao, J., and T. Warner, 1993: Treatment of on/off switches in the adjoint method: FDD experiments with a simple model. *Tellus*, **45A**, 525-538.
- Basara, J. B., 2001: The value of point-scale measurements of soil moisture in planetary boundary layer simulations. Ph.D Dissertation, School of Meteorology, University of Oklahoma, Norman. 225 pp.
- Benjamin, S. G., and T. N. Carlson, 1986: Some effects of surface heating and topography on the regional severe storm environment, I, Three-dimensional simulations. *Mon. Wea Rev.* **114**, 307-329.
- Bennett, A.F., L. M. Leslie, C. R. Hagelberg, P. E. Powers, 1993: Tropical cyclone prediction using a barotropic model initialized by a generalized inverse method. *Mon. Wea. Rev.*, **121**(6), 1714–1729.
- Bennett, A.F., 2002: Inverse modeling of the ocean and atmosphere. Cambridge University Press, 234pp. ISBN 0-821-81373-5.



- Bers, L., F. John, and M. Schechter, 1963: Partial differential equations. Wiley, NewYork.
- Betts, A.K., and J. H. Ball, 1996: The land surface-atmosphere interaction: A review based on observational and global modeling perspectives. *J. Geophys. Res.*, **101**, D3, 7209-7225.
- Bhumralkar, C. M., 1975: Numerical experiments on the computation of ground surface temperature in an atmospheric general circulation model, *J. Appl. Meteor.*, **14**, 1246-1258.
- Blackadar, A. K., 1976: Modeling the nocturnal boundary layer. *Prec. Third Symp. Atmos. Turb., Diffusion and Air Quality*, Boston, Amer. Metero. Soc., 46-49.
- Boni, G., F. Castelli, and D. Entekhabi, 2001: Sampling strategies and assimilation of ground temperature for the estimation of surface energy balance components, *IEEE Transactions on Geosciences and Remote Sensing*, **39**(1), 165-172.
- Bouttier, F., J.-F. Mahfouf, and J. Noilhan, 1993a: Sequential assimilation of soil moisture from atmospheric low level parameters. Part I: Sensitivity and calibration studies. *J. Appl. Meteor.*, **32**, 1335-1350.
- Bouttier, F., J.-F. Mahfouf, and J. Noilhan, 1993b: Sequential assimilation of soil moisture from atmospheric low level parameters. Part II: Implementation in a mesoscale model. *J. Appl. Meteor.*, **32**, 1351-1364.
- Bouyssel, F., V. Casse, and J. Pailleux, 1998: Variational surface analysis from screen level atmospheric parameters. HIRLAM 4 workshop on variational analysis in limited area models. Meteo-France, Toulouse, 23-25 February, 1998.
- Brooks, R. H., and A. T. Corey, 1964: Hydraulic properties of porous media, *Hydrol. Pap.* 3, Colo. State Univ., Fort Collins.
- Brotzge, J. A., and D. Weber, 2002: Land-surface scheme validation using the Oklahoma atmospheric surface-layer instrumentation system (OASIS) and Oklahoma Mesonet data: Preliminary results. *Meteor. Atmos. Phys.*, **80**, 189-206.
- Brotzge, J. A., 2000: Closure of the surface energy budget. PhD dissertation, School of Meteorology, University of Oklahoma, Norman. 208 pp
- Brutsaert, W., and M. B. Parlange, 1998: Hydrologic cycle explains the evaporation paradox. *Nature*, pp.396 (No. 6706, Nov. 5), 30.
- Buckley, A., and A. LeNir, 1983: QN-like variable storage conjugate gradients. *Math. Prog.*, **27**, 155-175.

- Businger, J. A., J. C. Wyngaard, Y. Izumi and E. F. Bradley, 1971: Flux profile relationships in the atmospheric surface layer. *J. Atmos. Sci.*, **28**, 181-189.
- Byun, D. W., 1990: On the analytical solutions of flux-profile relationships for the atmospheric surface layer. *J. Appl. Meteor.* **29**(7), 652-657.
- Caldwell, M. M., T. E. Dawson, and J. H. Richards, 1998: Hydraulic lift: consequences of water efflux from the roots of plants, *Oecologia*, **113**, no. 2, 151-161.
- , J. H. Richards, and W. Beyschlag, 1991: Hydraulic lift: ecological implications of water efflux from roots, *British Ecological Society Special Publication Series*, **10**, 423-436.
- , 1990: water parasitism stemming from hydraulic lift: a quantitative test in the field, *Israel Journal of Botany*, **39**, 4-6, 395-402.
- Callies U., A. Rhodin, and D.P. Eppel, 1998: A case study on variational soil moisture analysis from atmospheric observations. *J. Hydrol.*, **212-213**, 95-108.
- Calvet, J.-C., J. Noilhan, and P. Bessemoulin, 1998: Retrieving the root-zone soil moisture from surface soil moisture or temperature estimates: A feasibility study based on field measurements. *J. Appl. Meteor.*, **37**, 371-386.
- Carslaw, H. S., and J. C. Jaeger, 1959: *Conduction of Heat in Solids*. Clarendon Press, 150pp.
- Caughey, S. J., and S. G. Palmer, 1979: Some aspects of turbulence structure through the depth of the convective layer. *Quart. J. Roy. Meteor. Soc.*, **105**, 811-827.
- Chou, M-D., 1990: Parameterization for the absorption of solar radiation by O<sub>2</sub> and CO<sub>2</sub> with application to climate studies. *J Climate.*, **3**, 209-217.
- Chou, M-D, 1992: A solar radiation model for climate studies. *J Atmos. Sci.*, **49**, 762-774.
- Chou, M-D., and M. Suarez, 1994: An efficient thermal infrared radiation parameterization for use in general circulation models, NASA Tech Memo 104606, 85 pp. [Available from NASA Center for Aerospace Information, 800 Elkridge Landing Road, Linthicum Heights, MD 21090-2934].
- Clapp, R. B., and G. M. Hornberger, 1978: Empirical equations for some soil hydraulic properties. *Water Resour. Res.*, **14**, 601-604.
- Clarke, R. H., A. J. Dyer, R. R. Brook, D. G. Reid, and A. J. Troup, 1971: The Wangara Experiment: Boundary Layer Data. Tech. Paper 19, CSIRO, Division of Meteorological Physics, Aspendale, Australia, 362 pp

- Courtier, P., and O. Talagrand, 1987: Variational assimilation of meteorological observations with the adjoint vorticity equation. Part II: Numerical results. *Quart. J. Roy. Meteor. Soc.* **113**: 1348-1368.
- Courtier, P., and O. Talagrand, 1987: Variational assimilation of meteorological observations with the adjoint equation. Part I: Numerical results. *Quart. J. Roy. Meteor. Soc.*, **113**, 1329-1347.
- Deardorff, J. W., 1980: Stratocumulus-capped mixed layers derived from a three dimensional model. *Bound. -Layer Meteor.*, **18**, 495-527.
- Deardorff, J. W., 1978: Efficient prediction of ground surface temperature and moisture, with inclusion of a layer of vegetation, *J. Geophys. Res.*, **83**(C4), 1889-1903.
- Deardorff, J. W., 1977: A parameterization of Ground-Surface Moisture content for use in atmospheric prediction models, *J. Appl. Meteor.*, **16**, 1182-1185.
- de Vries, D. A., 1963: Thermal properties of soils. *Physics of Plant Environment*, W. R. V. Wijk, Ed., John Wiley & sons, Inc, 210-235.
- Dickinson, R. E., 1988: The Force-Restore model for surface temperatures and its generalizations, *J. Climate*. **1**, 1086-1097.
- Dickinson, R. E., 1984: Modeling evapotranspiration for three dimensional global climate models. Climate Processes and Climate sensitivity. *Geophys. Monogr.*, **29**, 58-72.
- Dickinson, R. E., A. Henderson-Sellers, P. Kennedy, and F. Giorgi, 1992: Biosphere-atmosphere transfer scheme (BATS) Version 1e as coupled to the NCAR Community Climate Model, *NCAR Tech. Note*.
- Dyer, A. J., and B. B. Hicks, 1970: Flux-gradient relationships in the constant flux layer. *Quart. J. Roy. Meteor. Soc.*, **97**, 168-180.
- Dyer, A. J., 1974: A review of the flux-profile relationships. *Bound. -Layer Meteor.*, **7**, 363-372.
- Entekhabi, D., H. Nakamura, and E. Njaku, 1995: Retrieval of soil moisture profile by combined remote-sensing and modeling. *Passive microwave remote sensing of land-atmosphere interactions*, B. J. Choudhury, Y. H. Kerr, E. G. Njoku, and P. Pampaloni, Eds., 485-498.
- Errico, R. M., 1997: What is an adjoint model. *Bull. Amer. Meteor. Soc.* **78**, 2577-2591.
- Feddes, R.A., P.J. Kowalik, and H. Zaradny, 1978: Simulation of field water use and crop yield. *Simulation Monographs. Pudoc*, Wageningen, 189 pp.

- Fletcher, C., and D. Reeves, 1964: Function minimization by conjugate gradients, *Computer J.* **7** 149-154.
- Galantowicz, F., D. Entekhabi, and E. Njoku, 1999: Tests of sequential data assimilation for retrieving profile soil moisture and temperature from observed L-band radiobrightness. *IEEE Transactions on Geoscience and Remote sensing*, **37**, 1860-1870.
- Giering, R., T. Kaminski, and T. Slawig, 2003: Applying TAF to a Navier-Stokes solver that simulates an Euler flow around an airfoil. To appear in *Future Generation Computer Systems*.
- Giering, R., and T. Kaminski, 1998: Recipes for adjoint code construction. *ACM Transactions on Mathematical Software*, **24** (4), 437-474.
- Giering, R., T. Kaminski, and T. Slawig, 2003: Applying TAF to a Navier-Stokes solver that simulates an Euler flow around an airfoil, to appear in *Future Generation Computer Systems*, Elsevier, Amsterdam, 2003.
- Gilbert, J. C., and C. Lemarechal, 1989: Some numerical experiments with variable storage quasi-Newton algorithms. *Mathematical Programming*, **45**, 407-435.
- Gill, P.E., and W. Murray, 1979: The numerical solution of a problem in the calculus of variations, in *Recent Mathematical Developments in Control*, D.J. Bell (editor), pp. 97-122, Academic Press, London.
- Gillies, R., and T. N. Carlson, 1995: Thermal remote sensing of surface soil water content with partial vegetation cover for incorporation into climate models. *J. Appl. Meteor.*, **34**, 745-756.
- Grunmann, P.J., K. Mitchell, and D. Zupanski, 1999: Adjoint method for soil moisture initialization. 8.5. Third WMO international symposium on assimilation of observations in meteorology and oceanography, Quebec City, Canada, 7-11 June 1999.
- Hall, M., and D. G. Cacuci, 1983: Physical interpretation of the adjoint functions for sensitivity analysis of atmospheric models. *J. Atmos. Sci.*, **40**, 2537-2546.
- Henderson-Sellers, A., K. McGuffie, and A. J. Pitman, 1996: The Project for Intercomparison of Land-Surface Parameterization Schemes (PILPS): 1992 to 1995, *Climate Dynamics*, **12**, 849-859.
- Henderson-Sellers, A., A. J. Pitman, P. Irannejad, and K. McGuffie, 2002: Land-surface simulations improve atmospheric modeling. *EOS, Trans, AGU*, **83**, 145-152.

- Herman, R. P., 1997: Shrub invasion and bacterial community pattern in Swedish pasture soil, *FEMS Microbiology Ecology*, **24**, 3, 235-242.
- Hillel, D., 1982: *Introduction to Soil Physics*. Academic Press, 364 pp.
- Holtslag, A., and C. Moeng, 1991: Eddy diffusivity and counter-gradient transport in the convective atmospheric boundary layer. *J. Atmos. Sci.*, **48**(14), 1690-1698.
- Holtslag, A., and B. A. Boville, 1993: Local versus nonlocal boundary layer diffusion in a global climate model. *J. Climate*, **6**, 1825-1842.
- Hong, S.Y., and H. L. Pan, 1996: Nonlocal boundary layer vertical diffusion in a medium-range forecast model. *Mon. Wea. Rev.*, **124**, 2322-2339.
- Hopf, L., 1948: *Introduction to the Partial Differential Equations of Physics*, Dover, New York.
- Horton, J. L., and S. C. Hart, 1998: Hydraulic lift: a potentially important ecosystem process, *Trends in Ecology and Evolution*, **13**, 6, 232-235.
- Idso, S.B., R. J. Reginato, R. D. Jackson, B. A. Kimball, and F.S. Nakayama, 1974: The three stages of drying of a field soil. *Soil Sci. Amer. Proc.*, **38**, 831-837.
- Ishikawa, C. M., and C. S. Bledsoe, 2000: Seasonal and diurnal patterns of soil water potential in the rhizosphere of blue oaks: evidence for hydraulic lift, *Oecologia*, **125**, 4, 459-465.
- Jackson, T. J., M. E. Hawley, and P. E. O'Neill, 1987: Preplanting soil moisture using passive microwave sensors, *Water Res. Bull.*, **23**(1), 281-296.
- , 1997: Southern Great Plains 1997 (SGP97) Hydrology Experiment Plan, <http://hydrolab.arsusda.gov/sgp97/>.
- , 1993: Measuring surface soil moisture using passive microwave remote sensing. *Hydrological Processes*, **7**, 139-152.
- Jacquemin, B., and J. Noilhan, 1990: Sensitivity study and validation of a land surface parameterization using the HAPEX-MOBILHY data set. *Bound. -Layer Meteor.*, **52**, 93-134.
- Jones, A., T. Vukievi, T. Vonder Haar, 2004: A microwave satellite observational operator for variational data assimilation of soil moisture. *J. Hydrol. Meteorology*, **5**(1), 213-229.
- Jury, W. A., W. R. Gardner, and W. H. Gardner, 1991: *Soil Physics*. -5<sup>th</sup> ed. John Wiley & Sons, Inc. 328pp.

- Karl, T. R., C. N. Williams, Jr., F. T. Quinlan, and T. A. Boden (ed), 1990: United States Historical Climatology Network (HCN) serial temperature and precipitation data. ORNL/CDIAC-30, NDP019/R1. Carbon Dioxide Information Analysis Center, Oak Ridge National Laboratory, Oak Ridge, Tennessee.
- Kool, J. B., J.C. Parker, and M. Th. van Genuchten, 1987: Parameter estimation for unsaturated flow and transport models-A review. *J. Hydrol.*, **91**, 255-293.
- Kostov, K. G., and T. J. Jackson, 1993: Estimating profile soil moisture from surface layer measurements-A review. *Proc. of SPIE-The International Society of Optical Engineering*, **1941**, 125-136, Orlando, USA.
- LeDimet, F. X., and O. Talagrand, 1986: Variational algorithms for analysis and assimilation of meteorological observations-Theoretical aspects, *Tellus*, **38A**, 97-110.
- Li, J., and S. Islam, 2002: Estimation of root zone soil moisture and surface fluxes partitioning using near surface soil moisture measurements. *J. Hydrology*, **259**, 1-14.
- Linsley, R., M. Kohler, and J. Paulhus, 1949: *Applied Hydrology*. McGraw-Hill, 689pp.
- Liou, K.N., 1992: *Radiation and Cloud Processes in the Atmosphere*, Oxford Press, 487pp.
- Liu, D.C., and J. Nocedal, 1989: On the limited memory BFGS method for large scale optimization. *Mathematical Programming*, **45**, 503-528.
- Long, R., and W. Thacker, 1989a: Data assimilation into a numerical equatorial ocean model. Part I: The model and assimilation algorithm. *Dynamics for Atmospheres and Oceans* **13**, 379-412.
- Long, R., and W. Thacker, 1989b: Data assimilation into a numerical equatorial ocean model. Part II: Assimilation Experiments. *Dynamics for Atmospheres and Oceans* **13**, 413-440.
- Lord, S. J., E. Kalnay, R. Daley, G. D. Emmitt, and R. Atlas, 1997: Using OSSEs in the design of the future generation of integrated observing systems. Preprint volume, 1st Symposium on Integrated Observation Systems, Long Beach, CA, 2-7 February 1997.
- Lorenc, A. C., 1986: Analysis methods for numerical weather prediction. *Quart. J. Roy. Meteor. Soc.*, **112**, 1177-1194.
- Lorenz, E. N., 1963: Deterministic nonperiodic flow, *J. Atmos. Sci.*, **20**, 130-141.
- Louis, J. F., 1979: A parametric model of vertical eddy fluxes in the atmosphere. *Bound.-Layer Meteor.*, **17**, 187-202.

- Mahfouf, J.-F., and P. Viterbo, 2001: Land surface assimilation. ECMWF Meteorological training course lecture series (Printed in March, 2001), pp. 1-23.
- Mahfouf, J. F., A. O. Manzi, J. Noilhan, H. Giordani, and M. Deque, 1995: The land surface scheme ISBA within the Meteo-France climate model ARPEGE. Part I: Implementation and preliminary results. *J. Climate*, **8**, 2039-2057.
- Mahfouf, J.-F., 1991: Analysis of soil moisture from near-surface parameters: A feasibility study. *J. Appl. Meteor.*, **30**, 1534-1547.
- Manabe, S., 1969: Climate and ocean circulation. 1. The atmospheric circulation and the hydrology of the earth's surface. *Mon. Wea. Rev.*, **97**, 739-774.
- Marchuk, G. I., 1994: Adjoint equations and analysis of complex systems, Mathematics and its applications 466 pp., Kluwer Academic Publishers.
- Marchuk, G. I., 1981: Methods of Numerical Mathematics, 2nd ed., 466 pp., Springer-Verlag.
- Marshak, A., A. Davis, W. Wiscombe, W. Ridgway, and R. Cahalan, 1998: Biases in Shortwave Column Absorption in the Presence of Fractal Clouds. *J. of Climate*, **11**, 431-446.
- Margulis, S. A. and D. Entekhabi, 2001: A coupled land surface-boundary layer model and its adjoint, *Journal of Hydrometeorology*, **2**(3), 274-296.
- Mass, E. V., and G. J. Hoffman, 1977: Crop salt tolerance-current assessment. *J. Irrig. And Drainage Div.*, ASCE 103, 115-134.
- McLaughlin, D., 1995: Recent developments in hydrologic data assimilation. *Rev. Geophys.*, **33** (suppl.), 977-984.
- Milly, P. C. D., and K. A. Dunne, 1994: Sensitivity of the global water cycle to the water-holding capacity of land. *J. Clim.*, **7**, 506-526.
- Milly, P.C.D., and Z. J. Kabala, 1986: Integrated modeling and remote sensing of soil moisture. Hydrologic Applications of Space Technology. IAHS Publ. no. 160, 1986.
- Milly, P.C.D., and P. S. Eagleson, 1980: The coupled transport of water and heat in a vertical soil column under atmospheric excitation. 234 pp. Massachusetts Institute of Technology, Dept. of Civil Engineering, Ralph M. Parsons Laboratory for Water Resources and Hydrodynamics, Cambridge.

- Mintz, Y., 1984: The sensitivity of numerically simulated climates to land-surface boundary conditions, in *Global Climate*, edited by J. H. Houghton, pp. 79-105, Cambridge University Press, Cambridge, England.
- Mitchell, H. L., P. L. Houtekamer, and G. Pellerin, 2002: Ensemble size, balance, and model-error representation in an ensemble Kalman filter. *Mon. Wea. Rev.*, **130**(11), 2791–2808.
- Navon, I., and D. Legler, 1987: Conjugate-gradient methods for large-scale minimization in meteorology. *Mon. Wea. Rev.*, **115**, 1479-1502.
- Navon, I.M., X. Zou, J. Derber, and J. Sela, 1992: Variational data assimilation with an adiabatic version of the NMC spectral model. *Mon. Weather Rev.* **120**, 1433-1446.
- Nijssen, B., R. Schnur, and D. P. Lettenmaier, 2001: Global retrospective estimation of soil moisture using the variable infiltration capacity land surface model, 1980-1993. *J. Climate*, **14**, 1790-1808.
- Noilhan, J., and J.-F. Mahfouf, 1996: The ISBA land surface parameterization scheme. *Global and Planetary Change* **13**, 145-159.
- Noilhan, J., and S. Planton, 1989: A simple parameterization of land surface processes for meteorological models. *Mon. Wea. Rev.*, **117**, 536-549.
- Ookouchi, Y., M. Segal, R. C. Kessler, and R. A. Pielke, 1984: Evaluation of soil moisture on the generation and modification of mesoscale circulations. *Mon. Wea. Rev.*, **112**, 2281-2292.
- Pitman, A.J., Z. Yang, J. Cogley, and A. Henderson-Sellers, 1991: Description of bare essentials of surface transfer for the Bureau of Meteorology Research Center AGCM. *BMRC Res. Rep.*, **32**, 117pp.
- Pleim, J. E., and A. Xiu, 1995: Development and testing of a surface flux and planetary boundary layer model for application in mesoscale models. *J. Appl. Meteor.*, **34**, 16-32.
- Qu, W., and coauthors, 1998: Sensitivity of Latent Heat Flux from PILPS Land-Surface Schemes to Perturbations of Surface Air Temperature. *J. Atmos. Sci.*, **55**, 1909–1927.
- Rabier, F., P. Courtier, J. Pailleux, O. Talagrand, J. N. Thepaut, D. Vasiljevic, 1993: Comparison of four-dimensional variational assimilation with simplified sequential assimilation. Proceedings of the ECMWF on variational assimilation, with special emphasis on three-dimensional aspects. ECMWF, Reading, UK, pp. 271-326.



- Reichle, R. H., J. P. Walker, R. D. Koster, and P. R. Houser, 2002: Extended versus Ensemble Kalman filtering for land data assimilation. *J. Hydrol. Meteorology*, **3**(6), 728–740.
- Ren, D., and M. Xue, 2002: An improved force-restore model for land surface modeling. Abstract Volume, *Mississippi River Climate and Hydrology Conf.*, New Orleans, Louisiana.
- , 2001: Scaling issues in the calculation of surface latent and sensible heat fluxes in Blue River Basin using SHEELS model, MS Thesis, School of Meteorology, University of Oklahoma, Norman.
- , M. Xue, and J. Gao, 2002: Parameter Retrieval in a Land-Surface Model, *Preprint of 19th Conf. on weather Analysis and Forecasting/15th Conf. on Numerical Weather Prediction*, San Antonio, TX.
- , and A. Henderson-Sellers, 2002: An analytical hydrological model and its implication in scaling issues for land surface modeling. Submitted to *J. Climate*.
- , and M. Xue, 2004: An improved force-restore model for land-surface modeling. *J. App. Meteor.*, In Press.
- , M. Xue, and A. Henderson-Sellers, 2004: Incorporating hydraulic-lift into a land surface model and its effects on surface soil moisture prediction. *Hydrol. Meteorology*, In Press.
- Richards, L.A., 1931: Capillary conduction of liquids through porous mediums. *Physics* **1**, 318-333.
- Richards, J. H., and M. M. Caldwell, 1987: Hydraulic lift: substantial nocturnal water transport between soil layers by *Artemisia tridentate* roots, *Oecologia*, **73**, 4, 486-489.
- Running, S., and E. Hunt, 1993: Generalization of a forest ecosystem process model for other biomes, BIOME-BGC and an application for global-scale models. In: J.R. Ehrlinger and C. Fields (Editors). *Scaling Physiological Processes: Leaf to Globe*. Academic Press, New York.
- Saltzman, B., 1962: Finite amplitude free convection as an initial value problem-I. *J. Atmos. Sci.*, **19**, 329-341.
- Santanello, J. A., and T. N. Carlson, 2001: Mesoscale simulation of rapid soil drying and its implications for predicting daytime temperature and dew point, *J. Hydrometeor.*, **2**, 71-88.
- Schaake, J., Q. Duan, P. Houser, E. Wood, D. Lettenmaier, A. Robock, D. Lohmann, W. Higgins, and R. Pinker, 2002: An intercomparison of North American LDAS soil

moisture fields. Abstract Volume, Mississippi River Climate and Hydrology Conf., New Orleans, Louisiana.

- Schroter, J., 1989: Driving of non-linear time dependent ocean models by observations of transient tracer-A problem of constrained optimization. In D. Anderson and J. Willebrand Eds., *Ocean Circulation Models: Combining Data and Dynamics*, pp. 257-285. Kluwer Academic Publishers.
- Scott, R. L., W. J. Shuttleworth, T. O. Keefer, and A. W. Warrick, 2000: Modeling multiyear observations of soil moisture recharge in the semiarid American Southwest. *Water Resour. Res.*, **36**(8), 2233-2247.
- Sellers, P. J., F. G. Hall, G. Asrar, D. E. Strebel, and R. E. Murphy, 1992: An overview of the First International Satellite Land Surface Climatology Project (ISLSCP) Field Experiment (FIFE). *J. Geophys. Res.*, **97**, 18 345-18 371
- Shanno, D. F., 1978: Conjugate gradient methods with inexact searches. *Math. Oper. Res.*, **3**, 244-256.
- Shanno, D.F., and K.H. Phua, 1980: Remark on algorithm 500: minimization of unconstrained multivariate functions. *ACM Transactions on Mathematical Software* **6**, 618-622.
- Shuttleworth, W.J., 1988: Macrohydrology-The new challenge for process hydrology. *J. Hydrology* **100**, 31-56.
- Smith, E. A., H. J. Cooper, W. L. Crosson, and H. Weng, 1993: Estimation of surface heat and moisture fluxes over a prairie grassland 3, design of a hybrid physical/remote sensing biosphere model. *J. Geophys. Res.*, **98**, 4951-4978.
- Song, Y, M. B. Kirkham, J. M. Ham, and G. J. Kluitenberg, 2000: Root-zone hydraulic lift evaluated with the dual-probe heat-pulse technique, *Australian journal of soil research*, **38**, 5, 927-935.
- Sun, W. Y., and M. G. Bosilovich, 1996: Planetary boundary layer and surface layer sensitivity to land surface parameters. *Bound. -Layer Meteor.*, **77**, 353-378.
- Sun, W. Y., and C. Z. Chang, 1986: Diffusion model for a convective layer. Part I: Numerical simulation of convective boundary layer. *J. Climate Appl. Meteor.*, **25**, 1445-1453.
- Talagrand, O., 1991: The use of adjoint equations in numerical modeling of the atmospheric circulation. In: Griewank, A., Corliss, G. F. (Eds.), *Automatic Differentiation of Algorithms: Theory, Implementation, and Application*. SIAM, Philadelphia, pp. 169-180.

- Talagrand, O., and P. Courtier, 1987: Variational assimilation of meteorological observations with the adjoint vorticity equation. Part I: Theory. *Quart. J. Roy. Meteor. Soc.*, **113**, 1311-1328.
- Tao, W-K, S. Lang, J. Simpson, C. Sui, B. Ferrier, and M. Chou, 1996: Mechanism of cloud-radiation interaction in the tropics and mid-latitude. *J. Atmos. Sci.* **53**, 2624-2651.
- Taylor, S. A., and G. M. Ashcroft, 1972: *Physical Edaphology*. Freeman and Co., San Francisco, California, 434-435.
- Thacker, W. C., 1987: Three lectures on fitting numerical models to observations. Technical Report, GKSS Forschungszentrum Geesthacht GmbH, Geesthacht, Federal Republic of Germany.
- Thacker, W. C., 1988: Fitting dynamics to data. *J. Geophys. Res.*, **93**, 1227-1240.
- Troen, I., and L. Mahrt, 1986: A simple model of the atmospheric boundary layer: Sensitivity to surface evaporation. *Bound.-Layer Meteor.*, **37**, 129-148.
- Van den Hurk, B., W. Bastiaanssen, H. Pelgrum, and E. Van Meijgaard, 1997: A new methodology for assimilation of initial soil moisture fields in weather prediction models using METEOSAT and NOAA data. *J. Appl. Meteor.*, **36**, 1271-1283.
- van Genuchten, M. Th., 1980: A closed form equation for predicting the hydraulic conductivity of soil. *Soil Science Society of America Journal* **44**, 892-898
- Wang, Z., 1993: Variational data assimilation with 2-D shallow water equations and 3-D FSU global spectral models. Ph.D Dissertation, College of arts and sciences, The Florida State University, Tallahassee, Florida, 234 pp.
- Wetzel, P. J., and J. T. Chang, 1988: Evapotranspiration from nonuniform surfaces: A first approach for short-term numerical weather prediction. *Mon. Weather Rev.* **116**, 600-621.
- Wetzel, P. J., and J. T. Chang, 1987: Concerning the relationship between evapotranspiration and soil moisture. *J. Climate Appl. Meteor.*, **26**, 18-27.
- Wetzel, P. J., D. Atlas, and R. Woodward, 1984: Determining soil moisture from geosynchronous satellite infrared data: A feasibility study. *J. Climate Appl. Meteor.*, **23**, 375-391.
- Xiu, A., and J. Pleim, 2001: Development of a land surface model. Part I: Application in a Mesoscale Meteorological Model. *J. Appl. Meteor.*, **40**, 192-208.

- Xu, Q., 1996a: Generalized adjoint for physical processes with parameterized discontinuities: Part I: Basic issues and heuristic examples. *J. Atmos. Sci.*, **53**(8), 1123-1142.
- Xu, Q., 1996b: Generalized adjoint for physical processes with parameterized discontinuities: Part II: Vector formulations and matching conditions. *J. Atmos. Sci.*, **53**(8), 1143-1155.
- Xu, Q., and C. Qiu, 1997: A Variational method for computing surface heat fluxes from ARM Surface Energy and Radiation Balance Systems. *J. Appl. Meteor.*, **36**, 3-11.
- Xu, Q., and B. Zhou, 2003: Retrieving soil water contents from soil temperature measurements by using linear regression. *Advances in Atmospheric Sciences*, **20**, 849-858.
- Xue, M., K. K. Droegemeier, V. Wong, A. Shapiro, and K. Brewster, 1995: *ARPS Version 4.0 User's Guide*. [Available from Center for Analysis and Prediction of Storms, University of Oklahoma, 100 E. Boyd St., Norman OK 73019], 380 pp.
- Xue, M., K. K. Droegemeier, and V. Wong, 2000: The Advanced Regional Prediction System (ARPS) - A multi-scale nonhydrostatic atmospheric simulation and prediction model. Part I: Model dynamics and verification. *Meteor. Atmos. Phys.*, **75**, 161.
- Xue M., D. Ren, 2002: Several recent modifications to ISBA land surface scheme and their implications for soil moisture simulation. To be submitted to *Monthly Weather Review*.
- Xue, M., and coauthors, 2001: The Advanced Regional Prediction System (ARPS) - A multiscale nonhydrostatic atmospheric simulation and prediction tool. Part II: Model physics and applications. *Meteor. Atmos. Physics*, **76**, 143-165.
- Ye, D., 1989: Sensitivity of climate model to hydrology, *Geophysical Monograph 52, IUGG Volume 7, Understanding Climate Change*, A Berger, R.E. Dickinson, John W. Kidson, Editors.
- Yu, L., and J. J. O'Brien, 1991: Variational Estimation of the wind stress drag coefficient and the oceanic eddy viscosity profile, *J. Phy. Ocean.*, **21**, 709-719, 1991.
- Zhang, D., and R. A. Anthes, 1982: A high-resolution model of the planetary boundary layer sensitivity tests and comparisons with SESAME-79 data. *J. Appl. Meteor.*, **21**, 1594-1609.
- Ziegler, C., T. Lee, and R. Pielke, Sr., 1997: Convective initiation at the dryline: A modeling study. *Mon. Wea. Rev.*, **125**, 1001-1026.

Zou, X., F. Vandenberghe, M. Pondera, and Y. H. Kuo, 1997: Introduction to adjoint techniques and the MM5 adjoint modeling system. *NCAR/TN-435-STR*.

Zupanski, D., 1997: A general weak constraint applicable to operational 4DVAR data assimilation systems. *Mon. Wea. Rev.*, **125**(9), 2274–2292.

## Appendix 1. General Philosophy of LSM-PBL Model

### *A1.1. Land Surface Components*

Land surface schemes, although developed based on different concepts and with different levels of complexity, are schemes to solve energy conservation (for soil temperatures) and water conservation (for soil moisture distribution) equations. The aim of land surface scheme is to provide temperature and specific humidity at the lower boundary of atmospheric models (Mahfouf and Viterbo 2001). These two variables are needed in the estimation of heat, water and momentum exchanges between the continental surfaces and the lower atmosphere.

Land surface schemes can be classified according to the intended application as those for global climate models, i.e., BUCKET (Manabe 1969), BATS (Dickinson *et al.* 1992), BEST (Pitman *et al.* 1991); for meso-scale/short range forecasting models, ISBA (NP89); and for eco-hydrological models, HYDRUS1D&2D (Scott *et. al* 2000), BGC (Running and Hunt 1993). Land surface models also evolved in their vertical level structure from single soil layer models (Manabe 1969) to force-restore models (NP89) and multiple-layer diffusion type models (Smith *et al.* 1993). Deardorff (1977&1978) pointed out the defect of bulk layer scheme in its description of surface soil moisture availability. Singling out a thin and rapid response surface layer enhances the surface evaporation description significantly, especially during short period of precipitation. Deardorff (1978) also introduced the “big leaf” representation of vegetation in LSMs. To date, multiple-layer diffusion type models are facing the problem of data availability among the vertical soil profile. The data assimilation schemes so far are limited to force-restore type of land surface schemes.

### A1.1.1. Soil Temperature

Soil temperature is governed by the following diffusion equation with variable coefficients:

$$\rho_{soil} C_{pSoil} \frac{\partial T_s}{\partial t} = \frac{\partial}{\partial z} \left[ \lambda_T \frac{\partial T_s}{\partial z} \right] + F(z, t), \quad (A1.1)$$

where  $\rho_{soil}$  is soil density, a function of vertical coordinate  $z$  (take as upward positive) and time  $t$ ,  $C_{pSoil}$  is soil heat capacity per unit mass (a function of  $z$  and  $t$ ), and the multiplication of  $\rho_{soil}$  with  $C_{pSoil}$  is volumetric heat capacity  $C_V$ . Here  $T_s$  is soil temperature,  $\lambda_T$  is soil thermal diffusivity (usually nonlinearly depend on soil moisture content). The forcing term  $F$  is introduced on one hand to facilitate the condition of extra heat source among soil profile and on the other hand to facilitate the treatment of the topmost layer, i.e., surface layer temperature. The surface temperature obtained by using Eq. (A1.1) satisfies the surface energy balance requirement and has a natural connection with the following soil layer, if

$$F(0, t) = \frac{R_n - LE - H}{d_1}, \quad (A1.2)$$

where  $R_n$  is the net input radiation (including solar radiation balance and longwave radiation balance),  $LE$  is the latent heat flux,  $H$  is the sensible heat flux, and  $d_1$  is the depth of the topmost soil layer. The sign convention of the symbols in Eq. (A1.2) is chosen so that the terms of energy fluxes are positive when flux is toward the ground interface, hence contributing to the temperature increment, and negative when it is away from the surface. The numerator on the right hand side of Eq. (A1.2) is also called ground

heat flux  $G$ . However, one should not confuse it with some field measurements of ground heat flux which actually is  $-\lambda_r \frac{\partial T_s}{\partial z}$  as applied to the shallower soil layer. In equation (A1.2),  $d_l$  should be thin enough so that one value of temperature represents the whole soil layer and thick enough so that no direct radiative forcing can make a direct penetration. Historically, either limited by computing capacity or for some specific study purposes, many simplified forms of Eq. (A1.1) were introduced and had been summarized by Deardorff (1978). Force restore method for surface soil temperature (Bhumralkar 1975; Blackadar 1976) was derived based on analytical solution (e.g., Carslaw and Jaeger 1959; Dickinson 1988) of the constant thermal diffusivity form of (A1.1).

Bhumralkar (1975) assumed the daily mean temperature is the same at all depths. This assumption may be valid in the spring and fall seasons of a year, but is certainly not true in most parts of the world at summer and winter (de Vries 1963; Ren and Xue 2004). If their proposal is directly applied, except for special days during a year, deep soil temperature (i.e., bulk layer temperature) is always dragged such that it possesses a same mean temperature as the surface temperature. Ren and Xue (2004) thoroughly discussed this phenomenon and their proposed method for proper removal of the soil temperature lapse rate works for a force restore type land surface scheme in ARPS.

Multiple-layer models based on numerical solving of (A1.1), i.e., using semi-implicit Crank-Nicolson scheme and with the lower boundary condition set as  $\lim_{z \rightarrow \infty} T_s(z, t) = \widetilde{T}_{sfc}$  (constant), are free of this problem because atmospheric forcing on various time scales (from daily cycle to annual cycle) are naturally included during the



continuous time marching. However, due to the lack of commensurate accurate measurements of soil textural properties, multiple-layer models are prone for systematic errors. Heavier computational load is also a constraint that limits the practical application of multiple layer soil models.

#### *A1.1.2. Soil Moisture*

On daily basis, evaporation constantly extracts water from land surface and this effect propagates to deeper soil through evaporation for bare soil or intercepted water reservoirs (snow cover, vegetation interception and dew) and through transpiration for vegetated areas. Of much less frequent is the precipitation process that recharges the soil of the hydraulically active layer.

The soil moisture conditions in hydraulically active layer control partitioning of surface energy fluxes (e.g., Santanello and Carlson 2001; Sun and Bosilovich 1996), ecosystems, and biogeochemical cycles (Caldwell *et al.* 1998; Richards and Caldwell 1987). The depth of this layer varies with surface cover types. The existence of roots facilitates the water flow through the soil-vegetation-atmosphere system through transpiration during daytime and hydraulic lift (now termed “hydraulic redistribution” since it can operate in both directions, M. Caldwell, personal communication) during nighttime. Thus, the existence of roots can significantly enlarge the hydraulically active soil depth. Precipitation and inter-precipitation patterns, heterogeneity in soil texture, vegetation and land use, and topography contribute to fluctuations in soil moisture spatial distribution and temporal variation.

In numerical models, the link between soil and atmospheric variables is provided through the expression of the surface fluxes, usually based on similarity theory. The

crucial variable here is the latent heat flux because its magnitude depends explicitly upon surface properties and because it is the bond to connect the thermal and hydraulic processes. Recent land surface schemes represent differently the grid box fractions covered by: a) bare soil, with evaporation controlled by soil moisture in a shallow top soil layer; b) vegetation, with transpiration controlled by soil moisture in the root zone affecting the magnitude of stomatal resistance; and c) snow or interception reservoir, evaporating at the potential (maximum) rate. These last two components require the existence of model prognostic equations for snow mass and interception reservoirs.

The difference between surface and lowest (atmospheric) model layer specific humidity is used to create the moisture potential in the similarity theory based schemes for calculating latent heat flux. Surface specific humidity is a weighted average of the saturated value at surface temperature and that of the lowest atmospheric model layer:

$$q_{sfc} = \alpha q_{sat}(T_{sfc}) + \beta q_l \quad (A1.3)$$

where  $q_{sfc}$  is surface specific humidity,  $q_l$  represents the value of specific humidity at the lowest atmospheric model layer. The quantity  $\alpha$  is called surface soil water availability and  $\beta$  is a non-local connection usually signifying the vegetation activities, i.e., the easiness of soil water extraction by vegetated surface. Both quantities depend upon soil moisture  $\theta$ . Using this philosophy, we can formally unify the expressions for bare soil evaporation and vegetation transpiration as:

$$LE = \frac{\rho_{air}}{R_a} [q_{sfc} - q_l] \quad (A1.4)$$

where  $\rho_{air}$  is air density,  $R_a$  is aerodynamic resistance. For example, for the ISBA scheme,  $\alpha$  and  $\beta$  are given by  $h_u(\theta)$  and 0 for bare surface ( $\alpha$  method for evaporation),

and  $R_a/R_a+R_c$  and  $R_c/R_a+R_c$  for vegetated surface, respectively.  $h_u(\theta)$  is closely related to the surface soil structural properties such as porosity, slope of log-retention curve, i.e., 'b' parameter (Clapp-Hornberger 1978), and air entry level soil suction. Noilhan and Planton (NP89) assumed evaporation takes place at the potential rate above a threshold value  $\theta_{fc}$  (field capacity) up to the saturation  $\theta_{sat}$ . Note that this expression for latent heat flux is in vapor-mass flux form, as is in the atmospheric component of ARPS. The energy form is easily obtained by multiplying the specific (per unit mass of water) latent heat of vaporization.

Any reasonably accurate mathematical description of water uptake by vegetations with heterogeneous soil and root properties is complicated. One viable approach however is to regard the root system as a diffuse sink which penetrates each depth layer of soil uniformly, though not necessarily with a constant strength throughout the root zone. This macroscopic root system approach circumvented the flow patterns at the immediate periphery of the absorbing roots and avoided geometric complications involved in analyzing the distribution of fluxes and potential gradients on a micro scale. Root water uptake is then represented as a sink term that is added to the Richards' equation (a combination of mass balance and Darcy's law, Hillel 1982; Jury *et al.* 1991; Richards 1931) which describes the water flow through the soil.

$$\frac{\partial \theta}{\partial t} = \frac{\partial}{\partial z} \left[ K(h) \frac{\partial h}{\partial z} \right] + \frac{\partial K(h)}{\partial z} - S \quad (\text{A1.5})$$

where  $\theta$  is volumetric soil water content ( $\text{m}^3 \text{ m}^{-3}$ ),  $K$  is the hydraulic conductivity ( $\text{m s}^{-1}$ ),  $h$  is soil water potential (m), and  $S$  is the root water uptake rate ( $\text{m}^3 \text{ m}^{-3} \text{ s}^{-1}$ ), which depends on root density,  $h$  or  $\theta$ , and osmotic head  $\pi$ . A more complete expression of  $S$  reads:

$$S(h, \pi, z) = \alpha_1(h)\alpha_2(\pi)S_p(z), \quad (\text{A1.6})$$

where  $\alpha_1$  and  $\alpha_2$  are two functions signifying the soil water pressure head (water stress function) and salinity (water reduction function due to salinity) dependence. The reader is referred to Taylor and Ashcroft (1972) for the expression of  $\alpha_1$  and Mass and Hoffman (1977) for the expression of  $\alpha_2$ . Feddes *et al.* (1978) showed that between the two reduction points, water uptake can take place at potential rate, and water uptake ceases when soil potential falls below wilting point or about oxygen efficiency (drawn point).  $S_p(z)$  in Eq. (A1.6) is the root water uptake under potential condition.  $S_p(z)$  is distributed among root zone soil layers by the root shape factor which is a macroscopic description of the root length density distribution  $r(z)$  ( $\text{m m}^{-3}$ ) through  $S_p(z) = \frac{r(z)}{\int_{-L}^0 r(z)dz} T_p$ . Here  $T_p$

is potential transpiration rate (atmospheric demanding), and  $L$  is the maximum root depth. To solve Eq. (A1.5), two extra things must be done first: a) to keep one of  $\theta$  or  $h$ , which is done usually through empirical relations (e.g., Brooks and Corey 1964; van Genuchten 1980); and b) to supplement it with conditions for the initial situation and for the top and bottom boundary of the flow system. Precipitation, runoff and infiltration are usually treated as upper boundary conditions. For the bottom boundary, either zero-flux boundary or fixed water content or the combination forms are usually applied.

Again, many simplifications for various purposes were made. For example, ISBA, following the pioneering work of Deardorff (1977), makes an analogy to the force restore treatment to the soil temperature. For the top layer, evaporation and precipitation were the only forcing terms and a restoration toward the equilibrium water content was assumed. ISBA as of 1989 also totally ignores the gravitational drainage. Transpiration

only exists for the water budget of the deep/bulk layer. Realizing that water transfer from the root zone to the atmosphere depends both on biological and physical controls (i.e., plants limit their water losses in unfavorable environmental conditions determined by soil moisture in the root zone, atmospheric water deficit, solar radiation, air temperature and carbon-dioxide concentration), four corresponding factors are used in ISBA to modify an unconstrained stomatal resistance.

### *A1.2. Vertical Mixing in and above Convective Boundary Layer*

Following is a description of the involved atmospheric component, namely, the surface layer, the convective boundary layer and the above free atmosphere. Suppose the turbulence in the convective boundary layer is both homogeneous and statistically stationary, the governing equation for a horizontally uniform planetary boundary layer (PBL) reads:

$$\left\{ \begin{array}{l} \frac{\partial \bar{u}}{\partial t} = -\frac{\partial \overline{u'w'}}{\partial z} + f(\bar{v} - v_g), \\ \frac{\partial \bar{v}}{\partial t} = -\frac{\partial \overline{v'w'}}{\partial z} - f(\bar{u} - u_g), \\ \frac{\partial \bar{\theta}}{\partial t} = -\frac{\partial \overline{\theta'w'}}{\partial z} - \overline{R_{radiative}}, \\ \frac{\partial \bar{q}}{\partial t} = -\frac{\partial \overline{q'w'}}{\partial z} + \overline{C_{condensation}}. \end{array} \right. \quad (A1.7a)$$

$$\left\{ \begin{array}{l} \frac{\partial \bar{u}}{\partial t} = -\frac{\partial \overline{u'w'}}{\partial z} + f(\bar{v} - v_g), \\ \frac{\partial \bar{v}}{\partial t} = -\frac{\partial \overline{v'w'}}{\partial z} - f(\bar{u} - u_g), \\ \frac{\partial \bar{\theta}}{\partial t} = -\frac{\partial \overline{\theta'w'}}{\partial z} - \overline{R_{radiative}}, \\ \frac{\partial \bar{q}}{\partial t} = -\frac{\partial \overline{q'w'}}{\partial z} + \overline{C_{condensation}}. \end{array} \right. \quad (A1.7b)$$

$$\left\{ \begin{array}{l} \frac{\partial \bar{u}}{\partial t} = -\frac{\partial \overline{u'w'}}{\partial z} + f(\bar{v} - v_g), \\ \frac{\partial \bar{v}}{\partial t} = -\frac{\partial \overline{v'w'}}{\partial z} - f(\bar{u} - u_g), \\ \frac{\partial \bar{\theta}}{\partial t} = -\frac{\partial \overline{\theta'w'}}{\partial z} - \overline{R_{radiative}}, \\ \frac{\partial \bar{q}}{\partial t} = -\frac{\partial \overline{q'w'}}{\partial z} + \overline{C_{condensation}}. \end{array} \right. \quad (A1.7c)$$

$$\left\{ \begin{array}{l} \frac{\partial \bar{u}}{\partial t} = -\frac{\partial \overline{u'w'}}{\partial z} + f(\bar{v} - v_g), \\ \frac{\partial \bar{v}}{\partial t} = -\frac{\partial \overline{v'w'}}{\partial z} - f(\bar{u} - u_g), \\ \frac{\partial \bar{\theta}}{\partial t} = -\frac{\partial \overline{\theta'w'}}{\partial z} - \overline{R_{radiative}}, \\ \frac{\partial \bar{q}}{\partial t} = -\frac{\partial \overline{q'w'}}{\partial z} + \overline{C_{condensation}}. \end{array} \right. \quad (A1.7d)$$

Here  $t$  is time,  $z$  is altitude,  $u$  is the zonal velocity component (eastward positive),  $v$  is the meridional velocity component (northward positive),  $w$  is vertical velocity, and  $\theta$  is virtual potential temperature, which is defined as  $\theta = \theta_d(1 + 0.61q)$ , here  $\theta_d$  is the potential temperature for dry air, and  $q$  is the mixing ratio of water vapor. Here  $u_g$  is the eastward component of the geostrophic wind,  $v_g$  is the northward component of the

geostrophic wind,  $f$  is the Coriolis parameter,  $\overline{R_{radiative}}$  is the radiative cooling rate, and  $\overline{C_{condensation}}$  is the sink term due to condensation (vanishes for clear boundary layer). Here the overbar '—' denotes the grid resolvable, or mean quantity while the superscription prime "' indicates sub-grid quantity or perturbation. The vertical turbulent flux of a quantity ( $q, \theta$ , or momentum) is expressed as the covariance between its perturbation and the vertical velocity perturbation. Specifically,  $\overline{u'w'}$  and  $\overline{v'w'}$  are components of the Reynolds stress tensor in the east and north directions, respectively; and  $\overline{\theta'w'}$  and  $\overline{q'w'}$  are the components of the turbulent heat and moisture fluxes, respectively.

Centered on how to parameterize eddy fluxes using grid mean properties, there are local- $K$  approach which uses local gradient of scale resolvable  $q, \theta, u$  or  $v$ ; non-local- $K$  approach which enhances the mixing process for convective PBL by including the effects from larger-scale eddies to the local flux (Hong and Pan 1996); and higher order closure that expresses the eddy mixing coefficient as proportional to the square root of sub-grid scale turbulent kinetic energy (TKE) and a length scale of eddies. The length scale is parameterized as stability-dependent and the vertical grid spacing-dependent for stable stratification and parameterized as a function of the height of inversion for unstable layers (Deardorff 1980; Caughey and Palmer 1979; Sun and Chang 1986). The following four points (in sections A1.2.1-A1.2.4) are mainly from the class material of Dr. E. Fedorovich's Planetary Boundary Meteorology offered in School of Meteorology, University of Oklahoma.

### A1.2.1. Empirical Approximations of the Universal Functions

Based on the Monin-Obukhov similarity hypothesis the dimensionless gradients of wind velocity, buoyancy, virtual potential temperature, and (invoking some additional assumptions and experimental evidence) also of potential temperature and specific humidity can be expressed in dimensionless form

$$\left\{ \begin{array}{l} \frac{\kappa z}{u_*} \frac{\partial U}{\partial z} = \varphi_m(\zeta), \end{array} \right. \quad (A1.8a)$$

$$\left\{ \begin{array}{l} \frac{\kappa z}{b_*} \frac{\partial b}{\partial z} = \varphi_b(\zeta), \end{array} \right. \quad (A1.8b)$$

$$\left\{ \begin{array}{l} \frac{\kappa z}{\theta_{v*}} \frac{\partial \theta_v}{\partial z} = \varphi_{\theta_v}(\zeta), \end{array} \right. \quad (A1.8c) ,$$

$$\left\{ \begin{array}{l} \frac{\kappa z}{\theta_*} \frac{\partial \theta}{\partial z} = \varphi_h(\zeta), \end{array} \right. \quad (A1.8d)$$

$$\left\{ \begin{array}{l} \frac{\kappa z}{q_*} \frac{\partial q}{\partial z} = \varphi_q(\zeta). \end{array} \right. \quad (A1.8e)$$

where  $\kappa$  is von Karman constant (0.4),  $z$  is the height from the surface,  $\varphi_m$  is a dimensionless wind gradient, and  $u_*$  is the surface frictional velocity (represents surface stress), and  $\varphi_b(\zeta) = \varphi_{\theta_v}(\zeta) = \varphi_h(\zeta) = \varphi_q(\zeta)$  are universal functions of the dimensionless height  $\zeta = z/L$ , here  $L$  is Monin-Obukhov length. The meanings of  $b_*$ ,  $\theta_*$ ,  $\theta_{v*}$ , and  $q_*$  can be analogously inferred and their relationship will be further discussed soon.

Similarity and dimensionality require that in the limit of the neutrally stratified atmospheric surface layer (ASL) ( $\zeta = \frac{z}{L} = 0$ , or  $L \rightarrow \infty$ ) the values of the universal functions become  $\varphi_m(0) = 1$ , and  $\varphi_b(0) = \varphi_{\theta_v}(0) = \varphi_h(0) = \varphi_q(0) = C_h$ , here  $C_h$  is a constant of order 1.

After a series of specialized ASL experiments performed mainly during the 1960s and 1970s, numerous sets of analytical universal functions have been proposed. Two most commonly used sets are those of Businger *et al.* (1971) and Dyer (Dyer and Hicks 1970, Dyer 1974).

✓ Stable ASL ( $\zeta = \frac{z}{L} \geq 0$ )

○ Dyer:  $\varphi_m(\zeta) = 1 + 5\zeta$  ,  $\varphi_h(\zeta) = 1 + 5\zeta$  , using  $\kappa = 0.41$  (A1.9)

○ Businger:  $\varphi_m(\zeta) = 1 + 4.7\zeta$  ,  $\varphi_h(\zeta) = 0.74 + 4.7\zeta$  , using  $\kappa = 0.35$

✓ Unstable ASL ( $\zeta = \frac{z}{L} \leq 0$ )

○ Dyer:  $\varphi_m(\zeta) = (1 - 16\zeta)^{-0.25}$  ,  $\varphi_h(\zeta) = (1 - 16\zeta)^{-0.5}$  ,  $\kappa = 0.41$  , (A1.10)

○ Businger:  $\varphi_m(\zeta) = (1 - 15\zeta)^{-0.25}$  ,  $\varphi_h(\zeta) = (P_r^{-0.74})(1 - 9\zeta)^{-0.5}$  , using  $\kappa = 0.35$ .

#### A1.2.2. Expressions for Turbulent Exchange Coefficients in terms of Universal Functions

Combining  $K \frac{\partial U}{\partial z} = \overline{-u'w'} = u_*^2$  and  $\frac{\partial z}{u_*} \frac{\partial U}{\partial z} = \varphi_m(\zeta)$ , one obtains the eddy

coefficients for momentum:

$$K = \frac{\kappa u_* z}{\varphi_m(\zeta)} = \kappa u_* L \frac{\zeta}{\varphi_m(\zeta)}, \quad (\text{A1.11})$$

which for the neutral conditions ( $L \rightarrow \infty$ ) reduces to  $K = \kappa u_* z$ . Similarly, taking into

account that  $K_h \frac{\partial \theta}{\partial z} = \overline{-\theta'w'} = u_* \theta'$  and  $\frac{\kappa z}{\theta_*} \frac{\partial \theta}{\partial z} = \varphi_h(\zeta)$ , we obtain expression for the

turbulent heat exchange coefficient

$$K_h(z) = \frac{\kappa u_* z}{\varphi_h(\zeta)} = \kappa u_* L \frac{\zeta}{\varphi_h(\zeta)}. \quad (\text{A1.12})$$



Note first that due to  $\varphi_q(\zeta) = \varphi_h(\zeta)$ , the eddy coefficients for humidity

$$K_q(z) = K_h(z). \quad (\text{A1.13})$$

Thus,  $\frac{1}{Sc} = \frac{1}{Pt} = \frac{K_h(z)}{K(z)} = \frac{\varphi_m(\zeta)}{\varphi_h(\zeta)}$ . Here  $Sc$  is turbulent Schmidt number.

In terms of Dyer's universal functions:

$$K(z) = \begin{cases} \kappa u_* z (1-16\zeta)^{0.25} & (\text{unstable}, \zeta \leq 0) \\ \frac{\kappa u_* z}{1+5\zeta} & (\text{stable}, \zeta \geq 0) \end{cases} \quad \text{and } K_h(z) = \begin{cases} \kappa u_* z (1-16\zeta)^{0.5} & (\text{unstable}, \zeta \leq 0) \\ \frac{\kappa u_* z}{1+5\zeta} & (\text{stable}, \zeta \geq 0) \end{cases}$$

Richardson numbers can also be expressed in terms of the dimensionless height:

$$Ri = \frac{\varphi_h}{\varphi_m^2} \zeta = \frac{P_t}{\varphi_m} \zeta, \quad Ri_{flux} = \frac{1}{\varphi_m} \zeta = \frac{P_t}{\varphi_h} \zeta. \quad \text{This implies that the turbulent exchange}$$

coefficients can also be expressed in terms of Richardson numbers.

### A1.2.3. Integral Forms of Flux-Profile Relationships

To introduce the information from the observed wind speed and humidity, we need to explore the integral form of the universal functions. Integration of

$$\varphi_m(\zeta) = \frac{\kappa z}{u_*} \frac{\partial U}{\partial z} \quad \text{between levels } z_1 \text{ and } z > z_1 \text{ in the ASL leads to the following expression}$$

for the wind velocity profile:

$$U(z) = U(z_1) + \frac{u_*}{\kappa} \left[ \ln \frac{z}{z_1} - \psi_m \left( \frac{z}{L}, \frac{z_1}{L} \right) \right], \quad \text{where}$$

$$\psi_m \left( \frac{z}{L}, \frac{z_1}{L} \right) = \psi_m(\zeta, \zeta_1) = \int_{\zeta_1}^{\zeta} [1 - \varphi_m(\zeta)] d \ln \zeta.$$

If the lower integral level is taken to be the surface roughness height/length  $z_0$ , where the mean flow velocity is assumed to be zero, the wind profile appears as

$U(z) = \frac{u_*}{\kappa} \left[ \ln \frac{z}{z_0} - \psi_m \left( \frac{z}{L}, \frac{z_0}{L} \right) \right]$ . A comparison with the neutral log-wind profile indicates

that function  $\psi_m \left( \frac{z}{L}, \frac{z_0}{L} \right) = \psi_m(\zeta, \zeta_0)$  describes the deviation of the velocity profile from the logarithmic law due to the effect of atmospheric stability. It is thus called the stability correction.

When  $\zeta_0 \ll 1$ , i.e.,  $z_0 \ll L$ , and  $\frac{z}{z_0} \gg 1$ , the stability correction function

$\psi_m(\zeta, \zeta_0)$  is approximated by  $\psi_m(\zeta) = \int [1 - \phi_m(\zeta)] d \ln \zeta + C$ , where the value of the integral constant is chosen to provide  $\psi_m(\zeta_0) = 0$ . Then, the velocity profile takes the approximation form

$$U(z) = \frac{u_*}{\kappa} \left[ \ln \frac{z}{z_0} - \psi_m \left( \frac{z}{L} \right) \right]. \quad (\text{A1.14})$$

Similarly, with respect to the temperature and humidity profiles, using the notions of roughness length for temperature and specific humidity ( $\theta = \theta_s$  at  $z = z_{0\theta}$ , and  $q = q_s$  at  $z = z_{0q}$ ), the temperature and humidity profiles can be expressed as:

$$\begin{aligned} \theta(z) &= \theta_s + \frac{\theta_*}{\kappa} \left[ \ln \frac{z}{z_{0\theta}} - \psi_h \left( \frac{z}{L}, \frac{z_{0\theta}}{L} \right) \right], \text{ and} \\ q(z) &= q_s + \frac{q_*}{\kappa} \left[ \ln \frac{z}{z_{0q}} - \psi_h \left( \frac{z}{L}, \frac{z_{0q}}{L} \right) \right]. \end{aligned} \quad (\text{A1.15})$$

In atmospheric modeling purposes, the following transformation on dependent variable yields (For Dyer's empirical approximations):

$$(unstable, \zeta \leq 0): \begin{cases} \psi_m(\zeta) = 2 \ln \frac{1+x}{2} + \ln \frac{1+x^2}{2} - 2 \arctan(x) + \frac{\pi}{2}, \text{ where } x = (1-16\zeta)^{0.25}, \\ \psi_h(\zeta) = 2 \ln \frac{1+y}{2}, \text{ where } y = (1-16\zeta)^{0.5} \end{cases}$$

$$(stable, \zeta \geq 0): \begin{cases} \psi_m(\zeta) = -5\zeta, \text{ where } x = (1-16\zeta)^{0.25}, \\ \psi_h(\zeta) = -5\zeta \end{cases}$$

#### A1.2.4. Expressions of the Monin-Obukhov Length $L$

There are six interchangeably definition forms of the Monin-Obukhov length  $L$ .

$$\begin{aligned} L &= -\frac{u_*^3}{\kappa w_* b_*} = -\frac{u_*^3}{\kappa \frac{g}{\theta_{v0}} w_* \theta_*} = \frac{u_*^2}{\kappa b_*} = \frac{u_*^2}{\kappa \frac{g}{\theta_{v0}} \theta_*} \\ &= \frac{u_*^2}{\kappa \frac{g}{\theta_{v0}} (\theta_* + 0.61 \theta_{v0} q_*)} = \frac{u_*^2}{\kappa (\frac{g}{\theta_{v0}} \theta_* + g 0.61 q_*)} \end{aligned} \quad (A1.16)$$

Note that  $L$  is related to both sensible heat flux and latent heat flux (the second expression on the right hand side of Eq. (A1.16)). Another fact is that Monin-Obukhov similarity theory, applied in the inner region of the atmospheric boundary layer, i.e., the surface layer, has proven to be a reliable way to obtain regional scale fluxes over rugged terrain. For instance, the mean wind speed profile  $U=U(z)$  in the ASL can be described by the well-known Monin-Obukhov model (A1.14).

In the PBL the characteristic horizontal length scales tend to be 10 to 100 times larger than the vertical scales. Therefore, application of (A1.14) with ASL wind speed measurements at heights around 100m above the surface may produce  $u_*$  values that are representative for upwind distances (or surface length scales) of the order of 1 to 10 km. In the same spirit, formulations that make use of  $U$  measurements at higher elevations, namely, in the outer region of the ABL, may be capable of producing  $u_*$  values that are

representative over even larger upwind fetches. Thus, the surface nonuniformity may be a concern for applying ASL formulations to larger horizontal regions. As an extension of the surface layer similarity into the mixed layer, bulk ABL modeling (Brutsaert and Parlange 1996) use a similar formulation to (A1.14) but with a vertically averaged (bulk) wind speed measured in the outer layer and a bulk stability correction function (prescribed according PBL experiments which provides  $u_*$  and PBL wind profiles). They found that their ABL formulation performed as well as the Monin-Obukhov surface layer similarity model for the determination of surface shear stress for uniformed surface roughness characteristics and may have the potential to be applied to estimate surface fluxes over even larger regions where ASL formulations do not necessarily apply.

In real application, the surface roughness characteristics of the site can be obtained through an analysis of those radiosonde wind speed profiles in the ASL measured under neutral stability conditions. The aim of field campaigns (i.e., for a forest and farm land interlaced region in south western France, Hydrologic Atmospheric Pilot Experiment-Modelisation du Bilan Hydrique, HAPEX-MOBILHY, Andre *et al.* 1986; for a moderately moist grassland in USA, First International Satellite Land Surface Climatology Project Field Experiment, FIFE, Sellers *et al.* 1992; for an arid part of Australia, Wangara boundary layer experiment, Clarke *et al.* 1971; and several scattered places with routine hydraulic observations located in the Whitcta Basin (Oklahoma), Southern Great Plains Hydrologic Field Experiment, SGP '99) are usually to determine the functional form of the stability adjust function, using the directly observed surface stress ( $u_*$ ) or surface flux components ( $H$  and  $LE$ ). Real application of the PBL scheme is a process of estimating  $u_*$  and  $L$ , usually an iterative procedure is involved.

## Appendix 2. A Review of 4DVAR Data Assimilation Technology

Data assimilation is the process of fitting dynamic model trajectory over some time interval to data using the model equations as a strong constraint, through adjusting its initial, boundary conditions or other model parameters (LeDimet and Talagrand 1986; Talagrand and Courtier 1987; Lorenc 1986). The goal is achieved by minimizing the cost function, which is a measure of the model-data misfit and is usually in the form of mean square error, or by maximizing the likelihood using minimization techniques. For each iteration step, the minimization routine usually takes two parameters, i.e., the value of the cost function and its gradient with respect to the control variables, which explicitly or implicitly appear in the cost function and their optimal values are the goal of the minimization procedure.

During the ensuing discussion, the following notational conventions are heavily used.

$Z \in R^m$ , observations that are taken at  $m$  irregular spatial grid points;

$x \in R^n$ , model output (state vector) that are distributed on  $n$  regular spatial grids;

$H$  (or its non-linear counterpart  $h$ ), projection matrix, which finishes two operations: *a*)

implementing the physical transition of model output to the corresponding observations (e.g., using  $Z$ - $R$  relationship to complete the transformation of precipitation rate to radar observed reflectivity; using Stephan-Boltzmann relation to relate the satellite brightness temperature to surface temperature), and *b*) making a projection from model space  $R^n$  to observation space  $R^m$  ( $H$  is an  $m$  by  $n$  matrix);

$V$ , noise inherent to the observations, which is of zero mean, additive, with known variance, and

is assumed to be temporally uncorrelated. For two time levels  $k$  and  $l$ ,

$$E(V(k))=0; E(V(k) V^T(l))=Q\delta_{k,l},$$

here  $\delta_{k,l}$  is the Kronecker delta, and superscript  $T$  denotes transpose.  $Q$  is called covariance matrix of observation noise and is assumed to be constant;

$\bar{x}(k) \in R^n$ , base state of variable  $x$  at time level  $k$ ;

$W \in R^{m \times m}$ , a symmetric, positive definite matrix called the weight matrix. It gives a weight to

model-data difference in the cost function. It is significant when the cost function includes more than one type of observational data. Usually,  $W=Q^{-1}$ ;

$J$ , cost function, a measure of the distance between the model forecast and observations.

Usually

defined as the quadratic form.

$\mathbf{J}_h$ , Jacobian matrix of function  $h$  with respect to state variable  $x$ .

$c$ , control variable, or a specific state variables that minimize the cost function. Finding control

variable  $c$  is the goal of conducting variational data assimilation.

$\mathbf{R} \in R^{m \times m}$ , resolvent matrix that signifies state transition of the forward dynamic system, also

called state transition matrix.

$M \in R^{m \times m}$ , the discrete form of resolvent  $\mathbf{R}$ .

The functional relationships will be extensively used throughout this section.

$$\delta J(c) = \langle \delta c, \nabla_c J(c) \rangle; \quad \langle x^T, Ay \rangle = \langle A^T x^T, y \rangle; \quad \langle a, y \rangle = \langle b, y \rangle, \forall x \rightarrow a = b; \text{ and } \langle x, y \rangle = x^T y.$$

where, angle bracket  $\langle \rangle$  signifies inner products in Hilbert space,  $\delta J(c)$  is the first order variation of cost function  $J$  with respect to  $c$ , and  $\nabla_c J(c)$  is the gradient of  $J$  with respect to state variables evaluated at  $c$ .

What follows is a succinct review of the 4DVAR formulism, using the optimal estimation of initial conditions in non-linear systems as an example. Both model nonlinearity and the nonlinearity between observations and model analysis are considered. Perturbation theory is the basis for solving this problem. This subsection is summarized from Dr. Varahan's lecture notes on Dynamic Data Assimilation, which was given on 1999.

Pick a  $c \in R^n$  and let  $\bar{x}(0) = c$ , the orbit can be computed using  $x(k) = M(x(k-1), \alpha) = \dots = M^{(k)}(c + \delta c, \alpha)$ . The actual evolution of the perturbation is given by

$$x(k) - \bar{x}(k) = M^k(c + \delta c, \alpha) - M^k(c, \alpha). \quad (\text{A2.1})$$

Since the computation of  $M^k(x, \alpha)$  is very difficult in general, this quantity is usually approximated using the first order Taylor series expansion:

$$M(x(0), \alpha) = M(\bar{x}(0) + \delta c, \alpha) \approx M(\bar{x}(0), \alpha) + J_M(\bar{x}(0), \alpha) \delta c.$$

Similarly  $\bar{x}(1) + \delta x(1)$  is an approximation to  $x(1)$  to a first order accuracy. Thus,  $M(x(1), \alpha) = M(\bar{x}(1) + \delta x(1), \alpha) \approx M(\bar{x}(1), \alpha) + \delta x(1) J_M(\bar{x}(1), \alpha)$ , by denoting  $\delta x(2) = \delta x(1) J_M(\bar{x}(1), \alpha)$ ,  $\bar{x}(2) + \delta x(2)$  is thus an approximation to  $x(2)$ .

Continuing this argument, inductively defining

$$\delta x(k+1) = \delta x(k) J_M(\bar{x}(k), \alpha), \quad (\text{A2.2})$$

results in  $\bar{x}(k+1) + \delta x(k+1)$  as an approximation to  $x(k+1)$ .

Note that Eq. (A2.2) is a non-autonomous linear dynamic system where the one step transition matrix  $J_M(\bar{x}(k), \alpha)$  is evaluated along the base state. Equation (A2.2) is known as the tangent linear system (TLS). For convenience, introducing the following notation  $J_M(k) = J_M(\bar{x}(k), \alpha)$ , then Eq. (A2.2) can be rewritten as  $\delta x(k+1) = \delta x(k) J_M(k) = J_M(k) J_M(k-1) J_M(k-2) \dots J_M(1) J_M(0) \delta c$ . If one further defines, for  $i \leq j$ ,  $J_M(i:j) = J_M(j) J_M(j-1) \dots J_M(i)$ , Eq. (A2.2) can be further reduced to  $\delta x(k+1) = J_M(0:k) \delta c$ , or  $\delta x(k) = J_M(0:k-1) \delta c$ .

The iterative scheme that defines the TLS as in (A2.2) can also be written in a matrix-vector form:  $F \delta x = b$ , (A2.3)

where  $F$  is an  $N$  by  $N$  block partitioned matrix given by

$$F = \begin{bmatrix} I & O & O & O \\ -J_M(1) & I & O & O \\ O & -J_M(2) & I & O \\ O & O & -J_M(3) & I & O \\ \dots & \dots & \dots & \dots & \dots \\ O & O & O & -J_M(N-1) & I \end{bmatrix}, \delta x = (\delta x(1), \delta x(2), \delta x(3), \dots, \delta x(N))^T, \text{ and}$$

$b$  is a block partitioned vector given by  $b = (J_M(0) \delta c, 0, 0, \dots, 0)^T$ .

In the following, an example will be given illustrating the usage of adjoint technique to get the gradient of cost function with respect to the control variable  $c$ .

$$\text{Define } J(c) = \frac{1}{2} \sum_{k=1}^N \langle [h(x(k)) - Z(k)], W [h(x(k)) - Z(k)] \rangle.$$



Since  $J(c) = \sum_{k=0}^N J_c(k)$ , and  $\delta J(c) = \sum_{k=0}^N \delta J(k)$  (the subscription 'c' is omitted). The general

term  $J(k) = \frac{1}{2} [h(x(k)) - Z(k)]^T W [h(x(k)) - Z(k)]$  and

$$\delta J(k) = \langle W [h(x(k)) - Z(k)], J_h(k) \delta x(k) \rangle = \langle J_M^T(0:k-1) J_h^T(k) W [h(x(k)) - Z(k)], \delta c \rangle,$$

Thus

$$\nabla J(c) = \sum_{k=0}^N \nabla J(k) = \sum_{k=0}^N J_M^T(0:k-1) J_h^T(k) W [h(x(k)) - Z(k)] \quad (\text{A2.4})$$

Here all Jacobians are taken with respect to  $x$  and  $J_M(0:-1) = I$ , the identity matrix.

Define forcing

$$f(k) = J_h^T(k) W [h(x(k)) - Z(k)] \quad (\text{A2.5})$$

, and  $\bar{\lambda}(k) \in R^n$  for  $K = N, N-1, N-2, \dots, 2, 1, 0$ . The gradient of  $J$  can be obtained by the

following iteration procedure

$$\bar{\lambda}(k) = J_M^T(k) \bar{\lambda}(k+1) + f(k), \quad (\text{A2.6})$$

starting from  $\bar{\lambda}(N) = f(N)$ . (A2.7)

Or, in matrix form,  $B\bar{\lambda} = f$ , with  $B$  an  $N+1$  by  $N+1$  block partitioned matrix given by

$$B = \begin{bmatrix} I & -J_M^T(0) & O & O & O \\ & I & -J_M^T(1) & O & O \\ & & I & -J_M^T(2) & O \\ \dots & \dots & \dots & \dots & \dots \\ & O & & I & -J_M^T(N-1) \\ & & O & & I \end{bmatrix},$$

$\bar{\lambda} = (\bar{\lambda}(0), \bar{\lambda}(1), \bar{\lambda}(2), \dots, \bar{\lambda}(N))^T$ , and  $f = (f(0), f(1), f(2), \dots, f(N))^T$ .

$\bar{\lambda}(0)$  is the gradient of the cost function with respect to the control variables.

Variational technique has a long tradition in hydraulics research and land surface modeling studies (see e.g. Kool *et al.* 1987). They are useful tools for finding optimal fits between model and data, for parameter identification, sensitivities, and error propagation. The ability of 4DVAR data assimilation to deal with data scattered in time has stimulated efforts to devise variational assimilation schemes for atmospheric models (Navon *et al.* 1992). Another reason why the variational method is considered to be superior (Rabier *et al.* 1993) to sequential methods (e.g., Nudging, Successive correction, Optimal interpolation, Kalman Filter, and Kalman smoother) is that it allows for nonlinear relation between observations and the model variables to be retrieved.

Kalman filter assimilate data this way: The analysis is a combination of background and a modified observation innovation. The analysis is then used as the background for next time level analysis. The Kalman gain applied to innovation vector depends on error covariance matrix, which evolves in time and also not easy to save and time cost to estimate

Like retrospective methods, the variational data assimilation methods would also necessarily depend on land model skill, however, the model strong constraint can be readily relaxed through adding an extra forcing term to represent the model error (Zupanski 1997). This extra forcing term can be determined in the data assimilation process. Assuming that this error is not related to model physics (but only parameterization uncertainties), the assimilation method's forward model dependency may be effectively quarantined.

### Appendix 3. An example of hand coding adjoint and its verification

The following is an example of the Lorenz system and its hand-coded adjoint (Fig 3A.1). Lorenz system (Lorenz 1963) is a well studied nonlinear system to describe the forced convection process between two large, parallel plates (an example of using “finite system systems of deterministic ordinary differential equations to represent forced dissipative hydrodynamical systems”-Lorenz 1963). Lorenz system can be viewed as a miniature of the atmospheric system, which is a forced (ultimately radiative forcings at surface and top of atmosphere) dissipative (hence non-conservative) system (thermal dissipation and viscous dissipation of momentum) governed by nonlinear partial differential equations. Phase changes of water (both latent heat releasing/absorption and the effects on radiative transfer from clouds) further complicated the process since the forcings put into the system through different manners have quite different consequences for the evolution of the system.

$$\begin{cases} \frac{dx}{dt} = -ax + ay & 3A.1(a) \\ \frac{dy}{dt} = -xz + rx - y & 3A.1(b) \\ \frac{dz}{dt} = xy - bz & 3A.1(c) \end{cases}$$

$a = 10$ ,  $b = 8/3$ ,  $0 < r < 30$ , following Saltzman (1962)

In Lorenz system, three variables are used ( $x, y$  and  $z$  in Eq. (3A.1a-c)) to describe a state of the forced dissipative system in phase space.  $x$ ,  $y$  and  $z$  signify the velocity and temperature structures of the flow system. The state of no convection is represented by setting  $x=y=z=0$ . The steady states are represented by time invariant  $x$ ,  $y$  and  $z$ . Lorenz system can possess very complicated nonlinear characteristics such as the behaviors of the system are very sensitive to initial values and the existence of attractors. The long

term behavior of the system depends on the initial region (in phase space) of the state variables. Taken the parameters as in Eq. (3A.1), every  $r$  greater than the critical Rayleigh number ( $\sim 24.74$ ) corresponds a subspace of zero volume in the phase space. All trajectories emanating from this region are non-periodic since any two points near each other in phase space cannot keep being so as time goes on.

The integration scheme for the forward model (Eqs. (3A.1a-c)) is the fourth order Runge-Kutta method (subroutine *rgkt* in Fig. 3A.1). It is required that the sum total of small time steps (e.g., *timestep(2)*-*timestep(5)* in Fig. 3A.1) equals three times the forward time integration step. The right hand side of the Lorenz system is evaluated in subroutine *ytend*.

```

!----- Lorenz system -----
! a=10, b=8/3, 0<r<30
! dx
! ----a*x+a*y
! dt
! dy
! ----x*z+r*x-y
! dt
! dz
! ----x*y-b*z
! dt
! It is a system to describe the convection process
! between two large, parallel plate, i.e., bernad flow
subroutine lorenz (nsys,p,timestep)
implicit none
integer :: i, nsys
double precision :: timestep(5)
double precision, dimension (1:nsys) :: p,y

do i=1,nsys
y(i)=p(i)
enddo
call rgkt (nsys,timestep,y)
do i=1,nsys
p(i)=y(i)
enddo
end subroutine lorenz

subroutine rgkt (nsys,timestep,y)
implicit none
integer i,j, nsys
double precision, dimension (1:nsys) :: y,ym,yw,yt
double precision timestep(5)

do i=1,nsys
ym(i)=y(i)
yw(i)=y(i)
enddo

do j=1,4
call ytend (nsys,ym,yt)

do i=1,nsys
ym(i)=yw(i)+timestep(j)*yt(i)
y(i)=y(i)+timestep(j+1)*yt(i)/3.0
enddo

enddo

return
end subroutine rgkt

!----- The adjoint of Lorenz system -----
subroutine adlorenz (nsys,timestep,p,ad_p)
implicit none
integer :: i, nsys
double precision :: timestep(5),temp (nsys,4)
double precision, dimension (1:nsys) :: p,y,ad_p,ad_y

do i=1,nsys
y(i)=p(i)
ad_y(i)=ad_p(i)
ad_p(i)=0.0
enddo

call adrgkt (nsys,timestep,y,ad_y)
do i=1,nsys
ad_p(i)= ad_p(i)+ad_y(i)
ad_y(i)=0.0
enddo

end subroutine adlorenz

subroutine adrgkt (nsys,timestep,y,ad_y)
implicit none
integer :: i,j,nsys
double precision :: timestep(5),temp (nsys,4)
double precision, dimension (1:nsys) :: y,ym,yw,yt,ad_y,ad_ym,
ad_yw, ad_yt

do i=1,nsys
ym(i)=y(i)
yw(i)=y(i)
ad_ym(i)=0.0
ad_yw(i)=0.0
ad_yt(i)=0.0
enddo

do j=1,4
do i=1,nsys
temp(i,j)=ym(i)
enddo
call ytend (nsys,ym,yt)
do i=1,nsys
ym(i)=yw(i)+timestep(j)*yt(i)
y(i)=y(i)+timestep(j+1)*yt(i)/3.0 !! not used later on...
enddo

do j=4,1,-1
do i=1,nsys
ad_yt(i)=ad_yt(i)+timestep(j+1)*ad_y(i)/3.0
ad_yt(i)=ad_yt(i)+timestep(j)*ad_ym(i)
ad_yw(i)=ad_yw(i)+ad_ym(i)
ad_ym(i)=0.0
enddo

do i=1,nsys
ym(i)=temp(i,j)
enddo

call adytend (nsys,ym,ad_yt,ad_ym)
enddo

do i=1,nsys
ad_y(i)=ad_y(i)+ad_yw(i)

```

**Fig. 3A.1** Lorenz system and its adjoint. The integration scheme for the forward model is the fourth order Runge-Kutta method.

In the adjoint code of *rgkt*, to avoid the expensive re-computation, a temporary array (*temp*) was used to hold the required base state values. Also, at the beginning of the subroutine *adlorenz* (adjoint code of subroutine *lorenz*), adjoint variable of local array *y* is set to zero, thus  $ad\_y=ad\_p$ , rather than the more general form of  $ad\_y=ad\_y+ad\_p$ . Also, a global dependency analysis shows that statement  $y(i)=y(i)+timestep(j+1)*yt(i)/3.0$  is useless in the adjoint code since *y* is no longer required. With user specified flow derivatives to avoid an expensive re-computation, automatic tool TAF (as of April 18, 2003) can also produce similarly effective code.

The adjoint and tangent linear codes of Lorenz system ( $a=10.0$ ,  $b=8.0/3.0$ , and  $r=28.0$ ) was verified using dot product test (i.e., method *a* in Section 3.1). The time series resulting from using  $X=10.0, Y=8.0, Z=11.7$ , and  $\delta X=0.005, \delta Y=0.2, \delta Z=0.006$  are given in Fig 3A.2, which clearly show the correctness of our code. TAFLINK provides another effective tool to check the correctness of the TLM/ADM models by a direct comparison with the finite difference results. The following (Fig. 3A.3) is a result of TAFLINK run. In Fig. 3A.3, the discrepancy to finite differences changes with the perturbation *eps* and will become very small if using double precision compilation and as *eps* is small. Also, the output of TLM and ADM is identical. Here the full Jacobian is compared not only the *Jacobian* $\times$ *vector* (TLM) or *vector* $\times$ *Jacobian* (ADM). In automatic differentiation technology, it is called vector mode testing. The hand-coded adjoint code of the land surface-atmospheric boundary layer model will be tested by all above three verification procedures.

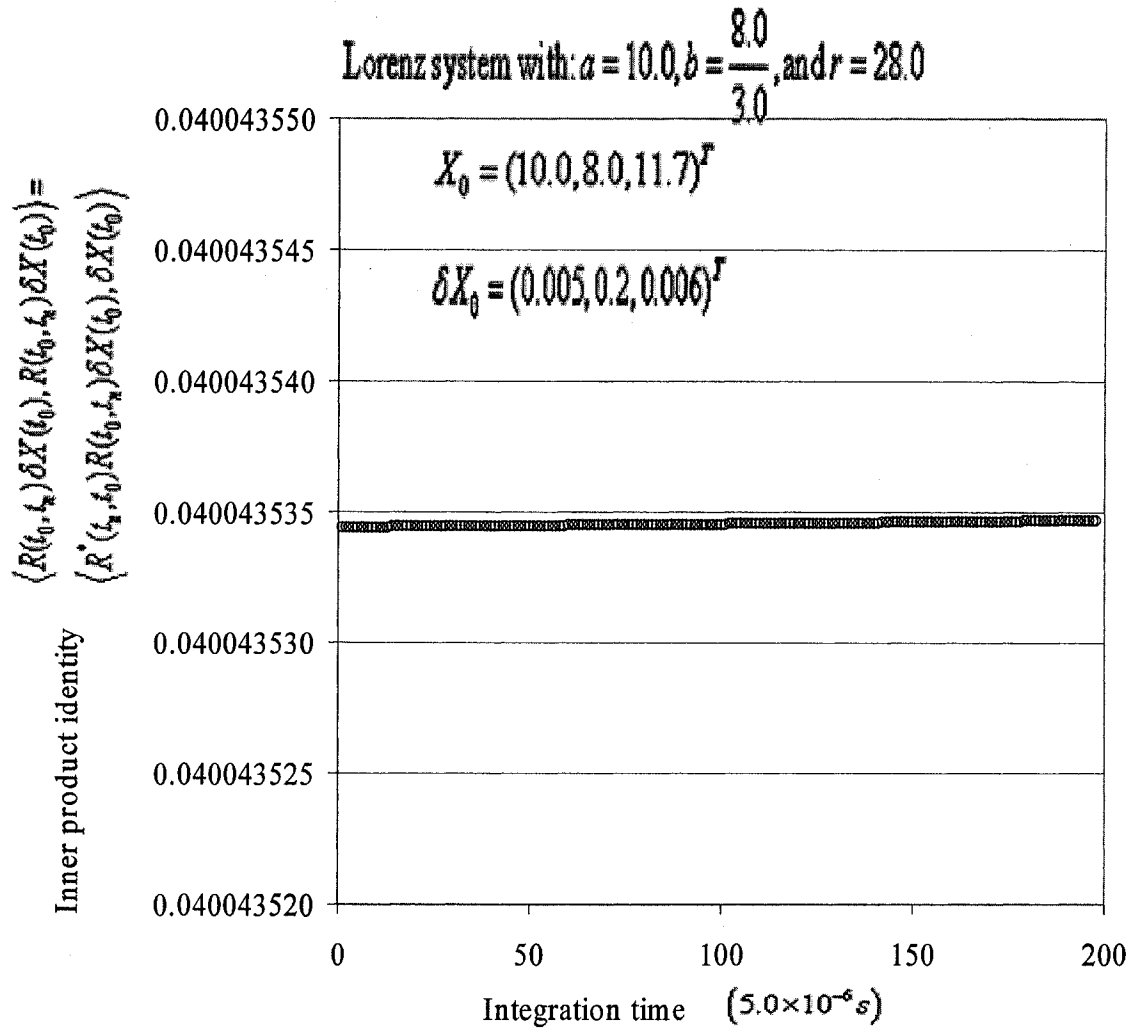


**Fig. 3A.2.** Dot product verification of TLM/ADM of Lorenz system.

```
(a)
./fchecktl
parameters for gradient check read
CHECK OF JACOBIAN USING eps = 0.100E-01

I  J  x(i)  finit. Diff  AutoDiff  DIFFERENCE
1  1  0.100000E+02  0.990179E+00  0.990179E+00  0.131077E-09
1  2  0.100000E+02  0.160665E-01  0.160665E-01  0.248410E-05
1  3  0.100000E+02  0.806622E-02  0.806615E-02  0.984188E-05
1  4  0.100000E+02  0.990179E+00  0.990179E+00  0.131077E-09
1  5  0.100000E+02  0.160665E-01  0.160665E-01  0.248410E-05
1  6  0.100000E+02  0.806622E-02  0.806615E-02  0.984188E-05
1  7  0.100000E+02  0.990179E+00  0.990179E+00  0.130955E-09
1  8  0.100000E+02  0.160665E-01  0.160665E-01  0.248411E-05
1  9  0.100000E+02  0.806622E-02  0.806615E-02  0.984189E-05
1 10  0.100000E+02  0.990228E+00  0.990228E+00  0.128922E-09
1 11  0.100000E+02  0.159865E-01  0.159865E-01  0.247138E-05
1 12  0.100000E+02  0.802516E-02  0.802509E-02  0.979374E-05
1 13  0.100000E+02  -.974177E+01  -.974177E+01  0.406305E-07
1 14  0.100000E+02  0.159953E+02  0.159954E+02  0.502766E-05
1 15  0.100000E+02  0.821215E+01  0.821200E+01  0.192503E-04
2  1  0.800000E+01  0.989588E-02  0.989588E-02  0.318186E-09
2  2  0.800000E+01  0.999036E+00  0.999036E+00  0.492375E-09
2  3  0.800000E+01  0.996234E-02  0.996229E-02  0.493898E-05
2  4  0.800000E+01  0.989588E-02  0.989588E-02  0.318186E-09
2  5  0.800000E+01  0.999036E+00  0.999036E+00  0.492375E-09
2  6  0.800000E+01  0.996234E-02  0.996229E-02  0.493898E-05
2  7  0.800000E+01  0.989588E-02  0.989588E-02  0.299425E-09
2  8  0.800000E+01  0.999036E+00  0.999036E+00  0.492377E-09
2  9  0.800000E+01  0.996234E-02  0.996229E-02  0.493896E-05
2 10  0.800000E+01  0.984642E-02  0.984642E-02  0.302641E-09
2 11  0.800000E+01  0.999041E+00  0.999041E+00  0.484919E-09
2 12  0.800000E+01  0.991221E-02  0.991216E-02  0.491425E-05
2 13  0.800000E+01  0.989167E+01  0.989167E+01  0.490520E-09
2 14  0.800000E+01  -.937808E+00  -.937807E+00  0.156655E-05
2 15  0.800000E+01  0.100254E+02  0.100254E+02  0.982307E-05
3  1  0.117000E+02  -.492049E-04  -.492049E-04  0.236094E-07
3  2  0.117000E+02  -.992240E-02  -.992240E-02  0.164025E-07
3  3  0.117000E+02  0.997301E+00  0.997301E+00  0.412006E-12
3  4  0.117000E+02  -.492049E-04  -.492049E-04  0.236094E-07
3  5  0.117000E+02  -.992240E-02  -.992240E-02  0.164025E-07
3  6  0.117000E+02  0.997301E+00  0.997301E+00  0.412006E-12
3  7  0.117000E+02  -.492051E-04  -.492051E-04  0.227807E-07
3  8  0.117000E+02  -.992240E-02  -.992240E-02  0.163753E-07
3  9  0.117000E+02  0.997301E+00  0.997301E+00  0.543144E-12
3 10  0.117000E+02  -.487127E-04  -.487127E-04  0.242582E-07
3 11  0.117000E+02  -.987267E-02  -.987267E-02  0.162136E-07
3 12  0.117000E+02  0.997315E+00  0.997315E+00  0.512412E-12
3 13  0.117000E+02  -.984858E-01  -.984858E-01  0.162317E-07
3 14  0.117000E+02  -.994503E+01  -.994503E+01  0.490837E-07
3 15  0.117000E+02  -.275867E+01  -.275867E+01  0.234424E-08

./fcheckad
parameters for gradient check read
```

```
(b)
=====
COMPUTATION OF FUNCTION AND JACOBIAN
IN REVERSE MODE
=====
CHECK OF JACOBIAN USING eps = 0.100E-01
=====
I  J  x(i)  finit. Diff  AutoDiff  DIFFERENCE
1  1  0.100000E+02  0.990179E+00  0.990179E+00  0.131076E-09
1  2  0.100000E+02  0.160665E-01  0.160665E-01  0.248410E-05
1  3  0.100000E+02  0.806622E-02  0.806615E-02  0.984188E-05
1  4  0.100000E+02  0.990179E+00  0.990179E+00  0.131076E-09
1  5  0.100000E+02  0.160665E-01  0.160665E-01  0.248410E-05
1  6  0.100000E+02  0.806622E-02  0.806615E-02  0.984188E-05
1  7  0.100000E+02  0.990179E+00  0.990179E+00  0.130956E-09
1  8  0.100000E+02  0.160665E-01  0.160665E-01  0.248411E-05
1  9  0.100000E+02  0.806622E-02  0.806615E-02  0.984189E-05
1 10  0.100000E+02  0.990228E+00  0.990228E+00  0.128922E-09
1 11  0.100000E+02  0.159865E-01  0.159865E-01  0.247138E-05
1 12  0.100000E+02  0.802516E-02  0.802509E-02  0.979374E-05
1 13  0.100000E+02  -.974177E+01  -.974177E+01  0.406305E-07
1 14  0.100000E+02  0.159953E+02  0.159954E+02  0.502766E-05
1 15  0.100000E+02  0.821215E+01  0.821200E+01  0.192503E-04
2  1  0.800000E+01  0.989588E-02  0.989588E-02  0.318186E-09
2  2  0.800000E+01  0.999036E+00  0.999036E+00  0.492375E-09
2  3  0.800000E+01  0.996234E-02  0.996229E-02  0.493898E-05
2  4  0.800000E+01  0.989588E-02  0.989588E-02  0.318186E-09
2  5  0.800000E+01  0.999036E+00  0.999036E+00  0.492373E-09
2  6  0.800000E+01  0.996234E-02  0.996229E-02  0.493898E-05
2  7  0.800000E+01  0.989588E-02  0.989588E-02  0.299425E-09
2  8  0.800000E+01  0.999036E+00  0.999036E+00  0.492375E-09
2  9  0.800000E+01  0.996234E-02  0.996229E-02  0.493896E-05
2 10  0.800000E+01  0.984642E-02  0.984642E-02  0.302639E-09
2 11  0.800000E+01  0.999041E+00  0.999041E+00  0.484918E-09
2 12  0.800000E+01  0.991221E-02  0.991216E-02  0.491425E-05
2 13  0.800000E+01  0.989167E+01  0.989167E+01  0.490518E-09
2 14  0.800000E+01  -.937808E+00  -.937807E+00  0.156655E-05
2 15  0.800000E+01  0.100254E+02  0.100254E+02  0.982307E-05
3  1  0.117000E+02  -.492049E-04  -.492049E-04  0.236094E-07
3  2  0.117000E+02  -.992240E-02  -.992240E-02  0.164025E-07
3  3  0.117000E+02  0.997301E+00  0.997301E+00  0.413548E-12
3  4  0.117000E+02  -.492049E-04  -.492049E-04  0.236094E-07
3  5  0.117000E+02  -.992240E-02  -.992240E-02  0.164025E-07
3  6  0.117000E+02  0.997301E+00  0.997301E+00  0.413564E-12
3  7  0.117000E+02  -.492051E-04  -.492051E-04  0.227807E-07
3  8  0.117000E+02  -.992240E-02  -.992240E-02  0.163753E-07
3  9  0.117000E+02  0.997301E+00  0.997301E+00  0.544925E-12
3 10  0.117000E+02  -.487127E-04  -.487127E-04  0.242582E-07
3 11  0.117000E+02  -.987267E-02  -.987267E-02  0.162136E-07
3 12  0.117000E+02  0.997315E+00  0.997315E+00  0.513859E-12
3 13  0.117000E+02  -.984858E-01  -.984858E-01  0.162317E-07
3 14  0.117000E+02  -.994503E+01  -.994503E+01  0.490837E-07
3 15  0.117000E+02  -.275867E+01  -.275867E+01  0.234424E-08

./fcompare
```

```
(c)
=====
CHECK OF REVERSE AND FORWARD MODE
A^t = A
=====
forward and reverse mode give identical results

./ftime
PRGFTIME : options have been read
iterations = 500

*****
TIMING OUTPUT, niter = 500
*****
control parameters N : 3
run time function : 1.337000
run time function + tangent : 3.183000
run time function + adjoint : 136.719000
rel. run time forward mode (FUNC+JAC)/FUNC = 2.380703
rel. run time reverse mode (FUNC+JAC)/FUNC = 102.258040
rel. run time forward mode(Finite Diff.)/(FUNC+JAC) = 0.168018E+01
rel. run time reverse mode(Finite Diff.)/(FUNC+JAC) = 0.391167E-01
*****

iterations = 500

*****
TIMING OUTPUT, niter = 500
*****
control parameters N : 3
run time function : 1.339000
run time function + tangent : 3.149000
run time function + adjoint : 136.850000
rel. run time forward mode (FUNC+JAC)/FUNC = 2.351755
rel. run time reverse mode (FUNC+JAC)/FUNC = 102.203137
rel. run time forward mode(Finite Diff.)/(FUNC+JAC) = 0.170086E+01
rel. run time reverse mode(Finite Diff.)/(FUNC+JAC) = 0.391377E-01
*****
```

Fig. 3A.3. TAFLINK checking of the correctness and efficiency of TLM/ADM of Lorenz system. Note that TAFLINK did the following tests:

- Test TLM/ADM against finite differences.
- Compare the tangent and adjoint computed Jacobian.
- The codes are timed at last.